Elucidation of Cellular Functions of the Deubiquitinases USP53 and USP54

Dissertation

for the achievement of the academic degree of the

Doctor of Natural Sciences

(Dr. rer. nat.)

Submitted to the

Department of Chemistry and Chemical Biology

TU Dortmund University

by

Kai Gallant

Dortmund 2025

The work presented in this thesis was performed during the period from May 2020 to April 2025 under the supervision of Dr. Malte Gersch at the Chemical Genomics Centre, the Max Planck Institute of Molecular Physiology Dortmund and the Faculty of Chemistry and Chemical Biology at the Technical University Dortmund.

Supervisor:	Dr. Malte Gersch
1st Examiner:	Dr. Malte Gersch
2nd Examiner:	Prof. Dr. Dr. h.c. Herbert Waldmann

Disclaimer

Results detailed in this thesis have contributed to the following publications:

Wendrich K[#], **Gallant K[#]**, Recknagel S, Petroulia S, Kazi NH, Hane J, Führer S, Bezstarosti K, O'Dea R, Demmers J, Gersch M, "Discovery and mechanism of K63-linkage-directed deubiquitinase activity in USP53", *Nat Chem Biol,* 2024, https://doi.org/10.1038/s41589-024-01777-0, [#]contributed equally

Kazi HK, Klink N, **Gallant K**, Kipka, GM, Gersch M, "Chimeric deubiquitinase engineering reveals structural basis for specific inhibition of USP30", *Nat Struct Mol Biol,* accepted in principle – a preprint was published on bioRxiv: https://doi.org/10.1101/2024.09.22.613429

Kim Wendrich contributed to work described in this thesis by providing *in vitro* generated tetra- and polyubiquitin chains and purified catalytic domain of USP53 and USP54. To facilitate a better understanding of experimental data acquired for this dissertation, her highly complementary work features in two panels throughout this thesis which is attributed accordingly. Siska Führer contributed to work described in this thesis by purification and biotinylation of the biotinylated pulldown reagents as well as support in developing the workflow of coupling TUBE-based ubiquitinome isolation to mass spectrometry and purification of OTUB1* together with Nafizul Haque Kazi. Dr. Stavroula Petroulia contributed to work described in this thesis by providing conditional *USP53* knockdown cell lines. The DPF and Dr. Malte Gersch contributed to work described in this thesis by purifying AMSH*. Dr. Zhou Zhao contributed to work described in this thesis by purifying OTUD1. Marvin Rötte contributed to work described in this thesis by purification and functionalisation of activity-based probes. Dr. Petra Janning and Malte Metz contributed by mass spectrometry sample measurement and initial steps of data analysis. Furthermore, Dr. Stefano Maffini contributed by support with live-cell imaging and fruitful discussions. Dr. Jeroen Demmers, Karel Bezstarosti and Wouter Doff contributed to work described in this thesis by processing diGly samples and initial bioinformatic analysis of raw data. Major contributions are also indicated in the respective figure captions.

Acknowledgments

I would like to express my gratitude to my supervisor, Malte, for his support and guidance throughout my PhD journey. I have greatly valued the scientific discussions we had, which not only deepened my understanding of the matter but also fostered a collaborative and stimulating environment. Your clear vision for the project and guidance helped me navigate the complex world of ubiquitination, deubiquitination and many others. I believe your attention to detail and encouragement to strive for excellence have made me a better scientist and I want to express my gratitude for this.

I also want to extend my sincere gratitude to Prof. Dr. Dr. Herbert Waldmann, not only for examining my thesis, but also for the fruitful and enriching time I had at the CGC which you enabled.

Furthermore, I want to thank Dr. Christian Schröter and Prof. Dr. Stefan Westermann for their support and input during the TAC meetings and beyond.

I want to also dedicate a special thanks to Lucia and Christa for their kindness and their support during my PhD. Your friendliness towards everyone in any situation has always been a beacon at the institute and the research school that I was always very happy to be a part of.

I am deeply grateful to each member of the Gersch group for enriching my time in the group not only with interesting discussions about science, insights into experimental details and help on how to improve the project and my skills, but also shared moments of joy, pain, frustration and happiness. I could not have asked for better colleagues because you all are not only incredibly smart but also amazingly friendly, helpful and open. I am also very grateful that I can call many of you true friends today with a shared passion for games, drinks, music, festivals and, last but not least, coffee. Thank you Christian, Evie, Mirko, Sarah, Mirko, Zhou, Helena, Rachel, Mira, Gian, Jan, Kim, Nafizul, Niko and Siska. I hope we will keep in touch as we move on with our lives.

I would especially like to thank you, Kim, for being such a wonderful person to share the passion for ‘our’ two DUBs with. Not only was discussing the intricacies of these two sUSPects with you always insightful and exciting but you are just a true joy to work and spend time with – both in and out of the lab. While we might not have shared the same taste in appropriate lab music, I believe we did share a really good time and I am grateful for everything.

I also want to thank you, Niko, for being not only an honest, passionate and helpful colleague, but also a true friend. While your passion for targeting countless proteins for degradation was infectious, your interest and joy were not limited to these molecules. I am so very happy that

we not only shared a good part of the PhD journey but also trips to the many sights of Dortmund. While these included not too many detours to the gym, I always ended up having a great time with you.

Life and science in the Gersch group would not have been the same without all the other members of the CGC. I really enjoyed running into all of you in the corridors on a daily basis, exchanging ideas on how to progress in our projects or what to do on the weekend (if not spent in the lab). Thank you for your constant support, the relatively few moments that tension was rising and your input over the past few years. This is particularly true for my wonderful office mate Yang – it has simply been a pleasure to share an office and thoughts with you.

Among the people who roam the corridors of the CGC and Department IV, I would like to especially thank you, Jen-Yao, Stefan, Kim, Jeff, Caitlin, Oguz, Eric, Georg, Jimin, Pascal and Jessica for sharing many memorable moments with me in the lab, on the fire escape, in Dortmund and beyond. Thank you for the great memories, your help, everything we experienced in this (sometimes) stressful time and your friendship.

To everyone I had the pleasure to go to lunch at Mensa with: I want to wholeheartedly thank you for providing an (often much needed) break from a hectic day in the lab. Discussions about rising Mensa prices or the culinary characteristics of salad dressings were often just what I needed to regain the energy to develop a new blot.

Many thanks to you Sabri, Arianna, Francesca, Fabian, Duccio, and Lara for many sunny, sandy days, your expert cineaste suggestions and being the heart not only of the institute but also of many of my happy hours in Dortmund.

I would also like to thank all the other incredible people at MPI that I was fortunate enough to get to know during my time here, whether it be in seminars, social gatherings at the institute or retreats. You provided so much support during every step of the project and my PhD and helped fill the institute and my time there with life. I especially want to thank Petra, Slava, Peter, Daniel, Oliver and Sebastian. Finally, I want to express my gratitude to you, Stefano, for your support, kindness and encouragement. I want to extend this gratitude also to you, Peter and Valentina for being positive role models and for taking responsibility to change the scientific community for the better.

Many thanks also to the collaborators in Rotterdam, in AG Summerer and the HRMS team in Dortmund for many enlightening meetings, your help with data analysis in proteomics research and a very positive and encouraging atmosphere. A big thanks also to the amazing DUB and ubiquitin community that was always a very kind, open and supportive group that I had the pleasure to get to know on conferences and in presentations.

A big thank you also to one of the kindest people I ever met: thank you Sophia for being a fabulous, kind and open flatmate and for keeping up with me and my working hours.

As I write these acknowledgements, I am reminded of how many people I have been lucky enough to meet during my time here in Dortmund and how they shaped me as a person and scientist. However, there were also many people that supported me with their friendship and love over many years and I would like to dedicate the following page to them.

I want to say thanks to my friends from home who were always there for me despite me not being in my hometown all too much during my studies and PhD. Thank you for all the evenings that still felt like the good ol' times.

Thanks to everyone who I regularly share my Monday evenings with. What started as a routine during COVID became a cherished tradition and I am so happy that we keep on meeting virtually and in person.

Many evenings would not have been the same without my dear horror film enthusiasts (and, most importantly, true friends). Thank you, Ani, Fabi and Nils for always keeping in touch, sharing your emotions and support and taking the time for us, despite being in different time zones or cities and overall life situations. It always feels as heartfelt and joyous as it did during our studies.

Thank you, Henriette, Erik and Svea from the bottom of my heart for many amazing hours during our studies and beyond, your open ear and heart in so many situations. Your friendship helped me through a lot and it sure was the source of countless good memories in the last years. I sincerely hope that, like the many hikes we have done together, our shared journey ahead of us is almost endless, with no end in sight.

You will not be surprised to find this section of my 'thank you' almost at the end, since this is where you have found me most of the time during our cycling tours: Thank you, Jozi, Thomi and Fabi. What started out as a relatively improvised summer tour, has become one of the most precious things I look forward to each year. Your constant support, encouragement and distraction have been really important to me during my PhD time and I am sure it will continue to be in the future.

I do not think words can do justice to what you have meant to me over the last few years, Rachel. With you, every wall seemed like a hurdle possible to overcome and your support and love gave me the energy I often needed to achieve my own and our shared goals. All of it while enjoying life to the fullest in every shared second. Thanks so much for all of it, my love.

Last but definitely not least I want to thank my family: Vielen Dank, dass ihr mich über all die Jahre bedingungslos unterstützt habt und immer für mich da wart. Ich habe mich jedes Jahr an Weihnachten und zu allen anderen Anlässen immer sehr auf eure Gesellschaft gefreut und bin euch unendlich dankbar, dass ich so viele unzählige schöne Momente mit euch erleben konnte. Vielen Dank Silke, Susanne, Connie, Carsten, Laura, Silvan, Kalea, Mikas und Hubbert. Tausend dank auch an euch, Dagmar, Thomas und Stephanie für eure Unterstützung in schweren Zeiten und euer immer offenes Ohr. Mein größter Dank gebührt meiner Oma, meinem Opa und meiner Mutter: Ihr habt mich zu der Person gemacht, die ich heute bin und mir alles ermöglicht, was ich erreicht habe – auch wenn Ihr dafür eure eigenen Bedürfnisse hintenanstellen musstet. Das werde ich euch niemals vergessen und euch für immer dankbar sein.

Table of contents

Disclaimer I

Acknowledgments I

Table of contents V

Abstract VII

Zusammenfassung VIII

1 Introduction 1

1.1 The Ubiquitin System 1

1.2 Ubiquitin Chain Topology dictates Substrate Fate and Function 3

1.3 Deubiquitinases – Important Enzymes shaping the Ubiquitin System 6

1.4 DUBs regulate a Plethora of Cellular Processes 8

1.4.1 Ubiquitination regulates membrane proteins in diverse ways 8

1.4.2 Tight junction proteins are tightly regulated by the ubiquitin system 10

1.4.3 DUBs regulating the cell cycle and microtubule organization 10

1.5 DUBs as promising Therapeutic Targets 11

1.6 USP53 – a DUB associated with Cholestasis and Hearing Loss 12

1.7 USP54 - an enigmatic DUB that promotes Cancer Progression 14

1.8 Tools for the Identification of Ubiquitinated Proteins 15

1.9 Methods to Investigate Ubiquitin Architectures on Proteins 18

2 Motivation and Aim 20

3 Elucidation of Cellular Functions of the Deubiquitinases USP53 and USP54 21

3.1 Catalytic Activity of USP53 and USP54 isolated from Cells 21

3.1.1 Reactivity of USP53 and USP54 with activity-based probes is indicative of their catalytic activity in cells 21

3.1.2 USP54 displays selective cleavage of K63-linked ubiquitin chains *ex cellulo* 24

3.2 Establishment of a Toolkit for the Identification of Cellular Substrates of USP53 and USP54 25

3.2.1 Different polyubiquitin binders allow selective enrichment of ubiquitin *in vitro* and *ex cellulo* 25

3.2.2 Monoubiquitin binders are valuable tools to enrich proteins decorated with short ubiquitin chains 27

3.2.3 Establishing ubiquitin binders as useful reagents to study the influence of DUB activity in the context of mitochondrial depolarisation 29

3.3 Identification of substrates of the human DUB USP53 31

3.3.1 Analysis of protein levels of USP53 mutants in cells 31

3.3.2 Establishing epithelial and epithelial-like knockdown cell lines to study USP53 effects 32
3.3.3 diGly-based ubiquitinomics identifies ubiquitination sites regulated by USP53 34
3.3.4 Ubiquitin binders complement diGly-based proteomics to assess substrate ubiquitylation 39
3.3.5 Ubiquitin chain restriction analysis identifies ubiquitin chain types on the putative USP53 substrate MARVELD2 42
3.3.6 Assessing the effect of ubiquitination of MARVELD2 in the context of endocytosis 46
3.4 Characterization of the Cellular Role of the Human DUB USP54 48
3.4.1 Total proteome analysis of the prostate cancer cell line PC-3 upon USP54 depletion reveals proteins regulated by the DUB 48
3.4.2 Elucidating the microenvironment of USP54 using proximity labelling 50
3.4.3 USP54 regulates the cell cycle and cytoskeleton organisation 56
3.4.5 U2OS cells expressing siRNA-resistant USP54 as a tool for future experiments to characterise cellular functions of the DUB 59
3.4.6 Localisation of USP54 and the impact of C-terminal domains on localisation 60
3.4.7 Ubiquitinome isolation coupled to mass spectrometry for the identification of substrates of USP54 63
4 Conclusion and Discussion 71
4.1 Tools identifying DUB Substrates demonstrate an Influence of USP30 Inhibition on Ubiquitination of TOM Complex Proteins 71
4.2 Regulation of Tricellular Junction Proteins by USP53 72
4.3 USP54 – an intricate Protein important for Cell Cycle Progression and Cytoskeletal Organisation 75
5 Appendix 79
6 Material and Methods 82
6.1 Material 82
6.2 Methods 88
7 References 106
8 Abbreviations 127

Abstract

Ubiquitylation is a reversible post-translational modification that is vital to most cellular processes. Deubiquitinases (DUBs), which modulate ubiquitylation, thus fulfil a critical role in maintaining a healthy cell state. Consequently, numerous pathological conditions are associated with misregulated or mutated DUBs. Two enzymes that have been linked to human pathologies are USP53 and USP54, two poorly characterised ubiquitin-specific protease (USP) family members which were annotated as catalytically inactive pseudoenzymes. Rudimentary knowledge about the cellular roles of USP53 and USP54 and limited insights into their potential substrates has, however, hampered a better understanding of their association with the reported diseases and phenotypes.

The endeavour to better understand both proteins in this dissertation began by establishing enzymatic activity of both proteins. In subsequent experiments, the herein presented work thus focused on filling the knowledge gap between DUB activity and reported pathologies. As such, this dissertation provides a model that establishes a link between *USP53* mutations and cholestasis as well as hearing loss. This was achieved by a combination of cell biological approaches, state-of-the-art mass spectrometry and a variety of enrichment tools allowing for the isolation and subsequent enzymatic treatment of ubiquitinated proteins. These methods facilitated the identification of two tricellular junction proteins, MARVELD2 and LSR, as substrates of USP53. For MARVELD2, significantly increased K63-linked ubiquitination upon depletion of the DUB could be demonstrated. Notably, the most prominent ubiquitinated species found to be emerging in these conditions is diubiquitinated MARVELD2, thus converging with *in vitro* work conducted within the group. Furthermore, this dissertation provides insights into the cellular functions of USP54, highlighting its role in cell cycle regulation and microtubule network organisation. In order to relate these phenotypic effects to catalytic activity, ubiquitin enrichment coupled to mass spectrometry was optimised which identified a set of proposed substrates. In addition, proximity labelling revealed USP54 interactors that localise to three discrete cellular compartments, centrioles, tight junctions and endolysosomal membranes. Orthogonal experiments furthermore supported interaction of the DUB with 14-3-3 proteins which indicates a regulation of USP54 protein abundance during the cell cycle.

In conclusion, this work advances the knowledge about the two underexplored DUBs USP53 and USP54, while demonstrating the utility of combinatorial ubiquitin enrichment approaches to study the nature of ubiquitination on DUB substrates. The findings in conjunction with the reported pathologies will pave the way to better understand the association of DUB and diseases and potentially allow hijacking USP54 for novel therapeutic opportunities.

Zusammenfassung

Die Ubiquitinierung von Proteinen stellt eine posttranslationale Modifikation dar, die für die Aufrechterhaltung zahlreicher zellulärer Prozesse essentiell ist und von Deubiquitinasen (DUBs) reguliert wird. Aufgrund der Bedeutung dieser Modifikation sind Fehlregulierung und Mutationen in diesen Enzymen oftmals mit bestimmten Krankheitsbildern assoziiert. Zwei Enzyme, die mit menschlichen Pathologien assoziiert werden, sind USP53 und USP54. Diese beiden unzureichend charakterisierten Proteine sind Teil der Ubiquitin-spezifischen Proteasen (USP)-Familie und wurden zuvor als katalytisch inaktiv beschrieben. Das begrenzte Wissen über ihre zellulären Funktionen, sowie ihre potenziellen Substrate stand bisher einem Verständnis zur Verknüpfung von DUB und Krankheit im Wege.

Die vorliegende Dissertation liefert ein Modell, welches Mutationen in *USP53* mit Cholestase und Hörverlust verknüpft. Diese Verknüpfung wurde durch eine Kombination aus zellbiologischen Ansätzen, moderner Massenspektrometrie und Ubiquitin-Anreicherungs-Reagenzien erstellt, die die Isolierung und anschließende enzymatische Untersuchung von ubiquitinierten Proteinen ermöglichen. Dies erlaubte die Identifikation der USP53 Substrate MARVELD2 und LSR. Diese beiden trizellulären Proteine weisen nach der Verminderung der DUB in den verwendeten Zellsystemen eine signifikant erhöhte K63-verknüpfte Ubiquitinierung auf. Interessanterweise ist die Bildung von diubiquitiniertem MARVELD2 unter diesen Bedingungen besonders bevorzugt, was mit den *in vitro* durchgeführten Arbeiten innerhalb der Gruppe übereinstimmt. Darüber hinaus bietet die Dissertation Einblicke in die zellulären Funktionen von USP54 und dessen Rolle in der Zellzyklusregulation und der Organisation des Mikrotubuli-Netzwerks hervor. Um diese phänotypischen Effekte mit der katalytischen Aktivität in Verbindung zu bringen, wurde die Kopplung von Ubiquitinanreicherung an Massenspektrometrie optimiert, wodurch eine Reihe von Substraten identifiziert wurde. Darüber hinaus wurden Interaktoren von USP54 durch lokal begrenzte Proteinmarkierung identifiziert. Diese lokalisieren in drei zellulären Kompartimenten, den Zentriolen, Zell-Zell-Verbindungen und endolysosomalen Membranen. Orthogonale Experimente stützen zudem die Interaktion der DUB mit 14-3-3-Proteinen - ein Indiz dafür, wie die Proteinlevel von USP54 während des Zellzyklus reguliert werden könnten.

Zusammenfassend erweitert diese Dissertation das Wissen über die beiden wenig erforschten DUBs USP53 und USP54 und vermittelt gleichzeitig die Nützlichkeit eines kombinatorischen Ansatzes zur Untersuchung der Art der Ubiquitinierung auf vorgeschlagenen DUB-Substraten. Gemeinsam mit den berichteten Pathologien ebnen diese Erkenntnisse den Weg, diese Proteine für neue therapeutische Möglichkeiten zu erschließen.

1 Introduction

1.1 The Ubiquitin System

Since the development of the cell theory by Schwann, Schleiden and Virchow, scientific progress elucidated that cells are not only highly complex but also incredibly dynamic systems. Within these systems, proteins fulfil a majority of the structural and functional roles. The fate of a protein, however, is not fully determined by its DNA-encoded amino acid sequence: post-translational modifications (PTMs) emerged as essential elements of life that regulate chemical and physical properties of many proteins vital to our cells.

These PTMs are not limited to small chemical entities such as phosphorylation but can be proteinaceous themselves. The most prominent example for a proteinaceous modifier in mammalian cells is ubiquitin (Ramazi & Zahiri, 2021). This highly conserved, 76-amino acid big polypeptide is mostly described to attach to the ϵ-amino group of a lysine side chain of a substrate protein via its C-terminal glycine residue. The formation of this iso-peptide bond is facilitated by E1 activating (2 members), E2 conjugating (35 members) and E3 ligating (>600 members) enzymes – the latter promote E2 and substrate protein selectivity (Q. Yang et al., 2021).

The roughly 8 x 10^7 copies of ubiquitin within a cell (amounting to approximately 85 µM in a human cell, Kaiser et al., 2011) are present in different ubiquitin pools: 'free' ubiquitin, ubiquitin participating in the conjugation cascade and conjugated ubiquitin (Clague et al., 2015) with conjugated ubiquitin being estimated to target ~100,000 protein sites (W. Kim et al., 2011; Prus et al., 2024; Wagner et al., 2011). 60% of the total ubiquitin pool in a mammalian cell is estimated to be present as monoubiquitination, meaning that one molecule ubiquitin is attached to one substrate protein (Clague et al., 2015). However, it is important to note that ubiquitination is not restricted to the attachment of one molecule ubiquitin to a given site. In fact, one of the fascinating properties of the ubiquitin system is the capacity to modify the modifier – meaning that ubiquitin itself can be modified by ubiquitin via one of its seven lysine residues (K6, K11, K27, K29, K33, K48 and K63) or its N-terminal methionine residue (M1, see Figure 1).

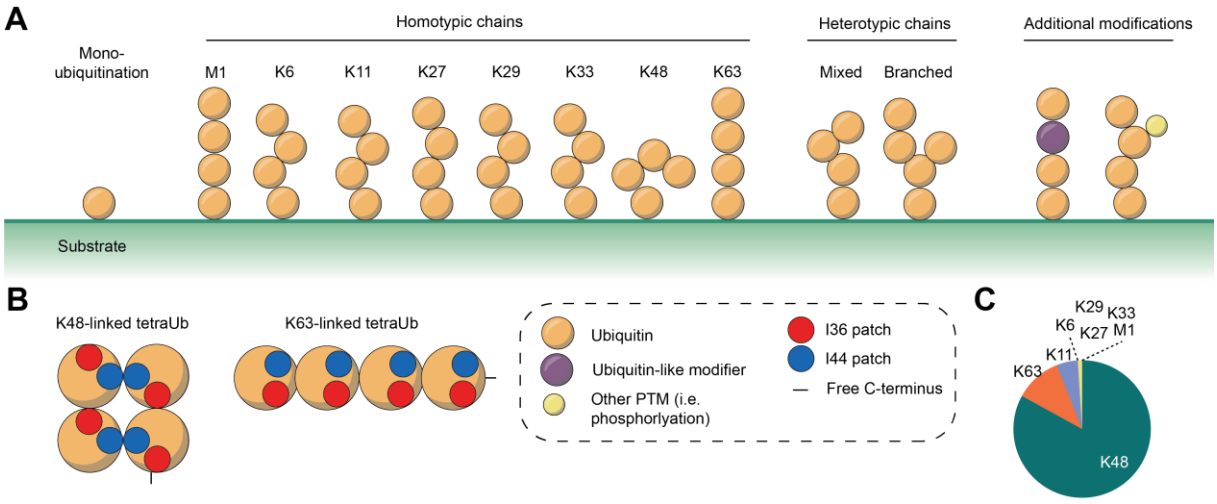

Figure 1. The intricate complexity of ubiquitin chain topology. (A) Schematic representation of the complex ubiquitin chain topology and its modifications. Figure adapted from Mevissen and Komander (2017). **(B)** Topology of tetraubiquitin chains made up from the two most abundant chain types, K48- and K63-linked chains. The interaction hotspots isoleucine 36 and isoleucine 44 patch are shown in the structures. The topologies were experimentally determined by crystallography, NMR or small-angle light scattering (Datta et al., 2009; Eddins et al., 2007). The panel was adapted from Komander and Rape (2012). **(C)** Distribution of linkage types among cellular polyubiquitin chains as measured in HEK-293 cells. Numbers were extracted from data presented in Kaiser et al. (2011).

The resulting ubiquitin chains (sometimes also referred to as ‘polymers’) can be either homotypic or heterotypic, meaning there could either be one linkage type present within one chain or several different ones (Fig. 1A). Furthermore, branched chains can form in which one molecule of ubiquitin is decorated with two or more other ubiquitin molecules (López-Mosqueda & Dikic, 2014; Meyer & Rape, 2014; Ohtake et al., 2016; Valkevich et al., 2014). Besides the combinatorial complexity of ubiquitin modifications, other modifiers can be incorporated in ubiquitin chains such as ubiquitin-like proteins or non-proteinaceous entities such as phosphorylation (Fig. 1A, Komander & Rape, 2012; Mevissen & Komander, 2017). The different linkages result in a plethora of different topologies effecting the structure of the polymer and expose different hot spots of interaction of ubiquitin such as the isoleucine patch 36 or 44 (Fig. 1B, Komander & Rape, 2012). Measurements of distribution of linkage types in polyubiquitin chains of human cells yielded that roughly 83% of linkages are K48-linkages, followed by K63- and K11-linkages (Fig. 1C, Kaiser et al., 2011).

Box 1. Comparing PTM properties of ubiquitylation and phosphorylation.

Phosphorylation is the only other post-translational modification exhibiting a scope and complexity comparable to ubiquitination. Interestingly, the number of writers (540) and erasers (190) as well as the estimated number of regulated sites (~100,000, Needham et al., 2019) in the phosphorylation system are very similar to the ubiquitin system. The two systems differ however in the occupancy of sites: the median occupancy of phosphorylation is ~3 orders of magnitude higher than ubiquitylation (Prus et al. 2024) which might be due to inherent system properties with ATP being generally not limiting (with an estimated cellular concentration of 2-12 mM, Song, 2021) while a cell has a finite number of ubiquitin molecules (Prus et al., 2024). The best-known and arguably most abundant ubiquitination occurs at the lysine side chain of proteins but the acyl transfer reaction can also occur at the N-terminal amino group of proteins and at the nucleophilic amino acid side chains of cysteine, serine, threonine and tyrosine (Kelsall, 2022). Phosphorylation, in turn, mostly regulates serine, threonine and tyrosine residues. However, also histidine, arginine and lysine phosphorylation have been described (Azevedo et al., 2024). The fascination for the ubiquitin system, in part, stems from its complexity conferred by the capacity to form homo- and heterotypical polyubiquitin chains while poly-phosphorylation is less well-known and displays limited complexity (Azevedo et al., 2015). Ubiquitin and phosphate groups not only compete for conjugation to certain amino acids but there is interplay within the system with ubiquitin being modified by phosphorylation thus influencing its properties (Koyano et al., 2014).

1.2 Ubiquitin Chain Topology dictates Substrate Fate and Function

The diversity of chain topology and length not only determines interactions with readers of the ubiquitin system, shaping substrate fate and function but also underscores the critical roles of specific chain types in biological processes.

Over the last centuries, homotypic chains have been associated with a plethora of biological processes (Fig. 2): (i) Linear ubiquitin chains built from M1-linked ubiquitin were shown to play a role in inflammation and immunity via the linear ubiquitin chain assembly complex regulating protein scaffolding and subsequent NF-κB signalling (Damgaard et al., 2012). (ii) K6-linked ubiquitin chains are upregulated upon UV genotoxic stress (Elia et al., 2015) and appear to be critical for mitophagy (Ordureau et al., 2015). (iii) K11-linked ubiquitin chains appear to mediate degradation in the cell cycle (which is potentially facilitated via branched chains, Yau et al., 2017). (iv) K27 linkages, while being considered the most enigmatic linkage type, were reported to be important in DNA damage response (DDR, Swatek & Komander, 2016). (v) K29-linked chains are associated with epigenetic regulation (Jin et al., 2016) and (iv) K33-

linked chains play a role in post-Golgi membrane protein trafficking (Yuan et al., 2014). The discovery of the ubiquitin-mediated protein degradation system (UPS) has been awarded with the Nobel prize in chemistry in 2004 (Hershko et al., 1979), which is regulated through K48-linked chains (vii) that are the most critical chain type for proteasomal degradation. Finally, K63-linked chains (viii) are arguably the most versatile chain type. They are involved in DDR (Haahr et al., 2018; Jackson & Durocher, 2013), kinase activation (Tang et al., 2019), endocytosis and other aspects of intracellular trafficking (Erpapazoglou et al., 2014), scaffolding (Damgaard et al., 2012), innate immune response (Wu & Karin, 2015) and autophagy (Dósa & Csizmadia, 2022). K63-chains were also identified as seeds for branched ubiquitin chains thus channelling proteins to the UPS. The appreciation of importance of such heterotypic chains and the role of other ubiquitin-modifications grew within the last decade. As such, other critical roles of K48/K63 branched chains in NF-κB signal regulation, K11/K63 mixed chains in endocytosis or M1/K63 hybrid chains in scaffolding have been revealed (Ohtake et al., 2016; Swatek & Komander, 2016).

Besides the importance of linkage types within a chain, analysis of ubiquitin chain interactors has shown that certain proteins interact with ubiquitin chains of a specific length indicating an important regulatory function of chain length (Waltho et al., 2024). This is further supported by the finding that epidermal growth factor receptors appear as tetra- to hexaubiquitylated rather than di- or triubiquitinated species (Tsuchiya et al., 2018).

For some of the chain types, ubiquitin binding domains (UBDs) of reader proteins were determined, and different concepts of ubiquitin recognition emerged. These include the recognition of linkage contexts by the UBDs, as well as the detection of distances between ubiquitin molecules and flexibility within the chain. Other UBDs recognise distinct surfaces built up by multiple ubiquitin molecules of a chain (Komander & Rape, 2012). Examples for ubiquitin binding by readers are the ubiquitin associated domain of UBQLN1 that binds individual ubiquitin molecules and shuttles ubiquitinated proteins to the 19S proteasome (Fig. 2B). This binding was shown for both K48- and K63-linked chains (D. Zhang et al., 2008) highlighting the flexibility of chains and the importance of cellular context. Other domains, such as the Npl4 zinc finger (NZF) domain of TAB2, bind two adjacent K63- or K6-linked diubiquitins within one domain, leading to activation of TAK1 triggering NF-κB signalling (Fig. 2C, Kulathu et al., 2009). Another recognition mode is employed in the use of different spacing between ubiquitin molecules in the ubiquitin-interacting motifs of RAP80 which binds K63-linked ubiquitin via the distinctly oriented isoleucine 44 patch. RAP80 then recruits BRCA1 to sites of DNA damage thus representing a key player in DDR (Fig. 2C, H. Kim et al., 2007).

Besides the fascinating insights into chain topology and its read-outs over the course of the last decades, other factors such as substrate localisation, timing and interactomes influence the cellular outcome of ubiquitylation and must be kept in mind when studying proteins involved in the ubiquitin system (Komander & Rape, 2012).

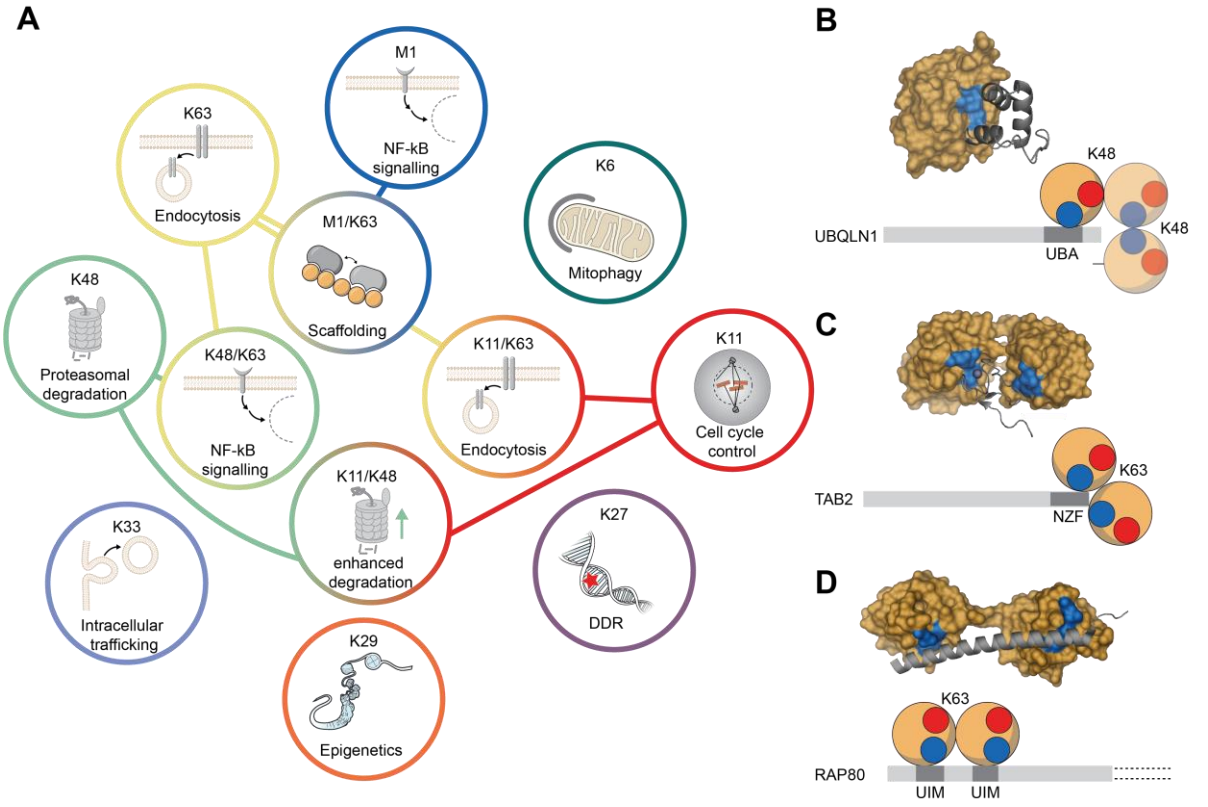

Figure 2. Ubiquitin chain topology dictates substrate fate and function. (A) Overview of different linkage types and their association with substrate fate and function in a cellular context upon protein decoration with the respective chain. The scheme was inspired by Swatek & Komander (2016). **(B-D)** Depiction of the interaction of ubiquitin binding domains from reader proteins involved in determining substrate fate. Ubiquitin binding domains and ubiquitin chains are shown in grey cartoon and orange surface representation, respectively. The critical isoleucine 44 patch is coloured in blue. Binding of a single ubiquitin molecule by the ubiquitin-associated (UBA) domain of UBQLN1 is shown in **(B)**, binding of the Npl4 zinc finger (NZF) ubiquitin-binding domain (UBD) to K63-linked diubiquitin in **(C)** and binding of the ubiquitin-interacting motif (UIM) of RAP80 to K63-linked diubiquitin in **(D)**. Structures are deposited with the PDB accession numbers 2JY6 for (B), 3A1Q for (C) and 2WWZ for (D). Sizes of proteins with binding domain are not to scale. Illustrations of mitochondrion, DDR and epigenetics were extracted from NIAID NIH Bioart and are licensed under public domain.

1.3 Deubiquitinases – Important Enzymes shaping the Ubiquitin System

The conceptional beauty of post-translational modifications is linked to their dynamic nature: besides conjugation of the modifiers by writers and readouts by distinct reader proteins, erasers remove or modulate the modification and thus ensure that the modifiers re-enter the cycle. The erasers (or better: modulators) within the ubiquitin system are termed 'Deubiquitylases' or 'Deubiquitinases' (DUBs).

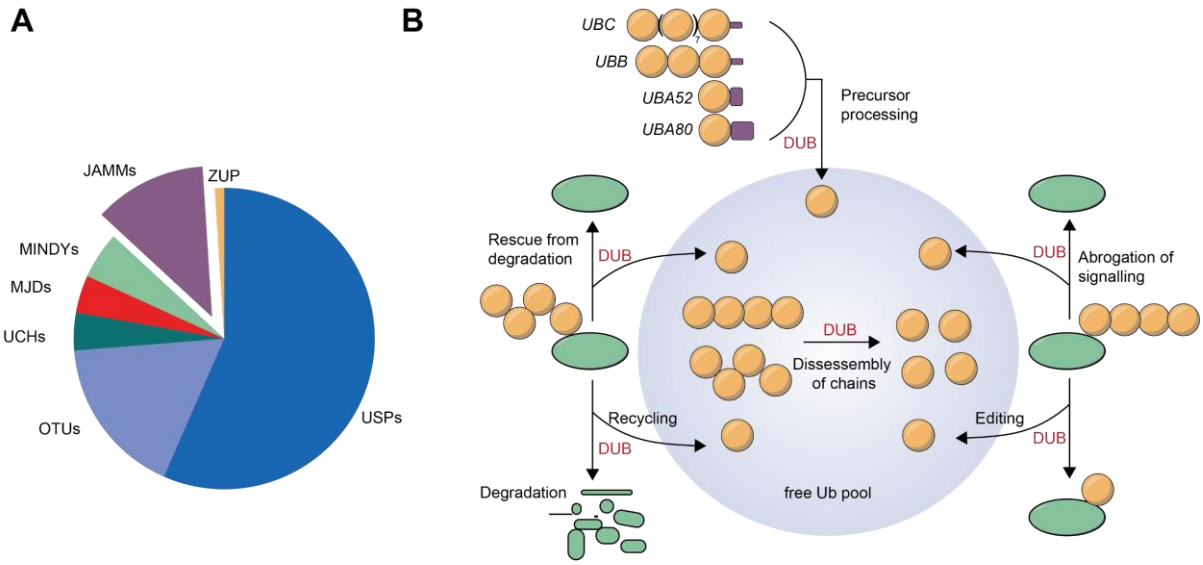

Figure 3. DUBs modulate all aspects of the ubiquitin system. (A) Pie chart depicting the seven DUB families found in humans with section sizes proportional to the number of members of each family. JAMMs are highlighted since they are the only metalloproteases among the DUB families (Clague, Urbe, et al., 2019). **(B)** DUBs fulfil a plethora of cellular functions, that all contribute to the regeneration of the free ubiquitin pool in a cell. The figure was slightly changed from Komander et al. (2009).

There are currently 99 DUBs identified in humans which are classified in seven structurally distinct families (Fig. 3A, Clague et al., 2019; Mevissen & Komander, 2017): the ubiquitin-specific proteases (USPs), ovarian tumour proteases (OTUs), ubiquitin C-terminal hydrolases (UCHs), the motif interacting with ubiquitin-containing novel DUB family (MINDYs) and Zinc finger containing ubiquitin peptidases (ZUPs, with ZUP1 as its only member to date) – all of which are cysteine-dependent proteases. In addition, there is the Zn-dependent JAB1/MPN/MOV34 metalloprotease family (JAMMs, Mevissen & Komander, 2017). Besides their structural differences, the DUB families differ in their tendency to display linkage specificity. The biggest family, the USPs generally show little linkage preference with notable exceptions (i.e. CYLD or USP30 - Gersch et al., 2017; Hrdinka et al., 2016). Other families such as the OTU DUBs have a high degree of linkage selectivity (Mevissen et al., 2013).

With roughly 1 x 10^7 aggregated copies per human cells, the number of DUBs is on par with the number of E2s. The most abundant DUBs are associated with major cellular machines such as the proteasome, the COP9 signalosome, LUBAC or the SAGA complex (Clague et

al., 2015). At the proteasome, DUBs recover ubiquitin from ubiquitinated proteins in a regulated manner (M. J. Lee et al., 2011). Beyond recycling ubiquitin and preventing proteins from proteasomal degradation, DUBs are also responsible for generating free ubiquitin at the start of the cycle since ubiquitin is either expressed as linear polyubiquitin or fused to ribosomal proteins (Fig. 3B, Komander et al., 2009). Furthermore, they regulate processes by either altering the interaction platform for proteins such as in LUBAC-associated processes or abrogate and edit cellular signalling (Fig. 3B).

Substrate specificity of DUBs is determined by their cellular localisation, interactions with substrates, mediating binding partners or ubiquitin itself. Moreover, specificity for distinct chains types influences these aspects (Clague et al., 2012).

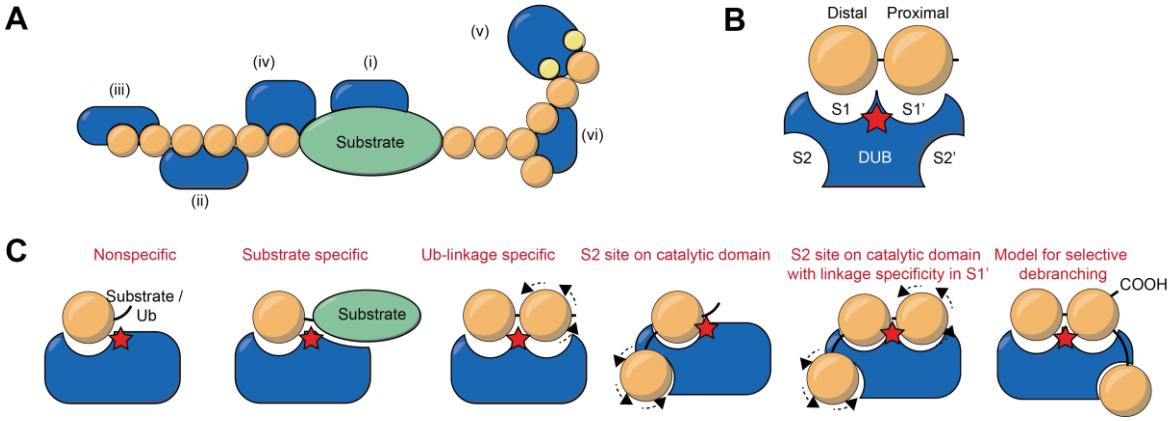

Figure 4. Cleavage of ubiquitin chains by DUBs. (A) DUBs can either directly bind to their substrates to remove ubiquitin (i) or recognize ubiquitin chains directly to perform either endo- (ii) or exo-cleavage at the distal (iii) or proximal (iv) terminus. Specialized ubiquitin cleavage modes include cleavage of modified ubiquitin (v) or cleavage of branched chains (vi). **(B)** Nomenclature for ubiquitin sites on the catalytic domain of DUBs. The red star indicates the catalytic centre. **(C)** Different ubiquitin binding modes and architectures of the catalytic domains of DUBs to recognise chains or specifically cleave them. Note the difference between chain specificity encoded in either S1' or S2 site. Figure was largely adopted from Mevissen & Komander, 2017 and slightly changed.

There are several possibilities how DUBs recognize their substrates or ubiquitin (Fig. 4A). Recognition of the distal ubiquitin by a DUB is facilitated by the S1 site that is shared between DUBs: it guides the C-terminus of ubiquitin and the scissile bond to the active site for its hydrolysis (Fig. 4B). For cleavage within a diubiquitin molecule, the distal ubiquitin molecule occupies the S1 site while the proximal ubiquitin occupies the S1' site (Fig. 4C, Mevissen & Komander, 2017). Some DUBs also feature additional ubiquitin binding sites in either the catalytic domain or in additional regions (S2, S2', S3 or S3', Fig. 4C). Specificity in cleavage of linkage types is often encoded in the S1' site with the S2 site being important for chain type recognition and chain-selective (proximal) exo-cleavage. It can also contribute to preferences for longer ubiquitin chains (Mevissen & Komander, 2017).

1.4 DUBs regulate a Plethora of Cellular Processes

Subcellular localisation is another critical factor determining substrate identities. Given ubiquitin's involvement in almost all cellular processes, DUBs have, consequentially, been identified across a large number of cellular structures (Fig. 5) and implicated in numerous cellular processes.

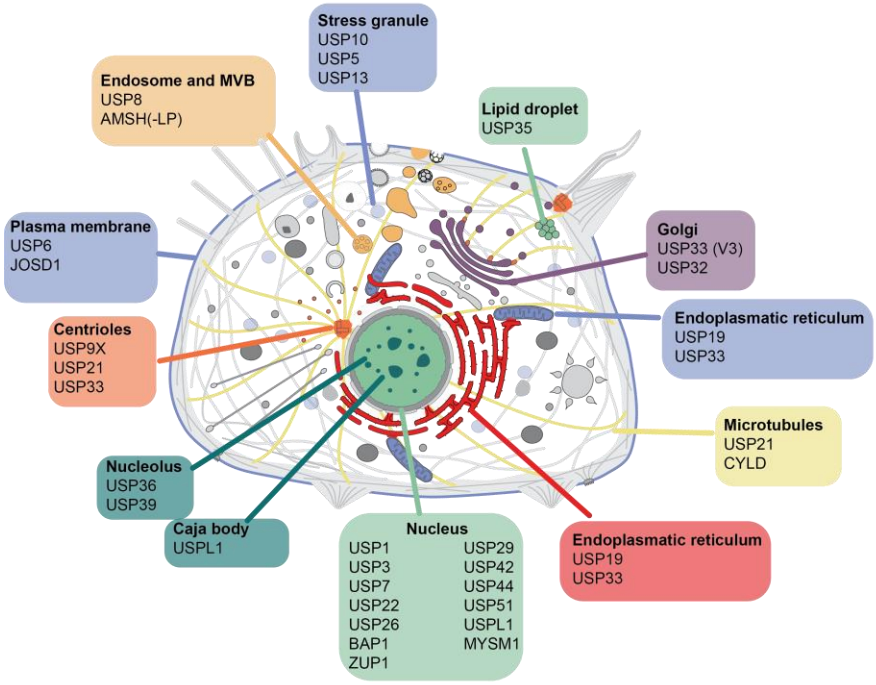

Figure 5. Subcellular localisation of DUBs determines set of substrates. Data derived from localisation screen in HeLa cells (Urbé et al., 2012) as shown in Clague et al. (2019). The depiction of the animal cell was extracted and changed from SwissBioPics (Le Mercier et al., 2022).

1.4.1 Ubiquitination regulates membrane proteins in diverse ways

Transmembrane proteins are estimated to make up roughly 20% of the cellular proteome (Foot et al., 2017) and fulfil numerous critical functions in a cell. They relay information from the extracellular space to the cell, provide anchors for cytoskeletal proteins and extracellular matrix, connect neighbouring cells or serve as signalling hotspots (S. Tan et al., 2008).

Given the importance of transmembrane proteins, it is not surprising that a delicate system has evolved that regulates signalling and membrane retention of the proteins and that ubiquitin plays a major role herein. As such it was found that ubiquitination is critical in determining their trafficking, abundance and localisation (Foot et al., 2017). The ubiquitin system exerts its influence starting with synthesis of the membrane proteins in the endoplasmic reticulum (ER), where ubiquitin controls the ER-associated degradation (ERAD) process (Christianson & Ye, 2014). A second level of protein quality control (PQC) for membrane proteins exists at the Golgi. While ERAD is governed by proteasomal degradation processes, degradation of proteins at the Golgi occurs only in a small fraction via the UPS. The majority of proteins are degraded via lysosomal pathways which involve the endosomal sorting complexes required

for transport (ESCRT)-machinery, sorting in multivesicular bodies (MVBs) and subsequent fusion with lysosomes (Buzuk & Hellerschmied, 2023). Proteins destined for integration in the plasma membrane that passed quality control in ER and Golgi are further balanced by ubiquitin modification which module their residence time and relative abundance (Foot et al., 2017).

One intricate example highlighting the fine-tuned regulation of ubiquitination of transmembrane proteins in mammalian cells, is the epidermal growth factor (EGF) receptor (EGFR). Several studies suggest that multi-mono-ubiquitylation serves as a signal sufficient for its efficient endocytosis (Haglund et al., 2003; Stringer & Piper, 2011) while other research articles indicate that K63-linked chains effect the sorting process rather than influence endocytosis (F. Huang et al., 2013).

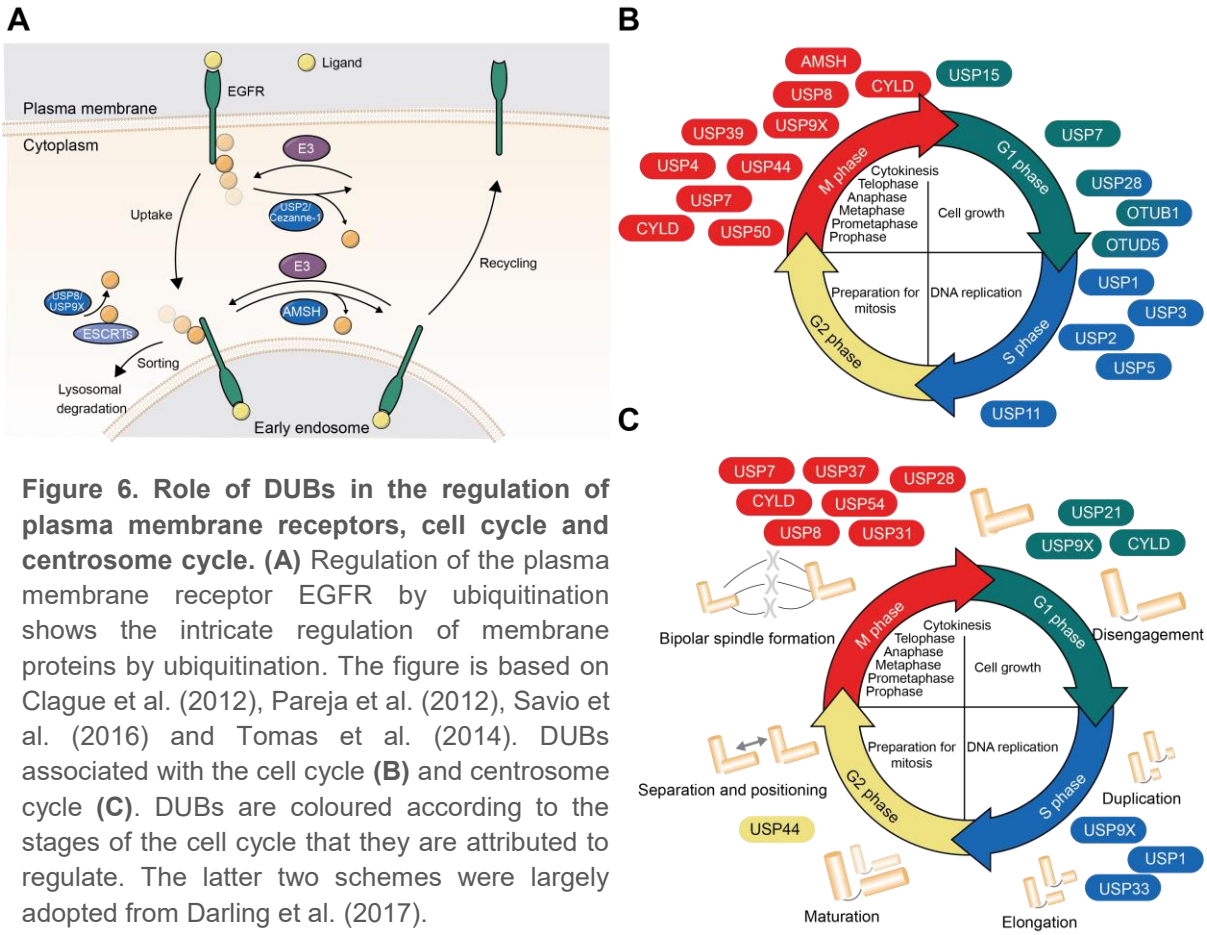

Figure 6. Role of DUBs in the regulation of plasma membrane receptors, cell cycle and centrosome cycle. (A) Regulation of the plasma membrane receptor EGFR by ubiquitination shows the intricate regulation of membrane proteins by ubiquitination. The figure is based on Clague et al. (2012), Pareja et al. (2012), Savio et al. (2016) and Tomas et al. (2014). DUBs associated with the cell cycle **(B)** and centrosome cycle **(C)**. DUBs are coloured according to the stages of the cell cycle that they are attributed to regulate. The latter two schemes were largely adopted from Darling et al. (2017).

Over the years, the direct and indirect regulation of EGFR fate by DUBs was reported. The K63-specific JAMM DUB AMSH was reported to regulate EGFR sorting into the degradative pathway (Fig. 6A, Tomas et al., 2014) while Cezanne-1, a K11-specific DUB and USP2, a promiscuous DUB, have been reported to prevent EGFR degradation by opposing receptor ubiquitination (Fig. 6A, Pareja et al., 2012; Savio et al., 2016). Furthermore, USP8 and USP9x

seem to modulate EGFR endocytosis by regulating turnover of ESCRT proteins or other adaptor proteins (Fig. 6A, Savio et al., 2016).

1.4.2 Tight junction proteins are tightly regulated by the ubiquitin system

A special configuration of transmembrane proteins at the plasma membrane are tight junction (TJ) proteins. They are located on the lateral side of epithelial cells and, together with scaffolding proteins, seal the spaces between neighbouring cells. Besides their barrier function, they act as pores to allow bypass of selected solutes and molecules, resemble a fence in preventing free diffusion of other membrane proteins and connect forces of cytoskeletal proteins (Reiche & Huber, 2020). TJs are composed of claudins, junction adhesion molecules and tight junction-associated MARVEL proteins (TAMPs). The latter includes occludin, tricellulin, and MARVELD3. Zonula occludens (ZO) proteins, also termed tight junction proteins (TJPs), link the intracellular domains of the transmembrane strands to actin.

For occludin, an integral membrane protein that contributes to TJ stabilization of bicellular junctions (Cummin, 2012), ubiquitination by the E3 ligase Itch after dissociation of tight junction protein 1 (TJP1) upon occludin phosphorylation has been described. Notably, the ubiquitination of occludin was connected to its proteasomal degradation (Reiche & Huber, 2020). Tricellular tight junctions (tTJs) ensure a tight seal to close the gap where three cells meet and differ significantly in molecular composition from bicellular junctions (Ikenouchi et al., 2005). However, also at tTJs, the E3 ligase itch was reported to ubiquitinate MARVELD2 (also called tricellulin), one of the key protagonists of tTJs (Jennek et al., 2017).

1.4.3 DUBs regulating the cell cycle and microtubule organization

Another critical cellular progress regulated by ubiquitination is the cell cycle. Cell cycle progression is a tightly regulated process driven by the sequential action of cyclin-dependent kinases (CDKs), polo-like kinases (PLKs) and the ubiquitin-mediated degradation of key effectors by E3 ligases, such as anaphase-promoting complex/cyclosome (APC/C) and Skp1-Cul1-F-box protein complex (Rhind & Russell, 2012).These enzymes ensure successful and controlled passage through the four stages: the initial growth phase (G1), replication of the genome (S-phase), a second growth phase (G2) to prepare for division and assemble cytoskeletal structures and the M-phase in which the genetic material is divided between the daughter cells (Hunt et al., 2011). Many DUBs play critical roles at almost every stage during the cell cycle (Fig. 6B, Darling et al., 2017).

The ubiquitin specific protease CYLD, for example, plays a critical role in several aspects of the cell cycle (Fig. 6B). This DUB with a specificity for cleavage of K63- and M1-linked chains

deubiquitinates the transcription factor BCL-3 inhibiting its nuclear translocation and transcription of cyclin D mRNA. This in turn, prevents CDK4/6 activation leading to a decrease in phosphorylation of retinoblastoma protein (Massoumi et al., 2006) thus preventing cell passage past the G1 restriction point. During metaphase and cytokinesis CYLD interacts with histone deacetylase 6 (HDAC6) leading to an increase in acetylated α-tubulin (Wickström et al., 2010). Additionally, it deubiquitinates dishevelled thus promoting correct spindle orientation (Fig. 6C, Y. Yang, Liu, et al., 2014). CYLD also contributes to mitotic spindle assembly through its interaction with the centrosomal protein CEP192 (Fig. 6C, Gomez-Ferreria et al., 2012). Furthermore, CYLD plays a pivotal role in ciliogenesis by deubiquitylating CEP70 which enables CEP70 to interact with y-tubulin at the centrosome (Y. Yang et al., 2014). This is not the only DUB important in regulating the centrosomes which are the dominant microtubule organising centres (Fig. 6C). USP33 for example localises to the centrioles where it stabilises CP110. Overexpression of either of the two proteins leads to centriole amplification. In addition, USP9X and USP1 are linked to regulating centrosome regulation (Darling et al., 2017). Other DUBs are involved in centrosome maturation, separation and mitotic spindle organisation. The importance of other DUBs in regulation of the cell cycle and the highly co-ordinated centrosomal cycle is shown in figure 6B and C.

The roles of DUBs in cell cycle progression and centrosomal organisation processes remain insufficiently characterised. Beyond the limited mechanistic understanding, regulation mechanisms of DUBs are largely unexplored. Furthermore, how a cell regulates certain DUBs and orchestrates their multifunctional roles across distinct cell cycle stages in regards to substrate recognition, activity and specificity, remains unclear (Darling et al., 2017).

1.5 DUBs as promising Therapeutic Targets

As established, DUBs are critical to almost all cellular processes with the regulation of transmembrane proteins and the cell cycle mentioned as two important examples. As such it does not come as a surprise that alterations of physiological levels and activity of DUBs are associated with various human diseases. The aforementioned K63-specific DUB CYLD, for example, is named after its associated syndrome: familial cylindromatosis (Biggs et al., 1995). Other DUBs are implicated in neurodevelopmental disorders (Jolly et al., 2022) and cancer (Snyder & Silva, 2021).

DUBs are appealing drug targets due to their well-defined catalytic clefts, their chemically accessible active site and their role in modulating protein stability and function, thus enabling targeting proteins that have previously been deemed undruggable or resistant to conventional approaches (Harrigan et al., 2018; P. Liu et al., 2025). USP30, for instance, has been established as a potential therapeutic target for Parkinson’s disease (PD, Fang et al., 2023).

Other enzymes within the system include USP28, USP7 or USP36 which could be addressed using small molecules in order to prevent stabilization of MYC (Sun et al., 2021). With the breakthrough of the field of induced proximity, DUBs have further entered into the focus of scientific research. Besides their importance in regulating the effects of proteolysis-targeting chimeras, DUB-targeting chimeras (DUBTACs) were developed that recruit a DUB to a (neo) substrates in order to stabilize it (Henning et al., 2022)

Moreover, with increasing evidence linking misregulation of K63-linked polyubiquitin chains to various pathologies (Cao et al., 2022; Dósa & Csizmadia, 2022; Lim & Lim, 2011; Yan et al., 2018), it is likely that research will intensify on DUBs involved in regulating specific chain modifications.

1.6 USP53 – a DUB associated with Cholestasis and Hearing Loss

One of the DUBs for which growing evidence suggests an association with human pathology is USP53 (Fig. 7C). Over the last six years, reports have linked its biallelic loss or mutations to progressive, intrahepatic cholestasis (Ahn et al., 2023; Alam et al., 2024; Alhebbi et al., 2020; Ateş et al., 2023; Gezdirici et al., 2023; Kamran et al., 2024; Maddirevula et al., 2019; Mangalath, 2023; Porta et al., 2021; Samanta et al., 2024; Shatokhina et al., 2021; Sankaranarayanan, 2021; J. Zhang et al., 2020; Zheng et al., 2024) often accompanied by hyperbilirubinemia (Kesavan et al., 2022). Some patients additionally presented with hearing problems or loss (Porta et al., 2021; J. Zhang et al., 2020). There is also evidence for its involvement in psychosis, schizophrenia and osteoporosis (Baek et al., 2021; Kanwal et al., 2023; Pardo et al., 2021). Mutations of *USP53* were furthermore identified as causative for progressive hearing loss in mice due to outer hair cell degeneration (Kazmierczak et al., 2015a). In other mouse studies, USP53 protected from a form of xenobiotic-induced liver injury (Ding et al., 2025) and regulated bone homeostasis (Hariri et al., 2021).

Despite its classification within the ubiquitin-specific protease family, the observed phenotypes were often ascribed to non-catalytic functions since USP53 was found to be inactive in a DUB screen (Quesada et al., 2004) and ubiquitin-probe reactivity assays (Kazmierczak et al., 2015). This was further cemented by absence of strongly conserved residues before the catalytic histidine (Quesada et al., 2004; Ye et al., 2009).

Recent evidence, however, challenges this view. Cellular studies claim catalytic activity of USP53 (Fig. 7C) by describing FKBP51 as a USP53 substrate in H1975 cells (Zhao et al., 2020), suggest K48-linked ubiquitin chain cleavage from scavenger receptor-A in smooth muscle cells (X. Liu et al., 2024), show deubiquitination of cytochrome c upon overexpression of USP53 (Yao et al., 2022) or catalysis of deubiquitination and subsequent stabilization of

ZMYND11 (Meng et al., 2024) and CRKL (Yi Liu et al., 2023). Other reports highlight the role of USP53 in clear cell renal cell carcinoma that was associated to its function in deubiquitinating IκBα (Gui et al., 2021) or β-catenin in osteogenic differentiation (Baek et al., 2021). On the other hand, the notion that catalytic activity of USP53 is critical for its function is also supported by the finding that for many of the USP53-associated diseases, mutations found in *USP53* cluster in its catalytic domain (Alhebbi et al., 2020; Kazmierczak et al., 2015; Maddirevula et al., 2019; Zhang et al., 2020; Zheng et al., 2024).

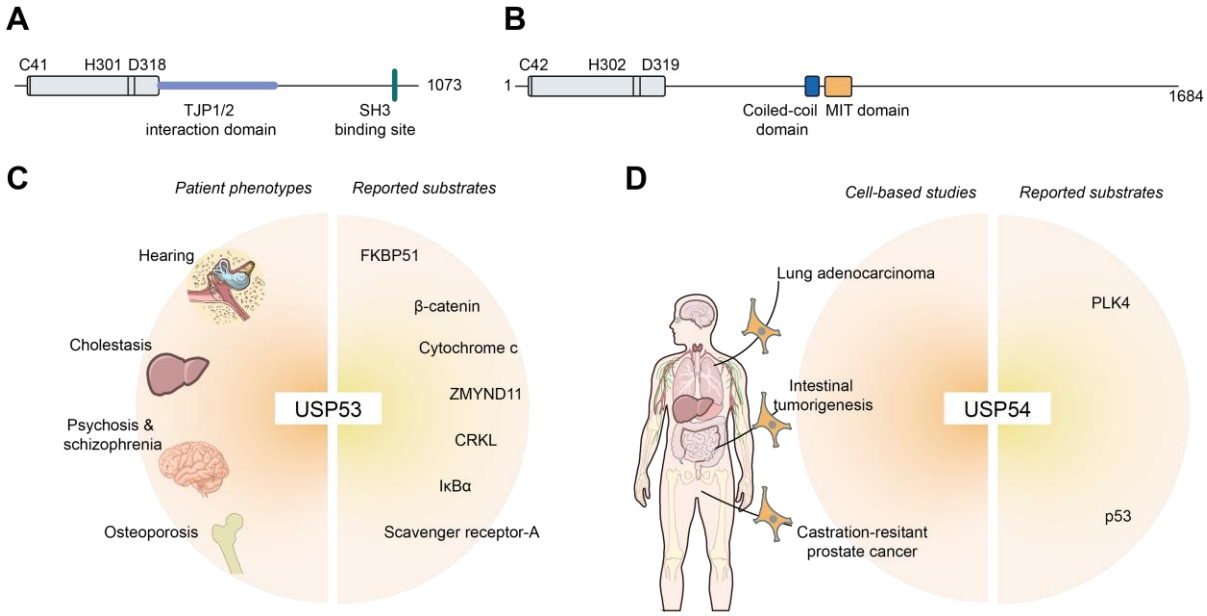

Figure 7. Architecture and role of USP53 and USP54. Domain architectures of human full-length USP53 **(A)** and USP54 **(B)**. Amino acids from the catalytic triad are indicated as lines. Information about domains and binding sites were taken from Kazmierczak et al. (2015); Rigden et al. (2009) and Wijdeven et al. (2017). Reports associate USP53 **(C)** and USP54 **(D)** with patient phenotypes or cancer progression in cell-based studies. Proteins reported as substrates of the DUBs are depicted on the right side. Illustrations of organs and human anatomy were extracted for NIAID NIH Bioart which are licensed under public domain.

Aside from its catalytic domain, USP53 has a short N-terminal sequence and an extensive C-terminal tail comprising of approximately 700 amino acids with an annotated Src homology 3 (SH3) binding site and an experimentally validated TJP1/2 binding part (Kazmierczak et al., 2015). Similar to TJP1/2, USP53 localises to cellular junctions, as observed in *in vivo* studies in hair cells and Deiters' cells of wild-type mouse organs of Corti (Kazmierczak et al., 2015).

The importance of recruitment of the catalytic potential of UPS53 to cellular junctions via C-terminal determinants appears critical in regards to observed patient phenotypes since impaired tight junctions at bi- or tricellular contact points are causative for deafness (Kamitani et al., 2015; Kitano et al., 2019; Nakano et al., 2009; Wang et al., 2015) and are attributed as one of the primary drivers of cholestasis (Anderson et al., 1989; S. Huang et al., 2021;

Kawaguchi et al., 1999; C. Z. Li et al., 2022; Metz & Bressler, 1979; Sonoi & Hagihara, 2021). This correlation presents an appealing connection between USP53 activity at tight junctions and patient pathophysiology.

1.7 USP54 - an enigmatic DUB that promotes Cancer Progression

USP53 has a homologue, which is USP54. According to phylogenetic analysis of their catalytic domains, both proteins are distinct from other USP family members and most similar to the SUMO isopeptidase USPL1 (Clague et al., 2019). Like USP53, USP54 has been annotated as inactive with the same reasoning as applied for USP53 (Quesada et al., 2004; Ye et al., 2009).

USP54 with its 1684 amino acids is the fifth biggest member of the ubiquitin-specific protease family (Komander et al., 2009). Its catalytic domain is located at the N-terminus with only a few amino acids preceding the hand-like structure typical for USPs (Fig. 7B). In its extended C-terminal tail, *ab initio* protein modelling revealed a microtubule interacting and transport (MIT) domain (Fig. 7B) which, in isolation, interacts with several proteins of the charged multivesicular body proteins (CHMPs) family. These proteins are components of the ESCRT machinery, that mediates sorting of ubiquitinated receptors to the lysosomes (Rigden et al., 2009). Other MIT domains have the capacity to bind to tubulin (Iwaya et al., 2010). Furthermore, USP54 possesses a coiled coil domain (Fig. 7B) which was proposed to result in interaction with cilia, as well as tight and adherence junction proteins (Wijdeven et al., 2017).

While reports on the physiological roles of USP54 are sparse (Fig. 7D), recent findings highlight its potential as a therapeutic target in castration-resistant prostate cancer (Zhou et al., 2024). Furthermore it was found to be overexpressed in colorectal cancer stem cells where it appears to promote intestinal tumorigenesis (Fraile et al., 2016). A recent report claims that it deubiquitinates and stabilizes p53 thus inhibiting lung adenocarcinoma progression (Chen et al., 2024). The most extensive study to date suggests USP54 to deubiquitinate polo-like kinase 4 (PLK4) following CEP120-induced expression and centrosome aggregation thus promoting centrosome amplification in gastric cancer. The destabilization of PLK4 upon USP54 protein level reduction was rescued upon proteasome inhibition, suggesting involvement of K48-linked ubiquitylation of PLK4 (Zhang et al., 2023).

1.8 Tools for the Identification of Ubiquitinated Proteins

In the human proteome, approximately 100,000 sites were found to be ubiquitinated (Kim et al., 2011; Prus et al., 2024), yet the occupancy of these sites is generally very low under physiological conditions, with a mean occupancy of 0.0081% and median occupancy of 0.059%. Furthermore, ubiquitination spans a large dynamic range, with only 1% of sites exhibiting occupancies greater than 1%, and has a rapid turnover, as 45% of ubiquitination sites show a half-life of less than ten minutes (Prus et al., 2024). These characteristics present significant challenges in studying ubiquitination and emphasize the importance of specialized and sensitive methodologies for measuring this dynamic PTM.

An advantage of studying protein ubiquitination is that it introduces a noticeable size shift of the substrate proteins when analysed with gel electrophoresis. Thus, in rare cases of cellular stress introducing high site occupancy, ubiquitylation events can be visualized by analysis of whole cell lysates with a Western Blot (Renart et al., 1979) as for example shown for some proteins of the outer mitochondrial membrane after mitochondrial depolarisation (Rusilowicz-Jones et al., 2020). For most proteins, however, this is unfeasible due to the aforementioned low occupancy. A commonly employed strategy to overcome this limitation is the ectopic expression of substrates either using introduced epitope tags (such as hemagglutinin, MYC or FLAG) or with antibodies binding the substrate. Following the isolation, immunoblotting with ubiquitin-targeting antibodies is supposed to reveal current ubiquitylation states of the proteins of interest (Chen et al., 2024; Li et al., 2002; Peng et al., 2019; Yi Liu et al., 2023; Zhang et al., 2023; Zhao et al., 2015). To enhance detection, these systems are often engineered to achieve higher occupancy rates by co-expressing ubiquitin (Peng et al., 2019; C. Zhang et al., 2023) and the corresponding E3 ligase (Li et al., 2002), combined with inhibition of the proteasome (Chen et al., 2024) or lysosome (Peng et al., 2020). One significant pitfall of this approach is that enrichment is often performed with non-stringent buffers thus increasing the likelihood of co-isolation of non-specifically bound ubiquitin or ubiquitinated proteins. Sometimes indirect methods for validating ubiquitylation of specific proteins are carried out which include ‘rescuing’ protein levels by either interfering with proteasomal or lysosomal degradation. Proteins whose abundance was subsequently stabilised by this intervention are often deemed ubiquitinated (Qu et al., 2021; Sun et al., 2018; Zhang et al., 2023).

The aforementioned methods inform about targeted approaches to investigate the ubiquitination state of specific proteins. However, in the majority of cases, substrates remain unidentified and thus unbiased approaches to identify differential ubiquitination of cellular proteins are needed. This is predominantly achieved by mass spectrometry (MS)-based proteomics. To detect ubiquitylated proteins, these proteins need to be enriched. The

enrichment approaches can broadly be categorized in methods that enrich ubiquitinated proteins on the protein level and methods that identify ubiquitinated proteins on the peptide level (Fig. 8, Sun & Zhang, 2022).

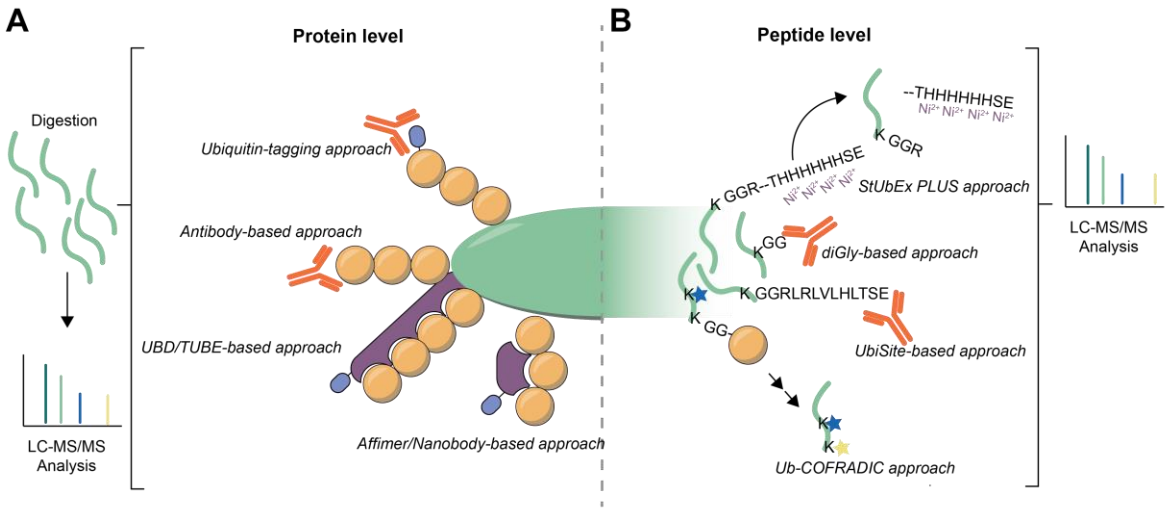

Figure 8. Approaches to identify ubiquitinated proteins on a protein and peptide level. (A) Methods that enrich ubiquitinated proteins on the protein level include ubiquitin-tagging, antibody- or nanobody-based approaches or make use of ubiquitin binding domains, tandem-repeated ubiquitin-binding entities (TUBEs) or affimers. **(B)** Approaches enriching peptides include the enrichment with antibodies recognising diGly-modified lysines or the UbiSite antibodies and the antibody-free approaches StUbEx PLUS and Ub-COFRADIC. The figure was in parts inspired by Sun & Zhang, 2022.

In the first category (Fig. 8A), proteins are enriched using either tagged ubiquitin (Peng et al., 2003; Trulsson et al., 2022; Xu & Jaffrey, 2013), ubiquitin- or ubiquitin linkage-specific antibodies (Denis et al., 2007), linkage specific affimers (Gersch et al., 2017; Michel et al., 2017), nanobodies (Lange et al., 2024) or ubiquitin binding domains of proteins (Hjerpe et al., 2009; Sims et al., 2012; Tan et al., 2008; Thorslund et al., 2015; Xolalpa et al., 2016; Zhang et al., 2022).

Ubiquitin tagging has been beneficial to verify DUB-substrate relations in many cases and allows usage of well-established purification tools (Akimov et al., 2014), but does have inherent pitfalls. One of them is that tagged ubiquitin might alter conjugation or deconjugation of ubiquitin from the substrate and thus might fail to mimic the behaviour of endogenous ubiquitin (Sun & Zhang, 2022). Antibody-based identification of ubiquitinated proteins allows for isolation of ubiquitinated proteins from animal or patient samples without the need for genetic manipulation (Takagi et al., 2002). In addition, chain-linkage specific antibodies allow for isolation of proteins decorated with a certain linkage type (Matsumoto et al., 2010; Xu & Jaffrey, 2013). However, this technique has disadvantages such as cross-reactivity and high costs associated with the use of antibodies (Sun & Zhang, 2022).

Ubiquitinated proteins can further be analysed using ubiquitin binding domains of proteins (UBDs). UBDs are often extracted from specific reader proteins and while single UBDs mostly show low affinity to ubiquitin, tandem-repeated ubiquitin-binding entities (TUBEs) exhibit much higher affinity (Hjerpe et al., 2009; Mattern et al., 2012; Sato et al., 2009; Sims et al., 2012; Sun & Zhang, 2022; Xolalpa et al., 2016). As such, a tandem UIM peptide derived from yeast Vps27, a protein involved in endosomal sorting, reaches sub-nanomolar affinity for ubiquitin chains (Sims et al., 2012). Since there is a need for reader proteins to differentiate between different ubiquitin linkages, consequentially, there are UBDs described that either unselectively or selectively bind to and isolate specific chain types. One of these examples is the UIM domain of RAP80 that specifically isolates K63-linked ubiquitin chains (Sato et al., 2009). However, the use of UBDs for isolation of ubiquitylated proteins does not come without challenges. As such, protein digestion after isolation can yield numerous peptides derived from the UBDs themselves, washing conditions might not be harsh enough to differentiate between ubiquitin interactome and ubiquitinome and TUBEs do not isolate proteins decorated with short ubiquitin chains very well (Sun & Zhang, 2022). Recent advancements have addressed most of these concerns. As such, a monoubiquitin-binder, derived from an *Orientia tsutusgamushi* DUB has been described displaying a low-nanomolar affinity for ubiquitin and stability to withstand harsh washing conditions (Zhang et al., 2022). Nevertheless, one must keep in mind that monoubiquitin binders might recognise intrinsic ubiquitin-like (UBL) domains of proteins thus leading to identification of contaminants (Kliza & Husnjak, 2020).

Enrichment of ubiquitinated proteins on the protein level allowing for their subsequent identification in mass spectrometry has been successfully employed in a number of studies over the last years. As such, the first proteome-wide identification of ubiquitinated proteins was achieved by Peng et al. in *Saccharomyces cerevisiae* using epitope-tagged ubiquitin (J. Peng et al., 2003). Since then, several methodologies expanded on this method for the proteome-wide identification of ubiquitination, as, for example, reported by Danielsen et al. (2011) or Akimov et al. (2014). In addition, immobilised ubiquitin-recognising antibody FK2 (Denis et al., 2007; Schwertman et al., 2012) and tandem-repeated ubiquitin binding domains (Lopitz-Otsoa et al., 2012; Y. Shi et al., 2011) have been used in proteome-wide studies to identify ubiquitination of proteins on the protein level.

All reagents that enrich ubiquitinated proteins at the protein level which were mentioned above can be used to isolate proteins for Western Blot based read-outs in addition to mass spectrometry-facilitated analysis. This allows for the combination and orthogonal verification of hits identified in MS-based proteomics. While this is not feasible with methods that identify ubiquitinated proteins at the peptide level, these methods have proven to be not only highly valuable in the identification of ubiquitinated proteins but especially in the identification of

ubiquitination sites. The peptide-based approaches can be categorized in methods that use specifically modified ubiquitin, such as in stable tagged ubiquitin exchange (StUbEx) PLUS (Akimov, Olsen, et al., 2018) and approaches that use selective masking of non-ubiquitinated proteins in combination with non-selective deubiquitination and modification of freed lysines (Fig. 8B, Stes et al., 2014; Sun et al., 2023). The most commonly employed tools, however, make use of antibodies (Fig. 8B). These antibodies either recognise the diglycine (diGly) remnant left on the substrate lysine after tryptic digest (Xu et al., 2010) or bind to the C-terminal 13 amino acids of ubiquitin after Lys-C digestion (UbiSite, Akimov, Barrio-Hernandez, et al., 2018). While the diGly-based approach cannot distinguish between the remnants left by NEDD8, ISG15 and ubiquitin (Akimov, Barrio-Hernandez, et al., 2018), it is the most widely used tool to study ubiquitination and is continuously improved. Subsequently, using data-independent acquisition (DIA) methods in conjunction with diGly antibodies, over 90,000 ubiquitinated peptides were identified, highlighting the enormous power and robustness of this technique (Hansen et al., 2021).

Asides from investigating the effect of extracellular stimulation on the ubiquitin system, these tools and established methods have also led to the identification of cellular DUB substrates over the past years (Bingol et al., 2014; B. Liu et al., 2018; Sapmaz et al., 2019; Steger et al., 2021, 2021). While most of these reports relied on antibody based peptide enrichment, few others employed tagging methods (Ramirez et al., 2021; Trulsson et al., 2022).

1.9 Methods to Investigate Ubiquitin Architectures on Proteins

The multifaceted nature of protein ubiquitination across various levels necessitates an equally versatile toolkit to analyse the specific ‘flavour’ of ubiquitination on the targeted protein. Besides a statement about site occupancy, length and linkage type on target proteins are critical to understand the role of ubiquitination. Information about ubiquitination pattern can be achieved with binders specifically recognising certain chain types. UBDs, affimers and nanobodies are tools that provide insights into ubiquitin chain architecture by enriching only proteins with the given linkage type (Kliza & Husnjak, 2020). The same concept is applied for chain-specific antibodies (Matsumoto et al., 2010, 2012; Newton et al., 2012). Other studies make use of isolation via ectopic expression of reporter-tagged mutated ubiquitin to identify the predominant chain linkage of a protein (Lee & Sharp, 2004).

Apart from studies that draw conclusions about the chain type from isolation behaviour with specific reagents, other methodologies have been developed throughout the years. The identification of a cornucopia of linkage-specific DUBs allowed the establishment of ubiquitin chain restriction (UbiCRest) analysis (Hospenthal et al., 2015). The initial idea of treating ubiquitinated substrates with different linkage-specific DUBs to characterize the ubiquitin chain

has been expanded to allow for the treatment of cellular samples (Panda & Gekara, 2018). Here, proteins are first isolated with TUBEs or antibodies and subsequently treated with the respective DUBs (Emmerich et al., 2016; Lafont et al., 2017; Satpathy et al., 2015).

Other approaches make use of mass spectrometry to identify chain architectures. As such, an approach using an engineered viral protease is used to quantify diGly-modified branching points, called Ub-clipping (Swatek et al., 2019). Furthermore, absolute quantification of ubiquitin (Ub-AQUA) strategies (Kaiser et al., 2011; Kirkpatrick et al., 2005) or ubiquitin chain enrichment middle-down mass spectrometry (UbiChEM-MS, Crowe et al., 2017) have been described over the years.

Box 2. Non-proteinaceous ubiquitination.

While protein ubiquitination governs a plethora of cellular processes, ubiquitination is not limited to modifications of proteinaceous substrates but extends to lipids, sugars and nucleotides (Kelsall et al., 2022; Otten et al., 2021; Sakamaki & Mizushima, 2023; Szczesna et al., 2024; Zhu et al., 2024). Ubiquitin is linked to most of these moieties via an ester bond. However, amide bond formation between ubiquitin and phosphatidylethanolamine has also been described (Sakamaki et al., 2022). Due to the low stability of most of these linkages and an incapability of most of the current ubiquitinomics workflows to detect non-proteinaceous ubiquitination, the physiological relevance of most of these unconventional ubiquitination events remains obscure. The development of novel tools, however, will mostly likely reveal an avenue to unravel this fascinating world (Lechtenberg & Komander, 2024).

2 Motivation and Aim

The regulation of cellular ubiquitination by Deubiquitinases is a process critical to almost every cellular process. Advances in our understanding of their molecular function may thus not only facilitate a more profound comprehension of this complex post-translational modification but also provide ways to address human pathologies associated with the misregulation or mutation of DUBs.

This work aimed to characterise the two underexplored DUBs USP53 and USP54 by means of cell biology, chemical biology approaches and mass spectrometry. Following the establishment of cellular activity, these investigations were focused on substrate identification to provide information about the molecular link of disease and DUB activity. In doing so, this work should complement and incorporate findings of *in vitro* experiments performed within the research group that focus on structural elucidation and cleavage specificity of these DUBs. For accomplishing these goals, diverse and efficient tools enabling the assessment of the catalytic effect of DUBs on ubiquitination state of substrate proteins with minimal perturbations of physiological cell states were to be tested, optimised and established in a variety of cellular settings.

3 Elucidation of Cellular Functions of the Deubiquitinases USP53 and USP54

3.1 Catalytic Activity of USP53 and USP54 isolated from Cells

Previously, USP53 and USP54 were considered to be catalytically inactive pseudoenzymes (Clague, Urbé, et al., 2019; Quesada et al., 2004). However, there is mounting evidence linking mutations within the catalytic domain of USP53 to pathologies. In addition, recent *in vitro* data from our group (Wendrich et al., 2024) has demonstrated DUB activity with specificity for cleavage of K63-linked ubiquitin chains.

3.1.1 Reactivity of USP53 and USP54 with activity-based probes is indicative of their catalytic activity in cells

The activity of proteases can be readily assessed using activity-based probes (ABPs). These probes are generally comprised of (i) a reporter tag – such as the human influenza hemagglutinin-derived HA-tag, (ii) a recognition element and (iii) a warhead that reacts covalently with an amino acid side chain (Fig. 9A-B). To investigate the activity of cellularly expressed USP53 and USP54, their reactivity with ubiquitin ABPs was assessed (Fig. 9C-E). To this end, the catalytic domains of these two proteins fused to enhanced monomeric green fluorescent protein (emGFP, Zacharias et al., 2002) were ectopically expressed in HEK-293 cells. In addition, the catalytically inactive version of these DUBs as well as the well-characterised, highly active DUB, USP2 were expressed. The lysate from these cells was then incubated with the HA-tagged ubiquitin ABP containing a propargyl amide (PA) warhead. Reactivity with the ABP was assessed by GFP immunoblotting to visualise the induced size shift of the reactive DUB of approximately 7,000 Dalton (7 kDa) due to the covalent addition of the probe. As demonstrated in Fig. 9C, the majority of USP2 reacted with the ABP, demonstrating the reactivity of the probe and maintained DUB activity throughout cell lysis (Fig. 9C). Strikingly, USP53 and USP54 were also observed to react with the ubiquitin ABP. Consistent with *in vitro* data that showed lower activity of USP53 (Wendrich et al., 2024) compared to USP54, the catalytic domain of USP53 reacted to a lesser extent with the probe in cell lysate. The lack of a molecular weight shift observed upon mutation of the catalytic cysteine demonstrated that the reaction with the probe is dependent on an intact catalytic triad of the enzymes (Fig. 9C). Immunoblotting for the HA tag confirmed that the shift in molecular weight of the DUBs was indeed due to ABP addition. Together, these results indicate that USP53 and USP54 are ubiquitin-reactive DUBs in a cellular context.

Given that the catalytic domain of USP54 did not display full reactivity with the PA-functionalized probe (Fig. 9C), I assessed whether changing the electrophilic group of the ABP

would enhance reactivity with the DUBs. Reactivity of USP54 with PA and vinyl sulfone (VS) warhead probes was compared in a similar manner as described above (Fig. 9D).

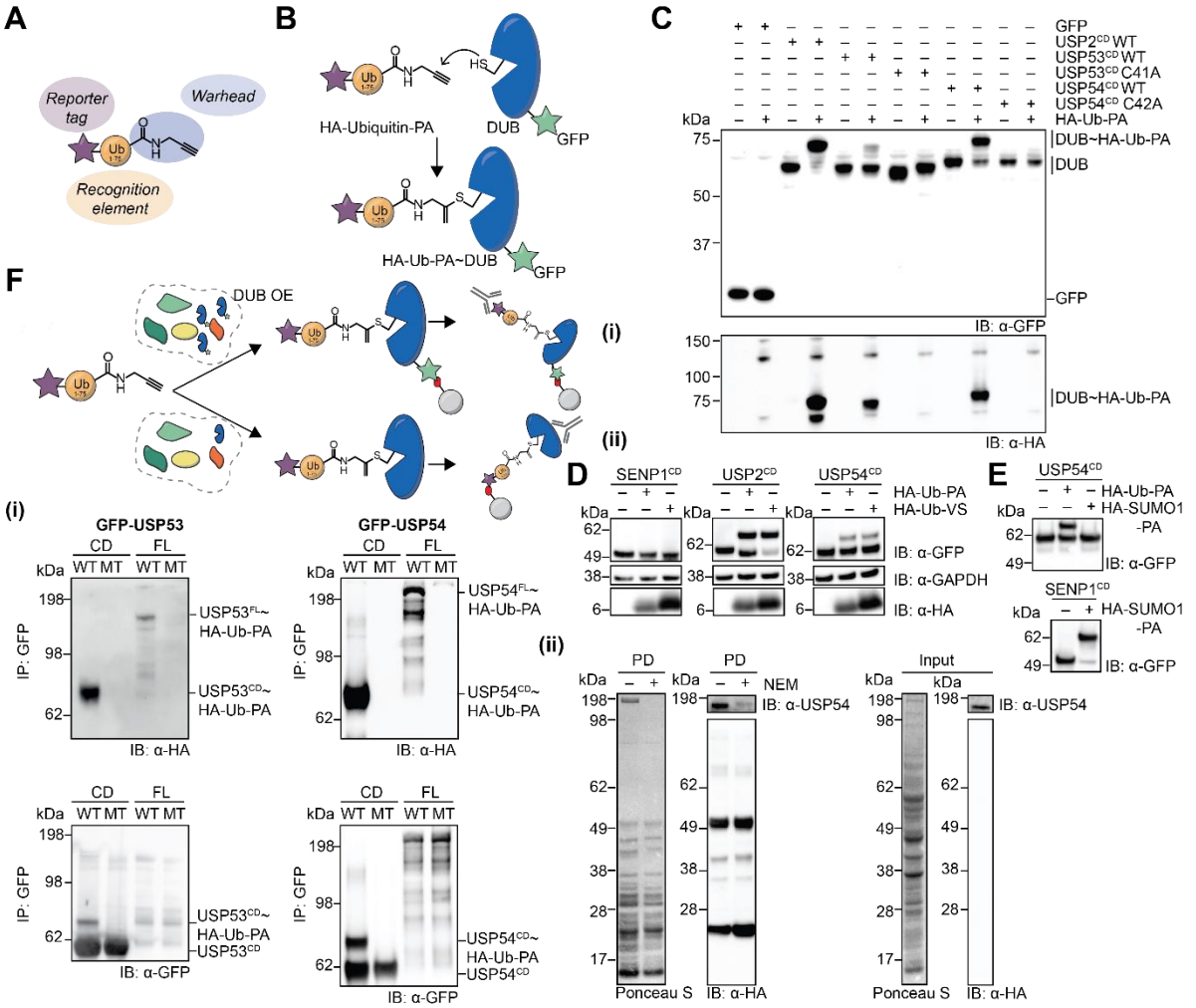

Figure 9. Reactivity of USP53 and USP54 with activity-based probes indicates their cellular activity. (A) Illustration of a ubiquitin-based ABP with an electrophilic PA warhead with annotated individual building blocks. **(B)** Scheme of the reaction of a PA-based ABP with cysteine-based DUBs which results in covalent bond formation between both entities. **(C)** Probe reactivity assay with GFP or GFP-tagged catalytic domains (CD) of various DUBs, as well as their catalytically inactive counterparts as ectopically expressed in HEK-293 cells. HA-ubiquitin-PA was incubated with the cell lysates for 30 min in reducing conditions. Probe reactivity was analysed by SDS-PAGE and Western Blotting. The reactivity with the probe is deduced from a size shift of the DUB of approximately 7 kDa as indicated. **(D)** Probe reactivity of the catalytic domains of the SUMO protease SENP1 and the ubiquitin proteases USP2 as well as USP54 with ubiquitin-based ABPs equipped with either propargyl amide (PA) or vinyl methyl sulfone (VS) warheads in a similar setup as described in (C). **(E)** Probe reactivity of the catalytic domains of USP54 and SENP1 with either ubiquitin- or SUMO1-based ABPs in a similar setup as described in (C). **(F)** Overview of methods that demonstrate reactivity of low-reactive full-length DUBs that were ectopically expressed with a GFP-tag **(i)** or endogenous protein isolated from cell lysate **(ii)**. In **(i)**, the ectopically expressed proteins were first isolated from cell lysate using their GFP-tag before addition of the ABPs and extensive washing steps. Emergence of a chemiluminescent signal upon anti-HA immunoblotting indicates reactivity of the protein with the probe. In **(ii)**, HA-Ub-PA was added to lysate derived from U2OS cells. Reactive proteins were isolated using immunoprecipitation with anti-HA beads. To verify that isolation is dependent on cysteine-reactivity, free cysteines were alkylated using NEM. Reactivity of endogenous USP54 was assessed using an anti-USP54 antibody.

While the exchange of the warhead impacted the fraction of USP2 that reacted, no effect was observed for USP54. In order to validate that the reactivity of the USPs was dependent on the recognition element of the ABP, the reactivity of a protease that does not possess ubiquitin-cleavage activity, SENP1, was tested (Fig. 9D). Indeed, SENP1 did not react with our probes thus indicating that the effect that I observed is dependent on the recognition of ubiquitin by the USPs. Experiments in which the recognition element was changed from ubiquitin to the ubiquitin-like modifier SUMO1 demonstrated that the recognition of ubiquitin is necessary for the reactivity of USP54 with the ABP (Fig. 9E).

Both, USP53 and USP54 have been shown to possess extended C-terminal tails that could influence their activity (Komander et al., 2009). Despite extensive efforts, full-length variants of both DUBs could not be purified in bacterial or insect cells (personal correspondence with K. Wendrich). Consequently, I endeavoured to assess ABP reactivity of full-length enzymes in human cell lysate. This approach was met with challenges, as their expression in cells was found to be relatively low, and the induced size-shift proved difficult to detect due to the relatively large size of the unconjugated enzymes. To overcome these challenges, I adopted two immunoprecipitation (IP)-based approaches. In the first approach (Fig. 9Fi), cell lysates ectopically expressing GFP-tagged full length DUBs were isolated from cells utilising immobilised GFP-nanobodies and washed extensively before the addition of the ABP. In the second approach (Fig. 9Fii), the probes were incubated with unperturbed cell lysates and immunoprecipitated using the reporter tag. The isolation of the endogenous DUB was subsequently assessed using immunoblotting with USP54-targeting antibodies in the second approach. Ectopically expressed full-length constructs of both, USP53 and USP54 demonstrated reactivity with the probes following isolation from lysate (Fig. 9Fi). This, again, was dependent on an intact catalytic triad. However, USP53 exhibited relatively low reactivity, consistent with prior observations. Furthermore, while isolation of endogenous USP53 was not successful (data not shown), the isolation of endogenous USP54 from U2OS cells proved successful (Fig. 9Fii). Detection of USP54 upon isolation was dependent on the presence of free cysteines since pre-incubation of the lysate with *N*-Ethylmaleimide (NEM) led to the failure to detect the DUB. The isolation of endogenous USP54 from U2OS cells suggests that not only ectopically expressed constructs are active in a cellular environment but that ubiquitin-reactivity is shared for endogenous USP54. The combined analysis of these data further substantiates the notion that USP53 and USP54 exhibit DUB activity in cells.

3.1.2 USP54 displays selective cleavage of K63-linked ubiquitin chains *ex cellulo*

Thorough biochemical data has demonstrated that the purified catalytic domains of USP53 and USP54 cleave K63-linked ubiquitin chains with high specificity *in vitro* (Wendrich et al., 2024). Since cellular environment and domains outside of the catalytic domain may influence DUB activity (Mevissen & Komander, 2017), I wanted to assess whether full-length USP54 expressed in human cells maintains this specificity. To this end, I expressed GFP-tagged USP54 in HEK-293 cells and purified it, utilising an agarose-coupled nanobody. Catalytically inactive USP54 and GFP alone were included as controls. Following extensive washing steps, *in vitro*-generated K48- and K63-linked polyubiquitin chains were added to the isolated DUB that was pre-immobilised on beads (Fig. 10A). Following an incubation period, the solution that contained the ubiquitin chains was analysed by SDS-PAGE and Coomassie stain. Upon incubation of wildtype USP54 with K63-linked ubiquitin chains, long ubiquitin chains collapsed (Fig. 10B). The cleavage of the chains was again dependent on the presence of the catalytic cysteine. The expression levels of both the mutant and wildtype enzymes were found to be comparable (Fig. 10C). However, cleavage of K48-linked chains was not observed for neither of the enzymes (Fig. 10B). This experimental setup was not conducive to the discernment of USP53 cleavage selectivity (see Appendix Fig. 1A, B), likely attributable to its inherently diminished reactivity in comparison to USP54. In order to verify that both polyubiquitin chain types were susceptible to cleavage, I overexpressed the promiscuous DUB USP28 in HEK-293 cells and repeated this experiment which demonstrated cleavage of both chain types (Appendix Fig. 1A). In summary, cellularly expressed full-length USP54 mimics the cleavage preference for K63-linked chains of *in vitro* purified catalytic domain-only enzymes.

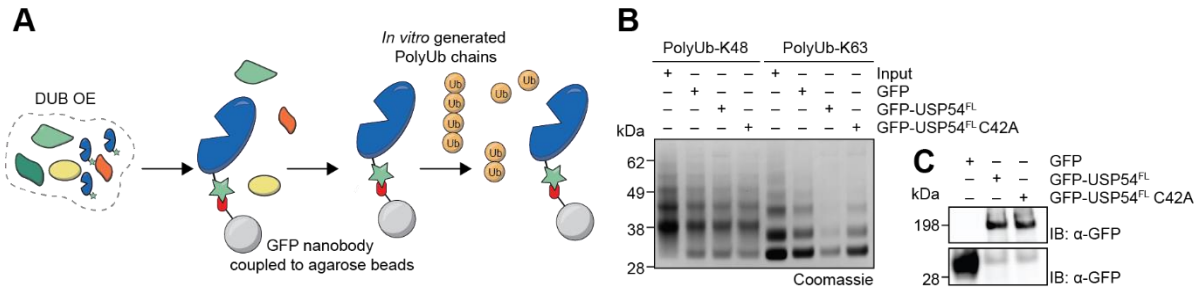

Figure 10. Full-length USP54 demonstrates selective cleavage of K63-linked ubiquitin chains. **(A)** Schematic for the experimental procedure for detecting the chain selectivity of GFP-tagged full-length DUBs as expressed in HEK-293 cells. **(B)** Polyubiquitin chain cleavage of full-length USP54 investigated by Coomassie staining of denaturing Bis-Tris gradient gels. USP54 and the respective controls were isolated from HEK-293 lysate with immunoprecipitation using their GFP-tag before extensive washing and addition of the polyubiquitin chains to the immobilised proteins. **(C)** Western Blot of the ectopically expressed proteins employed in the experiments shown in (B).

3.2 Establishment of a Toolkit for the Identification of Cellular Substrates of USP53 and USP54

Investigating ubiquitinated proteins has proven to be difficult – at least in parts because occupancy of ubiquitylation sites by the post-translation modifier is relatively low with a mean occupancy of 0.059% (Prus et al., 2024). This inherent property renders the development of suitable tools to enrich for ubiquitylated protein species imperative. However, despite the advent of several enrichment tools over the past decade, conclusive comparisons were still scarce. The following chapter thus sought to consolidate and optimise the usage of these tools for the purpose of identifying cellular substrates of USP53 and USP54.

3.2.1 Different polyubiquitin binders allow selective enrichment of ubiquitin *in vitro* and *ex cellulo*

The recent publication from our group which studied USP53 and USP54, in conjunction with the results presented above, demonstrated that both DUBs selectively cleave K63-linked polyubiquitin chains, exhibiting a preference for cleavage of longer polymers (Wendrich et al., 2024). Consequently, the experiments focused not only on indiscriminate isolation tools for the enrichment of ubiquitylated proteins but on the isolation of proteins bearing extended K63-linked ubiquitin chains (Fig. 11A). Enrichment agents that would allow for isolation of polyubiquitinated proteins consisted of binding domains found in either human Ubiquilin-1 (UBQLN1), Rap80 or yeast VPS27 with the latter two binding to K63-linked ubiquitin chains. All three binding domains have been described as tandem-repeated domains, which means that several domains were fused together, linked by spacer regions of varying lengths. This setup increases the affinity for ubiquitin chains to a high picomolar to low nanomolar range (Hjerpe et al., 2009; Sims et al., 2012).

In order to facilitate a comparison of the efficacy and specificity of the enrichment reagents in our experimental setup, I performed *in vitro* pulldowns utilising ubiquitin chains of different linkage types. To this end, the ubiquitin binding domains of the aforementioned proteins were fused to emGFP and purified. The fusion proteins were subsequently incubated with a panel of *in vitro*-generated and purified tetraubiquitin chains (Fig. 11B) and binding was assessed by immunoblotting for ubiquitin. The pan-polyubiquitin (pan-PolyUb) binder derived from UBQLN1 isolated all three chains, irrespective of the linkage type present in the ubiquitin chain. The binder derived from BRCA1-A complex subunit Rap80 (termed Rx3A7) demonstrated selective isolation of K63-linked polyubiquitin over K48-linked ubiquitin chains and the topologically most similar M1-linked chains (Fig. 11B). In contrast, the isolation reagent derived from yeast ESCRT-0 complex protein VPS27 demonstrated affinity not only

for K63-linked ubiquitin chains, but also for K48-linked polyubiquitin and, to a lesser extent, M1-linked ubiquitin chains (Fig. 11B). This observation could most likely be attributed to the reagent's remarkably high ubiquitin affinity, a property that has been noted before (Sims et al., 2012). In summary, two unspecific reagents and one reagent that allowed for selective isolation of K63-linked chains over K48- and M1-linked chains were purified and their specificity and efficacy assessed in an *in vitro* setting.

To identify cellular substrates of DUBs by detecting differential ubiquitination of proteins, these binders need to be adequate for the use in cellular settings. I thus assessed the efficacy of isolation of cellular ubiquitin pools by UBQLN1- and Rap80-derived binders (Fig. 11C). Both pulldown reagents isolated ubiquitin from HeLa cells over a wide range of molecular weights. However, it was noted that the UBQLN1-derived binder was able to isolate a larger fraction of ubiquitinated proteins (Fig. 11C). This finding is consistent with the observation that approximately 88% of cellular ubiquitin present in chains was found to be non-63-linked (information derived from Kaiser et al., 2011). Summed up, both tools facilitated the isolation of cellular ubiquitin over a wide range of molecular weight species.

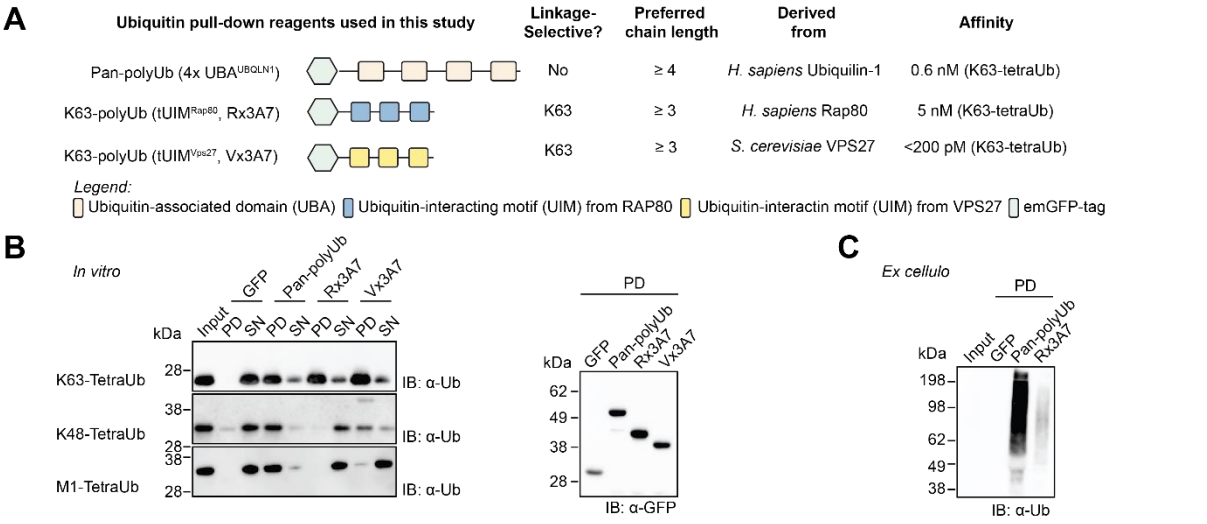

Figure 11. Polyubiquitin binding reagents allow for enrichment of ubiquitin *in vitro* and *ex cellulo*. **(A)** Overview of emGFP-tagged polyubiquitin binders used in this dissertation. The affinity data was derived from the original publications (Hjerpe et al., 2009; Sims et al., 2012). **(B)** *In vitro* studies demonstrate binding behaviour of reagents within a panel of three homotypic tetraubiquitin chains with different linkage types. The chains were incubated with equimolar concentrations of the respective enrichment reagent or GFP before isolating them using GFP-targeting nanobodies. The supernatant (SN) and the isolated tetraubiquitin chains (PD) were collected and analysed with SDS-PAGE and Western Blotting. The efficient isolation of all reagents is shown on the right. **(C)** Enrichment of ubiquitin-conjugated protein pool and direct comparison of ubiquitin isolation from HeLa cells between the UBQLN1- and Rap80-derived binders, pan-PolyUb and Rx3A7. The binders were pre-immobilised on beads before cell lysate was added to the beads. The protein suspension was incubated for 2 h to allow for binding and the isolated ubiquitinated proteins were analysed using SDS-PAGE and Western Blotting.

3.2.2 Monoubiquitin binders are valuable tools to enrich proteins decorated with short ubiquitin chains

The impact of denaturing lysis and washing conditions in separating the 'ubiquitinome' from the 'ubiquitin interactome' has recently been noted for ubiquitin isolation from yeast extract (Zhang et al., 2022). Thus, we endeavoured to optimise our established ubiquitin binding tools to also allow for more stringent isolation conditions. To this end, the emGFP-based enrichment tag was replaced by a biotin tag (Fairhead & Howarth, 2015). This modification was expected to facilitate denaturing lysis and washing, thereby enabling the discrimination between protein species that are ubiquitylated with intrinsically low occupancy and proteins that merely interact with these proteins or ubiquitin itself. In addition, we expanded our panel of ubiquitin binding tools to include the recently published monoubiquitin (monoUb) binder, derived from an *Orientia tsutsugamushi* DUB (OtUBD, Zhang et al., 2022) which was biotinylated at an internal ubiquitylation site (Fig. 12A).

To assess the capacity of these modified pulldown reagents to isolate ubiquitylated proteins, they were assessed in cell lysate under denaturing conditions (8 M urea) and isolation efficiencies of the PolyUb binders and the monoUb binder OtUBD were determined. As demonstrated in the Far Western using Alexa Fluor 488-coupled streptavidin, all isolation reagents were bound by the streptavidin-based agarose beads even under denaturing conditions (Fig. 12B). The bound pulldown reagents were able to isolate ubiquitin from human cells with the newly introduced OtUBD isolating free ubiquitin and diubiquitin (Fig. 12B). Free ubiquitin and diubiquitin was not isolated by neither the pan-PolyUb nor Rx3A7 since their high affinities to ubiquitin are largely attributable to avidity effects (Fig. 12B).

Ultimately, the isolation tools should provide evidence for differential ubiquitylation of specific cellular proteins. To confirm that our reagents allow for this, I assessed the modification of two proteins that would demonstrate a reported ubiquitylation state change upon the addition of a specific trigger (Fig. 12C and D). The first system to assess the capability of the isolation tools included the detection of ubiquitylated γH2AX. The histone variant H2AX is central to the process of DNA damage response (DDR, Luczak & Zhitkovich, 2018; Thorslund et al., 2015) and undergoes phosphorylation and subsequent ubiquitylation within this cellular response. In order to trigger DDR, DNA double-strand breaks (DSB) were induced by the supplementation of cell culture media with the topoisomerase II poison etoposide (Eto) which should lead to phosphorylation and ubiquitylation of H2AX (Le et al., 2023). Following DSB induction, ubiquitylated proteins were isolated using OtUBD, Rx3A7 and the pan-PolyUb binder (Fig. 12C). In the absence of DNA damage, pulldowns with OtUBD isolated a low amount of ubiquitinated γH2AX, while no ubiquitinated γH2AX was observed with UBQLN1 and Rx3A7.

When DSB was induced, the amount of ubiquitylated γH2AX, that was detected, was greatly enhanced for OtUBD and the pan-PolyUb binder. For Rx3A7, no ubiquitylated γH2AX was detected which is consistent with the extensive studies by Thorslund et al. (2015), who reported that γH2AX did not exhibit K63-linked ubiquitylation upon etoposide treatment. The isolation and visualisation of ubiquitylated species of γH2AX and the detected change in ubiquitylation state upon induction of DDR demonstrated the applicability of these tools to monitor differential ubiquitylation of individual proteins.

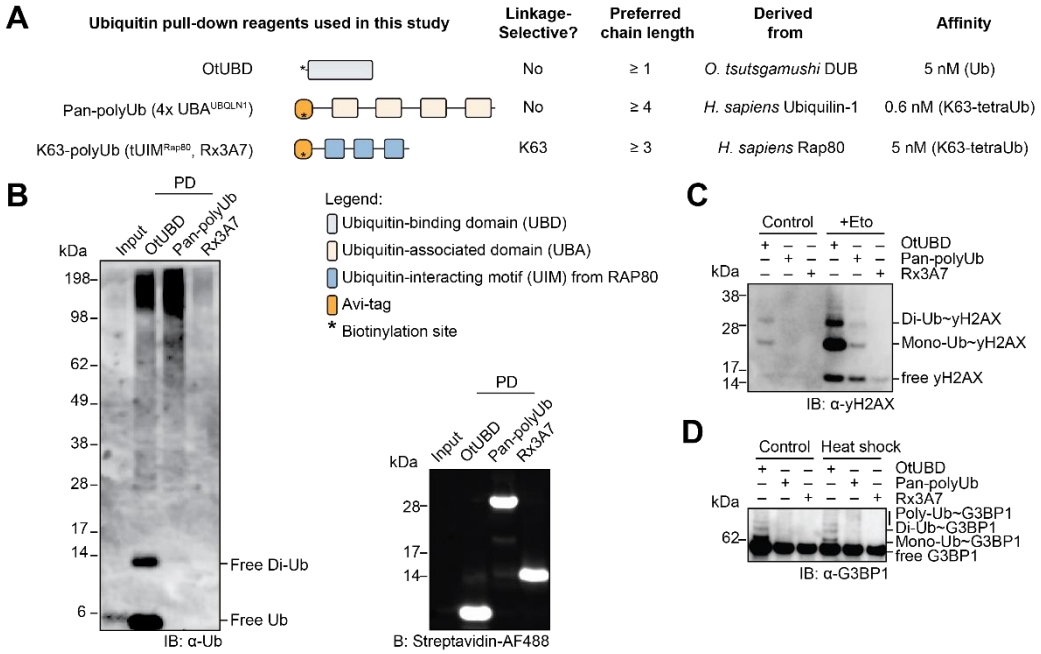

Figure 12. The high-affinity monoubiquitin binder derived from *O. tsutsugamushi* allows for enrichment of free ubiquitin and proteins decorated with short ubiquitin chains. **(A)** Overview of biotinylated mono- and polyubiquitin binders used in this dissertation. The affinity data for OtUBD was derived from Zhang et al. (2022). **(B)** Enrichment of free ubiquitin and ubiquitin-conjugated protein pool from U2OS cells. The cell lysate was added to ubiquitin binders pre-immobilised on streptavidin beads. After incubation, ubiquitin and ubiquitinated proteins were eluted from the beads and analysed by SDS-PAGE and Western Blotting. Alexa-Fluor 488-tagged streptavidin was used in Far Western to ensure presence of equimolar amounts of the binders in the pulldown. **(C)** Comparison of isolation-efficiency of ubiquitylated γH2AX between mono- and polyubiquitin binders in etoposide-treated U2OS cells versus control cells. **(D)** Comparison of isolation-efficiency of ubiquitylated G3BP1 between mono- and polyubiquitin binders in heat shock (43 °C, 1 h)-exposed U2OS cells versus control cells.

In a subsequent experiment, the performance of the binders was evaluated in relation to proteins that were reported to undergo extensive ubiquitination, such as G3BP1, in order to compare their efficacy in isolation with long ubiquitin chains (Fig. 12D). As previously reported, G3BP1 is ubiquitinated upon heat shock (HS, Maxwell et al., 2021) which led us employ this trigger. With Rx3A7 we did not detect any ubiquitylated G3BP1, contrasting the findings by Gwon et al. (2021) that identified K63-linked ubiquitination on G3BP1 after HS utilising lysine-depleted ubiquitin mutants. For OtUBD pulldowns, ubiquitylated G3BP1 was identified - the

isolated fraction of ubiquitylated protein, however, was unchanged upon HS. With the UBQLN1-based isolation, a slight induction of decoration of G3BP1 with long ubiquitin chains was demonstrated (Fig. 12D). This indicates an importance of long ubiquitin chains on G3BP1 upon cellular stress and highlights how the different isolation reagents can complement each other.

3.2.3 Establishing ubiquitin binders as useful reagents to study the influence of DUB activity in the context of mitochondrial depolarisation

Subsequent to the demonstration of the capacity of our binders to not only isolate ubiquitin chains *in vitro* and *ex cellulo*, but also to isolate ubiquitinated protein species from a complex protein suspension, the subsequent objective was to evaluate the efficacy of these tools in a system critically regulated by DUB activity. This approach was undertaken to approximate the experimental system to the objective of the thesis in discovering substrates of our DUBs of interest.

One biological system regulated by a DUB is the process of mitophagy. In this selective form of autophagy of damaged mitochondria, USP30 counteracts the ubiquitylation of proteins in the mitochondrial outer membrane (MOM, Fig. 13A, Kazlauskaite et al., 2014; Narendra et al., 2010). Due to its role in mitophagy, the DUB USP30 emerged as a promising target to tackle Parkinson's and Alzheimer's disease. Consequently, several inhibitors that target USP30 have been described, such as the small molecule inhibitor compound 39 (CMPD39) and its derivative NK036 (Kazi et al., 2024; Rusilowicz-Jones et al., 2022; Yue et al., 2014). In order to induce mitophagy, HeLa cells that stably express the yellow fluorescent protein (YFP)-tagged E3 ligase Parkin were treated with carbonyl cyanide *m*-chlorophenyl hydrazine (CCCP) which leads to depolarisation of mitochondria thus triggering mitophagy (Fig. 13B-E, Pickrell & Youle, 2015). Upon CCCP-treatment, Parkin was recruited to the mitochondria (Fig. 13C), a critical step in mitophagy. Subsequently, we isolated ubiquitylated proteins employing biotinylated OtUBD in denaturing conditions (Fig. 13D). Under physiological conditions, OtUBD did not isolate any ubiquitylated species of the investigated proteins – irrespective of the inhibition of USP30 (Fig. 13D). The combination of mitochondrial depolarisation and OtUBD isolation, however, led to the detection of ubiquitylated mitofusin 2 (MFN) and the translocase of the outer membrane proteins 40 and 20 (TOM40 and TOM20). For both TOM proteins, the detected ubiquitylation increased upon USP30 inhibition (Fig. 13D). The relatively large fraction of ubiquitylated TOM20 in this combinatorial treatment is supported by the finding that even without prior enrichment, monoubiquitylated TOM20 was identified (Fig. 13E). These findings supported that our system is capable of detecting DUB-specific effects on ubiquitylation patterns of individual DUB substrates.

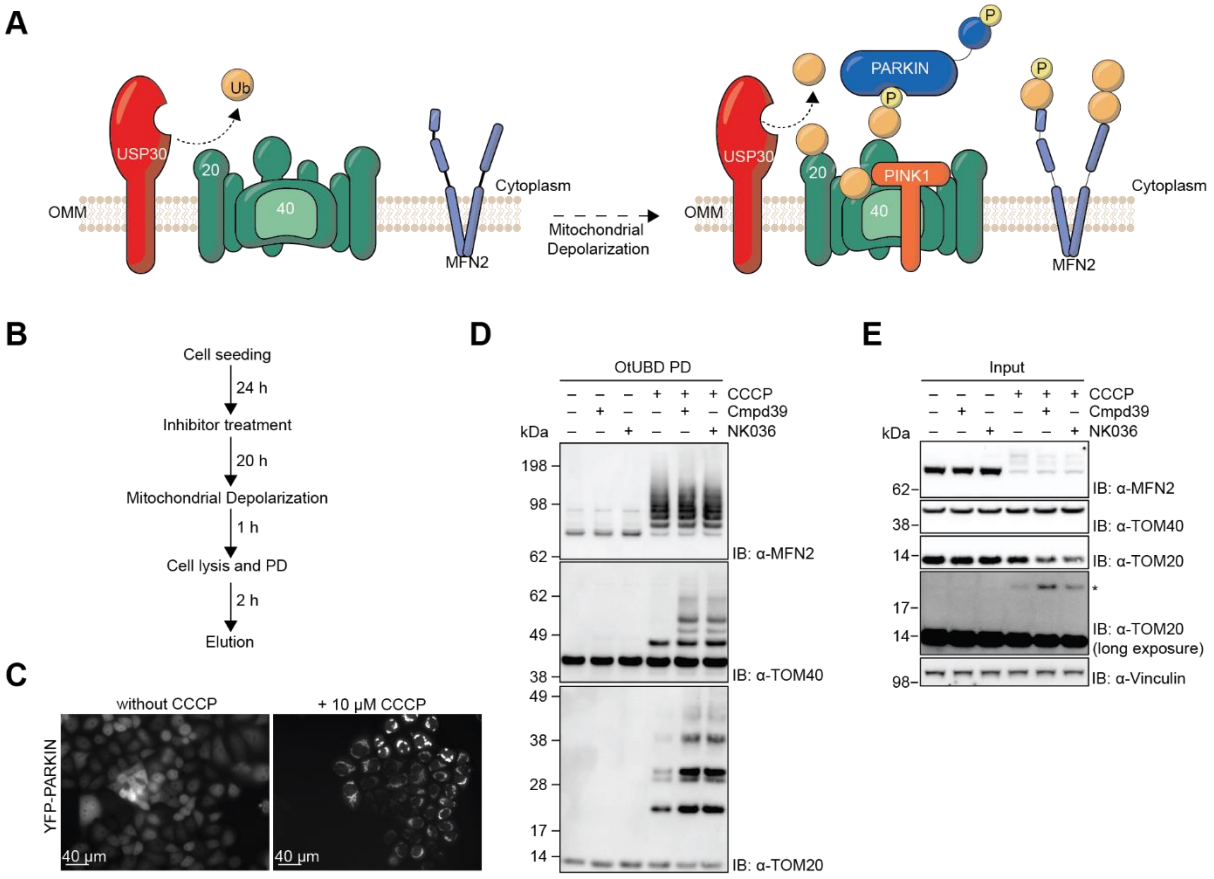

Figure 13. Ubiquitin binders as useful tools to study DUB activity and DUB inhibitors in a mitophagy setting. (A) Model of ubiquitination at the mitochondrial outer membrane after mitochondrial depolarisation. **(B)** Overview of treatment time course with USP30 inhibitors and mitochondrial depolarisation using CCCP. Cells were first treated with the USP30 inhibitors before mitochondria were depolarised for 1 h using CCCP. After induction of mitophagy, cells were lysed and ubiquitinated proteins isolated with OtUBD. **(C)** YFP-Parkin recruitment to the mitochondria of HeLa cells with constitutive expression of the YFP-tagged E3 ligase following treatment with CCCP. **(D)** Isolation of ubiquitinated proteins using biotinylated OtUBD after treatment of HeLa YFP-Parkin cells with CCCP and two different USP30 inhibitors. The samples were analysed by SDS-PAGE and Western Blot. **(E)** Input fractions of the pulldowns shown in (D). 'Long exposure' refers to extended exposure of the chemiluminescence reaction at the imager. The asterisk indicates monoubiquitinated TOM20 visible in total lysate fraction. OMM: Outer mitochondrial membrane.

The experiments investigating the effects of USP30 inhibition furthermore validated that TOM20 and TOM40 are regulated by USP30, while MFN2 was not. This highlighted selective deubiquitination at the mitochondrial outer membrane and supported diGly-based proteomics approaches (Ordureau et al., 2020). In addition, I could show that active USP30 preferentially deubiquitinated poly- or multiubiquitinated TOM20 and TOM40, while exerting relatively mild or no effects on their monoubiquitinated forms. Both tested compounds showed effects on ubiquitylation pattern of USP30 substrates which might render them as promising tools to regulate mitophagy and to dissect the role of USP30 in Parkinson's or Alzheimer's.

In conclusion, this work comprehensively compared and assessed previously established ubiquitin binders in cellular settings. This facilitated the identification of the most efficacious tools to study ubiquitination and the effect of DUBs in various settings. In the process, the effect of USP30 inhibitors on ubiquitination patterns of mitochondrial outer membrane proteins were elucidated, which provides avenues to study USP30 activity. These ubiquitin binders and experimental details have laid the foundation for studies of the hitherto underexplored DUBs USP53 and USP54, which will be presented in the ensuing chapters.

3.3 Identification of substrates of the human DUB USP53

Recent publications have indicated a correlation between mutations in *USP53* and progressive familial intrahepatic cholestasis, a hereditary liver disorder in children (Alhebbi et al., 2020, 2021; Gezdirici et al., 2023; Maddirevula et al., 2019; Srinivas Sankaranarayanan, 2021). However, mechanistic understanding of these observations was hampered by the annotation of USP53 as an inactive pseudoenzyme. Consequently, after demonstrating its activity the following chapter was initiated with the objective to investigate effects of USP53 depletion on ubiquitylation of cellular proteins in a relevant cell system.

3.3.1 Analysis of protein levels of USP53 mutants in cells

A comprehensive mapping of all cholestasis-associated missense and frameshift/nonsense mutations in *USP53* was inspected, as created for Wendrich et al. (2024, Fig. 14A). Interestingly, missense mutations clustered in the catalytic domain of the DUB thus underscoring the importance of integrity of this domain for USP53 functionality.

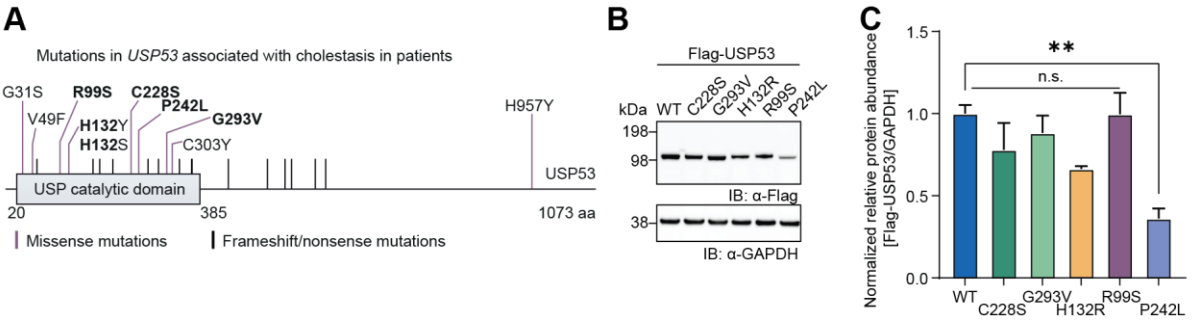

Figure 14. Stability assessment of USP53 after recapitulation of mutations associated with cholestasis in human patients. (A) Domain architecture of full-length USP53 with missense and frameshift/nonsense mutations annotated with the respective positioning. Figure slightly changed from Wendrich et al. (2024) created by Kim Wendrich with contributions by the author. **(B)** Western blot analysis of protein levels of USP53 carrying missense mutations highlighted in bold in (A). Vectors encoding for mutations in the Flag-USP53 full-length context were expressed in HEK-293 cells and cells were lysed 48 h after expression. Protein levels were analysed by Western Blot. **(C)** Quantification of protein levels of USP53 mutants from three independent experiments. The indicated *p*-value was calculated with a 2-way ANOVA and corresponds to $p=2.3 \times 10^{-3}$.

In order to ascertain whether these mutations simply impair the stability of the protein in cells, I generated vectors encoding for mutants in the Flag-USP53 full-length context, transfected them into HEK-293 cells and detected the protein levels of the mutants (Fig. 14B). We hypothesised that G31S and C303Y mutations would lead to structural perturbations in the immediate vicinity of the catalytic residues according to a homology model based on the structure of USP54 (Wendrich et al., 2024). Consequently, the subsequent analysis excluded these mutants. In triplicate measurements, only the P242L mutation led to a significant decrease in cellular levels of USP53 (Fig. 14C). Given that the other examined mutations did not affect total protein levels in cells, we hypothesised that these mutations primarily impeded catalytic activity. This hypothesis was later corroborated for mutations affecting the amino acids R99 and H132 *in vitro* (Wendrich et al., 2024).

3.3.2 Establishing epithelial and epithelial-like knockdown cell lines to study USP53 effects

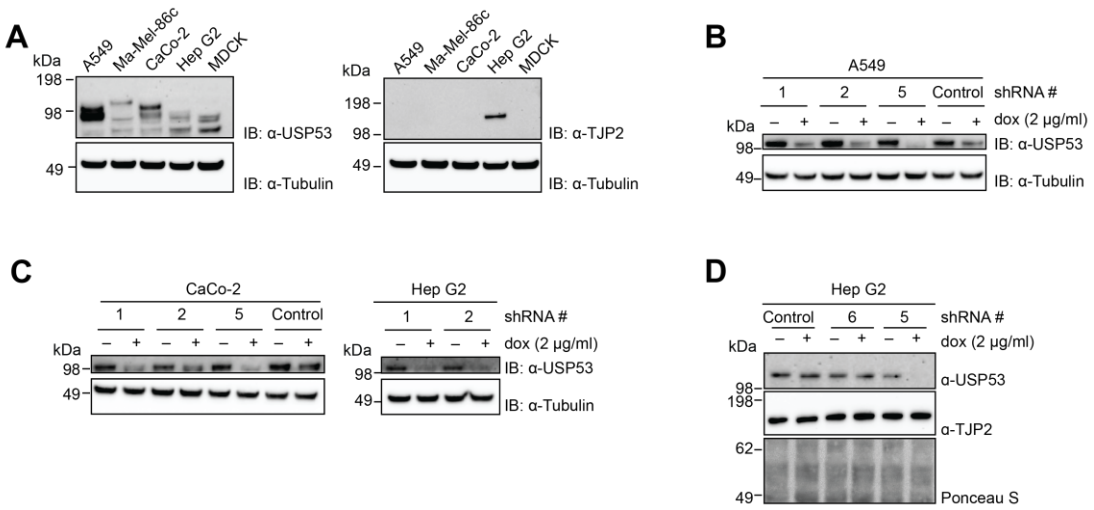

Figure 15. Cell line panel to identify suitable cell lines for USP53 studies. (A) Comparison of USP53 and TJP2 protein levels between four human and one canine cell line. Cells were grown to high levels of confluency and subsequently harvested before protein levels were analysed by Western Blot. **(B)** Efficiency of *USP53* knockdown in four A549 cell lines that have an integrated shRNA. This shRNA was introduced with a lentiviral system and target either *USP53* or a control sequence. **(C)** Efficiency of *USP53* knockdown in four CaCo-2 cell lines and two HepG2 cell lines with integrated shRNA targeting either *USP53* or a control sequence. **(D)** Efficiency of *USP53* knockdown in three additional Hep G2 cell lines with integrated shRNA, targeting either USP53 or a control sequence. In addition, investigations of the influence of USP53 depletion on TJP2 levels were conducted. In every experiment shown, doxycycline was added to cell culture medium at least 72 h before harvesting the cells and analysis of protein levels by Western Blot.

In order to better understand the function of USP53 in human cells in the context of tight junction protein localisation, we characterised the expression levels of USP53 across a panel of cell lines which have been reported to form cell-cell junctions. The lung epithelial cell line A549, the melanoma cell line Ma-Mel-86c, the colorectal adenocarcinoma cell line CaCo-2

and the hepatocellular carcinoma cell line Hep G2 were investigated. In addition to these, Madin-Darby Canine Kidney (MDCK) cells were included, despite their non-human origin, since they are commonly used for the investigation of tight junctions. In addition to USP53 levels, protein abundance of TJP2 was analysed (Fig. 15A) since Kazmierczak and colleagues who associated a *Usp53* mutation with hearing loss in mice subsequently identified TJP2 as an interaction partner. Among the cell lines examined, A549 and CaCo-2 exhibited the highest levels of USP53, while HepG2 displayed the highest levels of TJP2, one of the proposed interactors of USP53 (Fig. 15A). These three cell lines were therefore utilised in further studies.

In order to identify substrates in these cell lines, we established cell lines that carry a doxycycline (dox)-inducible short hairpin RNA (shRNA) targeting *USP53* to conditionally deplete the DUB (Fig. 15B-D). This objective was achieved using lentiviral transduction in conjunction with puromycin-based selection. Following dox induction, we identified several clones exhibiting a successful knockdown of the DUB (Fig. 15B-E). Given the high levels of the potential substrate of USP53, TJP2, in HepG2 cells, TJP2 level changes upon USP53 depletion were assessed in these cells (Fig. 15D). However, upon depletion of USP53 using shRNA#5, neither a change in TJP2 levels was detected (Fig. 15D), nor could ubiquitylated TJP2 be detected (data not shown).

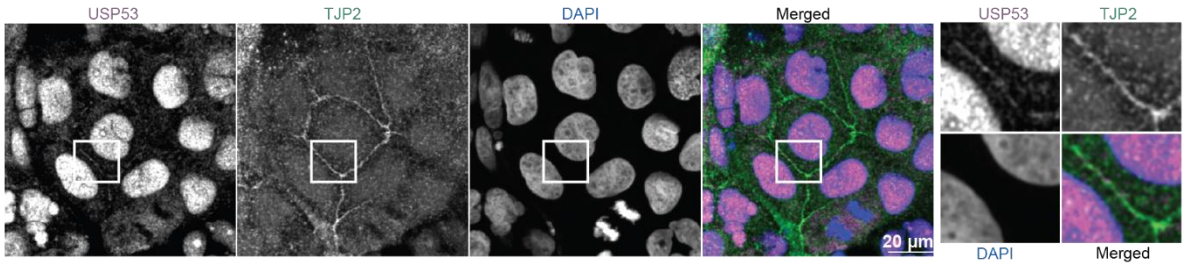

Figure 16. Confocal microscopy detects USP53 at cellular junctions. Representative confocal images of USP53 (in purple), TJP2 (in green) and DAPI (in blue), as detected with immunofluorescence in CaCo-2 cells. CaCo-2 cells were grown to high levels of confluency before proteins were fixed, permeabilization of the cellular membranes and immunofluorescent staining. Insets are magnified images of squares.

In order to validate that USP53 localised at tight junctions in the cell lines under investigation, we performed immunofluorescence (IF)-based confocal imaging. For CaCo-2 (Fig. 16), co-localisation of USP53 with the tight-junction marker TJP2 could be determined.

3.3.3 diGly-based ubiquitinomics identifies ubiquitination sites regulated by USP53

Following the identification of a suitable cell line for USP53 studies in cells with the propensity to establish tight junctions (also supported by Putt et al., 2017; Samak et al., 2016; Valenzano et al., 2015) and the subsequent establishment of a conditional knockdown cell line, I focused on the identification of potential substrates of USP53 in CaCo-2 cells. *In vitro* data, accumulated in the group by Kim Wendrich, demonstrated that USP53 has the propensity to remove ubiquitin completely from potential substrates – a surprising finding for a linkage-directed DUB.

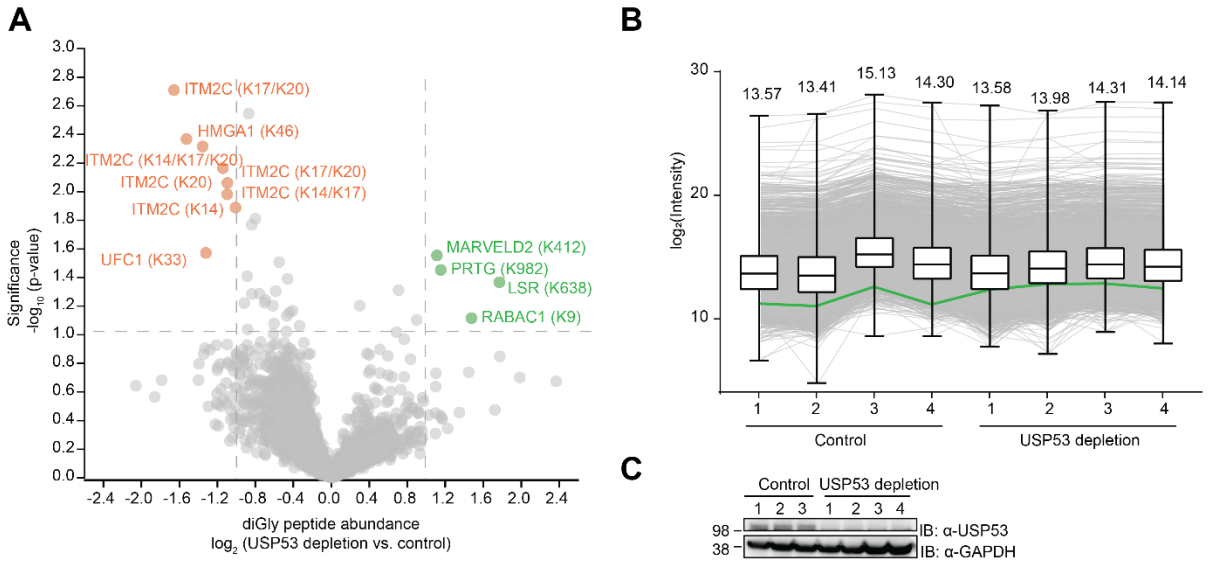

Figure 17. diGly-based ubiquitinomics reveals differentially ubiquitinated peptides after USP53 depletion in CaCo-2 cells. **(A)** Volcano plot showing log_2 fold changes of peptides with a diGly remnant upon depletion of USP53 in CaCo-2 cells using the conditionally expressed shRNA#5. diGly sites were unambiguously identified and given in brackets. Significance cut-offs are set to '0.05' and abundance cut-offs to '2' which are illustrated with dashed lines. The t-test for any given value analysed four samples per condition. Peptides with increased presence of diGly-modifications are shown in green, peptides with decreased abundance of diGly modifications are shown in orange. The lysine residues that are differentially regulated are shown in brackets. **(B)** Profile plot of all peptides identified after filtering. Medians of all intensities are given above the box plots with min-max borders. The green line indicates the diGly-labelled peptide from MARVELD2 modified at lysine 412. **(C)** Validation of successful knockdown of *USP53* in the samples analysed in this figure. Control sample number four is missing due to loss of sample. Sample processing and initial analysis was performed by K. Bezstarosti and J. Demmers.

To identify candidate substrates of USP53, we looked for proteins that are differentially ubiquitylated upon USP53 depletion. A suitable method to identify ubiquitylation of proteins is diGly-based ubiquitinomics. This method utilises a monoclonal antibody that specifically recognises the diGly remnant of ubiquitylated proteins resulting from trypsinolysis which allows identification and quantification of ubiquitylated proteins and sites of the modification

on a global scale (Fulzele & Bennett, 2018; W. Kim et al., 2011). The acquisition of data was conducted in collaboration with the research group led by Dr. Jeroen Demmers at the Erasmus University Medical Centre in Rotterdam. Using data-independent acquisition (DIA) mass spectrometry, 8500 peptides with diGly-modified lysines were identified after initial processing in *Spectronaut*. Subsequent rigorous filtering in *Perseus* (Tyanova et al., 2016) reduced the dataset to 3320 peptides, corresponding to 1472 distinct proteins, which were identified as ubiquitinated (all filtering steps are recorded in Appendix Fig. 5). Among the proteins whose ubiquitination state was significantly upregulated upon USP53 depletion with an at least 2-fold increase in lysine ubiquitination, we identified peptides corresponding to two tricellular junction proteins, MARVELD2 and LSR (Fig. 17A, Table 1). Conversely, a reduction in ubiquitination was observed for several peptides of the integral membrane protein 2C (ITM2C, Fig. 17A, Table 1). In order to verify the robust change in ubiquitination state of the detected peptides, the profile plot was inspected for differentially enriched ubiquitinated peptides between the individual samples (Fig. 17B). The abundance of the ubiquitinated MARVELD2 peptide was visualised in the plot that showed upregulated ubiquitination upon USP53 depletion. While the robust upregulation of MARVELD2 ubiquitination could be visualised, it became apparent, that measured intensities between the samples fluctuated (Fig. 17B). This fluctuation was likely attributable to the acquisition of data on two different days. Since peptides for USP53 were not identified in mass spectrometry, I verified the successful knockdown of USP53 in our samples using Western Blot (Fig. 17C).

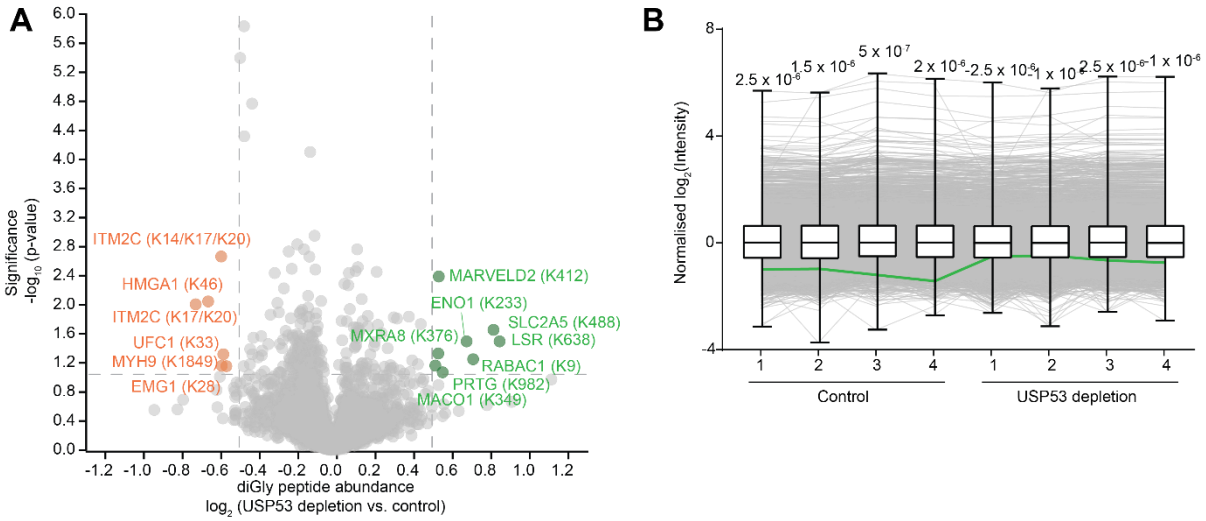

Figure 18. Normalisation of diGly ubiquitinomics data shows differentially regulated ubiquitination sites after USP53 depletion. (A) Volcano plot showing the same samples as processed in Fig. 17C with an additional Z-normalisation based on the column medians of peptides signal. Significance cut-offs are set to '0.05' for the significance and '1.414' for abundance change and illustrated with dashed lines. The t-test for given value was obtained analysing four samples per condition. **(B)** Profile plot with identical parameters as in Fig. 17C after Z-normalisation.

To address the fluctuation of the measured intensities between the individual samples, a normalisation step was introduced in data processing using Z-score normalisation, integrated within the *Perseus* software (Fig. 18A). Following the normalisation and statistical analysis, it was found that each protein identified with significant changes in ubiquitination prior to normalisation was also identified after normalisation. Furthermore, we identified an additional set of potential substrates that demonstrated an abundance change of peptides of at least 1.414 (see Table 2). In order to identify other regulated ubiquitination sites upon USP53 depletion, the top three ubiquitination sites with a similar profile as MARVELD2 across the samples were identified using the '*Profile Plot*' feature integrated in *Perseus*. This analysis led to the identification of several previously unidentified substrate candidates (Fig. 18B, Table 3). Among these, we identified the tight-junction associated protein and direct TJP1/TJP2-binder claudin 6 (CLDN6).

In conclusion, diGly-based ubiquitinomics identified ten candidate substrates. These candidates and the positioning of their ubiquitylation sites are illustrated in Fig. 19 and Fig. 20.

Table 1. Significantly changed diGly sites of the respective proteins in CaCo-2 cells upon USP53 depletion versus control. The asterisk indicates that the PTM site location corresponds to the location in the predominant isoform of the respective protein.

$-\log_{10}$ (*p*-value)	$\log_2$(Fold change)	Gene name	PTM site location*
1.37	1.77	LSR	K638
1.12	1.48	RABAC1	K9
1.45	1.15	PRTG	K982
1.55	1.11	MARVELD2	K412
1.89	-1.01	ITM2C	K14
2.06	-1.09	ITM2C	K20
1.98	-1.10	ITM2C	K14/K17
2.16	-1.14	ITM2C	K17/K20
1.57	-1.32	UFC1	K33
2.32	-1.35	ITM2C	K14/K17/K20
2.37	-1.53	HMGA1	K46
2.71	-1.66	ITM2C	K17/K20

Table 2. Significantly changed diGly sites of the respective proteins in CaCo-2 cells upon USP53 depletion versus control after Z-score normalisation. The asterisk indicates that the PTM site location corresponds to the location in the predominant isoform of the respective protein.

$-\log_{10}$ (*p*-value)	$\log_2$(Fold change)	Gene name	PTM site location*
2.39	0.56	MARVELD2	K412
1.16	0.54	MACO1	K349
1.50	0.70	ENO1	K233
1.66	0.84	SLC2A5	K488
1.07	0.58	PRTG	K982
1.50	0.87	LSR	K638
1.33	0.55	MXRA8	K376
1.25	0.73	RABAC1	K9
1.16	-0.57	MYH9	K1849
2.67	-0.57	ITM2C	K14/K17/K20
2.01	-0.70	ITM2C	K17/K20
2.05	-0.64	HMGA1	K46
1.16	-0.54	EMG1	K28
1.32	-0.56	UFC1	K33

Table 3. Top four protein hits isolated from the profile plot of the MARVELD2 peptide harbouring lysine 412 after Z-score normalisation. The asterisk indicates that the PTM site location corresponds to the location in the predominant isoform of the respective protein.

$-\log_{10}$ (*p*-value)	$\log_2$(Fold change)	Gene name	PTM site location*
2.39	0.56	MARVELD2	412
2.46	0.12	PLLP	7
2.45	0.23	CLDN6	217
1.58	0.12	MXRA8	428

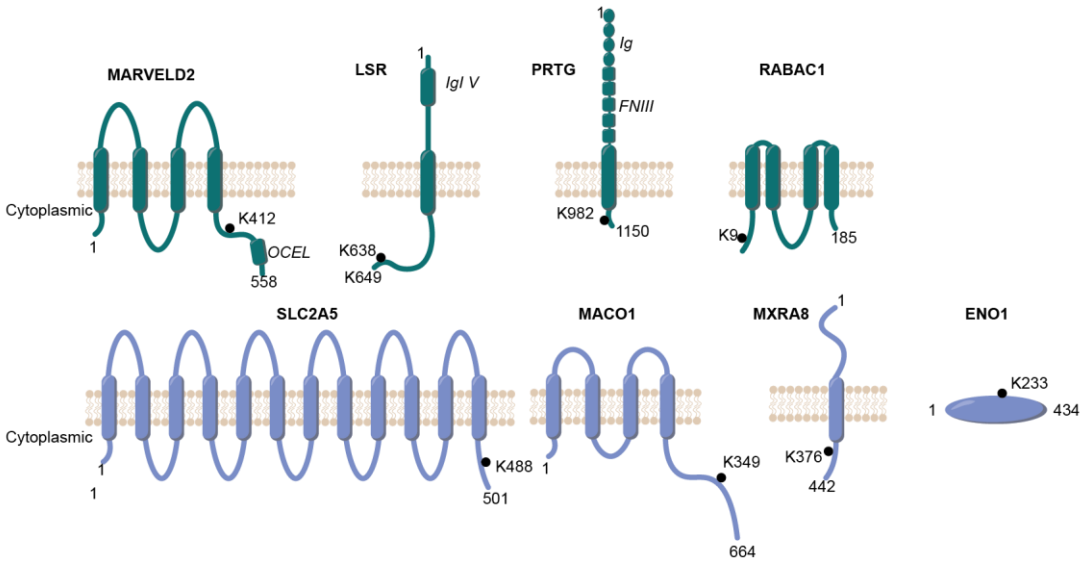

Figure 19. Ubiquitination site positioning in the proteins identified by diGly-based ubiquitinomics. Ubiquitination site are indicated by a black dot on the protein. Numbers correspond to either N- and C-terminal amino acids or the identified ubiquitination site. Annotated domains of proteins are given in italics. All proteins except ENO1 possess transmembrane domains. Proteins depicted in dark green and lavender were found to be upregulated in ubiquitination after USP53 depletion in normalised and non-normalised data or only in normalised data, respectively.

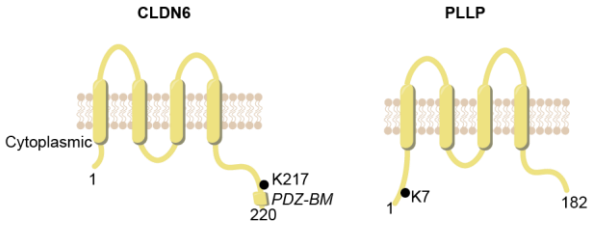

Figure 20. Ubiquitination site positioning in proteins identified by diGly-based ubiquitinomics and profile plot analysis with the MARVELD2 peptide harbouring lysine 412. Ubiquitination sites are indicated by a black dot on the protein. Numbers correspond to either N- and C-terminal amino acids or the modified ubiquitination site. Annotated domains of proteins are given in italics.

To explore whether increased identification of the respective peptides upon their diGly-based enrichment was simply a function of upregulated protein abundance, we inspected total protein abundance within the samples subjected to diGly enrichment (Fig. 21). This was possible since samples that were submitted to diGly-based enrichment were split off and subjected to total proteome analysis by mass spectrometry, analysed by DIA and processed in *Spectronaut*. In the analysis of the total proteome, two thirds of the proteins, for which a change in ubiquitination state was detected (Fig. 18A), were identified. Most proteins showed only a minor change in overall abundance upon depletion of USP53 with the exception of the non-histone chromatin protein HMGA1 (Fig. 21A). CLDN6 is slightly downregulated in the proteome upon USP53 depletion (Fig. 21A). To exclude that USP53 depletion resulted in a change of overall protein abundance, the intensities of peptides identified in the different samples were compared. However, no remarkable change was observed (Fig. 21B). In the total lysate, we did not identify peptides corresponding to MARVELD2. In order to identify

changes in its protein levels, we turned to Western Blot-based detection (Fig. 21C). However, no change in protein levels of MARVELD2 was detected upon USP53 depletion.

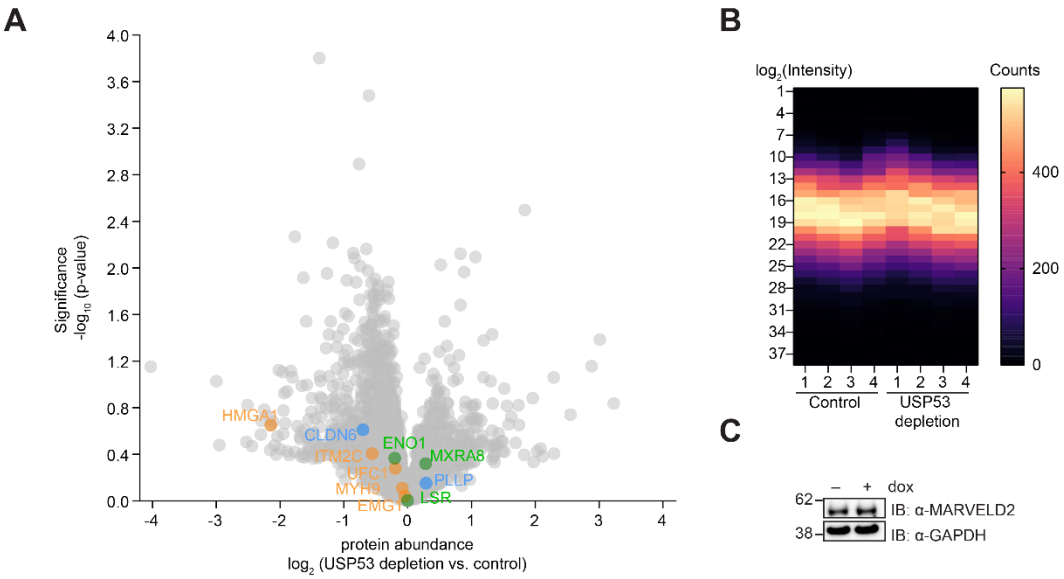

Figure 21. Comparison of total proteome samples of CaCo-2 cells upon USP53 depletion. (A) Volcano plot depicting proteins with altered abundance upon depletion of USP53 using the conditionally expressed shRNA#5. Proteins were highlighted in green or orange dependent on their increased diGly or reduced diGly modifications in diGly ubiquitinomics setup. Bright blue colouring highlights proteins with a similar profile plot as MARVELD2. **(B)** Comparison of log_2 intensities of identified peptides between USP53 depletion samples and control samples. **(C)** Western blot detection of MARVELD2 which could not be detected in total proteome samples. Sample processing and initial analysis was performed by K. Bezstarosti and J. Demmers.

3.3.4 Ubiquitin binders complement diGly-based proteomics to assess substrate ubiquitylation

As established above, the diGly remnant-recognising antibodies employed for the exploration of USP53 substrate candidates are an efficacious tool for the identification and quantification of ubiquitinated proteins and sites on a peptide level. However, it should be noted that they are not suited for Western blot-based readouts and investigations into ubiquitin architecture on substrates due to the need for prior trypsinolysis. In order to validate the regulation of ubiquitination sites discovered with diGly proteomics in orthogonal assays, the tools established in chapter 3.2 were utilised. Denaturing lysis after USP53 depletion was conducted prior to enrichment of ubiquitylated cellular proteins with OtUBD and the pan-PolyUb binder (Fig. 22A). The orthogonal validations were focused on MARVELD2 (also termed tricellulin) and LSR (also termed angulin-1) since ubiquitylation of lysine 412 and lysine 638, respectively, were identified with high confidence in the diGly data set. Our choice to further investigate those two proteins was further informed by the fact that there is data

showing that genetic mutations in both proteins result in similar phenotypes as observed for *USP53* mutations (Maddirevula et al., 2019; Riazuddin et al., 2006).

The enrichment of ubiquitylated proteins with the pulldown reagent derived from OtUBD resulted in a striking difference in ubiquitylation of MARVELD2 in response to USP53 depletion (Fig. 22B). While there was only a modest increase in monoubiquitination of MARVELD2 upon depletion of the DUB, the most significant difference was found in diubiquitinated protein (Fig. 22B). This finding is consistent with *in vitro* data demonstrating that USP53 possesses an S2 site that contributes significantly to ubiquitin binding and catalysis of chains (Wendrich et al., 2024). The increase in diubiquitinated species was found to be significant (Fig. 22C) and is not derived from an increase in overall protein abundance (Fig. 22D) as already shown in Fig. 21C. The pan-polyUb binder, derived from human UBQLN1, only exhibited a modest increase in the presence of long ubiquitin chains on MARVELD2 (Fig. 22E).

While the results for MARVELD2 showed a marked difference in ubiquitination, thus validating the diGly-based proteomics approaches, no such difference in ubiquitination was detected for the other tricellular protein, LSR in CaCo-2 cells (Fig. 22F). The lack of identification of distinct bands corresponding to LSR species with few ubiquitin molecules attached, potentially hampered this identification. I verified that LSR does not show abundance changes in these experiments with LSR levels being overall unchanged and independent of USP53 levels (Fig. 22G) which is consistent with our proteomics data (Fig. 21A). I thus focused the experimental efforts on MARVELD2

In order to exclude any potential off-target effects of the *USP53*-targeting shRNA that was utilised in these assays, the experiment was repeated with a CaCo-2 cell line that harboured a different shRNA (#1) which has also been shown to deplete USP53 efficiently (Fig. 22H). In this cell line, the increase in diubiquitinated MARVELD2 species upon USP53 depletion was confirmed (Fig. 22H). To exclude any effect of doxycycline treatment on MARVELD2 ubiquitination state, the parental CaCo-2 cell line, which did not harbour any artificially introduced shRNA, was employed. However, the ubiquitination levels were not changed in these conditions (Fig. 22I). This indicates that altered ubiquitination of MARVELD2 is indeed dependent on the induced USP53 depletion rather than doxycycline treatment

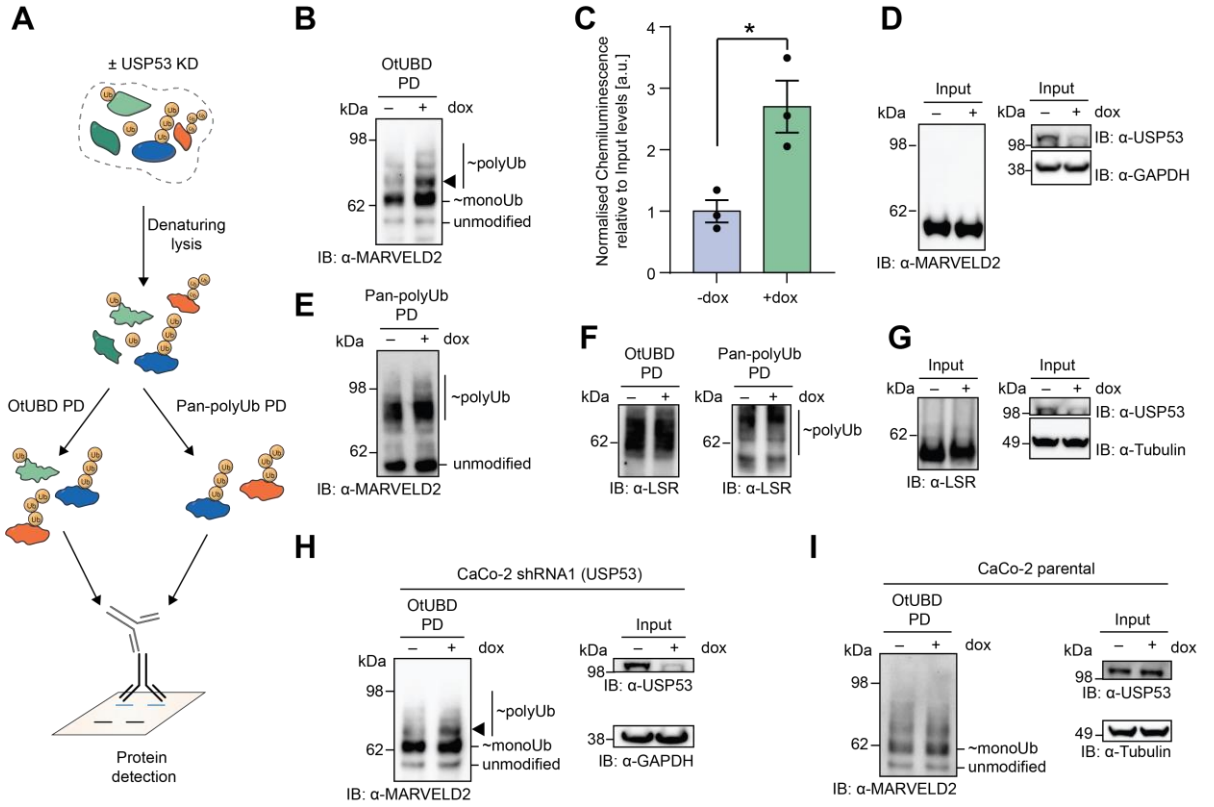

Figure 22. Change in ubiquitination pattern on substrates of USP53 upon its depletion in CaCo-2 cells. (A) Model of isolation of the ubiquitinome with a pan-PolyUb binder or OtUBD after knockdown of *USP53*. **(B)** Change in ubiquitination of MARVELD2 after USP53 depletion with *USP53*-targeting shRNA#5. The arrow indicates the MW of diubiquitinated MARVELD2. **(C)** Analysis of diubiquitin-modified MARVELD2 signal after isolation with OtUBDs in three independent experiments. The chemiluminescence signal from diubiquitinated MARVELD2 in the OtUBD pulldown was normalised to the MARVELD2 levels in the input for each condition and repeat and subsequently normalised. **(D)** Analysis of protein levels in cell lysate for samples processed in panel (B). **(E)** Analysis of ubiquitinated MARVELD2 after pan-PolyUb pulldown. **(F)** Analysis of ubiquitinated LSR after OtUBD- or pan-polyUb pulldown upon USP53 depletion. **(G)** Analysis of protein levels in cell lysate for samples processed in panel (F). **(H)** Same assay as in panel (B) with the *USP53*-targeting shRNA #1. **(I)** Same assay as in panel (B) and (H) with the parental CaCo-2 cell line not expressing *USP53*-targeting shRNA. All experiments were typically repeated at least once and showed similar results. For statistical analysis, the experiments were repeated twice. The asterisk indicates a *p*-value of 0.0209 in a two-tailed unpaired t-test.

Following the demonstration that USP53 specifically cleaved K63-linked ubiquitin chains *in vitro*, we hypothesised that USP53 depletion should mainly facilitate emergence of this chain type on MARVELD2 and LSR. To test this hypothesis, the selective K63-polyUb binder Rx3A7 (Fig. 23A) was utilised. The results obtained demonstrated indeed an increase in K63-linked chains on MARVELD2 in the absence of USP53 (Fig. 23B). Consistent with observations made in figure 22 no such change in K63-polyUb was detected for LSR (Fig. 23C).

In conclusion, I could orthogonally verify MARVELD2 ubiquitination, highlighting the most prominent influence of USP53 presence on diubiquitinated MARVELD2.

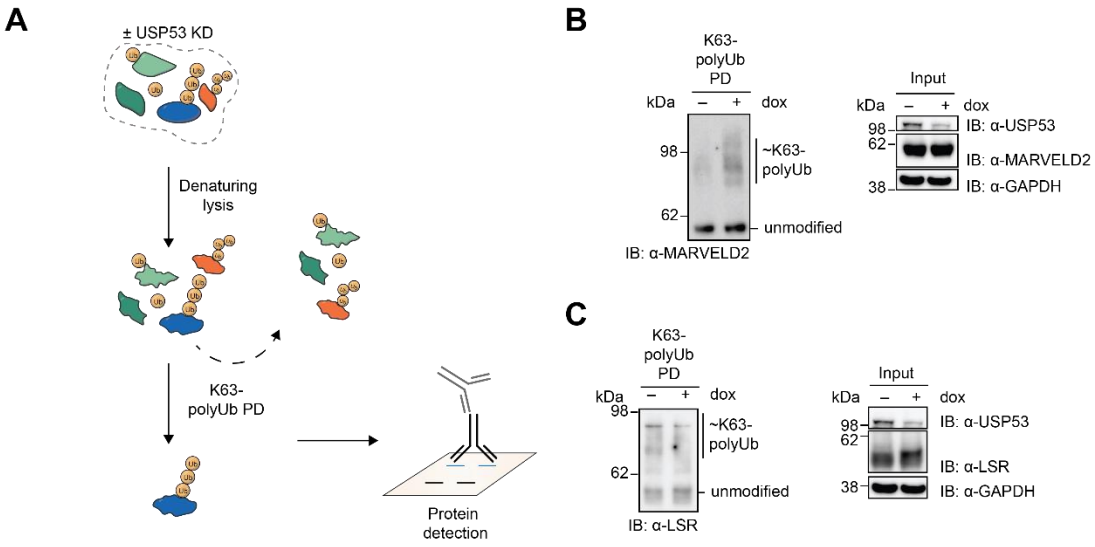

Figure 23. Change in K63-linked ubiquitin chains on substrates of USP53 upon its depletion in CaCo-2 cells. (A) Isolation method to enrich K63ylated proteins in the assay. **(B)** Change in K63-linked ubiquitin chains bound to MARVELD2 upon knockdown of *USP53* in CaCo-2 cells and isolation with Rx3A7, the K63 polyUb enrichment tool. **(C)** K63-linked ubiquitin chains on LSR upon knockdown of USP53. Proteins decorated with K63-linked ubiquitin chains were isolated with the ubiquitin binder Rx3A7 from CaCo-2 cell lysate. The depletion of USP53 was induced using doxycycline in the CaCo-2 cell line harbouring the *USP53*-targeting shRNA #5.

3.3.5 Ubiquitin chain restriction analysis identifies ubiquitin chain types on the putative USP53 substrate MARVELD2

Ubiquitin chain restriction (UbiCRest) analysis has emerged as a method to analyse the ubiquitin decoration of proteins (Hospenthal et al., 2015). In this method, DUBs with distinct specificity for the cleavage of certain ubiquitin chains are employed to digest ubiquitin chains on proteins to allow for analysis of these chains. This method was first established to identify specificity of E3 ligases *in vitro* (Hospenthal et al., 2015) but has since been expanded to the characterization of ubiquitin chains of proteins expressed in various cell types (Panda & Gekara, 2018). I intended to employ this system to investigate the ubiquitin chains on putative USP53 substrates that emerged following the depletion of the DUB.

Since the OtUBD reagent has not been utilised in UbiCRest studies, a suitable protocol needed to be established that would allow for an efficient ubiquitin chain digestion. To this end, three different approaches were tested (Fig. 24). Approach (i) entailed the initial incubation of cell lysate with the enzymes, prior to the isolation of ubiquitinated species. In approach (ii), the ubiquitinated protein species were first isolated before the enzymes were added to the beads. In the (iii) approach, ubiquitinated proteins were first isolated, then the bound proteins were eluted using acidic elution and finally, the eluted protein suspensions were neutralised and enzymes added. To assess the efficacy of these approaches, MARVELD2 was selected as protein of interest with the catalytic domain of USP2 and Lambda

Phosphatase (λPP) as the enzymes of choice. USP2 represented a highly active and promiscuous DUB which would allow to assess whether the high MW weight species of MARVELD2 that we deemed to be ubiquitylated MARVELD2, were indeed ubiquitylated forms of the proteins and to test if ubiquitin chains on the protein of interest were accessible for cleavage. λPP was included to assess whether the isolated species are phosphorylated forms of the proteins.

The findings demonstrated a collapse of high-MW species of MARVELD2 upon addition of the catalytic domain of USP2, both in native lysis (i) and following acidic elution (iii, Fig. 24). For the cleavage of ubiquitin chains on beads (ii), the DUB exhibited a minimal effect, which can be attributed to the protective effects of the pulldown reagent - consistent to observations made for pan-PolyUb binders (Hjerpe et al., 2009). As anticipated, the unmodified variant of the protein was not detected in the pulldown when the enzyme treatment was done prior to isolation with only a marginal increase of free protein in the supernatant (SN, Fig. 24i). This finding is consistent with the prevailing notion that the ubiquitinated fraction of a protein at any given moment is generally low. Notably, while the addition of λPP did not lead to a collapse of high MW species of MARVELD2, it resulted in a slight reduction in size of the deubiquitylated species (Fig. 24i), indicating that the isolated MARVELD2 was ubiquitinated and phosphorylated.

In summary, I concluded that the sequential elution, neutralisation and enzymatic digestion was the favourable experimental setting since it enabled the circumvention of the protection effects of the binders. Furthermore, DUB activity correlated with the emergence of unmodified protein species supporting the conclusion that the isolated MARVELD2 species were in fact ubiquitylated proteins (Fig. 24iii).

Having established the UbiCRest assay on samples enriched with the OtUBD reagent, the subsequent aim was to expand this setup to linkage-specific DUBs to investigate the type of ubiquitin-linkage that has emerged on MARVELD2 upon USP53 depletion. To this end, a panel of DUBs was set up which demonstrate differential cleavage of ubiquitin chains. Their specificity was assessed *in vitro* in the post-elution buffer over a range of concentrations. This panel included the promiscuous and highly potent catalytic domain of the DUB USP2, the reportedly K48-linkage specific DUB OTUB1 and K63-linkage specific DUBs OTUD1 and AMSH, as well as two differently linked polyubiquitin chains. For OTUB1 and AMSH, enzymes were used that demonstrated improved properties, as indicated by the asterisk: OTUB1 has been fused to the inactive E2 UBE2D2 resulting in OTUB1* while AMSH has been fused to mSTAM2 VHS-UIM yielding AMSH* (Michel et al., 2015).

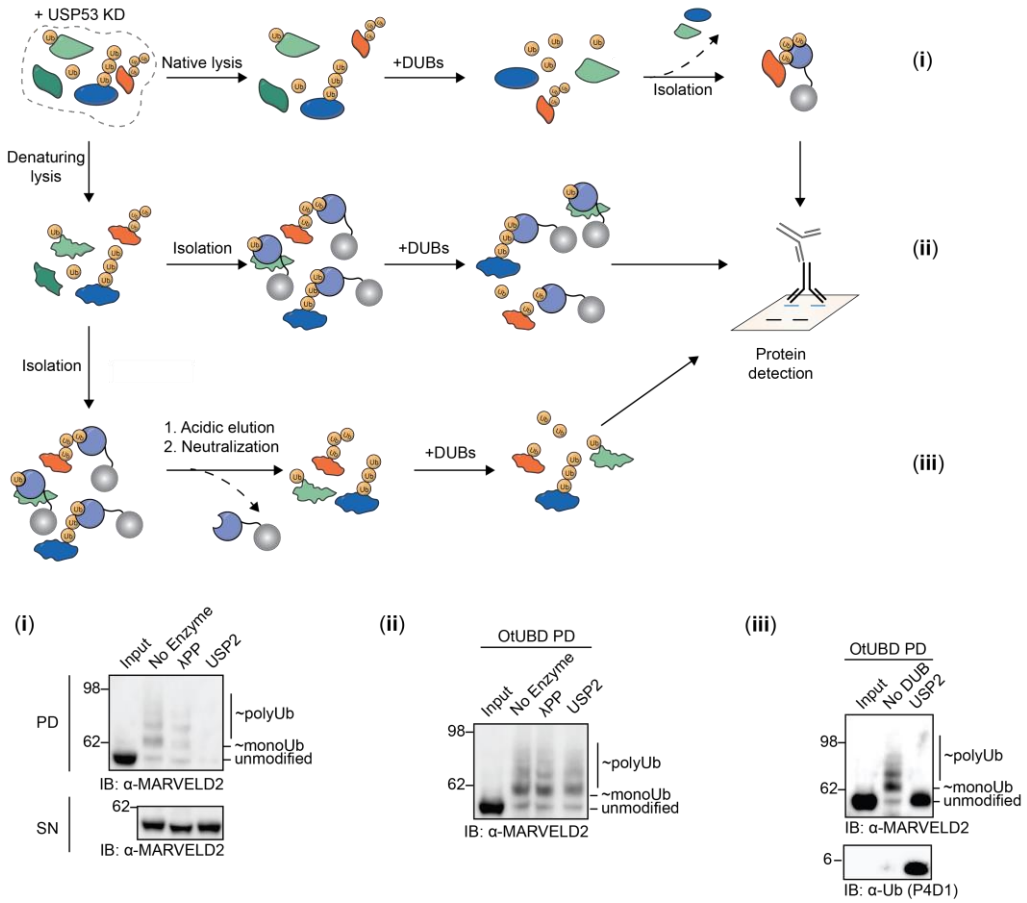

Figure 24. UbiCRest variations to investigate the nature of high MW species on potential DUB substrates extracted from cells. Model of three different setups to investigate high MW species in an UbiCRest related manner in cell lysate from CaCo-2 cells depleted of USP53. The methods differ in lysis condition, sequencing of isolation and DUB addition as well as in elution steps. **(i)** Native lysis of cells is followed by addition of the indicated enzymes. Following enzyme treatment, the cellular ubiquitinome was isolated using the ubiquitin binder OtUBD. Subsequently, ubiquitylation levels of MARVELD2 were analysed by Western Blot. **(ii)** Denaturing lysis is followed by isolation with the ubiquitin binder OtUBD. The indicated enzymes were added directly to the proteins immobilised on the beads before the analysis of MARVELD2 ubiquitination by Western Blot. **(iii)** Denaturing lysis is followed by isolation of the cellular ubiquitinome with the OtUBD reagent. Ubiquitinated proteins were eluted from the ubiquitin binder with acidic elution before the suspension was neutralised and the indicated enzymes were added. The cell line used for all experiments shown here was CaCo-2 shRNA #5. PD: pulldown, SN: supernatant.

USP2 was found to cleave both, K48- and K63-linked homotypic chains, as evidenced by the disappearance of high MW bands and the emergence of free ubiquitin as indicated in the Coomassie-stained gel. OTUB1* was found to cleave K48-linked chains with a notably reduced capability to process diubiquitin (Fig. 25A). AMSH* could be validated as a highly active K63-specific DUB with no processivity of K48-linked chains across the tested range of concentrations (Fig. 25A). OTUD1 was identified as a highly potent K63-processing enzyme that shows processivity of K48-linked chains at modest enzyme concentrations (Fig. 25A). With this experiment, the appropriate enzyme concentrations for the subsequent experiments in our conditions were determined.

The following UbiCRest experiments investigated the identity of the ubiquitin chains on MARVELD2. To this end, the ubiquitinome was isolated with OtUBD prior to acidic elution and neutralisation as tested in Fig. 24. Subsequently, the enzymes were incubated with the eluate with the concentrations determined in Fig. 25A. While USP2 incubation led to complete collapse of the ubiquitin chain, resulting in unmodified MARVELD2, OTUB1* did not alter the ubiquitin chain on the protein (Fig. 25B). AMSH* led to the emergence of a stronger monoubiquitinated MARVELD2 band, as would be expected for a DUB with high linkage specificity cleaving ubiquitin from a protein decorated with a K63-linked chain and contributions from S1 as well as S1' side (Shrestha et al., 2014, Fig. 25B). Surprisingly, OTUD1 led to the emergence of the unmodified substrate. This finding is consistent with the hypothesis that MARVELD2 is decorated with K63-linked ubiquitin, yet suggests that the interaction between the S1' site of OTUD1 and the proximal ubiquitin is less important for catalysis (see also Mevissen et al., 2013). Importantly, the results indicate that K63-linked ubiquitin chains are the most prevalent ubiquitin chain on MARVELD2 upon depletion of USP53.

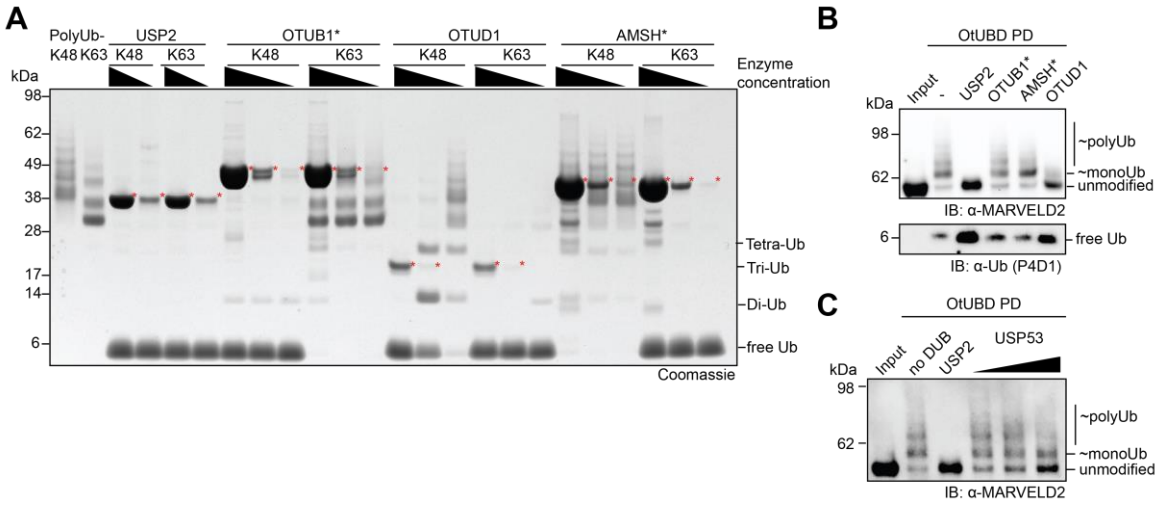

Figure 25. UbiCRest assays to investigate ubiquitin chain composition on MARVELD2 upon USP53 depletion. (A) *In vitro* assay to investigate specificity range for cleavage of PolyK48- and PolyK63-linked ubiquitin chains by different DUBs used throughout the thesis. The chains were incubated with the respective enzymes before cleavage was analysed by SDS-PAGE and Coomassie staining. The concentrations used were 5 and 1 µM for USP2, 20, 2 and 0.2 µM for both, OTUB1* and AMSH*, and 2, 0.2 and 0.02 µM for OTUD1. The red asterisk indicates the position in the gel at which the respective DUB is found. **(B)** UbiCRest assay with the ubiquitinome of CaCo-2 cells upon USP53 depletion after denaturing lysis, isolation with the ubiquitin binder OtUBD and acidic elution. Enzyme concentrations were 1 µM for USP2, 0.2 µM for both OTUB1* and AMSH* and 0.02 µM for OTUD1**. (C)** *En bloc* cleavage mechanism of the catalytic domain of USP53 (0.5, 2 and 5 µM) shown for its substrate MARVELD2 upon incubation for 2 h at 37 °C.

In order to investigate whether the catalytic domain of USP53 has the capacity to remove ubiquitin chains from the ubiquitinated and thus isolated MARVELD2, I incubated purified

USP53^{cat} with the isolated ubiquitinome and blotted for MARVELD2 (Fig. 25C). The results obtained from this process clearly demonstrated the emergence of unmodified MARVELD2 after incubation with increasing concentrations of the DUB of interest. This outcome is consistent with the observations from *in vitro* studies, which demonstrated that USP53 possesses the ability to cleave ubiquitin *en bloc* from proteins (Wendrich et al., 2024).

Collectively, the demonstrate that, upon USP53 depletion, K63-linkages on the tricellular protein MARVELD2 increase, suggesting it to be a cellular substrate of the DUB. Furthermore, we have demonstrated that USP53 predominantly cleaves ubiquitin completely from substrates.

3.3.6 Assessing the effect of ubiquitination of MARVELD2 in the context of endocytosis

I set out to explore the effects of increased ubiquitylation of MARVELD2 upon depletion of USP53. Since the most prominent outcome of K63-linkage addition to transmembrane proteins located in the plasma membrane is altered presence at the membrane by means of endocytosis (Erpapazoglou et al., 2014), I assessed whether endocytosis of MARVELD2 is effected upon USP53 knockdown (Fig. 26).

To this end, CaCo-2 cells depleted from USP53 were incubated with sulfo-NHS-SS-biotin, a water-soluble reagent that cannot pass the plasma membrane which labels primary amines of the extracellular domains of transmembrane proteins. The extracellular biotin is susceptible to cleavage by a reducing agent, such as sodium 2-mercaptoetanesulfonate (MESNA), while endocytosed biotin-labelled proteins are protected from this cleavage. The levels of endocytosis can be inferred from the levels of biotinylated protein still present after treatment with the reducing agent. Thus, utilising streptavidin-based isolation of biotinylated proteins, I was able to assess the amount of endocytosed and plasma-resident proteins (Fig. 26A). The results obtained demonstrated that a substantial proportion of the protein underwent internalisation following a 30 min period (Fig. 26B). However, no difference in internalised MARVELD2 was detectable between USP53-depleted and non-depleted cells using this approach (Fig. 26B).

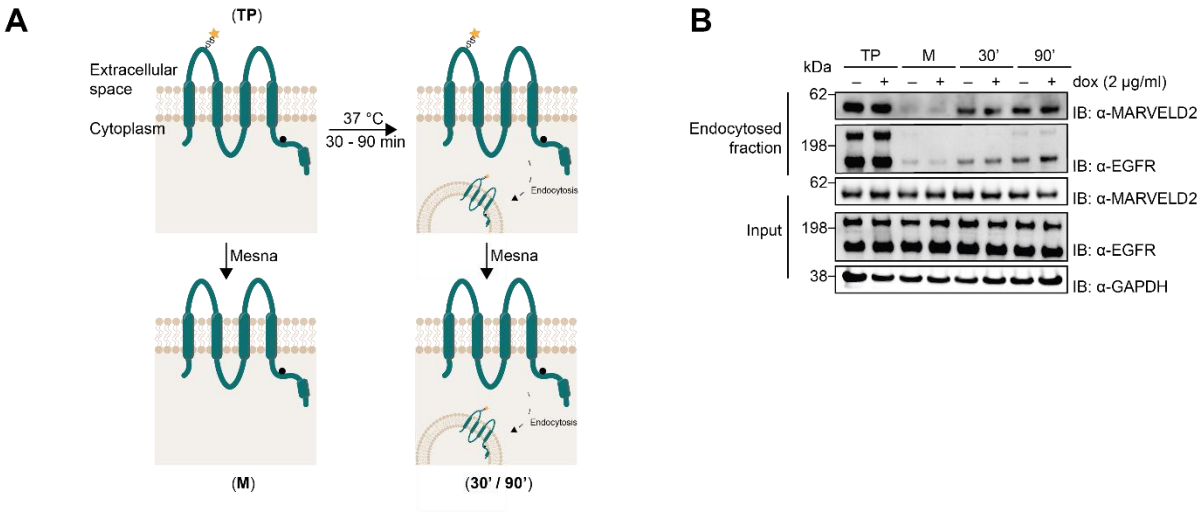

Figure 26. Influence of increased K63-linked ubiquitin chains on endocytosis of MARVELD2 after USP53 depletion. (A) Model for experimental setup for endocytosis analysis. The star represents the biotin fragment of the reagent Sulfo-NHS-SS-Biotin. **(B)** Visualisation of the fractions for either total surface protein (TP), control samples (M) or samples for which endocytosis was allowed to proceed for either 30 min (30') or 90 min (90'). Biotinylated proteins were isolated from CaCo-2 cell lysate using agarose beads functionalised with streptavidin to yield samples M, 30' and 90'.

In summary, the results presented in this subchapter have yielded substrates of USP53 which allow an association of the observed pathologies in human patients with the activity of this intricate USP DUB. In doing so, the experiments provided an example how ubiquitin binders can complement the commonly employed method of diGly substrate identification, thereby facilitating a more profound comprehension of the impact of enzymes on ubiquitin decoration of proteins. Future research directions include investigating whether the intricate cleavage mechanism is necessary for controlling cellular processes that MARVELD2 and LSR are involved in. These considerations along with other implications of the research will be discussed in more depth in chapter 4.3.

3.4 Characterization of the Cellular Role of the Human DUB USP54

Similar to USP53, the DUB USP54 has been linked to diseases albeit lacking mechanistic understanding. Altered gene expression of USP54 has been associated with cancer progression since USP54 was found to be overexpressed in colorectal cancer stem cells (Fraile et al., 2016) and castration-resistant prostate cancer (Zhou et al., 2024), while it appears to inhibit adenocarcinoma progression (Chen et al., 2024). We thus attempted to provide a better understanding of the cellular role of USP54.

3.4.1 Total proteome analysis of the prostate cancer cell line PC-3 upon USP54 depletion reveals proteins regulated by the DUB

In order to study cellular USP54 function, cell lines suitable for investigations into its functions needed be stablished. To this end, mRNA and protein levels of USP54 were determined by quantitative reverse transcription polymerase chain reaction (RT-qPCR) and Western Blot across a panel of cell lines.

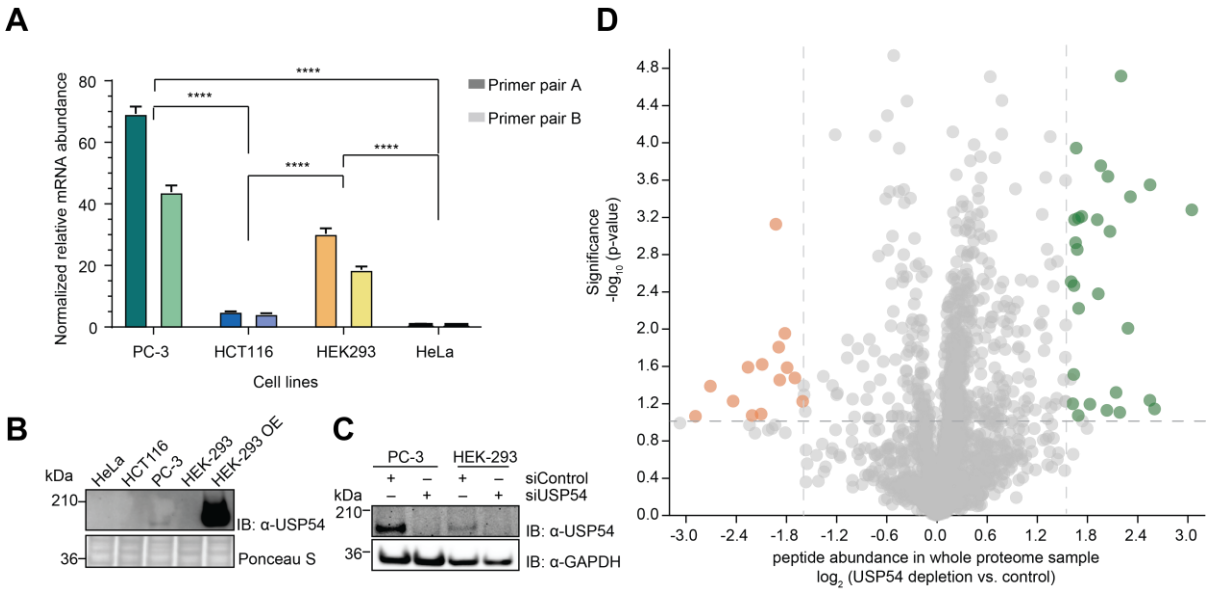

Figure 27. Cells of the prostate cancer cell line PC-3 show elevated levels of USP54. (A) qPCR-based evaluation of mRNA levels of *USP54* mRNA, across a small panel of cell lines with two different primer pairs (indicated by differently coloured bars). Values were normalised to expression levels in HeLa cells. Statistical testing was done using two-way ANOVA with **** representing an adjusted *p*-value <0.0001. **(B)** USP54 protein levels in different cell lines. HEK-293 OE represents transient overexpression of human USP54 in the cell line by transfection. **(C)** Comparison of protein levels and knockdown efficiencies of USP54 in the two cell lines with the highest *USP54* mRNA levels. **(D)** The volcano plot depicts proteins with altered abundance upon depletion of USP54. The depletion was induced with a pool of siRNAs and incubation for 48 h in PC-3 cells before cell lysis and whole proteome analysis. Proteins were highlighted in green or orange dependent on whether their abundance either increased or decreased upon depletion of the DUB.

Given the reported role of USP54 in colorectal and prostate cancer (Fraile et al., 2016; Zhou et al., 2024), mRNA levels between the colorectal cancer model cell line HCT116, the prostate cancer model cell line PC-3 and the commonly employed embryonic kidney cell line HEK-293, as well as the cervical cancer cell line HeLa were compared to identify cell lines high in USP54 (Fig. 27A-C). The mRNA levels between these cells varied significantly with the highest expression profiles observed for PC-3 and HEK-293 cells (Fig. 27A). While no USP54 protein was detected in HeLa and HCT116 cells, a faint band was observed in HEK-293 with highest protein levels detected in PC-3 cells (Fig. 27C). The identity of this band was determined to be USP54 by ectopic expression of a gene construct corresponding to USP54 (Fig. 27B) and siRNA-mediated knockdown (Fig. 27C). Based on the elevated amounts of USP54 detected in PC-3 cells, these cells were chosen for further investigations.

A major function of ubiquitination is the regulation of protein degradation. As such, I first assessed whether the depletion of USP54 led to changes in protein abundance. This was achieved by performing a total proteome analysis in cells depleted of USP54 by siRNA in PC-3 cells (Fig. 27D). Following protein precipitation and a combination of trypsin- and Lys-C-catalysed digestion and data-dependent acquisition, 2736 proteins were identified with 40 proteins displaying significant changes in total protein levels after USP54 depletion (Fig. 27D). Of note, many of the proteins that showed significantly lowered abundance, possess transmembrane domains (Table 3). There was a notable increase in the abundance of DTX3L, an E3 ligase that is involved in DDR (Yan et al., 2009), interferon-mediated antiviral responses (Zhang et al., 2015) and required for the recruitment of several proteins to endosomes (Holleman & Marchese, 2014). Furthermore OTUD6B, a DUB regulating protein synthesis, cyclin D1 translation and c-MYC protein stability (Sobol et al., 2017). However, these experiments did not yield a clear indication of the cellular processes or location that USP54 is involved in.

Table 3. Proteins with lowered or elevated abundance in PC-3 cells upon USP54 depletion. Proteins with a transmembrane domain are marked with an asterisk. The annotations were extracted from UniProt (The UniProt Consortium, 2025).

Reduced			***Increased***		
$-\log_{10}$ (*p*-value)	**$\log_2$ (Fold change)**	**Gene name**	**$-\log_{10}$ (*p*-value)**	**$\log_2$ (Fold change)**	**Gene name**
1.62	-2.09	MAGT1*	3.18	1.65	OTUD6B
1.07	-2.21	DPAGT1*	1.51	1.64	DBI
1.23	-1.61	PSAP	1.20	1.62	UCK2
1.46	-1.88	ATP5J2	2.47	1.64	COPS6
1.09	-2.10	TMEM205*	2.22	1.69	HSF1

Reduced			*Increased*		
-log$_{10}$ (*p*-value)	**log$_2$ (Fold change)**	**Gene name**	**-log$_{10}$ (*p*-value)**	**log$_2$ (Fold change)**	**Gene name**
3.13	-1.93	QDPR	3.21	1.73	DNM1L
1.23	-2.44	ATP2B4*	3.55	2.55	IFIT3
1.48	-1.70	SEC61B*	4.72	2.20	HAT1
1.07	-2.89	PLP2*	2.93	1.66	AKR7A2
1.39	-2.71	YIPF6*	2.38	1.93	ACSL4*
1.81	-1.89	SLC35E1*	1.24	2.55	HEXIM1
1.59	-1.79	CLPTM1L*	3.05	2.07	IFIT1
1.95	-1.82	EIF2B3	1.32	2.14	COX5B
1.59	-2.26	C1orf123	1.19	1.83	RPA2
Increased			3.28	3.05	MX1
-log$_{10}$ (p-value)	**log$_2$ (Fold change)**	**Gene name**	3.75	1.96	RRM2
3.19	1.69	OAS3	3.42	2.31	GBP1
1.13	2.03	NTMT1	3.17	1.92	TMPO*
1.11	2.18	HIGD2A*	2.01	2.28	SF3B4
2.51	1.60	UQCR10*	1.14	2.60	CARM1
3.64	2.04	SAMHD1	1.07	1.69	TOM5*
2.86	1.68	SNX5	3.94	1.66	DTX3L

3.4.2 Elucidating the microenvironment of USP54 using proximity labelling

Due to this lack of a strong indicator of the role of USP54 in the total proteome, I sought to understand the cellular role of USP54 by identifying its interaction partners and microenvironment. To this end, proximity labelling was used in HEK-293 cells (Roux et al., 2013). In this approach, a biotin ligase is fused to a protein of interest which, in presence of biotin, biotinylates nearby proteins with a radius of approximately 10 nm (Kim et al., 2014). Thereby, this method allows for the identification of candidate interactors and provides information on proteins in close proximity, sometimes also referred to as 'microenvironment' of the protein of interest. The improved biotin ligase BioID2 (Kim et al., 2016) was fused to the N-terminus of USP54, and the generated fusion protein was then ectopically expressed in HEK-293 cells. The process of protein biotinylation was induced by supplementing the medium with biotin prior to the enrichment of biotinylated proteins with streptavidin-based pulldown reagents and the subsequent submission of the resulting peptides to mass spectrometry after digestion (Fig. 28A). The positioning of the biotin ligase in close proximity to the catalytic

domain at the N-terminus of the protein was furthermore reasoned to promote the labelling of substrates.

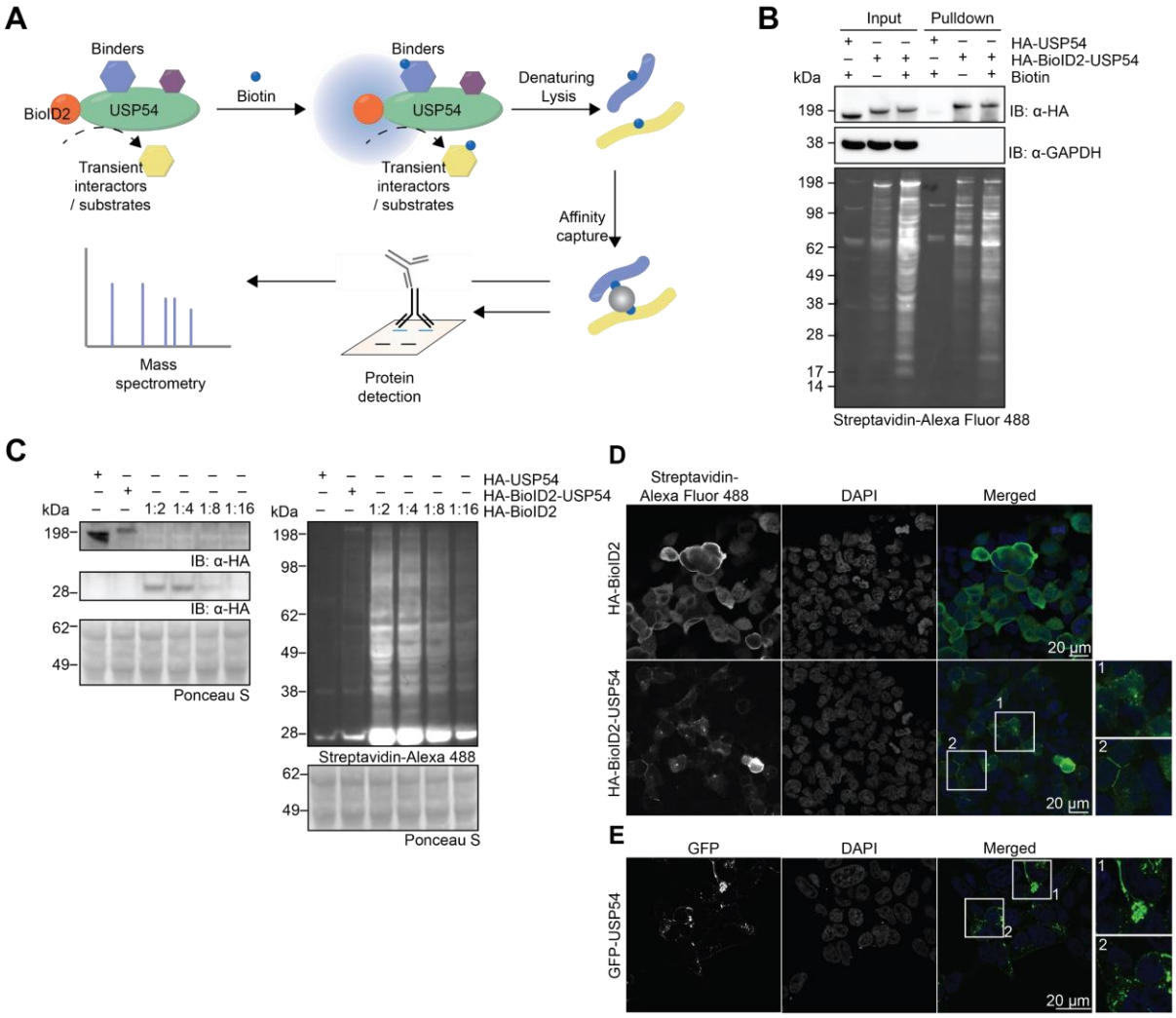

Figure 28. Setup of proximity labelling in HEK-293 cells to identify the interactors of USP54. (A) Schematic illustration of the proximity labelling experiment. **(B)** Detection of proteins ectopically expressed in HEK-293 cells and proteins biotinylated by the biotin ligase BioID2. To yield the PD fraction, biotinylated proteins were isolated from lysate using agarose beads functionalised with streptavidin. Biotinylation was induced by supplementation of biotin. Biotinylated proteins were detected in Far Western using Streptavidin coupled to the fluorescent dye Alexa Fluor 488. **(C)** Dilution series to identify suitable ratio to induce expression of BioID2 and USP54 as well as the BioID2-USP54 fusion protein. The ratio indicates the proportion of plasmid DNA encoding for the respective protein to 'empty' plasmid DNA. The levels were analysed by Western or Far Western blot while an equal loading was ensured by analysis of Ponceau Staining of the membrane. **(D)** Localisation of biotin-labelled proteins after expression of either USP54 fusion protein or BioID2 alone in HEK-293 cells and the subsequent addition of biotin to the medium. Inserts depict different patterns of signal. **(E)** GFP signal of GFP-USP54 fusion protein in HEK-293 cells. Inserts depict different patterns of signal.

In initial experiments, the properties of the established system were assessed. To this end, the proteins were ectopically expressed in the HEK-293 cells, biotin added to the medium and the biotinylated proteins isolated using streptavidin-coated beads. We observed biotinylation

of cellular proteins dependent on the transfection of a biotin ligase fusion protein that also correlated with the addition of biotin (Fig. 28B). Since fusion constructs of the biotin ligase are often expressed at lower levels than then ligase alone, titration experiments were performed to determine the optimal ratio of transfected plasmids (Fig. 28C) that ultimately would lead to equivalent amounts of biotinylated proteins.

In order to ensure that biotinylation, induced by the USP54 biotin ligase fusion protein, occurred in close proximity of cellular entities that USP54 localises to, the localisation of biotinylation signal upon expression of BioID-tagged USP54 was compared to the localisation of GFP-tagged USP54. To this end, confocal imaging with Alexa Fluor 488-tagged streptavidin was utilised to visualise biotinylated proteins and compared to the localisation of GFP-tagged USP54 (Fig. 28D). As anticipated, the expression of the USP54 fusion construct resulted in the biotinylation of cellular entities at endosome-like and cell-cell contact sites in HEK-293 cells. Conversely, the expression of BioID2 alone led to the biotinylation of entities throughout the cytoplasm (Fig. 28D). The localisation of biotinylated proteins thus indeed recapitulated the localisation of the GFP-USP54 fusion protein (Fig. 28E), thereby indicating that the BioID2-USP54 fusion construct performed biotin labelling in close proximity to the localisation of USP54.

For the identification of biotinylated proteins in mass spectrometry, three sets of samples were prepared. They ectopically expressed either BioID2-USP54, USP54 or the biotin ligase BioID2 alone. Biotinylation was induced by the addition of biotin 24 h before cell lysis. Subsequently, biotinylated proteins were enriched with streptavidin-functionalised beads, the enriched proteins were digested ‘on-bead’ and measured using DDA. The following analysis utilising *MaxQuant* and *Perseus* identified numerous proteins found to be differentially biotinylated (Fig. 29 A-B). With the application of stringent cut-offs, 57 proteins were identified that were significantly enriched in both comparisons, BioID2-USP54 versus HA-USP54 and BioID-USP54 versus BioID2 (Fig. 29C). The enriched proteins were found at the clathrin coat and endolysosomal membranes, centrosomes/centrioles and cell junctions (Fig. 29D-E, as well as table 4). They included several subunits of the heterotetrameric clathrin adaptor protein complexes 2 (AP2) and a subunit of the AP3 complex as well as TJP1 and TJP2. Among the centrosomal proteins that were identified were the polo-like kinase 1 (PLK1) which is a critical regulator of mitosis, CEP85, a regulator of centriole duplication, CEP55, a microtubule-bundling protein that associates with centralspindlin to control cell abscission, the K63-specific USP DUB CYLD as well as CEP135 and CSPP1, two proteins found at centriolar satellites, centrioles and cilia (Gupta et al., 2815). The cellular roles of the identified proteins are associated with clathrin-dependent endocytosis and receptor internalisation, microtubule cytoskeleton organisation and the cell cycle (Table 5).

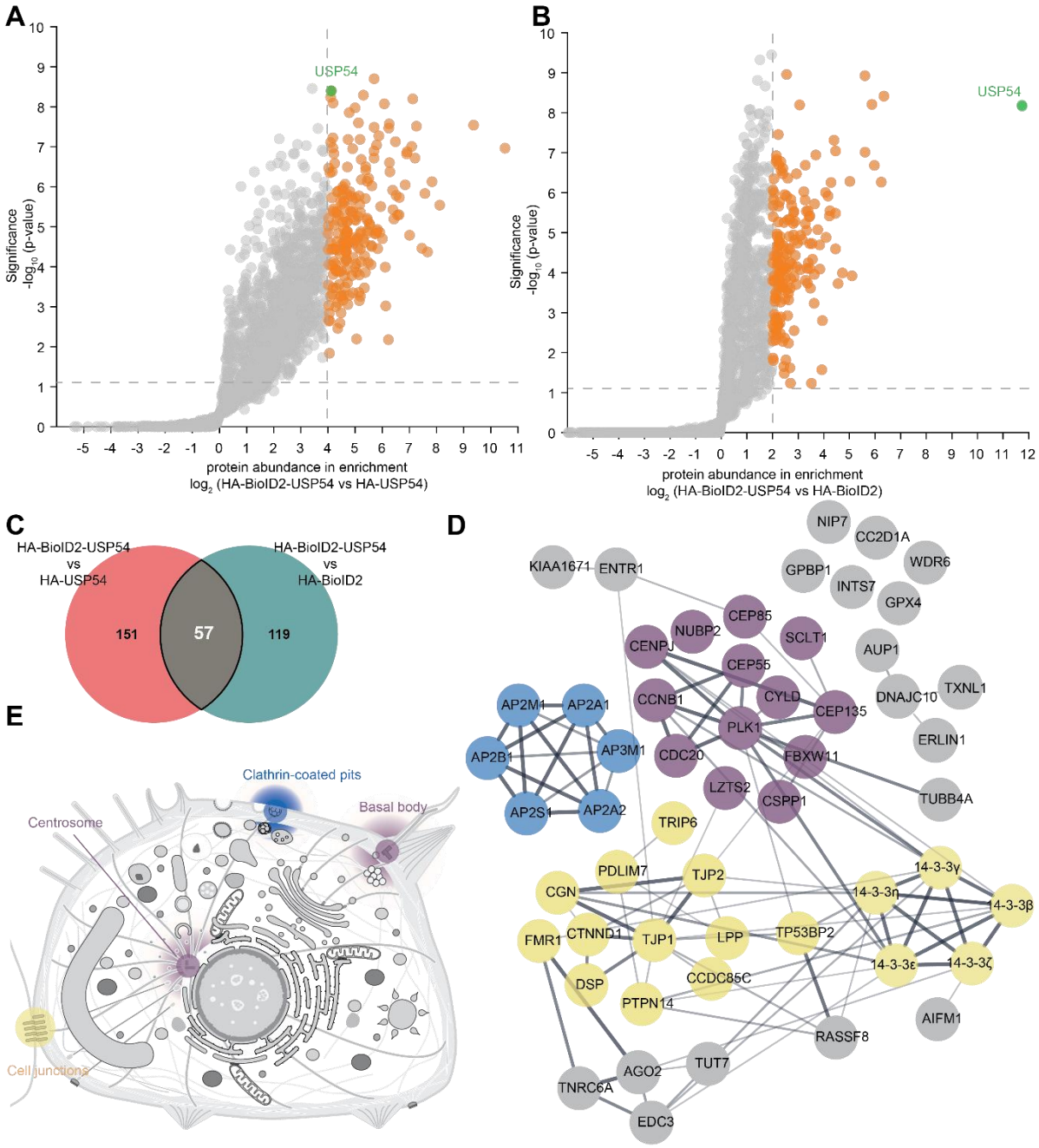

Figure 29. Proximity labelling reveals microenvironment and interactors of USP54. MS-based analysis of proteins biotinylated by the biotin ligase BioID2 upon supplementation with biotin. The biotinylated proteins were isolated from HEK-293 cell lysate using agarose beads functionalised with streptavidin. One-sided volcano plot depicting $\log_2$ fold-changes in protein abundance after streptavidin-based enrichment of biotinylated proteins in HEK-293 cells expressing HA-BioID2-USP54 versus cells expressing HA-USP54 (**A**) or HA-BioID2 (**B**). USP54 was labelled in green throughout both panels. Significance cut-offs were set to '0.05' for all of the plots. Proteins exceeding the set cut-offs were labelled in orange. (**C**) Venn diagram depicting the overlap between significantly enriched proteins in both statistical tests. For downstream analysis, I focused on the shared proteins. (**D**) STRING network cluster analysis of the 57 shared hits. The thickness of the edges represents strength of data support for an interaction of any given two proteins. Colouring was done according to g:Profiler-based annotations (Kolberg et al., 2023). (**E**) Cellular components that are linked to the proteins identified in proximity labelling experiments. The mammalian cell was extracted and changed from SwissBioPics (Le Mercier et al., 2022).

To complement the interactor identification by proximity labelling, I sought to identify interactors that strongly bind to USP54. To this end, GFP-based affinity-purification mass spectrometry (AP-MS) with GFP-USP54 as a bait protein was used (Fig. 30A). It should be noted that this method has inherent downsides, including the potential loss of information regarding cellular localisation and the inability to isolate transient interactors. However, when combined with information obtained from proximity labelling, the identification of interactors is facilitated with a high degree of fidelity. Subsequently, GFP-USP54 and GFP were ectopically expressed in HEK-293 cells and, utilising mild lysis and washing conditions, immunoprecipitated using GFP nanobodies (Fig. 30C). The bait and the isolated preys were subjected to mass spectrometry. Following data acquisition and statistical analysis, proteins that had previously been identified in the proximity study were highlighted (Fig. 30A-B). The most prominent hits were five of the seven 14-3-3 protein isoforms found in humans (14-3-3ζ, 14-3-3ε, 14-3-3γ, 14-3-3β, 14-3-3η). These were annotated as cell-cell junction proteins in Fig. 29D and table 4 but are reported to play a role in many cellular processes (Bridges & Moorhead, 2005). In line with their identification in AP-MS, eight positions within USP54 were consistently predicted as 14-3-3 interaction sites with high confidence by three independent interaction prediction methods (Table 6).

Table 4. Enrichment of proteins linked to cellular components as found by BioID experiments.

Clathrin coat / Endolysosomal membrane		**Centrosome / Centrioles**			
AP2M1	AP2S1	CENPJ	PLK1	CEP85	LZTS2
AP2A1	SCLT1	NUBP2	CEP55	CYLD	CCNB1
AP2B1	AP2A2	CEP135	CDC20	FBXW11	
AP3M1		CSPP1	SCLT1	CC2D1A	
Cell junction					
TRIP6	AP2A1	CTNND1	AP2B1	AP2A2	14-3-3ζ
LPP	14-3-3γ	PDLIM7	14-3-3ε	TP53BP2	
AP2M1	DSP	TJP2	TJP1	CCDC85C	
14-3-3η	FMR1	CGN	AP2S1	14-3-3β	

Table 5. Enrichment of proteins linked to biological processes as found by BioID experiments.

Clathrin-dependent endocytosis / Receptor internalization		**Microtubule cytoskeleton organisation**		
AP2M1	AP2A2	CENPJ	CDC20	LZTS2
AP2A1	FMR1	CEP135	CEP85	CCNB1
AP2B1		PLK1	CYLD	TUBB4A
AP2S1		CGN	FBXW11	

Cell cycle			
INTS7	PLK1	WDR6	FBXW11
CENPJ	14-3-3ε	CEP85	LZTS2
CEP135	CEP55	TP53BP2	CCNB1
CSPP1	CDC20	CYLD	TUBB4A
Intracellular protein transport			
AP2M1	AUP1	PTPN14	AP2A2
14-3-3η	AP2B1	AP3M1	
AP2A1	14-3-3ε	AP2S1	

In addition to the components shared with the BioID experiments, the presence of many members of the chaperonin containing tailless complex polypeptide 1 (CCT) or tailless complex polypeptide 1 ring complex (TRiC) was noted. This complex is integral to the function of an essential eukaryotic molecular chaperon (Fig. 30B, Grantham, 2020). Furthermore, a number of centrosomal (NUBP2, LZTS2, FBXW11), cell-junction- (TJP2, TJP1) and clathrin-coat-associated (AP2B1, AP2M1, AP2S1, AP2A2) proteins were identified as significantly enriched with the stringent requirement of 16-fold enrichment over the background (Fig. 30A-B).

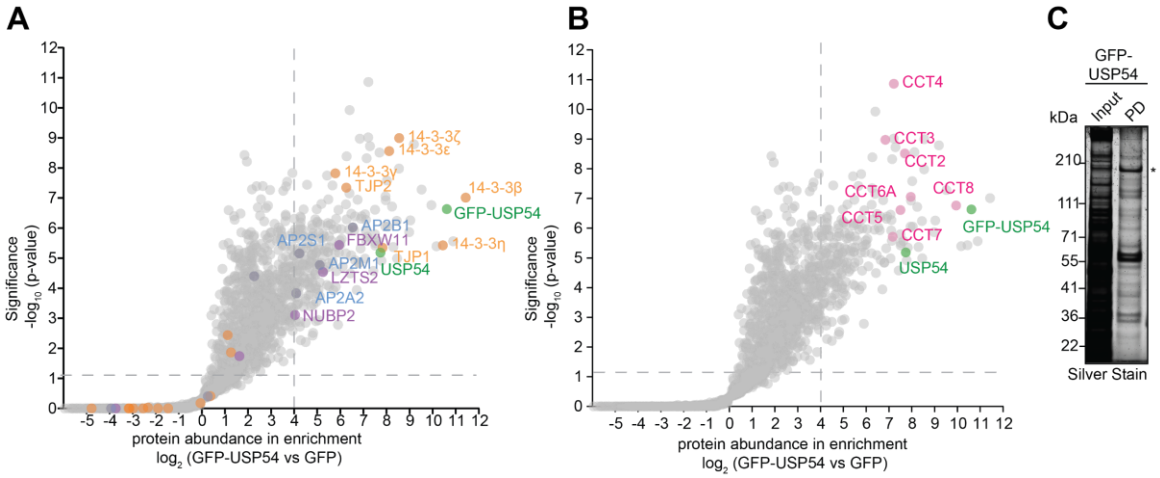

Figure 30. AP-MS reveals interactors of USP54 following GFP-based isolation from HEK-293 lysate. For affinity purification, the fusion protein emGFP-USP54 or emGFP alone were ectopically expressed in HEK-293 cells. Isolation of the respective proteins and their interactors was achieved using GFP-targeting nanobodies immobilised on agarose beads and mild lysis conditions. The isolated proteins were analysed in mass spectrometry. **(A)** One-sided volcano plot showing protein abundance in enrichment. Significance cut-off are set to '0.05' and '4' for log_2 fold change. Proteins are coloured according to proximity labelling results with proteins found at cell junctions coloured orange, proteins attributed to the centrosome in purple and proteins found at the clathrin-coat in purple. **(B)** Same one-sided volcano plot as shown in (A) with annotations for the components of the TRiC complex in hot pink. **(C)** Silver staining of gel depicting input and pulldown fraction of nanobody-based experiments isolating GFP-tagged USP54 from HEK-293 lysate experimental setup as in used for mass spectrometry-based proteomics (A) and (B). The asterisk indicates the MW which GFP-tagged USP54 is supposed to possess.

Table 6. Candidate 14-3-3 binding sites in USP54. The amino acid predicted to be phosphorylated and bound by the 14-3-3 protein is shown in brackets with the surrounding amino acids shown next to it. The sites were identified using a 14-3-3 prediction server (Madeira et al., 2015).

Position	Peptide [-6:4]	Position	Peptide [-6:4]
496	QAPRNA[S]KPSS	1362	MGRRLH[S]AHDP
670	SSERNS[S]SPVS	1420	RISRSL[S]GTVV
1156	FKDRSL[S]GSLR	1457	RCSSSS[S]LPVI
1163	GSLRKN[S]SPSD	1558	IGTRFL[T]TPGC

3.4.3 USP54 regulates the cell cycle and cytoskeleton organisation

Analyses of USP54 interactors and its microenvironment identified a number of proteins implicated in the regulation of the cell cycle, centrosome function and cytoskeleton organisation. To determine the function of USP54 in these processes, knockdown studies were conducted in the osteosarcoma cell line U2OS, a cell line frequently used to study these processes, with the objective to determine the influence of USP54 depletion on cell cycle progression and tubulin network structure by live-cell fluorescence microscopy. Tubulin staining revealed that cells exhibited a more peripheral and linearly organised tubulin network upon USP54 depletion while cells with physiological levels of USP54 displayed a much more centralised structure (Fig. 31A). This indicates that USP54 plays a critical role in microtubule organisation.

To allow for insights into the effect of USP54 depletion on cell cycle progression, U2OS cells were monitored for 18 h in live-cell microscopy and the number of cells were recorded that exhibited DNA condensation with subsequent chromosome alignment at the metaphase plate within this time span. This analysis revealed a substantial decline in cells entering M-phase (Fig. 31B), suggesting that USP54 fulfils a critical function not only in microtubule organisation but also cell cycle progression.

Proteins implicated in cell cycle progression are frequently subjected to phospho-regulation or modulation in protein abundance across different cell cycle stages (Vermeulen et al., 2003). In view of the observed phenotypes associated with *USP54* knockdown, I assessed whether protein levels of USP54 were altered throughout the cell cycle. To this end, U2OS cells were subjected to a double thymidine block or a thymidine block and nocodazole treatment, thereby arresting cells in G1/S phase or M-phase (Fig. 31D). The cells were then released for different time spans to obtain a homogeneous cell population with cells populating different cell cycle stages. With this approach, an elevated level of USP54 was observed in S/G2 phase and a reduced level in Prometa-, Meta- and Anaphase (Fig. 31E), largely mimicking the abundance

profile of the S/G2 cell cycle marker cyclin A (Müller et al., 2023). These findings indicate that USP54 protein abundance is regulated in a cell cycle dependent manner.

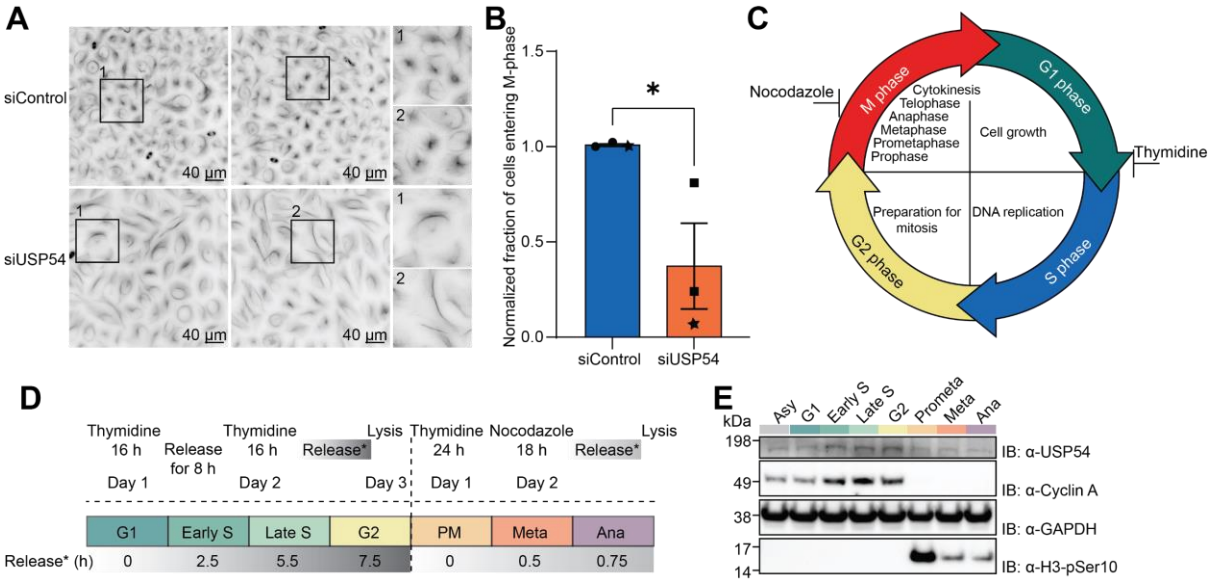

Figure 31. Influence of USP54 depletion on microtubule network and cell cycle progression in U2OS cells. (A) Representative image of the microtubule network after USP54 depletion using siRNA-mediated knockdown versus siRNA control sequence as visualised with SiR-tubulin. The U2OS cells were treated with siRNA and the respective dye 22 h and 1 h before image acquisition was started, respectively. **(B)** Relative quantification of cells entering mitosis over a time period of 18 h as visualized with SiR-DNA in three independent experiments (N=3). Analysis with an unpaired, two-tailed t test yielded a *p*-value of 0.04. In total, 2286 and 2242 cells were analysed for cells treated with control siRNA or *USP54*-targeting siRNA, respectively. The star indicates that data was acquired from an experiment which additionally included microtubule staining with SiR-tubulin. **(C)** Different phases of the cell cycle with annotation of the two compounds used for cell synchronisation in (D-E) that inhibit cell cycle progression at certain stages. Inspired by Ligasová et al. (2023). **(D)** Scheme showing the cell cycle arrest protocol with a dashed line separating mitotic phases from non-mitotic phases. Schedules for drug treatments were largely adopted from Bertsoulaki et al. (2022). **(E)** Western blot analysis of presence of USP54 throughout the cell cycle with the two cell cycle markers Cyclin A and H3-pSer10. The cells were captured in the different cell cycle stages using the protocol shown in (D). The experiment was repeated twice with similar results.

In order to identify the effect of USP54 depletion in mitosis and whether it exerts an effect at the G2/M transition, cells were arrested in G2/M-phase using RO-3306 (Vassilev, 2006), a well-characterised CDK1 inhibitor (Fig. 32A-B). For U2OS cells with physiological USP54 levels, the majority of cells demonstrated DNA condensation 30 min after release from RO-3306 (Fig. 32C). In cells where USP54 was depleted, this condensation took much longer and was observed less frequently, consistent with the results depicted in Fig. 31B. Furthermore, cells that underwent cell division despite USP54 depletion appeared to show reduced spreading of the tubulin network after division (Fig. 32D).

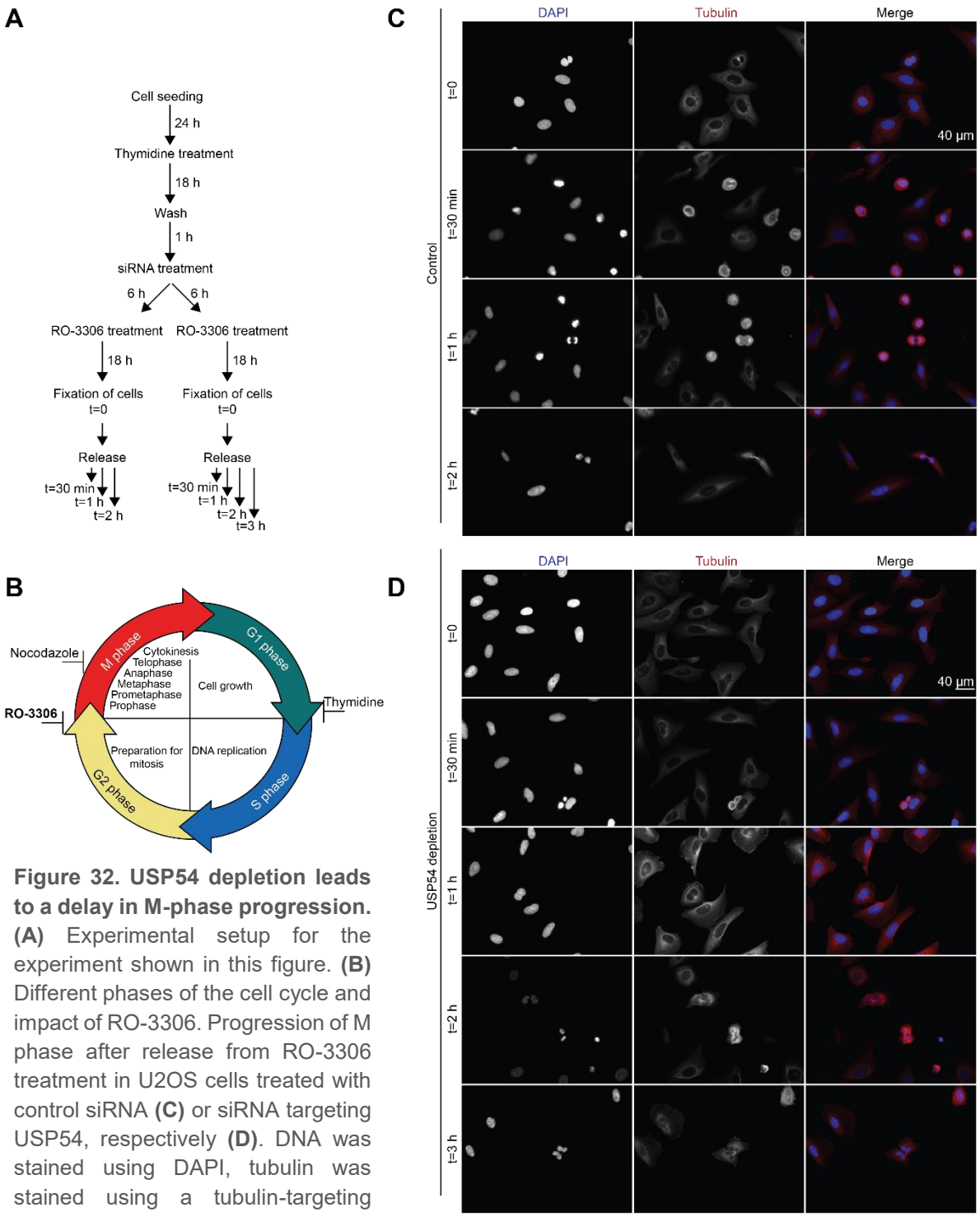

Figure 32. USP54 depletion leads to a delay in M-phase progression. **(A)** Experimental setup for the experiment shown in this figure. **(B)** Different phases of the cell cycle and impact of RO-3306. Progression of M phase after release from RO-3306 treatment in U2OS cells treated with control siRNA **(C)** or siRNA targeting USP54, respectively **(D)**. DNA was stained using DAPI, tubulin was stained using a tubulin-targeting antibody.

In mammalian cells, a pair of centrioles constitutes the core of the centrosome, a structure that is imperative for cell division. However, centrioles are also critical in the process of ciliogenesis as they function as a nucleating basal body for cilia (Kobayashi & Dynlacht, 2011). Consequently, a large number of proteins are shared between these structures (Dantas, 2020). Since centriolar proteins were identified in our BioID screen, I interrogated the role of USP54 on cilia formation upon serum starvation as monitored by confocal microscopy detecting acetylated tubulin (Fig. 33). To this end, GFP-USP54 was ectopically expressed in

RPE-1 cells and cilia formation manually assessed in cells that either did or did not display GFP signal. While 52.2% of the 180 RPE-1 cells without visible USP54 expression exhibited cilia formation, none of the cells expressing GFP-USP54 (n=9) displayed cilia formation. This finding demonstrated that USP54 not only influences microtubule organisation and cell cycle progression but also regulates cilia formation.

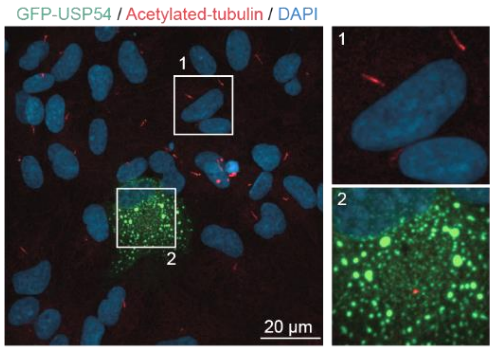

Figure 33. Effect of USP54 on cilia formation. Representative z-projection of confocal images of GFP-USP54 (in green), acetylated tubulin (in red) and DAPI (in blue) in RPE-1 cells are shown. Cells were serum starved for 24 h prior to fixation, immunostaining and subsequent visualisation. Insets are magnified images of dashed squares with the respective numbering.

3.4.5 U2OS cells expressing siRNA-resistant USP54 as a tool for future experiments to characterise cellular functions of the DUB

In view of the finding that transient overexpression of USP54 resulted in a heterogenous cell population with different protein levels, I set out to create stable cell lines with GFP-tagged USP54 variants. To facilitate rescue experiments, the USP54 mRNA should be resistant to commercially available siRNA used throughout the study that targets the endogenous DUB. The siRNA resistance (termed siR) was achieved through introduction of silent mutations in DNA coding for USP54 by splicing-by-overlap extension (SOE) PCR. To confirm the resilience of *USP54* mRNA to siRNA-mediated degradation, the DNA was transiently expressed in U2OS cells together with non-targeting or *USP54*-targeting siRNA. Subsequently, a comparison of the protein levels was conducted using Western Blot (Fig. 34A). The expression of the siR construct resulted in the presence of GFP-tagged USP54 even upon the addition of the siRNA in HEK-293 cells (Fig. 34A).

To create cell lines with a stable integration of siR GFP-USP54, U2OS Flp-In T-REx cells were employed. Following the integration and selection of clones, Western Blotting was used to identify clones that conditionally express our protein of interest (Fig. 34B). This analysis revealed the conditional expression of GFP, the GFP-tagged wild-type DUB and a catalytically inactive variant (Fig. 34B). The protein levels were adequately controlled by the addition of doxycycline for both variants (Fig. 34B). Due to the additional size of the GFP-tag, separation of the siRNA-resistant variants from endogenous USP54 was achieved utilising SDS-PAGE (Fig. 34C). It was determined that the protein levels upon induction of GFP-USP54 expression were only slightly higher than endogenous levels. While the levels of endogenous USP54 were

strongly reduced upon knockdown, both wild-type and catalytically inactive constructs were insensitive to siRNA treatment (Fig. 34C).

In conclusion, the established system provides a suitable tool with which to study USP54 in U2OS cells.

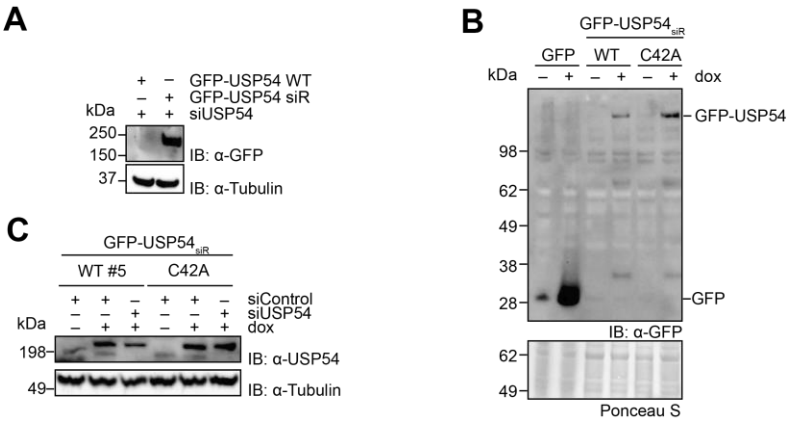

Figure 34. Generation of U2OS cells that conditionally express siRNA-resistant GFP-USP54. **(A)** Transient overexpression of vectors with (siR) or without (WT) mutations in *USP54* that render the sequence insensitive to the siRNA in HEK-293 cells. Both shown in a knockdown background. **(B)** Stable U2OS Flp-In T-REx cells allow for conditional expression of GFP and GFP-USP54$_{siR}$ upon addition of 1 µg/ml doxycycline as visualised by Western Blot. **(C)** Assessment of USP54 levels upon siRNA-induced knockdown of *USP54* in the U2OS Flp-In T-REx cells. Doxycycline was added to induce expression of the siRNA resistant mutants where indicated. Note the size difference between endogenous and GFP-tagged siRNA-resistant USP54. The cells for the overexpressed USP54$_{siR}$ stem from single-colony clone #5.

3.4.6 Localisation of USP54 and the impact of C-terminal domains on localisation

Given the indications of the microenvironment of USP54 and its associated phenotypes, I addressed the paucity of information regarding the subcellular localisation of USP54 using confocal microscopy. To this end, endogenous and GFP-tagged USP54 were visualised by immunofluorescence (IF) in HEK-293, HeLa and U2OS cells. Endogenous USP54 and transiently overexpressed GFP-USP54 displayed a cytosolic punctae-like localisation, resembling endosomal structures (Fig. 35A-E). GFP-USP54 stably expressed from a U2OS Flp-In T-REx cell line also formed cytosolic punctae (Fig. 35F). However, the GFP signal was predominantly present at a structure, which, owed to its position and doublet properties resembled centrosomes. Although some differences were observed in the patterns, in all cases, USP54 was found in cytosolic punctae.

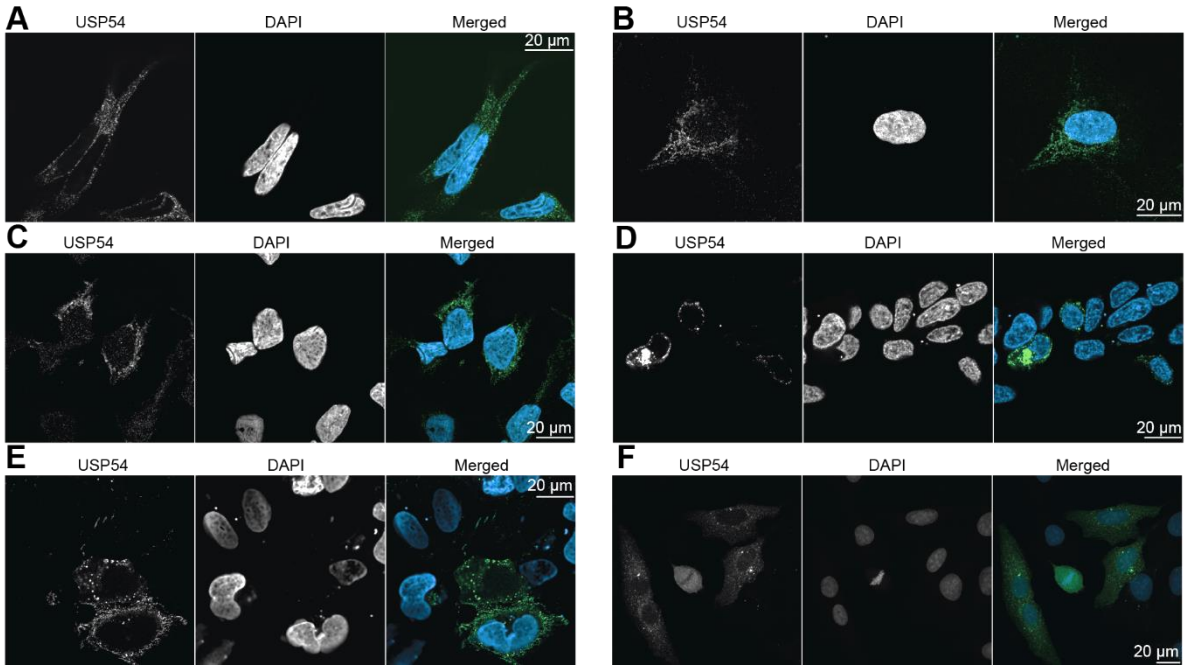

Figure 35. Evaluation of the localisation of USP54 using confocal microscopy. Localisation of endogenous USP54 in HeLa **(A)**, HEK-293 **(B)** and U2OS **(C)** cells visualised using the USP54-binding antibody HPA047663. Ectopic expression of GFP-USP54 was achieved using transient expression and was visualised utilising the GFP signal in HEK-293 **(D)** and U2OS **(E)** cells. U2OS Flp-In T-REx cells with stably integrated DNA, coding for GFP-USP54 are shown in **(F)** for which USP54 visualisation was achieved using their GFP signal with confocal microscopy.

Given its complex localisation and findings that highlight the capacity of C-terminal fragments to bind to specific proteins, I sought to determine critical factors of USP54 localisation encoded in its C-terminus. To this end, fragments of various lengths were created starting with the catalytic domain alone that was tagged with GFP. Other fragments included the short N-terminal sequence preceding the catalytic domain, the region between the catalytic domain and the annotated coiled-coil, the coiled-coil and MIT domain itself, and the remaining stretch of the C-terminus (Fig. 36A-B). This design was aided by secondary and tertiary structure predictions by Jnetpred and AlphaFold to define suitable cut-offs for the fragment-design (Cuff & Barton, 2000; Drozdetskiy et al., 2015; Jumper et al., 2021). Confocal microscopy demonstrated that the catalytic domain and extended constructs up to the coiled-coil domain localised throughout the cell - including the nucleus (Fig. 36B). The inclusion of the coiled-coil and MIT domain resulted in localisation to the aforementioned endosomal-like structures and inclusion of the C-terminal stretches led to redirection of USP54 to the plasma membrane (Fig. 36B). Consistent with aforementioned experiments, full-length protein resembled the localisation of endogenous protein with its punctae-like structures.

These experiments highlight the effect of C-terminal stretches for USP54 localisation. They support the BioID findings that USP54 most likely exerts its function at confined cellular localisations.

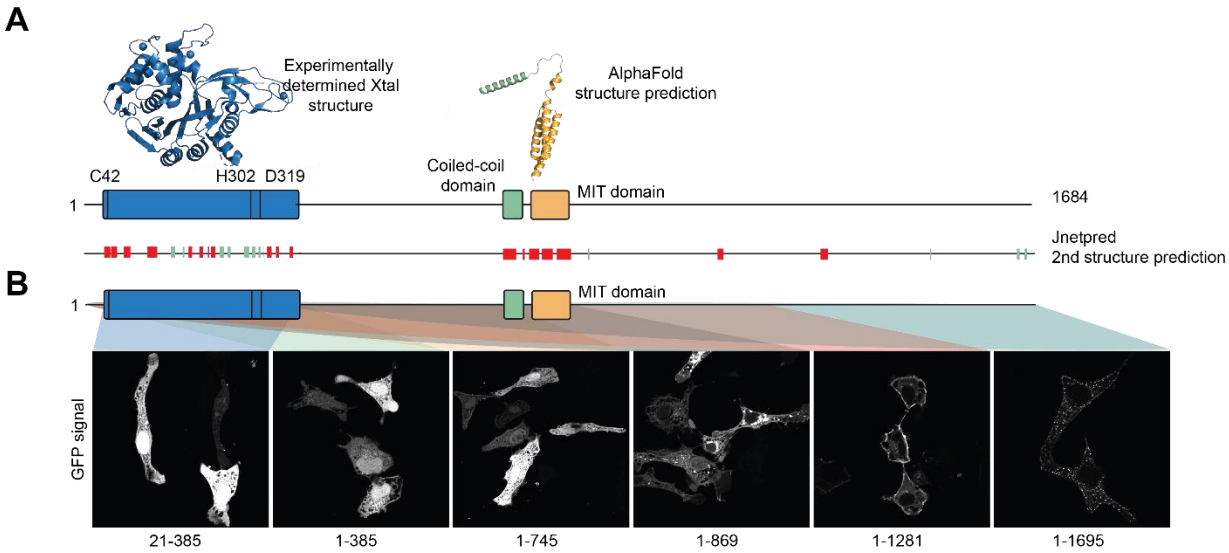

Figure 36 Experimental evaluation of factors determining the localisation of USP54. (A) Domain architecture of human full-length USP54 with a secondary structure prediction using Jnetpred (below) and the identified tertiary structures of USP54 from an experimentally determined crystal structure (PDB ID: 8C61, Wendrich et al., 2024) and AlphaFold (Jumper et al., 2021). MIT domain and coiled-coil domain were described in Rigden et al. 2009 and Wijdeven et al., 2017. **(B)** Different (shortened) constructs of USP54 were transiently expressed in HeLa cells and localisation investigated utilising their GFP signal with confocal microscopy.

After demonstrating the effect of C-terminal stretches on localisation, I sought to identify whether the C-terminus exerts a negative effect on the reactivity of USP54 with ABPs. To this end, the fragments described in Fig. 36 were expressed in HEK-293 cells and lysates were incubated with the aforementioned ABP. In order to verify the validity of the experimental setup, the catalytically inactive C42S variant was included as negative control and eGFP-tagged USP28 was included as a positive control. Analysis of the size shift following the covalent addition of the probe demonstrated that all catalytically competent constructs were capable to react with the probe, indicating that the assessed C-terminal stretches did not abolish USP54 reactivity (Fig. 37).

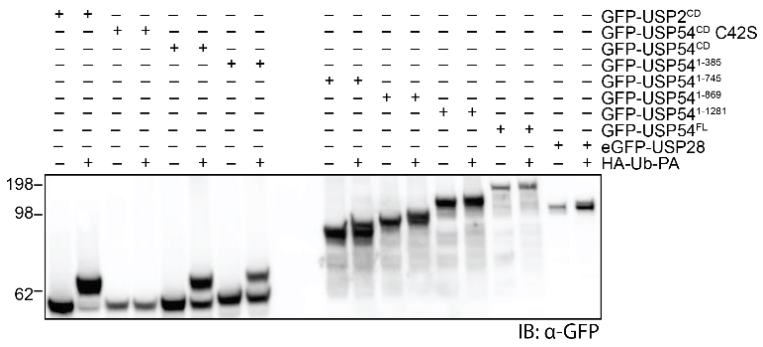

Figure 37. Reactivity of USP54 fragments with ubiquitin-based ABPs indicates that C-terminal stretches do not exert a negative effect on its activity. USP54 fragment were expressed in HEK-293 cells, lysates harvested and the probes added to lysate. The borders of the constructs are indicated and correspond to the borders in Fig. 28. The reactivity with the probe is indicated by a size shift of the DUB of approximately 7 kDa.

3.4.7 Ubiquitinome isolation coupled to mass spectrometry for the identification of substrates of USP54

The investigations thus far indicated that USP54 plays a role in clathrin-dependent endocytosis, microtubule organisation, cell cycle regulation and intracellular protein transport. To interrogate whether USP54 has substrates implicated in these processes, I performed ubiquitinome analyses in USP54 depleted cells.

Since several isolation tools to study ubiquitylated proteins had been established within the group, it was necessary to determine the most suitable approach for the identification of the substrates of USP54. To this end, we first assessed the effect of USP54 enzymatic activity on isolated, K63-ubiquitylated proteins. In *in vitro* data, USP54 exhibited a preference for cleavage of long, K63-linked ubiquitin chains, which are comprised of more than two ubiquitin molecules. While USP54 shares this preference with USP53, it has been shown that USP54 leaves a ubiquitin remnant at a model substrate, as demonstrated for polyUb-GFP cleavage *in vitro* (Fig. 38A, Wendrich et al., 2024).

To assess whether the *in vitro* cleavage behaviour of USP54 could be recapitulated for isolated, ubiquitinated proteins, the purified catalytic domain of USP54 was incubated with the ubiquitinome that was enriched from crude cell lysate using the OtUBD reagent. MARVELD2 was visualised in the experiment since we established earlier that this protein is decorated with K63-linked chains which can be isolated with our approach. The effect of the catalytic domain of USP54 was subsequently compared to the effect of USP53 (Fig. 38B). Consistent with previous data, USP53 led to the emergence of unmodified MARVELD2 with a reduction of overall chain abundance. The incubation with USP54 left a ubiquitin remnant on MARVELD2, whilst concomitantly reducing other ubiquitinated species – most notably the diubiquitinated protein species. This is consistent with the *in vitro* data, demonstrating that USP54 preferentially cleaves long K63-linked ubiquitin chains but does not favour removal of the most proximal ubiquitin.

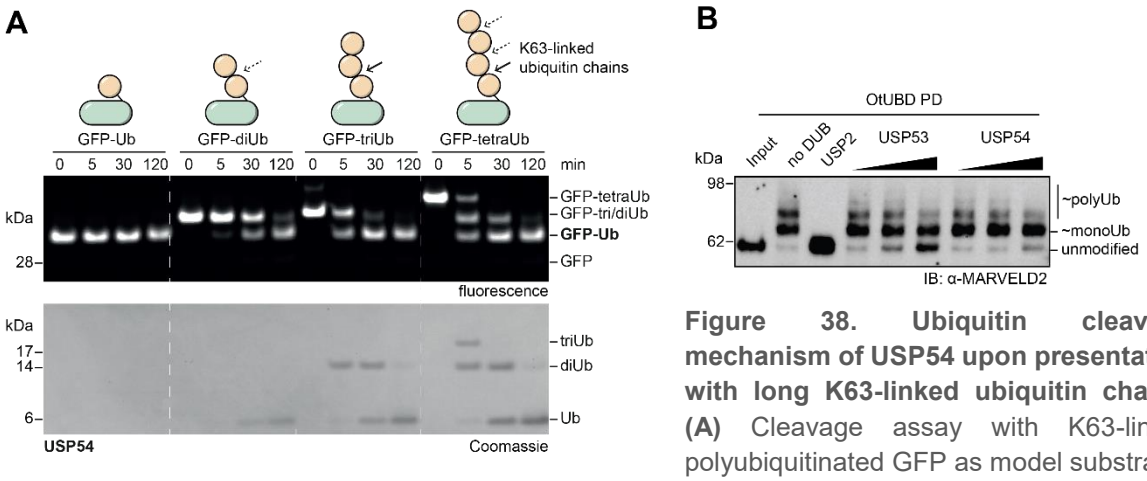

Figure 38. Ubiquitin cleavage mechanism of USP54 upon presentation with long K63-linked ubiquitin chains. **(A)** Cleavage assay with K63-linked polyubiquitinated GFP as model substrate. The model substrate (1 µM) was incubated with the catalytic domain of USP54$^{21-369}$ (300 nM). Cleavage activity was analysed after SDS-PAGE. In-gel fluorescence scanning visualised the GFP species. Coomassie staining of the same gel visualised ubiquitin chains formed during the assay. Cleavage sites are indicated with arrows. The assay was performed by Kim Wendrich and the figure was adopted from Wendrich et al. (2024). **(B)** UbiCRest assay with the isolated ubiquitinome of CaCo-2 cells upon depletion of USP53 after denaturing lysis, isolation with the OtUBD and acidic elution. MARVELD2 was chosen as a model substrate since previous experiments showed its decoration with K63-linked ubiquitin chains upon depletion of USP53. The assay was performed with the same conditions as in figure 17C with USP53$^{20-383}$ (0.5, 2 and 5 µM) and USP54$^{21-369}$ (0.3, 1 and 3 µM) and an incubation for 1 h at 37 °C.

In line with the findings that USP54 affected most prominently longer ubiquitin chains on proteins, the K63-polyUb binder Rx3A7 was utilised in enrichment steps prior to mass spectrometry-based substrate identification.

To isolate ubiquitylated proteins, lysis buffer with Rx3A7 was added to the cells depleted of USP54 (Fig. 39A). The lysis buffer was spiked with the enrichment tool to further reduce the likelihood of chain cleavage in the lysate. In addition, ethylenediaminetetraacetic acid (EDTA) and 1,10-phenanthroline (o-PA) was added to inhibit metalloproteases, NEM to inhibit cysteine-dependent DUBs as well as the broad-range DUB inhibitor PR-619 (Altun et al., 2011). The efficacy of this approach was demonstrated by the successful isolation of ubiquitin chains from U2OS cells (Fig. 39B), both with and without USP54 depletion (Fig. 39A). The isolated proteins were subjected to trypsin and Lys-C digest and submitted for mass spectrometry analysis. Peptides with the highest overall abundance were found for our pulldown reagent, as would be expected for a protein-based on-bead digest (Fig. 39C). On average, the second most abundant protein that was identified was ubiquitin, which confirmed the successful isolation of (conjugated) ubiquitin chains. Following USP54 depletion, an increased abundance of KIF23 (also known as MKLP1), ANLN, IQGAP1, TPX2, LUZP1 and TOP2A was detected in the K63-linked ubiquitinome (Fig. 39C). Increased detection of KIF23 upon USP54 depletion was also visualised in the profile blot (Fig. 39C).

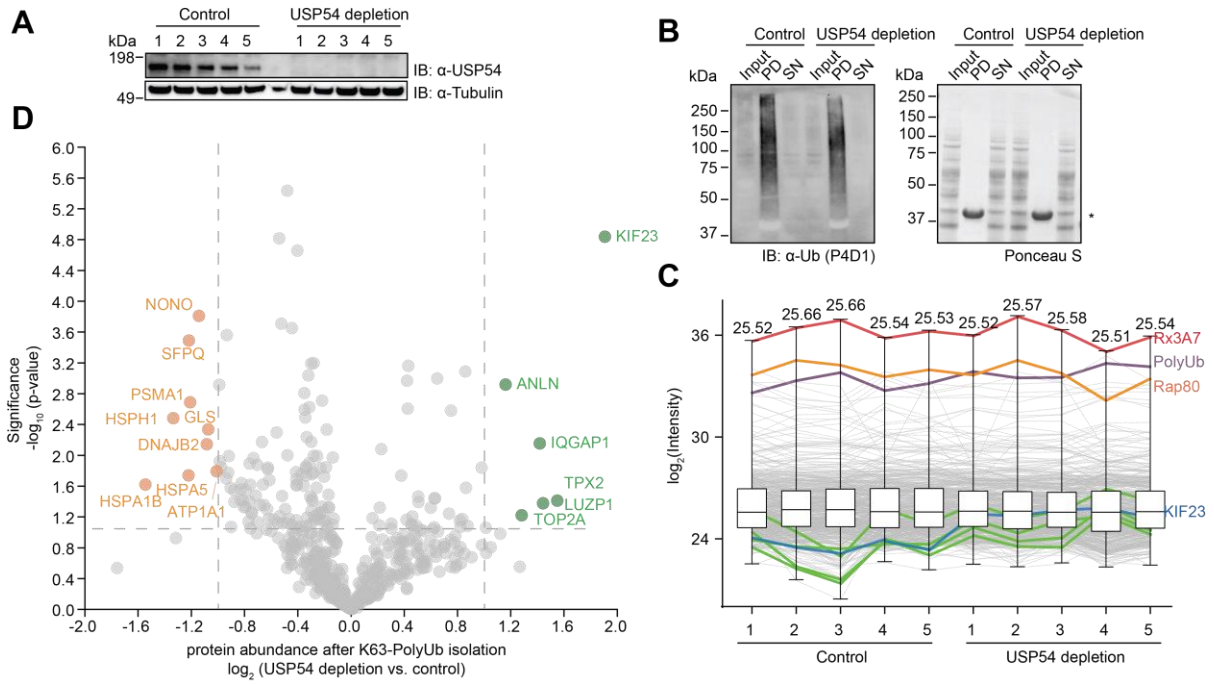

Figure 39. Influence of USP54 depletion on K63-linked ubiquitinome. (A) Input of control and USP54-depleted U2OS cells used in (C) and (D). The knockdown was induced using an siRNA pool. **(B)** Pulldown efficiency of the emGFP-tagged Rx3A7 used in the experiment. The asterisk indicates the MW at which to expect the enrichment reagent. PD: pulldown, SN: supernatant. **(C)** Profile plot depicting label-free intensities of all peptides identified after filtering. The medians of all intensities are given above the box plots with min-max borders. The red and orange lines indicate the abundance of the pulldown reagent which was annotated as RAP80 for the orange line. The purple line corresponds to polyubiquitin-C, the blue line to KIF23 and green lines to ANLN, IQGAP1, TPX2, LUZP1, TOP2A (top to bottom) **(D)**. Volcano plot depicting log_2 fold changes of protein abundance in K63-polyUb isolation upon depletion of USP54 in U2OS cells using siRNA. The significance cut-off is set to '0.05' with a cut-off for increased abundance of '2' as illustrated with the dashed lines. The t-test for given value was obtained analysing five samples per condition. Significantly enriched proteins are indicated in green, proteins with decreased abundance are indicated in orange.

In view of the strongly increased abundance of KIF23 in the USP54-depleted U2OS samples following K63-linked ubiquitinome isolation, I set out to orthogonally validate increased ubiquitylation of KIF23. Despite extensive efforts, the isolation of a ubiquitylated fraction of cellular KIF23 proved unsuccessful, despite making use of all ubiquitin enrichment reagents established in chapter 3.2. These assays were supported by KIF23 and ubiquitin co-overexpression followed by reporter-tag enrichment, as well as with isolation of ubiquitylated protein after the arrest of U2OS cells in different cell cycle stages (data not shown). This observation indicated that either KIF23 ubiquitylation has a very low occupancy, even under USP54 depletion conditions, or that the increased detection was due to increased abundance of unmodified KIF23 protein which accumulated in the background signal.

To test the latter hypothesis, overall protein levels of KIF23 upon USP54 depletion were assessed. In addition, I assessed the protein abundance change of RacGAP1 (also known as CYK4) since this protein forms the centralspindlin complex with KIF23, a structural element

that facilitates the bundling of microtubules to assemble the central spindle. To this end, knockdown studies were replicated in U2OS cells and combined with Western Blot analysis. In doing so, a significantly increased abundance of KIF23 and increased abundance of RacGAP1 were detected in the total cell lysate of U2OS cells following USP54 depletion (Fig. 40A and 39B). Upon further inspection, I detected not only an increase in abundance of the most prevalent cellular KIF23 species, but also of a KIF23 species characterised by slightly higher molecular weight (Fig. 40A and 39B), likely representing an isoform of KIF23, sometimes also referred to as CHO1 (Kuriyama et al., 2002).

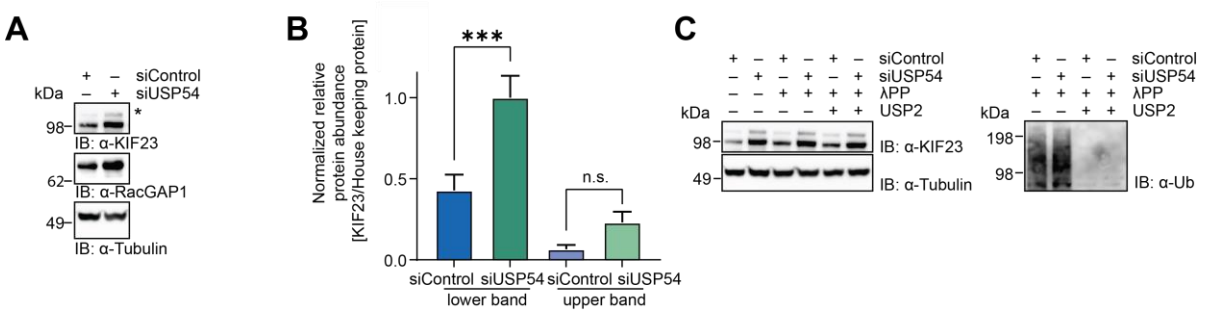

Figure 40. USP54 depletion leads to increased abundance of centralspindlin proteins. (A) Protein levels of the top hit from enrichment proteomics, KIF23, and its binding partner RacGAP1 upon USP54 depletion. The asterisk indicates the emerging upper band. **(B)** Normalised relative abundance of KIF23 lower and upper band in three independent experiments. The indicated *p*-value was calculated with a 2-way ANOVA and corresponds to $p=7x10^{-4}$. **(C)** Western blot identification of protein abundance after treatment of lysate with λPP (Lamda Phosphatase) and the catalytic domain of USP2.

In order to exclude the possibility that the higher molecular weight species represented ubiquitylated or phosphorylated KIF23, we incubated the lysate with λPP and the catalytic domain of USP2 (Fig. 40C). This did not result in a collapse of the upper band of KIF23, supporting the hypothesis that this upper band is not a ubiquitylated or phosphorylated KIF23 species. To ensure activity of USP2 in the cell lysate, the resulting cellular ubiquitination was probed which demonstrated that USP2 led to a decrease in the ubiquitin-smear, thereby supporting that USP2 was active in the lysate (Fig. 40C). In conclusion, we identified the two constituents of the centralspindlin complex, KIF23 and RacGAP1 as two proteins increased in abundance upon USP54 depletion.

In addition to the analysis of the ubiquitinome defined by K63-linkages, I set out to identify the effect of USP54 depletion with the pan-PolyUb reagent derived from UBQLN1, since ubiquitin chains on USP54 substrate may exist in mixed or branched chains. The GFP affinity handle was substituted with a biotin handle that allowed for denaturing lysis and washing conditions, thereby reducing the risk of isolating ambiguously bound proteins. In order to avoid of detection saturation due to highly abundant peptides derived from the ubiquitin binder thus allowing for increased sensitivity of low-abundant proteins, the ubiquitinated proteins were

eluted from the ubiquitin binder with acidic elution. In addition, to identify effects that arise from altered protein abundance, we included total lysate measurements in parallel to our pulldown studies. To enhance the depth of detection and circumvent the inherent limitations of mass spectrometry-coupled pulldowns, in skewing the results by unrepresentative imputation of missing values in the subsequent analysis, Tandem Mass Tags (TMTs) were utilised. Finally, the peptides were pre-fractionated after TMT labelling at a high pH to increase coverage and depth. The resulting methodology which was developed together with my colleague Siska Führer, is depicted in Fig. 41A.

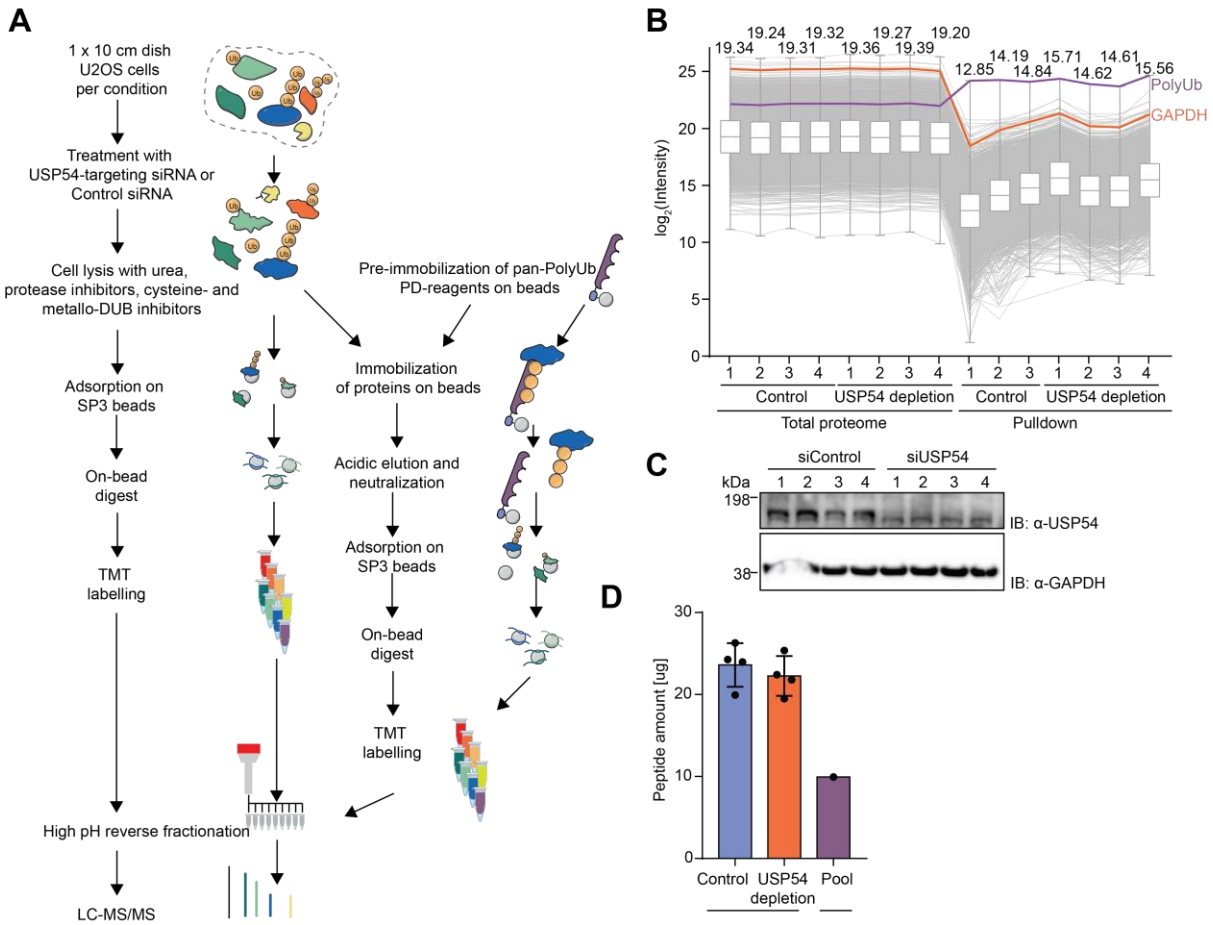

Figure 41. Optimised experimental procedure to identify substrates of USP54. (A) Schematic illustration of the experimental procedure in which total proteome and pan-PolyUbiquitinome samples were obtained from same dishes. This workflow has been developed together with Siska Führer. **(B)** Profile plot of all proteins identified after filtering in both, total proteome and pulldown samples. Medians of all intensities are given above the boxes with min-max borders. The orange lines reflect on abundance of GAPDH and the purple line of polyubiquitin-C. Note that one sample of the pulldown control did not pass quality control and was subsequently removed from analysis. **(C)** Input of control and USP54 depleted U2OS cells used in (A) and (B). **(D)** Peptide amounts in different samples as analysed by fluorescent peptide labelling. PD: pulldown.

The efficacy of the enrichment process was demonstrated by the increased detection of ubiquitin in the pulldown fraction (shown in orange in figure 41B) whilst household genes such as GAPDH were clearly deriched (shown in purple in the same figure). Furthermore, a

satisfactory knockdown efficiency was demonstrated in the U2OS samples (Fig. 41C). To facilitate a comprehensive comparison of peptide levels between the whole proteome samples and the pulldowns, fluorescent quantitative peptide detection was employed which detected equal peptide amounts between the total proteome samples and reduced peptide levels in the pulldowns (Fig. 41D). This finding corroborated the observations made in the mass spectrometry analysis (Fig. 41B). Following analysis of the samples, a significant increase in ubiquitination was detected for ZNF384, RPLP2, TMEM109, HSPB8, CDK6, MYL6, PSME1, VPS11, SUCLG1 and METTL14 (Fig. 42A), while DAXX, CEP290 and DCAF8L2 were found to be significantly reduced in ubiquitination. Notably, the depletion of USP54 did not result in an accumulation of ubiquitinated KIF23 in this experimental setting. The isolation of ubiquitinated proteins with the pan-PolyUb binder revealed a new subset of potential USP54 substrates that need be verified in additional assays. Interestingly, the use of the K63-specific Rx3A7 and the pan-PolyUb binder led to the identification of two different sets of proteins that were affected in ubiquitin chain decoration upon USP54 depletion.

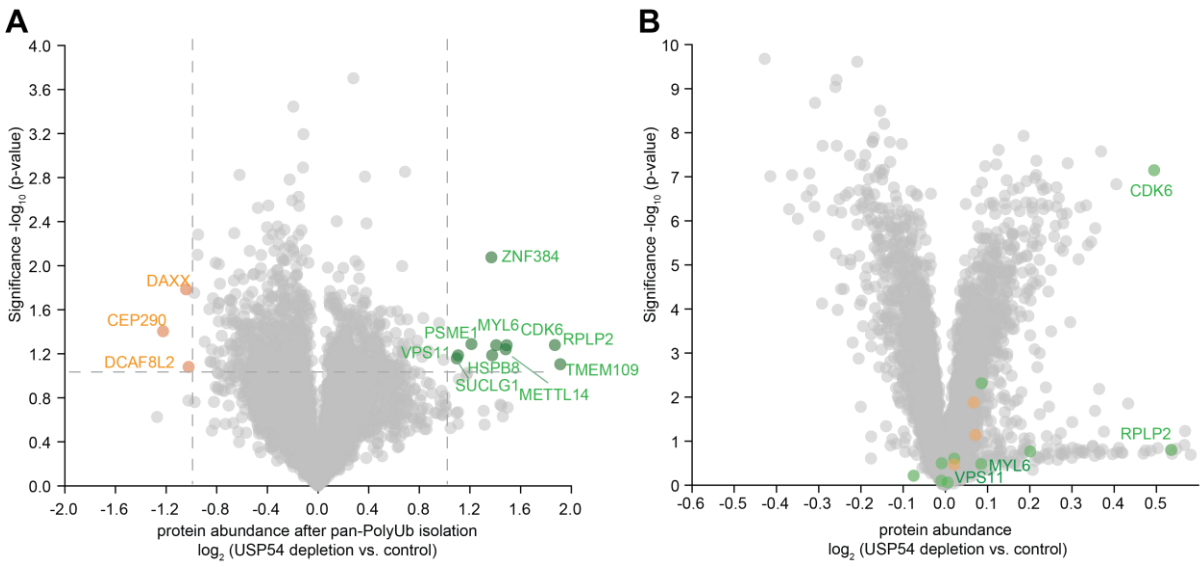

Figure 42. Denaturing pan-PolyUb enrichment isolates USP54 substrate candidates. (A) Volcano plot depicting log_2 fold changes of enriched proteins following pan-polyUb isolation upon depletion of USP54 in U2OS cells using siRNA. Significance cut-offs are set to '0.05' for the significance and '1' for abundance change and illustrated with dashed lines. The t-test for given value was obtained analysing three samples in the control and four samples for in USP54 depletion samples. Significantly enriched proteins are indicated in green, proteins with decreased enrichment are indicated in orange. **(B)** Volcano plot showing log_2 fold changes of protein abundance in total proteome samples from same lysate used in (A). Proteins are colour-coded according to their enrichment in (A).

In order to investigate the impact of protein changes on the detection of differentially ubiquitinated proteins, overall changes of protein abundance were analysed (Fig. 42B). The total proteome analysis revealed that CDK6 and RPLP displayed drastic abundance changes

upon USP54 depletion. This may provide an explanation for their increased detection in the pan-PolyUb-based isolation. Besides these two proteins, no drastic change in abundance was detected. Consistent with Western-Blot-based readouts and previously collected mass spectrometry data, total KIF23 levels increased upon USP54 depletion by 18%.

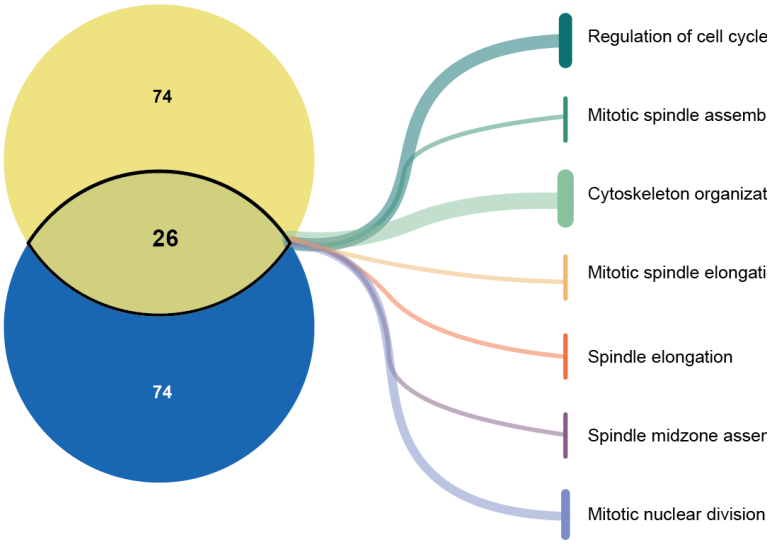

Figure 43. Influence of USP54 depletion on total proteome. Venn diagram depicting proteins with increased abundance after USP54 depletion in U2OS cells in two independent proteomics experiments. For each of the pools, the 100 proteins with the highest abundance change and a *p*-value <0.05. Subsequent analysis of the proteins shared between both experiments were investigated utilising gene enrichment analysis by g:Profiler (Kolberg et al., 2023). Biological processes that were identified with high confidence (adjusted *p*-value <1 x 10^{-3}) were depicted on the right with the thickness of the lines representing the number of proteins in the cluster.

In addition to these analyses with data-dependent acquisition, protein abundance changes in the total proteome in this dataset were compared to the changes detected in a dataset acquired using DIA. Both experiments were performed in the same conditions in regard to cell line, type of siRNA and duration of knockdown with the only differences in lysis buffer and downstream analysis. In order to analyse the impact of USP54 depletion on biological processes, the top 100 proteins for which the largest increase in significant abundance (p<0.05) were detected, were analysed. We observed that the proteins that were found to be upregulated the most, were predominantly associated with cell cycle processes and cytoskeletal organisation, along with associated processes (Fig. 43). This included the previously mentioned KIF23 and CDK6 (see tables 8 and 9).

Table 7. Increased abundance of proteins shared between two data sets for USP54 depletion in U2OS.

Gene names			
PHLDB1	RACGAP1	CBFB	DPY19L1
RASA2	PDGFRB	OXSR1	KIF23
TAGLN	PPP6R3	TPM2	ANKRD52
DTX3L	TPX2	SFXN1	SGPL1
CASP7	OTUD6B	CNN3	PRC1

Gene names		
CDK6	LRRFIP2	SLC16A1
ANXA1	TBC1D2B	ANLN

Table 8. GO-term enrichment of proteins increased in abundance between two data sets for USP54 depletion in U2OS. Terms for biological process were identified with an adjusted *p*-value of ≤ 1 x 10^{-3}.

Term name	Intersections
Regulation of cell cycle	DTX3L, CDK6, ANXA1, RACGAP1, PDGFRB, TPX2, ANLN, KIF23,
Mitotic spindle midzone	RACGAP1, KIF23, PRC1
Cytoskeleton	PHLDB1, ANXA1, RACGAP1, PDGFRB, TPX2, TPM2, CNN3,
Mitotic spindle elongation	RACGAP1, KIF23, PRC1
Spindle elongation	RACGAP1, KIF23, PRC1
Spindle midzone assembly	RACGAP1, KIF23, PRC1
Mitotic nuclear division	RACGAP1, PDGFRB, TPX2, ANLN, KIF23, PRC1

Accordingly, proteins with decreased abundance upon USP54 depletion were analysed (Table 9). The twelve share proteins between both experiments yielded proteins that did not cluster in particular biological processes.

Table 9. Decreased abundance of proteins shared between two data sets for USP54 depletion in U2OS.

Proteins			
WWP2	HNRNPM	NUDCD3	CHMP2B
IRAK1	STXBP2	PPP1R9B	VAT1L
HMOX1	HMGCL	CFDP1	YIPF5

In conclusion, the results of this study have provided new insights into phenotypes observed for USP54 depletion in human cells and highlight the importance of this underexplored DUB in a cellular context. The combination of the cellular characterisation of the DUB with the identification of proteins affected by USP54 depletion and proposed cellular substrates should provide a clear focus for future studies which will be discussed in more depth in the following chapter.

4 Conclusion and Discussion

Ubiquitination has been shown to regulate a plethora of cellular processes; frequently, enzymes effecting the intricate ubiquitin system are altered in pathological conditions. Consequently, proteins regulating the modification emerged as potential candidates for therapeutic intervention. Nevertheless, significant efforts have to be directed to better understand the cellular roles and substrates of DUBs, paving the way for the development of effective treatments. To shed light on substrates of the therapeutically intriguing enzymes USP53 and USP54, ubiquitin enrichment strategies have proven invaluable.

4.1 Tools identifying DUB Substrates demonstrate an Influence of USP30 Inhibition on Ubiquitination of TOM Complex Proteins

In the course of benchmarking efficacious tools for the isolation of DUB substrates, this dissertation has provided novel insights into the role of USP30 in response to mitochondrial stress. The findings have not only demonstrated the efficacy of ubiquitin binders to elucidate DUB functions and small molecule inhibitor effects in cells but also revealed how USP30 activity plays a pivotal role in regulating the ubiquitination pattern on TOM proteins in response to mitochondrial stress.

Most remarkably, our methodology demonstrated a strict regulation of TOM40 polyubiquitination by USP30 in mitochondrial depolarisation conditions within the examined time span. The fact that the monoubiquitinated TOM40 species has remained unchanged upon USP30 inhibition is consistent with the preference of USP30 to cleave specific linkage types and its weakened distal ubiquitin binding site and might in addition be influenced by phosphorylated ubiquitin species (Gersch et al., 2017). In addition, it was demonstrated that USP30 activity dampens TOM20 ubiquitylation (Fig. 44). These alterations in ubiquitination pattern on TOM proteins propose how USP30 exerts an effect on mitophagy, in line with findings from other studies (Bingol et al., 2014; Gersch et al., 2017; Rusilowicz-Jones et al., 2022). The complementary nature of ubiquitin-enrichment using OtUBD with other commonly employed tools in DUB and mitophagy research can be exemplified by investigating evidence from diGly mass spectrometry. This method has been instrumental in facilitating the exploration of numerous DUB substrates and has yielded a large set of ubiquitylation sites that are regulated by USP30 (Ordureau et al., 2020; Rusilowicz-Jones et al., 2020). However, diGly mass spectrometry cannot provide insights into the regulatory influence of the USP30 on ubiquitination patterns expanding on mono- or multi-monoubiquitylation. Thus, the combination of both approaches provides a more holistic insight in DUB function, as exemplified with TOM40. Moreover, this approach can complement affimer-based studies

which provide precise information on the type of ubiquitin decoration of mitochondrial proteins (Gersch et al., 2017), but inherently miss information about monoubiquitination and other chain types that decorate the substrates due to their very targeted nature.

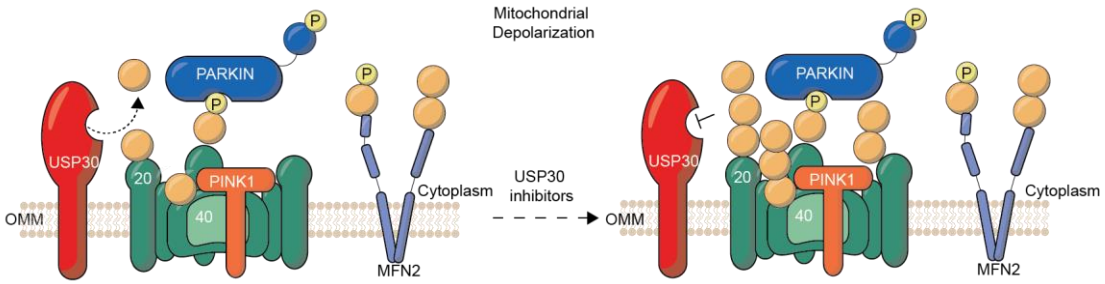

Figure 44. Schematic illustration of the effect of USP30 inhibition on ubiquitination states of mitochondrial outer membrane proteins. The presence of phosphorylated ubiquitin was derived from other publications (Ikeda, 2020; Matsuda, 2016; Shiba-Fukushima et al., 2014). OMM: outer mitochondrial membrane. P: phosphorylation

Further investigations are needed to determine the chain types built up on USP30 substrates upon inhibition or depletion of the DUB. To this end, the protocols established in this thesis should be employed in thorough UbiCRest analyses of USP30 substrates. In addition, the effects of increased ubiquitination of TOM proteins upon USP30 inhibition should be investigated in both, physiological conditions and upon mitochondrial stress, to study the potential of USP30 inhibitors to target Alzheimer's and Parkinson's disease. Furthermore, these experiments should be extended to other cell systems, such as induced neurons (iNeurons, Xue et al., 2013), derived from embryonic stem cells or neuronal cells from animal models to approximate cellular conditions mimicking pathology-relevant systems.

4.2 Regulation of Tricellular Junction Proteins by USP53

Within this thesis, deubiquitination of the tricellular junction proteins LSR and MARVELD2 are reported as a missing link between patient pathologies and observed mutations in USP53. The reported pathologies in humans could also be phenocopied in mouse models with mutations in MARVELD2 that display rapidly progressing hearing loss accompanied by loss of mechanosensory cochlear hair cells (Nayak et al., 2013). The rapidly progressing hearing loss (Porta et al., 2021; J. Zhang et al., 2020) and degenerated outer and inner hair cells in mice is shared for a mutation in the catalytic domain of USP53 (Kazmierczak et al., 2015a). The association of USP53 and MARVELD2 with impaired hearing, however, is not limited to mouse models but extends to human patients for which several cases have been described (Mašindová et al., 2015; Nayak et al., 2015; Shi et al., 2024; Srinivas Sankaranarayanan, 2021; Taghipour-Sheshdeh et al., 2019).

Furthermore, biallelic mutations in the *LSR* gene were found to cause intrahepatic cholestasis in human patients (Uehara et al., 2020) – an observation that was recently also described for biallelic mutations in *USP53* (Alhebbi et al., 2020; Gezdirici et al., 2023; Maddirevula et al., 2019; Srinivas Sankaranarayanan, 2021; J. Zhang et al., 2020). This intriguing connection was even noted recently (Ananda Kesavan et al., 2022) albeit without mechanistic explanation or experimental validation of this connection.

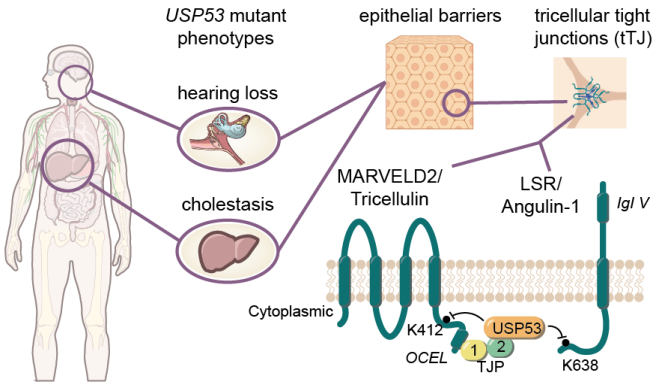

Figure 45. Model linking USP53-associated phenotypes to USP53-modulated ubiquitination of tricellular junction proteins. Genetic defects in *Usp53* and *Marveld2* share patient phenotypes with reports linking both to hearing loss and cholestasis. Our experiments provide evidence that catalytic activity of USP53 deubiquitinates these proteins thus connecting the observations and medical data. Domains and ubiquitination sites are annotated. The figure was adapted from Wendrich et al. and originally designed by Dr. M. Gersch. Illustrations of human anatomy and organs were extracted from NIAID NIH Bioart and licensed under public domain.

Within the presented dissertation, we demonstrated not only orthogonal verification of altered ubiquitination of MARVELD2 but could also show that specifically K63-linkage decoration on MARVELD2 increased upon USP53 depletion. The observed increase converges with *in vitro* findings that demonstrated specificity in cleavage of this chain type by USP53, a rare trait in the ubiquitin specific protease family. In the USP53 depletion experiments, we found that especially the diubiquitinated fraction of MARVELD2 increased among the identified shorter ubiquitin chains, suggesting that this species represents the dominant chain length that is regulated by USP53 *in cellulo.* This finding is consistent with the recently discovered S2 binding site in USP53, which is crucial for the preferential cleavage of longer ubiquitin chains (Wendrich et al., 2024). Length recognition and cleavage of specific ubiquitin chain lengths could be crucial in certain cellular settings since specific lengths of proteins can be read out by a differential set of readers leading to highly specific cellular responses (Waltho et al., 2024). In line with the *in vitro* data and ubiquitin chain restriction analysis, in which we provided evidence for the propensity of USP53 to cleave K63-linked chains *en bloc* from its substrates, we suggest that USP53 removes ubiquitin decoration completely from its substrates MARVELD2 and LSR. Such e*n bloc* cleavage activity has so far only been reported for the two proteasome-associated DUBs USP14 (Lee et al., 2016) and PSMD14 (also termed RPN11, Jonsson et al., 2022) which exhibit no linkage chain preference and it is going to be exciting to investigate the impact of this activity in future studies.

Interestingly, not only LSR and USP53, but also TJP2, is associated with intrahepatic cholestasis (Li et al., 2022; Sambrotta et al., 2014). The TJP2 protein has been shown to interact with the C-terminus of USP53 and reported to interact with TJP1 (Zihni et al., 2016) which, in turn, binds to the occludin/ELL (OCEL) domain in the C-terminus of MARVELD2. Thus, we propose USP53 to interact with MARVELD2 via TJP1 and TJP2. The combined findings accumulated throughout this thesis for the cellular function of USP53 is put into the context of pathology-association and depicted in figure 2.

Since the altered ubiquitination of MARVELD2 after USP53 depletion did not result in altered cellular protein levels of MARVELD2, we reason that ubiquitination in this case neither dictates its proteasomal nor lysosomal degradation. Ubiquitination of other plasma membrane proteins was described to alter endocytosis (Marmor & Yarden, 2004). However, we did not observe a notable difference in endocytosis upon USP53 depletion.

In the future, it should be assessed (i) if only catalytically active USP53 is able to reduce K63-linked ubiquitination of MARVELD2, (ii) the molecular functions and biological consequences of (poly-) ubiquitination of MARVELD2, (iii) the significance of K63-linked ubiquitin decoration of MARVELD2, (iv) if the propensity of USP53 to remove ubiquitin *en bloc* from its substrate is critical to its role. In the context of the investigation into (i), it should also be addressed what kind of effect a mimicking of patient mutations in *USP53* have on the ubiquitination state of tricellular proteins.

To address the molecular functions and biological consequences of (poly-)ubiquitination of MARVELD2, several possibilities can be considered. While the total endocytosed protein fraction seems to be unaffected by USP53 depletion, K63-linked chains could be critical for recycling and re-shuttling of MARVELD2. This could be addressed with a slightly adjusted experimental setup to allow for detection of recycled protein as described in Reyes-Alvarez et al., 2022. Furthermore, steric effects of the ubiquitin modifications (Chernorudskiy & Gainullin, 2013) should be investigated since the ubiquitination site is in close proximity to the interaction site of α-catenin and TJP1 (Cho et al., 2022; Higashi & Chiba, 2020) thus potentially affecting anchoring of the tricellular junction with the cytoskeletal network. This might lead to leaky tricellular junctions which could be investigated using fluorescently labelled dextrans or electric resistance measurement (Cho et al., 2022). In the CaCo-2 model, however, these investigations did not yield conclusive results.

To support these investigations, the USP53 depletion may be combined with mutational analysis replacing K412 in MARVELD2 or depleting the E3 ligase responsible for ubiquitination of tricellular proteins (i.e. with the E3 ligase ITCH which has been proposed by Jennek et al. in 2017 to ubiquitinate MARVELD2).

Other genetic approaches might include direct fusion of ubiquitin to the C-terminus of MARVELD2 to investigate the role of permanent (mono-)ubiquitylation for the system (see Asimaki et al., 2022) or the very recently developed Ubiquiton system that allows linkage- and substrate-specific polyubiquitination (Renz et al., 2024) which has the potential to address the significance of K63-linked ubiquitin decoration of MARVELD2 (iii). Approaching the importance of the *en bloc* deubiquitination activity of USP53 will most likely present a difficult question. However, fusion of different DUBs with different specificities and cleavage mechanisms to the C-terminus of MARVELD2 might present a feasible pathway to address this (see Huang et al., 2013).

While MARVELD2 and LSR are the most promising substrates of USP53, it might prove impactful to investigate the effect of USP53 on ITM2C ubiquitination and the other potential substrates that were identified in the mass spectrometry-based experiments. ITM2C represents a protein of elevated interest since several lysines at its cytoplasmic side showed decreased ubiquitin decoration following USP53 depletion. Since this observation cannot be explained by direct enzymatic function of USP53, there might be an indirect effect. However, since ITM2C (also termed BRI3) was connected to Alzheimer's disease (Dolfe et al., 2018), potentially due to its function as physiological inhibitor of amyloid precursor protein processing and Aβ oligomerization, the effect of USP53 on this process should be investigated. Furthermore, the NRBP1-containing CRL2/CRL4A was reported to target ITM2C for degradation thus highlighting ubiquitin-dependent regulation of the protein (Yasukawa et al., 2020).

4.3 USP54 – an intricate Protein important for Cell Cycle Progression and Cytoskeletal Organisation

Within this dissertation, several attributes of the underexplored DUB USP54 could be unravelled. Among the applied methods to characterise the enzyme was proximity labelling that identified interactors and the microenvironment of USP54. The interactors localise to endolysosomal membranes, clathrin coats, centrioles and cellular junctions. Their identification is not only complementary to our own AP-MS experiments with GFP-tagged USP54 but also to fragment-based AP-MS from Wijdeven et al. (2017) which identified interactors of USP54 fragments. The cellular compartments shared between these experiments included tight junctions, cilia and the homotypic fusion and vacuole protein sorting (HOPS) complex which is recruited to endolysosomal structures. The association of USP54 with centrosomes and centrioles was further supported by findings of Firat-Karalar et al. (2014) and Gupta et al. (2015) who found USP54 to be enriched in their proximity-studies with a variety of centrosomal and centriolar proteins as bait proteins (Firat-Karalar et al., 2014; Gupta

et al., 2015). Among the shared proteins in those studies and our own proximity labelling studies were CEP85, LZTS2, PLK1 and CYLD which are essential for cell cycle regulation. Notably, our experiments did not yield PLK4 as USP54 interactor which was not only one of the bait proteins in the studies by Firat-Karalar et al. but was also proposed as a substrate by Zhang et al. (2023). These findings, complemented by confocal microscopy across several cell lines, suggest USP54 to display distinct subcellular localisation. Alongside the multitude of experiments that show cellular activity and specificity of full-length USP54 presented in the thesis, this proposes that USP54 regulates K63-linked ubiquitination at these specific cellular sites.

Asides from the regulation of its activity through localisation, USP54 was found to be regulated in abundance throughout the cell cycle with reduced levels of the DUB in mitotic stages. It remains to be investigated how this cell cycle-dependent regulation is mediated. However, the identification of several 14-3-3 proteins as strong interaction partners of USP54 indicates a phospho-dependent regulation of the DUB, supported by the identification of eight candidate binding sites for these regulatory proteins in USP54. Considering the established function of 14-3-3 proteins in the regulation of the cell cycle, particularly with regard to the G2/M checkpoint, this association appears plausible (Gardino & Yaffe, 2011; Y. Zhang et al., 2024).

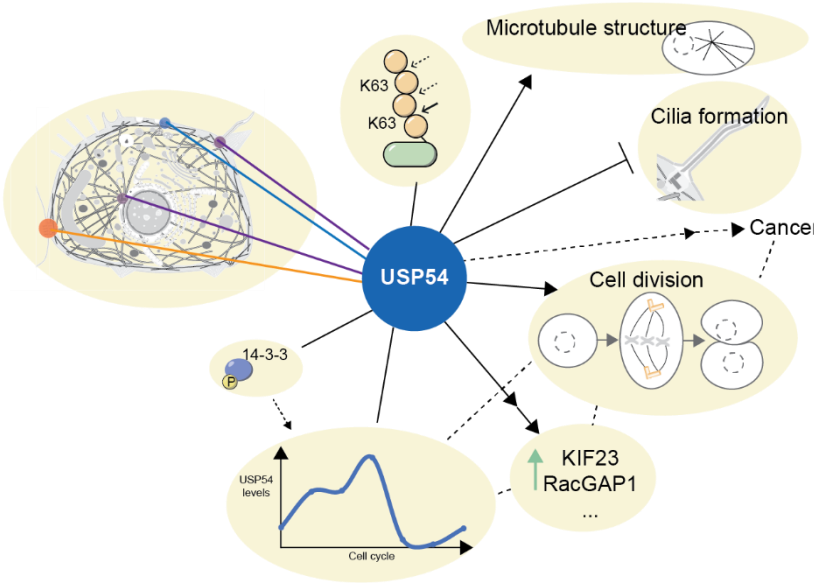

Figure 46. Visual representation of the characterisation of USP54 accumulated throughout the dissertation.

Dotted lines represent some of the hypothetical interconnections between individual findings. The green arrow indicates increased protein abundance. T-shape-ended lines indicate inhibitory effect of USP54.

Our hypothesis that the presence of USP54 at centrioles might result in defects in cell division and microtubule organisation upon mutation or depletion of the DUB held true. Depletion of USP54 does not only lead to a significant reduction in cells progressing through mitosis but also shifts the microtubule structure of cells from a radial to a peripheral structure. The latter indicating defects in a microtubule-organising centre (MTOC), such as the centrosome (Sanchez & Feldman, 2017). The influence of USP54 on centrioles is further supported by suppression of cilia formation upon ectopic expression of USP54 and induction of cilia

formation upon USP54 depletion as observed by Kasahara et al. (2018) since centrioles are key building blocks of cilia. The defects in cell cycle progression most likely stem from stalling of USP54-depleted cells between the entry in S-phase and entering PM phase due to the reduced number of cells displaying DNA condensation and findings acquired in fluorescence-activated cell sorting (FACS) experiments by Wijdeven et al.

Interestingly, CYLD, another K63-specific DUB has not only been described to regulate G2/M phase transition but was also found to be an interactor of USP54 in our screens. The observation of shared function and interaction evokes the question whether both K63-specific DUBs are redundant or whether they fulfil slightly different roles in their respective cellular contexts which should be addressed in upcoming experiments.

Notably, the two proteins consistently upregulated upon USP54 depletion, KIF23 and RacGAP1, have also been reported to peak in G2/M phase (Seguin et al., 2009), consistent with cell cycle arrest in this phase upon *USP54* knockdown. In cell cycle processes, it has to be always kept in mind that there is a risk of the causality dilemma – provoking the question whether alterations in proteins are affecting the cell cycle or whether cell cycle alterations are responsible for a change in protein properties. Thus, the identification of both midbody constituents in our K63-ubiquitinome enrichment experiments might be due to their increased protein abundance considering that KIF23 has been described to be ubiquitinated as a requisite for midbody ring degradation (Isakson et al., 2013), which takes place upon completion of cytokinesis, a cell cycle stage less populated upon USP54 depletion with reduced levels of USP54 in a physiological state.

It has been shown that utilisation of denaturing lysis and denaturing enrichment conditions for the isolation of ubiquitinated proteins can significantly improve the ration of proteins that are members of the ubiquitinome versus ubiquitin interactome (Zhang et al., 2022). The application of these conditions combined with the pan-PolyUb binder yielded cyclin-dependent kinase 6 (CDK6), vacuolar protein sorting-associated protein 11 (VPS11), and myosin light chain 6 (MYL6), among others, as significantly increased in ubiquitination. These proteins are of pronounced interest, since the kinase CDK6 is a critical regulator of cell cycle progression (Fassl et al., 2022) and VPS11 being a core component of both, the HOPS and class C core endosomal vacuole tethering (CORVET) complex which are both regulating the endolysosomal pathway (Terawaki et al., 2023). MYL6 has been suggested to be required for spindle and midbody orientation (Tomaiuolo, 2016). Considering their localisation and cellular function, the three proteins represent promising substrate candidates. Nevertheless, additional orthogonal validation is necessary to substantiate this hypothesis. In these experiments, the effects of USP54 depletion on K63-linked ubiquitin chains should be the

primary focus, as described in the identification and validation of USP53 substrates. These future experiments should be supported using the U2OS cell lines established in this dissertation that conditionally express siRNA-resistant USP54 thus allowing a separation of catalytic activity of USP54 and non-catalytic functions.

The enhanced comprehension of USP54 might hopefully facilitate the targeting of this DUB in subsequent studies employing small molecules or alternative chemical modalities. In this regard, it is imperative to acknowledge the diverse biological processes in which USP54 is engaged and to carefully dissect the contribution of USP54 in these processes. Its function in cell cycle regulation and reported involvement in centrosomal clustering render it a promising target for cancer treatment with chemotherapeutic drugs.

In conclusion, the understanding of the cellular roles of the two underexplored DUBs USP53 and USP54 was expanded in this dissertation using chemical biology, cell biology and mass spectrometry-coupled ubiquitinome enrichment. In doing so a foundation for future studies was laid out which paves the way for a holistic understanding of both enzymes and their roles in cellular processes and human pathologies.

5 Appendix

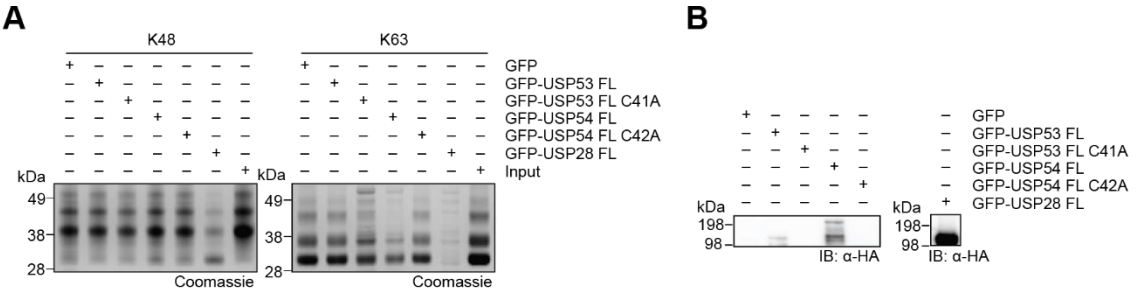

Appendix Figure 1. USP53 cleaves neither K48 nor K63-linked chains in the assay setup of main Fig. 10. (A) Polyubiquitin chain cleavage of full-length USP53, USP54 and USP28 after ectopic expression in HEK-293 cells and isolation via their GFP-tags as assessed by Coomassie staining of denaturing Bis-Tris gradient gels. **(B)** Ectopically expressed proteins used for isolation of proteins tested in (A). USP28 had to be visualised on a separate blot since its expression levels were much higher than expression levels of USP53 and USP54.

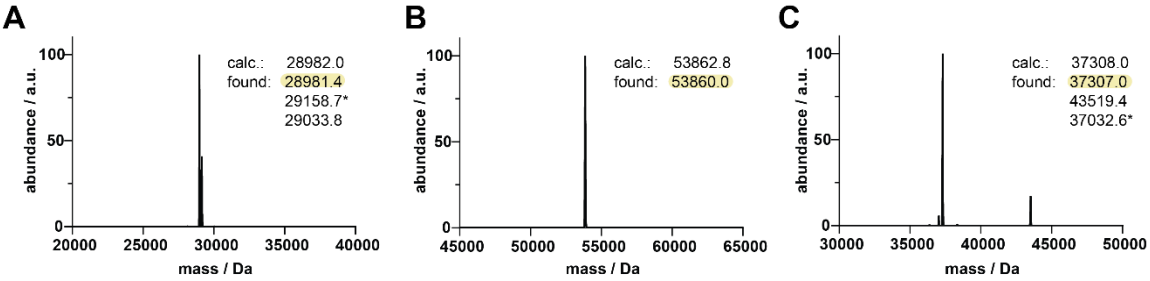

Appendix Figure 2. Deconvoluted intact protein mass spectra of emGFP-tagged ubiquitin enrichment reagents used in main Fig. 11C. (A) emGFP, **(B)** emGFP-pan-PolyUb and **(C)** emGFP-RX3A7. Calculated and observed molecular weights are given in Dalton. The calculated values take cleavage of the N-terminal methionine and maturation of emGFP into account. The protein species with highest abundance is highlighted in yellow for each measurement. The species in (A) denoted with an asterisk corresponds to a species with a retention of the N-terminal methionine and a non-covalent acetonitrile adduct. The species in (C) denoted with an asterisk corresponds to a species with cleavage of the first four amino acids and emGFP maturation.

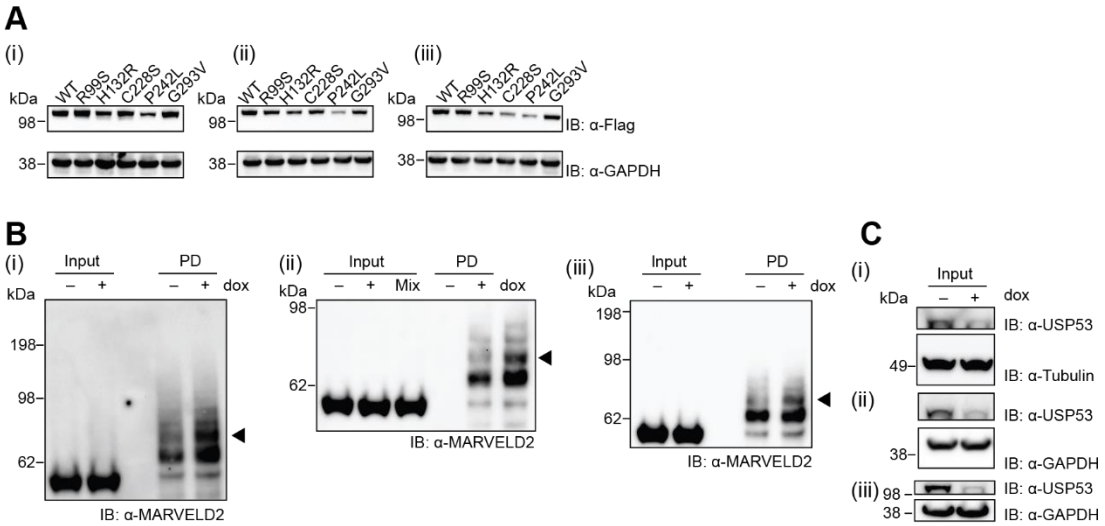

Appendix Figure 3. Western blots used for statistical testing of biological data in chapter 3. (A) Flag-USP53 levels of full-length USP53 carrying missense mutations highlighted in bold in Fig. 14A. The levels were analysed for Fig. 14C. **(B)** Levels of diubiquitinated MARVELD2 upon ubiquitinome enrichment with the OtUBD reagent as assessed in Fig. 22C. The intensity of the bands was extracted using Fiji (Schindelin et al., 2012) and values were normalised to input levels of MARVELD2. **(C)** USP53 levels in experiments shown in (B).

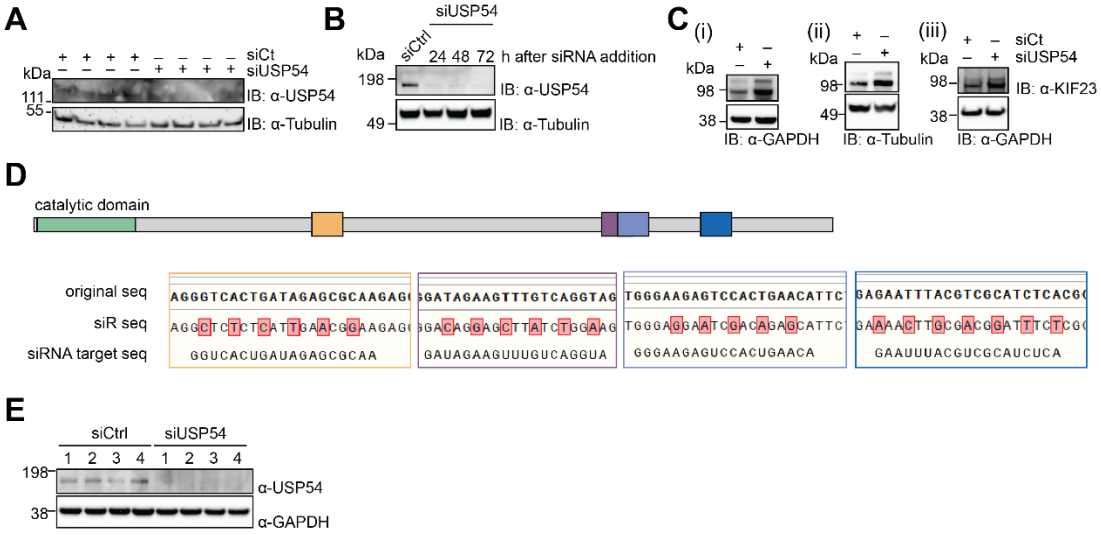

Appendix Figure 4. Western blots supporting data in chapter 4. (A) USP54 levels in the total proteome analysis shown in Fig. 27C. **(B)** Robust knockdown of *USP54* across the time span used in live-cell microscopy as assessed in Fig. 31B. **(C)** Levels of KIF23 upon USP54 depletion as statistically tested in Fig. 40B. **(D)** siRNA resistant *USP54* mRNA was established by introducing silent mutation to the siRNA pool target sequences. **(E)** Western Blot analysis of efficient USP54 depletion in the samples used in total proteome analysis with DIA in Fig. 43 as well as Table 7-9.

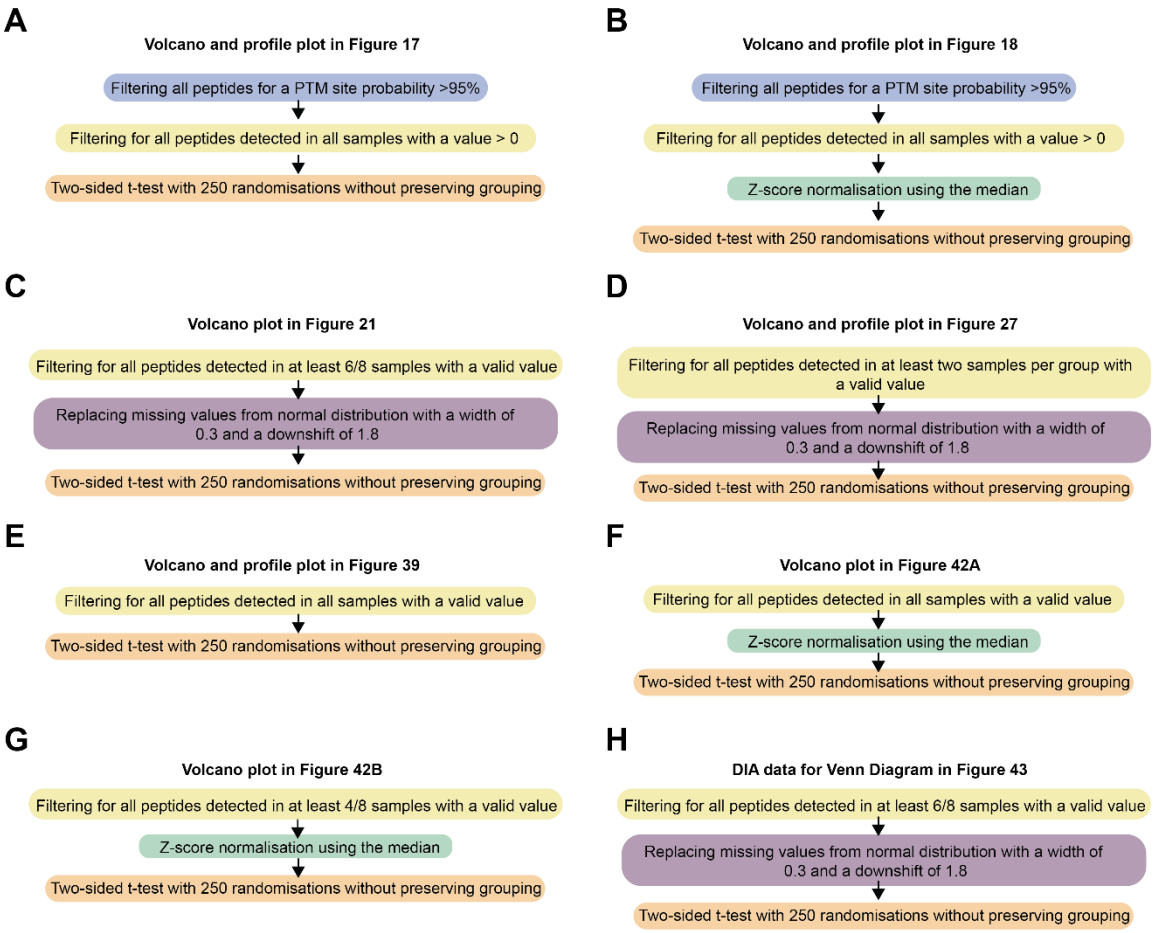

Appendix Figure 5. Critical processing steps of proteomics data in Perseus. Prior to these processing steps was pre-processing in *MaxQuant* and, in case of DIA analysis, in *Spectronaut*. In addition, prior to the steps shown here were several other common annotations as well as $\log_2$ transformation of data. **(A)** Volcano and profile plot in Fig. 17. **(B)** Volcano and profile plot in Fig. 18. **(C)** Volcano plot in Fig. 21. **(D)** Volcano and profile plot in Fig. 27. **(E)** Volcano and profile plot in Fig. 39. **(F)** Volcano plot in Fig. 42A. **(G)** Volcano plot in Fig. 42B. **(H)** Venn diagram in Fig. 43.

6 Material and Methods

6.1 Material

Oligonucleotides used in qPCR studies

Table 10. Oligonucleotides used in qPCR studies.

Name	Nucleotide Sequence (5'->3')	Corresponding gene
qPCR_GAPDH_fw	GTCTCCTCTGACTTCAACAGCG	*GAPDH*
qPCR_GAPDH_rv	ACCACCCTGTTGCTGTAGCCAA	*GAPDH*
qPCR_USP54_1_fw	CTCCCCAAGCTGAGTTCCAG	*USP54*
qPCR_USP54_1_rv	GACCACAGACTCATGGTGGG	*USP54*
qPCR_USP54_2_fw	GCAATGAGCAGGGCAAAAC	*USP54*
qPCR_USP54_2_rv	CGGAGAGTGTCAGATGGAAGC	*USP54*

Templates of key proteins

Table 11. Source of proteins from the two key proteins within this study. The asterisk indicates that the DNA sequence lacked three nucleotides coding for cysteine 190 which were inserted using SOE.

Coding for	Identifier	Source
USP54	DU49060	MRC PPU
USP53	OHS5894-202502340 *	Dharmacon

siRNA

Table 12. siRNA smartPools used throughout this thesis.

Target gene	Identifier	Supplier
USP54	M-016853-01-0005	Dharmacon
Control	D-001206-14-05	Dharmacon

Antibodies

Table 13. Antibodies used throughout this thesis. WB: Western Blot; IF: Immunofluorescence.

Antigen	Identifier	Supplier	Method
GFP	ab6673	Abcam	WB
HA	16B12	BioLegend	WB
USP54	HPA047663	Sigma	WB, IF
Ubiquitin	P4D1	Cell Signaling	WB

Antigen	Identifier	Supplier	Method
γH2AX-pSer 139	9718	Cell Signaling	WB
G3BP1	Sc-365338	Santa Cruz Biotech	WB
MFN2	12186-1-AP	Proteintech	WB
TOM40	18409-1-AP	Proteintech	WB
TOM20	11802-1-AP	Proteintech	WB
Vinculin	V9131	Sigma	WB
Flag M2	F3165	Sigma	WB
GAPDH	AM4300	Thermo Fisher	WB
USP53	HPA035844	Sigma	WB, IF
Tubulin	T6199	Sigma	WB
TJP2	sc-514557	Santa Cruz Biotech	WB, IF
MARVELD2	700191	Proteintech	WB
LSR	18216-1-AP	Proteintech	WB
EGFR	Sc-03	Santa Cruz Biotech	WB
Cyclin A	4656	Cell Signaling	WB
H3-pSer10	Ab5176	Abcam	WB
Acetylated tubulin	T6793	Sigma	IF
KIF23	28587-1-AP	Proteintech	WB
RacGAP1	13739-1-AP	Proteintech	WB
SQSTM1	sc-28359	Santa Cruz Biotech	IF
γ-tubulin	T5192	Sigma	IF
Mouse IgG	115-035-003	Jackson Immunoresearch	WB
Mouse IgG	NXA931V	Amersham	WB
Rabbit IgG	GENA934	Sigma	WB
Goat IgG	sc-2354	Santa Cruz Biotech	WB
Mouse IgG	4410	Santa Cruz Biotech	IF
Rabbit IgG	4412	Santa Cruz Biotech	IF
Mouse IgG	A21235	Thermo Fisher	IF
Rabbit IgG	A21245	Thermo Fisher	IF

Other detection tools

Table 14. Other tools to detect proteins or chemical entities used throughout this thesis. WB: Western Blot; IF: Immunofluorescence.

Ligand	Detection probe	Identifier	Supplier	Method
Biotin	Streptavidin-Alexa Fluor 488	S11223	Invitrogen	WB, IF
DNA	DAPI	268298	Merck	IF

Ligand	Detection probe	Identifier	Supplier	Method
DNA	SiR-DNA (Hoechst)	SC007	Spirochrome	Live-cell imaging
Tubulin	SiR-tubulin (Docetaxel)	SC002	Spirochrome	Live-cell imaging

Affinity gels

Table 15. Affinity gels used throughout this thesis.

Ligand	Material	Identifier	Supplier
HA (EZview)	Agarose resin	E6779	Sigma
GFP Trap	Agarose resin	gta-20	Chromotek
Biotin (High-capacity Neutravidin)	Agarose resin	29204	Thermo Fisher Scientific
Biotin (NeutrAvidin)	Agarose resin	29201	Thermo Fisher Scientific
Control (Pierce Control)	Agarose resin	26150	Thermo Fisher Scientific

Software

Table 16. Software used to analyse data or create figures. Occasional grammar checking of self-written sentences was done using DeepL Write Pro (indicated with an asterisk). This only affected replacement of words with synonyms and did not result in generation of extended text passages.

Name	Version number	Supplier
Excel	-	Microsoft Corporation
Prism	9	GraphPad Software
Perseus	1.6.14.0	Cox lab
Perseus	2.0.7.0	Cox lab
Illustrator	2021	Adobe Creative Cloud
PyMOL	2.5.2	DeLano Scientific LLC, Schrödinger Inc
SnapGene	6.0.4	Dotmatics
Image Lab	6.0.1	Bio-Rad Laboratories
ImageJ	1.54	NIH, USA
CFX Maestro	4.1.2433.1219	Bio-Rad Laboratories
SoftWoRx	7.2.0	Cytiva
DeepL Write Pro*	-	DeepL SE
ProMass	-	Novatia LLC
Cytoscape	3.10.1	Cytoscape Consortium (Shannon et al., 2003)

Web servers

Table 17. Web servers used to analyse data.

Name	Web page	Citation
VolcanoseR	huygens.science.uva.nl/VolcaNoseR2/	Goedhart & Luijsterburg, 2020
Venn webtool	bioinformatics.psb.ugent.be/webtools/Venn/	-
Reverse Complement	bioinformatics.org/sms/rev_comp.html	-
Uniprot	uniprot.org/	The UniProt Consortium, 2025
RCSB PDB	rcsb.org	Berman et al., 2000
g:Profiler	https://biit.cs.ut.ee/gprofiler/gost	Kolberg et al., 2023
14-3-3-Pred	compbio.dundee.ac.uk/1433pred/	Madeira et al., 2015
Jpred 4	compbio.dundee.ac.uk/jpred/	Drozdetskiy et al., 2015
String-DB	String-db.org/	Szklarczyk et al., 2023

Organisms

Prokaryotic strains

Two Escherichia coli (*E. coli*) strains were used throughout the thesis and are listed in table 18. The Top10F' strain was used for the amplification of plasmids, the Rosetta 2 (DE3)pLacI strain was used for protein expression.

Table 18. Prokaryotic *E. coli* strains used throughout the thesis.

Name	Genotype
Top10F'	F'mcrA Δ(mrr-hsdRMS-mcrBC) φ80lacZΔM15 ΔlacX74 recA1 araD139 Δ(ara-leu) 7697 galU galK rpsL endA1 nupG
Rosetta 2 (DE3)pLacI	F- ompT hsdSB(rB- mB-) gal dcm (DE3) pLacIRARE2 (CamR)

Mammalian cell lines

Several cell lines were used throughout the thesis that are listed in table 19 and referenced in the respective figure captions. U2OS FlpIN T-REx used to generate the stable U2OS cell lines that conditionally express our POI were kindly provided by the Nilsson lab (University of Copenhagen). HeLa cells that constitutively express YFP-Parkin were kindly provided by the Youle lab (NIH, Bethesda).

Table 19. Mammalian cell lines used throughout the thesis.

Cell line	Genotype	Supplier	Code
HEK-293	Wildtype	DSMZ	ACC 305
U2OS	Wildtype	DSMZ	ACC 785
HeLa	Wildtype	DSMZ	ACC 57
CaCo-2	Wildtype	Dept. IV	ATCC HTB-37
A549	Wildtype	DSMZ	ACC 107
Ma-Mel-B6c	Wildtype	AG Imig	-
HepG2	Wildtype	DSMZ	ACC 180
MDCK	Wildtype	Dept. II	-
HCT 116	Wildtype	DSMZ	ACC 581
PC-3	Wildtype	DSMZ	ACC 465
RPE-1	Wildtype	Dept. II	-
HeLa	YFP-Parkin	R. Youle lab (NIH Betheshda)	-
U2OS	GFP	This thesis	15-3
U2OS	GFP-USP54	This thesis	15-4
U2OS	GFP-USP54 C42A	This thesis	15-5
CaCo-2	shRNA5_100	This thesis	shRNA5
CaCo-2	shRNA1_100	This thesis	shRNA1
CaCo-2	Scrambled CF_100	This thesis	shCt

Cell culture media, buffers and supplements

Table 20. Media used for the cultivation of mammalian cells.

Name	Supplier
DMEM (high-glucose) + GlutaMAX	Thermo Fisher Scientific
F12K	Thermo Fisher Scientific
RPMI 1640	Corning
DMEM:F12K (1:1)	Thermo Fisher Scientific
FBS	Thermo Fisher Scientific
FBS – Tet-System Approved	Gibco
PenStrep	Sigma
Opti-MEM Reduced Serum medium w/o phenol	Thermo Fisher Scientific
Trypsin-EDTA (0.25%), w/ phenol red	Thermo Fisher Scientific
PBS pH 7.4	Gibco

Reagents and kits for proteomics

Table 21. Reagents and kits used in proteomics experiments.

Name	Supplier
Trypsin proteomics grade	Promega
LysC	Promega
TMTpro 16-plex	Thermo Fisher Scientific
Acetonitrile	VWR
Methanol	Riedel-de Haen
Formic acid	Acros
Pierce Fluorescent quantitative	Thermo Fisher Scientific
Pierce High pH Reversed-phase	Thermo Fisher Scientific

Mass spectrometers used in proteomics experiments

Table 22. Mass spectrometers used to generate data for the analysis shown in this thesis.

Mass spectrometer	Yielded data analysed in Fig.	Supplier
Q-Exactive Plus	27, 29, 30, 39	Thermo Fisher Scientific
Q-Exactive HF	41, 42, 43	Thermo Fisher Scientific
Exploris 480	17, 18, 21, 43	Thermo Fisher Scientific

6.2 Methods

Cloning and constructs

For bacterial expression, DNA sequences were cloned in either pOpin-B or pOpin-E vectors. For mammalian expression and most bacterial expressions, DNA sequences were cloned in pOpin-E vectors using the In-Fusion HD Cloning Kit (Takara Clonetech). Site-directed mutagenesis and generation of fusion constructs was carried out using splicing-by-overlap extension (SOE) PCR or Quickchange reactions using HF Phusion Polymerase. For the generation of stable protein expression in U2OS FlpIn-T-REx cells, gene sequences coding for the desired protein were integrated in the pcDNA5/FRT/TO expression vector using SOE. Integrity of DNA was verified using agarose gel electrophoresis. When only a desired DNA band of appropriate size was visible, the band was purified using a PCR purification kit - otherwise DNA species were separated by gel electrophoresis, excised and purified using a gel purification kit. All DNA sequences were analysed by Sanger sequencing services – either provided by GATC/Eurofins Genomics or Microsynth.

Transformation of chemically competent *E. coli*

A volume of 80 µl of chemically competent TOP10F' cells was transformed with 1–3 µl of plasmid DNA obtained through the cloning methods detailed above. The mixture was incubated on ice for 30 minutes, followed by a 45-second heat shock at 42 °C, and then cooled on ice for 2 minutes.

Afterwards, 1 ml of LB medium was added, and the cells were incubated at 37 °C for 1h while shaking at 800 rpm. Approximately 50 - 200 µl of bacterial suspension was spread onto a LB agar plate with the respective antibiotics. The plates were incubated overnight at 37 °C and individual colonies picked for subsequent steps.

Protein expression and purification in *E. coli*

For bacterial expression of emGFP, emGFP-panPolyUb and emGFP-Rx3A7, chemically competent Rosetta2(DE3)pLacI cells were transformed with the vectors and plated on agar plates with appropriate antibiotics. The following day, 2xTY medium was inoculated with colonies from the plates and grown over-night at 37 °C while shaking. Fresh 2xTY medium was inoculated with the over-night culture and grown at 37 °C until OD_{600nm} reached 0.8 – 1.2. Medium was cooled to 18 °C before protein expression was induced with 0.5 mM isopropyl-1-thio-β-D-galactopyranoside (IPTG) and over-night expression at 18 °C. Cells were harvested the next day by centrifugation and the pellets stored at -80 °C. For purification, the pellets were thawed, resuspended in lysis buffer (50 mM H_2NaPO_4, 300 mM NaCl, 20 mM imidazole, pH

8.0, supplemented with lysozyme and DNAse) and lysed by sonication (55% amplitude, 5 s on, 5 s off) on ice. Remaining debris was removed by centrifugation at 22000*g* for 30 min at 4 °C and filtration through a 45 µm filter. A pre-equilibrated (50 mM H_2NaPO_4, 300 mM NaCl, 20 mM imidazole, pH 8.0) HisTrap column (5 ml, GE Healthcare) was charged with the protein solution before extensive washing and elution of the His-tagged proteins with elution buffer (50 mM H_2NaPO_4, 300 mM NaCl, 500 mM imidazole, pH 8.0). The protein solution was dialysed overnight against SEC buffer (20 mM Tris, 100 mM NaCl, 4 mM DTT, pH 8.0). The dialysed protein suspension was loaded on a HiLoad16/600 Superdex 75 pg column. In preparation for the subsequent purification step, the protein suspensions were dialysed against low salt buffer (25 mM Tris, 50 mM NaCl, 4 mM DTT, pH 8.5) and loaded on a Resource Q column (GE Healthcare) for anion exchange chromatography. Following column loading and washing with low salt buffer, bound proteins were eluted with a salt gradient ranging from 50 to 500 mM NaCl by supplementing high salt buffer (25 mM Tris, 50 mM NaCl, 4 mM DTT, pH 8.5). Fractions containing the respective proteins were combined and concentrated. For storage, glycerol was added to a final concentration of glycerol of 5% and the samples were snap-frozen following the analysis of the proteins with intact mass spectrometry.

Sodium dodecylsulphate polyacrylamide gel electrophoresis (SDS-PAGE) for direct protein staining

SDS-PAGE was used to separate proteins according to their respective molecular weights. Samples were prepared by the addition of NuPAGE LDS sample buffer to protein solutions which served to denature the proteins. The protein samples were loaded onto NuPAGE Bis-Tris gradient gels (Invitrogen) and proteins were separated at a constant voltage of 160 V for 60 - 150 min in NuPAGE 2-(N-morpholino) ethane sulfonic acid (MES) running buffer. For protein band detection, the gels were either imaged directly, stained with InstantBlue solution while gently shaking and then washed with deionized water, or silver stained using the Silver Stain Plus kit (Bio-Rad) according to the instructions provided. Imaging was done using a Chemidoc MP Imaging System (BioRad).

Western blotting

For detection of protein levels via Western Blotting, proteins were first separated according to their molecular weights using SDS-PAGE. Afterwards, proteins were transferred on nitrocellulose membranes (0.45 µm pore size) using a Trans-Blot Turbo system (Bio-Rad) with either 1.3 A, 25 V, 10 min or 1.0 A, 25V for 30 min for detection of unmodified proteins or ubiquitylated proteins, respectively. For detection of USP54 levels, tank-blotting was performed for 18 h at 30 V and 4 °C. A successful transfer and equal loading was ensured by

Ponceau staining of the membrane. The membranes were blocked with 5% (w/v) non-fat milk in PBS-T buffer or TBS-T buffer (in case of phospho-Antibodies) and incubated with indicated primary antibodies overnight at 4 °C. Then the membranes were incubated with the respective secondary antibody coupled to horseradish peroxidase. The chemiluminescent reaction was initiated using a Clarity Western ECL substrate (Bio-Rad) with the addition of 20% Clarity Max Western ECL substrate (Bio-Rad) in in case of USP54 blots. In case of Far Westerns, the solution with the fluorophore-coupled proteins were incubated overnight at 4 °C in the dark and after washing, imaged directly. Images were recorded on a ChemiDoc MP Imaging System (Bio-Rad).

Intact protein mass spectrometry

For protein mass determination, protein samples were diluted to approximately 0.5–1 mg/ml in PBS and desalted using an AdvanceBio Desalting RP 2.1 × 12.5 mm cartridge (Agilent). The desalting process employed a gradient ranging from 5% to 95% solvent B (solvent A: HPLC-grade water with 0.1% trifluoracetic acid - TFA; solvent B: HPLC-grade acetonitrile - ACN with 0.1% TFA) at a flow rate of 0.4 ml/min.

Analysis was carried out on an Agilent 1260 II Infinity system (Agilent) equipped with an electrospray ion source operating in positive mode. The capillary voltage was adjusted to 4 kV, while the desolvation gas flow was maintained at 80 l/min at a temperature of 350 °C. Mass spectra were deconvoluted using the ProMass software (Novatia LLC).

Cell culture

Cells were cultivated in adequate medium supplemented with either 20% fetal bovine serum (FBS) for CaCo-2 cells or 10% FBS for all other cell lines and 1x penicillin/streptomycin at 5% CO_2 and 37 °C.

Transfection and siRNA-mediated knockdown

To allow for ectopic expression of proteins, human cells were typically plated to reach between 70 to 90% confluency the day after seeding. The plasmids were transfected using polyethylenimine (PEI) by mixing PEI:DNA in a 3:1 ratio in OPTI-MEM followed by incubation at RT for 15 min and the addition to cells. For siRNA mediated depletion of proteins, siRNA pools were pre-diluted in RNAse free water to 10 µM stock solutions. These stocks were incubated with RNAiMAX Lipofectamine in OPTI-MEM in a 1:3 ratio in OPTI-MEM followed by incubation at RT for 10 min. Experiments with cells ectopically expressing proteins or with depletion of a certain protein were typically performed 48 h after transfection to allow for successful proteins synthesis.

Cellular activity-based protein profiling

For activity-based protein profiling in cell lysate, cells were washed with ice-cold PBS and lysed in ABP buffer (50 mM Tris pH 8.0, 150 mM NaCl, 1% (v/v) IGEPAL, 5% (v/v) glycerol) supplemented with 5 mM Dithiothreitol (DTT). The lysate was scraped off the dish, cleared by centrifugation and the protein concentration between individual samples was equilibrated using Bradford solution. The activity-based probes were added to the lysates at a final concentration of 1 µM and incubated for 30 min at 37 °C. The reaction was stopped by the addition of LDS sample buffer. The samples were resolved by SDS page using a 4-12% Bis-Tris gel with MES SDS running buffer at 160 V.

Activity-based protein profiling following GFP-based enzyme enrichment

For activity-based protein profiling following enrichment of enzymes from cell lysate, cells were lysed using ABP buffer, supplemented by 2 mM Tris (2-carboxyethyl) phosphine (TCEP). The ectopically expressed enzymes were isolated by adding the lysate to pre-washed GFP-Trap agarose beads. This suspension was incubated for 2 h at 4 °C with permanent agitation. The beads were washed for four times with ABP buffer followed by addition of 2.5 µM HA-Ub-PA in ABP buffer. This was incubated for 1 h at 25 °C. The beads were washed three times with ABP buffer to remove excess ubiquitin probe. The immobilised proteins were eluted from the beads for 5 min at 95 °C with 2x LDS sample buffer supplemented with 25 mM DTT. For HA-blots of USP53, the bead eluates from the catalytic domain-only constructs were diluted 20-fold and the samples were resolved by SDS page using a 4-12% Bis-Tris gel with MES SDS running buffer at 160 V.

Isolation of USP54 from U2OS cell lysate using activity-based probes

U2OS cells were seeded in 10 cm dishes and grown for 48 h before being washed with ice-cold PBS and lysed in lysis buffer (50 mM Tris HCl pH 8, 300 mM NaCl, 1% (v/v) IGEPAL, 5% (v/v) glycerol, 1 mM phenylmethylsulfonyl fluoride-PMSF, 1 mM DTT, 5 mM $MgCl_2$ and 1:4000 benzonase). Cells were incubated with lysis buffer for 10 min at 4 °C before being scraped off the dish. The lysate was homogenized using sonication for 1 s (0.2 s on and 0.2 s off) at 10% amplitude and subjected to centrifugation for 10 min at 14,000 and 4 °C. The protein concentration in lysate was determined and split in two tubes with 500 µg protein per tube. One sample was treated with 10 mM NEM and one condition with the respective volume of isopropanol and a final concentration of 1 mM DTT. 10 µg HA-Ub-PA was added to each of the samples. Afterwards the samples were diluted 1:1 with lysis buffer and added to 25 µl pre-washed HA-EZview bead. The samples were rotated at 4 °C overnight. On the next day, the beads were washed with lysis buffer and two times with ice-cold PBS before adding 2x LDS sample buffer with 25 mM DTT and boiling for 5 min at 95 °C**.**

In vitro isolation of tetraubiquitin chains with enrichment reagents

For the isolation of *in vitro* generated tetraubiquitin chains, the three differently linked homotypic chains were diluted to 0.2 mg/ml in TUBE PD buffer (20 mM Na_2HPO_4, 20 mM NaH_2PO_4, 1% IGEPAL, 2 mM EDTA) supplemented with 1 mM DTT and incubated with an equimolar amount of enrichment reagent or GFP. These suspensions were added to 4 µl pre-washed GFP-Trap agarose beads and incubated for 2 h at 4 °C with permanent agitation. The beads were spun down according to the manufacturer's protocol and the supernatant was taken. Subsequently, the beads were washed four times with ice-cold PBS-T before the proteins were eluted in 2x LDS sample buffer.

Isolation of ubiquitin chains from HeLa cell lysate with enrichment reagents

HeLa cells were seeded in a 10 cm dish and grown for 72 h before being harvested with lysis buffer (10 mM Tris HCl pH 7.5, 150 mM NaCl, 5 mM EDTA, 0.5% IGEPAL) supplemented with 1x EDTA-free protease inhibitor cocktail, 50 µM PR619, 5 mM *N*-ethylmaleimide, 4 mM 1,10-phenanthroline. The lysate was subjected to centrifugation at 14,000*g* and 4 °C. After transfer of the input fraction to a new tube, the remaining lysate was split in three and added to the emGFP-tagged enrichment reagents which were pre-immobilised on 10 µl pre-washed GFP-Trap agarose beads. After 2 h incubation with permanent agitation at 4 °C, the beads were washed thrice with wash buffer (10 mM Tris HCl pH 7.5, 150 mM NaCl, 5 mM EDTA, 0.05% IGEPAL) supplemented with 50 µM PR619, 5 mM *N*-ethylmaleimide, 4 mM 1,10-phenanthroline. Elution was carried out using 2x LDS sample buffer with 25 mM DTT and boiling for 5 min at 95 °C. After pelleting of the beads at 500*g* for 1 min, the supernatant was transferred and analysed by SDS-PAGE and Western blotting as described above.

Comparative isolation of ubiquitin chains from U2OS cell lysate with enrichment reagents

One 10 cm dish with U2OS cells with a confluency of approximately 95% was lysed with lysis buffer (150 mM NaCl, 50 mM Tris HCl pH 7.4, 1% IGEPAL, 5% glycerol) supplemented with 1x EDTA-free protease inhibitor cocktail, 1 mM PMSF and 50 mM NEM. The lysate was homogenized using sonication for 1 s (0.2 s on and 0.2 s off) at 10% amplitude and subjected to centrifugation for 10 min at 14,000*g* and 4 °C. 1.25 nmol of each of the enrichment reagents were immobilised on 10 µl pre-washed high-capacity neutravidin beads and incubated for 1 h at 4 °C with permanent agitation. Excess reagent was washed away with ice-cold PBS before lysate was added to the immobilised enrichment reagents. These were then incubated for 1 h at 4 °C with rotation, pelleted by centrifugation at 500*g* for 1 min and the supernatant was removed. Beads were then washed once with lysis buffer, once with high-salt buffer (50 mM Tris HCl pH 8, 1 M NaCl) and twice with PBS. Elution was carried out using 2x LDS sample

buffer with 25 mM DTT and boiling for 5 min at 95 °C. After pelleting of the beads at 500*g* for 1 min, the supernatant was transferred and analysed by SDS-PAGE and Western blotting as described above.

For the isolation of the ubiquitinome from U2OS cell lysate for detection of ubiquitylated γH2AX and G3BP1 and, cells in 10 cm dishes were either treated with 30 µM etoposide or incubated at 43 °C for 1 h, respectively. For etoposide treatment, the control cells were treated with the equivalent volume of dimethyl sulfoxide (DMSO) while the control for the induced heat-shock were left at 37 °C. The cells were lysed with urea lysis buffer (8 M urea, 50 mM Tris HCl pH 8, 150 mM NaCl, 1% IGEPAL, 2 mM EDTA, 5% glycerol, 1x EDTA-free protease inhibitor cocktail, 2 µM MG132, 1 mM PMSF, 10 µM PR619, 20 mM *N*-ethylmaleimide, 4 mM 1,10-phenanthroline) and harvested by scraping. Directly after lysis, the obtained suspension was diluted 1:1 with dilution buffer (lysis buffer devoid of urea). Cells were homogenised using sonication for 1 s (0.2 s on and 0.2 s off) at 10% amplitude and subjected to centrifugation for 10 min at 14,000*g* and 4 °C. In parallel, biotinylated ubiquitin-binding entities were immobilized on 10 µL high-capacity neutravidin agarose bead slurry as described above. Lysate of each condition was distributed to three different Eppendorf tubes containing the respective pre-immobilized pulldown reagents and incubated for 1 h at 4 °C with rotation and downstream processing was in line with the description above.

Enrichment of endogenously ubiquitinated proteins in mitochondrial depolarisation background

HeLa cells that constitutively express YFP-Parkin were treated with 2 µM of the respective compounds or an equivalent volume of DMSO on the day after seeding. 19 h after compound treatment, 10 µM of carbonyl *m*-chlorophenyl hydrazone (CCCP, Acros Organics) or DMSO of the equivalent volume was added for 1 h before cells were washed with ice-cold PBS. Cells were then lysed in urea lysis buffer (4 M urea, 50 mM Tris HCl pH 8, 150 mM NaCl, 1% (v/v) IGEPAL, 2 mM EDTA, 5% (v/v) glycerol, 1x EDTA-free protease inhibitor cocktail, 1 mM PMSF, 10 µM PR619, 20 mM N-ethylmaleimide, 4 mM 1,10-phenanthroline) and harvested by scraping. Cells were homogenised by sonication for 10 s (2 s on and 2 s off) at 10% amplitude and subjected to centrifugation for 10 min at 14,000*g* and 4 °C. Biotinylated OtUBD (2 nmol, prepared as described elsewhere) was immobilized on 35 µl high capacity neutravidin agarose bead slurry per condition for 1 h at 4 °C with rotation. Excess reagent was washed away with ice-cold PBS. The beads were then equilibrated in urea lysis buffer. For each condition, an equal amount of 3 mg of protein (as determined per Bradford assay, in 1 mL of lysis buffer, typically obtained from one 10 cm dish), was added to the beads. These were then incubated for 2 h at 4 °C with rotation, pelleted by centrifugation at 500*g* for 1 min and

the supernatant was removed. Beads were then washed once with lysis buffer, once with high-salt buffer (50 mM Tris HCl pH 8, 1 M NaCl) and twice with PBS. Elution was carried out using 2x LDS sample buffer with 25 mM DTT and boiling for 5 min at 95 °C. After pelleting of the beads at 500*g* for 1 min, the supernatant was transferred and analysed by SDS-PAGE and Western blotting as described above.

Enrichment of endogenously ubiquitinated proteins from epithelial cells

CaCo-2 cells (stably transduced with USP53 shRNA where indicated) were treated as described above for the ubiquitinome analysis. 72 h after induction of the knock-down, cells were washed twice with ice-cold PBS and lysed in urea lysis buffer (8 M urea, 50 mM Tris HCl pH 8, 150 mM NaCl, 1% IGEPAL, 2 mM EDTA, 5% glycerol, 1x EDTA-free protease inhibitor cocktail, 2 µM MG132, 1 mM PMSF, 10 µM PR619, 20 mM *N*-ethylmaleimide, 4 mM 1,10-phenanthroline) and harvested by scraping. Directly after lysis, the obtained suspension was diluted 1:1 for OtUBD and 1:3 for pan-polyUb and K63-polyUb enrichment experiments with dilution buffer (urea lysis buffer devoid of urea). Cells were homogenised using sonication for 12 s (3 s on and 3 s off) at 10% amplitude and subjected to centrifugation for 10 min at 14,000*g* and 4 °C. In parallel, 17 nmol of the biotinylated ubiquitin-binding entities were immobilized on 240 µL high-capacity neutravidin agarose bead slurry (Pierce, Thermo Fisher Scientific) for 1 h at 4 °C with rotation. Excess reagent was washed away with ice-cold PBS. The beads were then equilibrated in diluted lysis buffer before being split up in two tubes. For each condition, an equal amount of 8-10 mg of protein (as determined per Bradford assay, in 2 mL of diluted lysis buffer, derived from two confluent 10 cm dishes per condition) was added to the pre-immobilized pulldown reagents and incubated for 2 h at 4 °C with rotation. Beads were pelleted by centrifugation at 500*g* for 1 min and the supernatant was removed. The resin was washed once with diluted lysis buffer, once with high-salt buffer (50 mM Tris HCl pH 8, 1 M NaCl) and once with ice-cold PBS. The pulldown reagent and bound proteins were eluted using 2x LDS sample buffer with 25 mM DTT and boiling for 5 min at 95 °C. After pelleting of the beads at 500*g* for 1 min*,* the supernatant was transferred and analysed by SDS-PAGE and Western blotting as described above.

Sample preparation for diGly enrichment

CaCo-2 cells stably transduced with USP53 shRNA#5 were seeded in eight 10-cm dishes, with each dish giving rise to one analysed sample. Knockdown of *USP53* was induced in four dishes using 2 µg/ml doxycycline 24 h after seeding and ultrapure water was used as the control in the other four dishes. The medium was changed every 24 h to medium with the respective treatment solution. Then, 72 h after induction of the knockdown, cells were washed thrice in ice-cold PBS and lysed in lysis buffer (50 mM Tris HCl pH 8.5 and 1% (w/v) sodium

deoxycholate). Cells were scraped off the dish and proteins were denatured at 95 °C for 10 min. Cell lysates were snap-frozen in liquid nitrogen. Subsequent steps were performed by the collaboration partners in the Demmers' group. These steps include, cell lysis by sonication in a Bioruptor Pico (Diagenode). Subsequently, protein concentrations were measured using the BCA assay (Thermo Fisher Scientific). Diglycine-modified peptides were enriched by immunoprecipitation using the PTMScan ubiquitin remnant motif (K-ε-GG) antibody–bead conjugate (kit 5562, Cell Signaling Technology) starting from 800 µg of total protein according to the manufacturer's protocol. Unbound peptides were removed by washing and the captured peptides were eluted with a low-pH buffer. Eluted peptides were analysed by nanoflow LC–MS/MS.

Ubiquitinome analysis following diGly enrichment

DIA raw data files were analysed with the *Spectronaut* Pulsar X software package (version 17.0.221202), using directDIA for DIA analysis including MaxLFQ as the LFQ method and *Spectronaut's* IDPicker algorithm for protein inference. The Q-value cut-off at precursor and protein level was set to 0.01. All imputation of missing values was disabled. Data were further analysed in Perseus (version 2.0.7.0). Peptide mass spectral intensity values were log2-transformed. Ubiquitinated peptides were filtered for sites that were quantified in all samples and in which the modified lysine was unambiguously identified (peptides with a PTM site probability greater than 95%). Changed ubiquitination sites upon USP53 knock-down were determined with a significance threshold of $-\log_{10}(p\text{-}value) \geq 1.12$ and a fold change threshold of $\log_2(\text{change in abundance}) \geq 1$ or and ≤ -1. For normalisation of the data, the integrated Z-score normalisation of Perseus (version 2.0.7.0) was utilized with use of the median and column access. For these ubiquitination site analyses, changed ubiquitination sites upon USP53 knock-down were determined with a significance threshold of $p\text{-}value \geq 0.05$ and a fold change threshold of $\log_2(\text{change in abundance}) \geq 1$ or and ≤ -1 before Z-score normalisation and a fold change threshold of $\log_2(\text{change in abundance}) \geq 0.5$ or and ≤ -0.5 after Z-score normalisation.

Total Proteome Analysis for diGly samples

DIA raw data files were analysed with the *Spectronaut* Pulsar X software package (version 17.0.221202), using directDIA for DIA analysis including MaxLFQ as the LFQ method and *Spectronaut's* IDPicker algorithm for protein inference. The Q-value cut-off at precursor and protein level was set to 0.01. All imputation of missing values was disabled. Data were further analysed in Perseus (version 2.0.7.0). Peptide mass spectral intensity values were $\log_2$-transformed. Only proteins which were detected in two thirds of all samples were quantified.

To allow for analysis, missing values were replaced from normal distribution with a width of 0.3 and a down-shift of 1.8 separately for each column.

UbiCRest assay in cell lysate

CaCo-2 cells (with dox-inducible shRNA#5 targeting USP53) were lysed in ABP lysis buffer (50 mM Tris HCl pH 7.4, 150 mM NaCl, 1% (v/v) IGEPAL, 2 mM EDTA, 5% (v/v) glycerol, 1x EDTA-free protease inhibitor cocktail, 2 µM MG132, 1 mM PMSF, 20 mM NEM) and harvested by scraping. Cells were homogenised using sonication for 12 s (3 s on and 3 s off) at 10% amplitude and subjected to centrifugation for 10 min at 14,000*g* and 4 °C. 25 mM DTT and 10 mM $MgCl_2$ were added to neutralize NEM and EDTA, respectively. The protein concentration was determined and the cell lysate distributed to individual tubes before addition of enzymes and incubation for 1 h at RT. The reaction was stopped by the addition of urea to a final concentration of 4 M. Afterwards the cell lysate was transferred to high-capacity neutravidin agarose bead slurry with immobilized biotinylated OtUBD for 2 h at 4 °C with rotation. Beads were pelleted by centrifugation at 500*g* for 1 min and the supernatant (SN) was kept. Beads were washed once with lysis buffer (4 M urea), once with high-salt (50 mM Tris HCl pH 8, 1 M NaCl) and once with ice-cold PBS before proteins were eluted from the beads with 2x LDS with 25 mM DTT and boiling for 5 min at 95 °C. After pelleting of the beads at 500*g* for 1 min, the supernatant was transferred and analysed by SDS-PAGE and Western blotting as described above.

UbiCRest assay with isolated ubiquitinome

Ubiquitinated proteins from CaCo-2 cells (with dox-inducible shRNA#5 targeting USP53) were isolated as described above using the OtUBD pulldown reagent. After the above-mentioned washing steps, beads were additionally washed twice with water. Subsequently, ubiquitinated proteins were eluted from OtUBD using 50 µL of a 100 mM glycine solution at pH 2.5 with an incubation time of 5 min at room temperature. Beads were pelleted by centrifugation at 500*g* for 1 min. The supernatant was transferred to a new tube and brought immediately to a neutral pH with 5 µL of 1 M Tris at pH 9.0. This step was repeated once, the resulting supernatants were combined and supplemented with final concentrations of 5 mM DTT, 5 mM $MgCl_2$ and 100 mM NaCl. For UbiCRest assays, supernatants were incubated with USP2 (1 µM), OTUB1* (0.2 µM), AMSH* (0.2 µM) or OTUD1 (0.02 µM) for 1 h at 37 °C. The reactions were stopped by adding 4 x LDS sample buffer (supplemented with 50 mM DTT) and visualized by SDS-PAGE and Western blotting as described above. To assess the activity of the catalytic domains of USP53 or USP54 on ubiquitinated proteins, enzymes were added to the supernatants at final concentrations of 0.5, 2 and 5 µM or 0.3, 1 and 3 µM, respectively. Samples were incubated for 1-2 h at 37 °C and analysed as described above.

UbiCRest assay with *in vitro* generated ubiquitin chains

USP2 (5 and 1 µM) and OTUB1*, AMSH* (20, 2 and 0.2 µM) and OTUD1 (2, 0.2 and 0.02 µM) were incubated with polyubiquitin chains for 1 h at 37 °C and supplemented with final concentrations of 5 mM DTT, 5 mM $MgCl_2$ and 100 mM NaCl.

Analysis of endocytosis of cell-surface exposed proteins

0.8 x 10^6 CaCo-2 cells (with dox-inducible shRNA#5 targeting USP53) were seeded in 35 mm dishes with addition of 2 µg/ml doxycycline and change of medium every day where indicated. Cells were grown until they formed a confluent monolayer after 96 h before being washed twice with ice-cold PBS* (PBS with 1 mM $MgCl_2$ and 0.1 mM $CaCl_2$). To each plate, 0.5 ml of cold Binding buffer (PBS with 10 mM HEPES, 1 mM $MgCl_2$, 0.1 mM $CaCl_2$, 10 mM glucose and 0.5 mg/ml Sulfo-NHS-SS-Biotin) was added and left at 4 °C for 45 min to allow for biotinylation of the surface proteins. Binding Buffer was removed and the plates were incubated twice with ice-cold PBS* containing 100 mM glycine for 5 min at 4 °C. At this stage the 'total protein' samples (TP) were harvested. The 'control' dishes (M) were left on ice and all other dishes incubated with pre-warmed culture media at 37 °C and 5% CO2. At the indicated time points, cells were placed on ice. Cells were washed twice with ice-cold PBS* and MESNA buffer (100 mM NaCl, 50 mM Tris HCl pH 8.6, 1 mM $MgCl_2$, 0.1 mM $CaCl_2$ and 8.2 mg/ml sodium 2-Mercaptoethanesulfonate) was added. MESNA buffer was replaced by fresh MESNA buffer after 20 min at 4 °C and left for another 20 min at 4 °C. After incubation, cells were washed twice with PBS* and harvested by scraping with lysis buffer (50 mM Tris HCl pH 8, 150 mM NaCl, 1x EDTA-free protease inhibitor cocktail, 4 M urea and 1 %IGEPAL). Cell lysate was cleared for 10 min at 14,000*g* and 4 °C. For each condition, an equal amount of 0.9 mg of protein (as determined per Bradford assay, in 0.3 mL of diluted lysis buffer) was distributed to 40 µl pre-washed high-capacity neutravidin agarose bead slurry and incubated over-night at 4 °C with rotation. The next day beads were washed with lysis buffer without protease inhibitor cocktail, once with high-salt buffer and once with ice-cold PBS before adding 40 µl 2x LDS containing 25 mM DTT and boiling for 5 min at 95 °C. After pelleting of the beads at 500*g* for 1 min, the supernatant was transferred and analysed by SDS-PAGE and Western blotting as described above.

qPCR

For the analysis of relative mRNA abundance, target threshold cycle (Ct) was determined automatically for the experiment. ΔCt was calculated by:

$$\Delta Ct = Ct_{target\ gene} - Ct_{reference\ gene}$$

With *GAPDH* as the reference gene. ΔΔCt was calculated for each cell line by normalizing ΔCt values to the respective value calculated for HeLa cells. Fold change (f) of mRNA levels were calculated by:

$$f = 2^{\Delta\Delta\mathrm{Ct}}$$

Assuming an ideal qPCR reaction with perfect doubling time.

To calculate the error, first variances of target and reference genes were calculated by:

$$v = \frac{\sum(x - \overline{x})^2}{(n-1)}$$

with x as the individual Ct value and $\bar{x}$ as the average of the values and the sample size n

Then, covariances were calculated with:

$$c = \frac{\sum(x - \overline{x})(y - \overline{y})}{n}$$

Where $\bar{x}$ and $\bar{y}$ are the sample means and n the sample size.

Finally, the relative standard deviation was calculated with:

$$\ln(2) * \sqrt{v_{target\ gene} + v_{reference\ gene} + 2 * c}$$

With this, the absolute standard deviation was calculated by multiplying the fold change with the relative standard deviation.

Total proteome analysis in PC-3 cells

1.8 x 10^5 PC-3 cells were seeded in 6-well plates with four plates per condition. 24 h after seeding, USP54 knock-down was induced using siRNA MAX reagent and the aforementioned siRNA mix targeting *USP54.* 24 h after the addition of siRNA, medium was exchanged. Following another 24 h, the cells were lysed in the wells using ABP lysis buffer (50 mM Tris pH 7.5, 150 mM NaCl, 1% (v/v) IGEPAL, 5% (v/v) glycerol and 1x EDTA-free protease inhibitor cocktail). After centrifugation at 14,000*g* for 10 min at 4 °C, the supernatant was adjusted to 2 mg/ml using Bradford reagent and a total volume of 50 µl of sample was transferred to loBind Eppendorf tubes. The samples were reduced with a final concentration of 10 mM Tris-(2-carboxyethyl)-phosphine (TCEP) for 30 min at 55 °C and alkylated with a final concentration of 15 mM chloroacetamide (CAA) for 30 min at RT in the dark. The proteins were precipitated by adding 200% precipitation solution with a 4:1:2 ratio of methanol:chloroform:water. Upon centrifugation for 5 min at 14,000*g* at 4 °C, protein pellet was washed with ice-cold methanol twice. The pellet was dried and subsequently resuspended in 4 M urea in Tris buffer (pH 7.5).

Then the solution was diluted to a final concentration of urea of 1 M before 2 µg trypsin was added. The protein suspension and trypsin were incubated overnight (approximately 14 h) before an addition 2 µg LysC was added and incubated for 2 h at RT. The digestion reaction was stopped by addition of 100% (v/v) TFA and desalted using C18-based StageTips.

Proximity labelling experiments

HEK-293 cells were seeded in four 10 cm dishes per condition before being transfected on the following day using PEI**.** 48 h after transfection, the cell culture medium was replaced with medium with 50 µM biotin. 72 h after transfection, the cells were washed twice with ice-cold PBS before detachment with trypsin. Cell culture medium was added to neutralise trypsin and the cells were spun down at 350*g*. The Cell pellet was washed with ice-cold PBS once more before being lysed in 0.5 ml lysis buffer (50 mM Tris pH 8.0, 150 mM NaCl, 1% IGEPAL, 0.5% (w/v) sodium deoxycholate, 0.1% (w/v) SDS and 1x EDTA-free protease inhibitor cocktail supplemented with 4 mM $MgCl_2$ and 0.025% (v/v) benzonase). The lysates were subjected to centrifugation for 10 min at 14,000*g* and 4 °C before protein concentration was adjusted using Bradford reagent. The protein concentration was adjusted and the suspension was diluted with 1:1 wash buffer (50 mM Tris pH 8.0, 150 mM NaCl). The samples were pre-cleared using 10 µl control bead slurry and incubated for 1 h at 4 °C. The pre-cleared lysate was transferred to 50 µl high capacity neutravidin agarose bead slurry per condition overnight at 4 °C with rotation. The next day, the beads were washed twice in wash buffer supplemented with 50 mM $MgCl_2$ before being washed twice with PBS. Afterwards, proteins were digested and peptides desalted as described above.

GFP-based affinity purification to enable interactome studies

HEK-293 cells were seeded in four 10 cm dishes per condition before being transfected on the following day using PEI. The cells were incubated with adjusted ABP lysis buffer (50 mM Tris pH 7.5, 150 mM NaCl, 0.5% (v/v) IGEPAL, 5% (v/v) glycerol, 5 mM EDTA and 1x EDTA-free protease inhibitor cocktail) for 10 min at 4 °C before being scraped off the dish and subjected to centrifugation for 10 min at 14,000*g* and 4 °C. The protein concentration in lysate was determined using Bradford reagent. 0.5 ml of 6 mg/ml proteins suspension were added to 20 µl GFP nanobody slurry and incubated overnight at 4 °C with permanent agitation. Following the incubation period, the beads were washed twice with lysis buffer and twice with lysis buffer without any detergent. The bound proteins were first reduced for 30 min at RT using 50 µl denaturing buffer (8 M urea, 50 mM Tris pH 7.5, 1 mM DTT) before being alkylated for 30 min at RT using a final concentration of 5 mM chloroacetamide. Afterwards, the proteins were digested for 1 h at 37 °C using 1 µg Lys-C. The supernatant was transferred to a new tube and 165 µl of 50 mM Tris pH 7.5, containing 1 µg trypsin was added to the beads and

incubated for 1 h at 37 °C. The supernatants of both digests were combined and another 2 µg of trypsin was added for an overnight digest at 37 °C. The digestion reaction was stopped on the next day by addition of TFA to a final concentration of 1% (v/v) and desalted using C18-based StageTips.

Analysis of the K63-linked ubiquitinome using the ubiquitin-binder Rx3A7

U2OS cells were seeded in 1 T75 flasks per sample before the knockdown was induced with siRNA targeting either *USP54* or a control sequence. 24 h after the induction of the knockdown, cells from the 10 cm dishes were trypsinated and transferred to 15 cm dishes. 48 h after the induction of the knockdown, U2OS cells were harvested using lysis buffer (10 mM Tris HCl pH7.5, 150 mM NaCl, 5 mM EDTA, 0.5% IGEPAL) supplemented with 1x EDTA-free protease inhibitor cocktail, 50 µM PR619, 5 mM *N*-ethylmaleimide, 4 mM 1,10-phenanthroline. msfGFP-Rx3A7 was already supplied in the lysis buffer. The lysate was subjected to centrifugation at 14,000*g* and 4 °C and the protein concentration was adjusted using Bradford reagent. 1.7 mg/ml protein suspension at a total volume of 1.2 ml was added to pre-washed GFP-Trap agarose beads. After 2 h incubation with permanent agitation at 4 °C, the beads were washed once with wash buffer (10 mM Tris HCl pH 7.5, 150 mM NaCl, 5 mM EDTA, 0.05% IGEPAL) supplemented with 50 µM PR619, 5 mM *N*-ethylmaleimide, 4 mM 1,10-phenanthroline. Subsequently, the beads were washed three times with detergent-free wash buffer (10 mM Tris HCl pH 7.5, 150 mM NaCl). The bound proteins were first reduced for 30 min at RT using 50 µl denaturing buffer (8 M urea, 50 mM Tris pH 7.5, 1 mM DTT) before being alkylated for 30 min at RT using a final concentration of 5 mM chloroacetamide. Afterwards, the proteins were digested for 1 h at 37 °C using 1 µg Lys-C. The supernatant was transferred to a new tube and 165 µl of 50 mM Tris pH 7.5, containing 1 µg trypsin was added to the beads and incubated for 1 h at 37 °C. The supernatants of both digests were combined and another 2 µg of trypsin was added for an overnight digest at 37 °C. The digestion reaction was stopped on the next day by addition of TFA to a final concentration of 1% (v/v) and desalted using C18-based StageTips before they were measured in DDA.

Analysis of the ubiquitinome using the pan-PolyUb binder

U2OS cells were grown in 1 10 cm dish per sample for 24 h before the knockdown was induced with siRNA targeting either *USP54* or a control sequence. 24 h after the induction of the knockdown, cells from the 10 cm dishes were trypsinated and transferred to 15 cm dishes. 72 h after the induction of the knockdown, U2OS cells were washed from dishes, transferred to Falcon tubes and pelleted. The pellets were washed three times with ice-cold PBS and flash frozen in falcon tubes. Cells were thawed on ice and lysed in urea lysis buffer (8 M urea, 50 mM Tris HCl pH 7.4, 150 mM NaCl, 1% IGEPAL, 2 mM EDTA, 5% Glycerol, 1x cOmplete

protease inhibitor cocktail, 2 µM MG132, 1mM PMSF, 10 µM PR619, 20 mM NEM, 4 mM o-PA). After 5 minutes of incubation, urea lysis buffer was diluted 1:1 with dilution buffer (50 mM Tris HCl pH 7.4, 150 mM NaCl, 1% IGEPAL, 2 mM EDTA, 5% Glycerol, 1x cOmplete protease inhibitor cocktail, 2 µM MG132, 1mM PMSF, 10 µM PR619, 20 mM NEM, 4 mM o-PA). Cell lysate was incubated for another 5 min on ice. DNA was sheered using a micro sonicator before cell debris was pelleted by centrifugation. Protein concentration was adjusted using Bradford reagent. 100 µg of protein suspension was transferred to separate Eppendorf tubes and flash frozen to constitute whole proteome sample. The pan-PolyUb binder was immobilized on High-capacity Neutravidin beads (agarose) for 2 h at 4°C. Excess reagent was washed away before addition of 2,3 mg of protein to 30 µl beads and rotated for 2 h at 4°C. Beads were washed with wash buffer (4 M urea, 50 mM Tris HCl pH 7.4, 150 mM NaCl, 1% IGEPAL, 2 mM EDTA, 5% Glycerol, 1x cOmplete protease inhibitor cocktail, 2 µM MG132, 1mM PMSF, 10 µM PR619, 20 mM NEM, 4 mM o-PA) once before being washed with high-salt buffer (1 M NaCl, 50 mM Tris HCl pH 7.4). Afterwards, beads are washed once with PBS and once with ddH_2O. After the last pelleting step, the samples were eluted with elution buffer (100 mM glycine HCl, pH 2.5). The supernatant was immediately neutralized with neutralization buffer (1 M HEPES pH 7.4). This step was repeated once and the two supernatants were combined. Samples were frozen until they were further processed for SP3 sample preparation.

SP3 sample preparation

The complete eluted pulldown suspension and 50 µg of whole proteome samples were boiled for 5 min at 95 °C in a buffer with the final concentration of 1% SDS, 10 mM TCEP, 40 mM CAA, 50 mM HEPES. A 1:1 mix of pre-washed hydrophobic and hydrophilic SeraMag beads (50 mg/ml) was added to both sample types (WP and PD). Protein precipitation was induced using Ethanol for 20 min at 24°C while shaking at 1000 rpm on a ThermoMixer. The beads were washed three times with 80% Ethanol before digestion was induced using trypsin and Lys-C (Promega) in 50 mM TEAB. Digestion proceeded for 18 h at 37 °C. Samples were flash frozen the next day. Peptide concentration was determined to roughly 10 µg in 100 µl buffer for PD and 10 µg in 300 µl buffer for WP using Quantitative Fluorometric Peptide Assay (Pierce). Peptide amounts between WP and PD were equilibrated and solubilized in 50 mM TEAB buffer

StageTip-based desalting of protein suspensions for proteomics

StageTips were prepared by stacking two C18 discs in a pipette tip using a special syringe. The C18 column material was primed using methanol. Then the StageTips were washed with buffer B (80% acetonitrile – ACN, 0.1% formic acid – FA) and twice with buffer A (0.1% FA).

Samples were loaded on C18 tips and incubated for 1 min at RT before they were washed with buffer A. The peptides were eluted in LoBind Eppendorf tubes with a total volume of 40 µl buffer B and subsequently dried in a SpeedVac at 30 °C for approximately 2 h.

Mass spectrometry analysis for data-dependent acquisition

For analysis of all samples measured in DDA, an Ultimate 3000 RSLC nano-HPLC system and a Hybrid-Orbitrap mass spectrometer (Q Exactive Plus or Q Exactive HF, as indicated in Table 22) equipped with a nano-spray source (Thermo Fisher Scientific) was used. Proteins were relatively quantified by using MaxQuant60 v.2.0.3.1, including the Andromeda search algorithm and searching the Homo sapiens reference proteome of the UniProt database. Briefly, an MS/MS ion search was performed for enzymatic trypsin cleavage, allowing two missed cleavages. Carbamidomethylation was set as a fixed protein modification, and oxidation of methionine and acetylation of the N-terminus were set as variable modifications. The mass accuracy was set to 20 parts per million (ppm) for the first search and to 4.5 ppm for the second search. The false discovery rates for peptide and protein identification were set to 0.01. Only proteins for which at least two peptides were quantified were chosen for further validation. Relative quantification of proteins was performed by using the label-free quantification algorithm implemented in MaxQuant.

STRING network cluster analysis and gene ontology analysis

The proteins identified from the proteomics data were submitted to the online resource of STRING-DB (Szklarczyk et al., 2023). Full STRING network was chosen as setting with edges representing the calculated confidence scores with a lower cut-off of 0.4. For visualization of the STRING analysis, the resulting graph was loaded into Cytoscape (Shannon et al., 2003). For functional enrichment analysis, g:Profiler was used with an organism search in *H. sapiens,* a statistical domain scope of only annotated genes and use of a g:SCD threshold of 0.05.

Immunofluorescence microscopy

Cells were either grown on 8-well cell culture slides or on coverslips that were pre-coated with poly-D-lysine (Sigma-Aldrich). For pre-coating, coverslips were first washed in 100% ethanol. Then 50 µg/ml Poly-D-lysine was added dropwise to the slides. The solution was left on the slides for 1 h before the coverslips were washed twice in PBS. Cells were fixed in Roti-Histofix for 10 min at room temperature before being permeabilized in 0.1% Triton-X100 for 10 min at room temperature. Unspecific binding was suppressed by blocking with 4% FBS in PBS (blocking buffer) for 1h at room temperature. Samples were incubated over-night at 4 °C with the primary antibodies in blocking buffer. After washing the coverslips thrice in PBS, secondary antibodies were applied in blocking buffer for 1 h at RT. Finally, DNA was visualized using

300 nM 4′,6-diamidino-2-phenylindole (DAPI). Ibidi mounting medium was used as mounting medium. Images were acquired either using the Zeiss LSM800 or Zeiss Axio Observer Z1.

Live cell microscopy for identification of defects in cell cycle and microtubule structure

U2OS cells were seeded in µ-plate 24 well (Ibidi). 24 h after seeding, when cells reached a confluency of roughly 30 – 50%, treatment with the respective siRNA was started. 18 h later, medium was exchanged to Leibovitz medium with 10% FBS. Three hours after medium exchange, SiR DNA and SiR-tubulin (Spyrochrome) were added according to manufacturer's manual. Cells were imaged 1 h after addition of the dyes on a Deltavision Elite System (GE Healthcare) equipped with an IX-71 inverted microscope (Olympus), a UPlanFLN 40×/1.3 NA objective (Olympus) and a pco.edge sCMOS camera (PCO-TECH Inc.). Images were acquired as Z-sections at 0.2 µm and deconvoluted using SoftWoRx (Cytiva) for 18 h at 37 °C and 5% CO2. For visualization in the thesis, images were converted into maximum-intensity-projection TIFF files. For analysis of data acquired with live-cell imaging, individual files for different point of views were blinded for an unbiased evaluation. Cell division events were assessed manually by recording DNA condensation in the SiR-DNA channel and tracked. Graphic representation was done using GraphPad Prism.

Lambda Phosphatase and USP2 treatment for KIF23 species analysis

Cells were either lysed in ABP lysis buffer with additional 20 mM NEM, 1 mM PMSF, Biotin-OtUBD and 5 mM EDTA (for complete protease inhibition), ABP lysis buffer with additional 10 mM $MnCl_2$ and 20 mM $MgCl_2$ (for Lambda phosphatase treatment) or with ABP lysis buffer with additional 20 mM $MgCl_2$ and 40 mM DTT (for DUB treatment). The lysate was incubated with either 10 µM Lambda phosphatase and/or 1 µM USP2 for 30 min at 37 °C.

Determination of cells entering mitosis

The first frame of each field-of-view time progression was used to determine the cell counts at the beginning of the experiment. For this frame, pixels in the SiR-DNA channel were filtered with Fijis median calculation with a radius of five pixels. To allow for further processing, the image was changed to an 8-bit image in Fiji. For thresholding, the Huang algorithm was used with standard settings. To separate the nuclei, watershedding was used. Afterwards particles were analysed with a lower micron^2 cut-off of 50 µm^2 and a circularity of 0-1.

Measurement of peptide amount in samples

Peptide concentrations were assessed using the Quantitative Fluorometric Peptide Assay according to the manufacturer's protocol

TMT labelling

TMT labels (LOT#: YB367250) from a TMT 16-plex labelling kit (Thermo Fisher) were dissolved in 42 µl anhydrous ACN. 20 µl of the dissolved labelling reagent was added to approximately 10 µg peptides for each, pulldown and total proteome. Samples were briefly vortexed and labelling proceeded for 2 h at RT. To each sample, 8 µl 5% (v/v) hydroxylamine were added and incubated for 15 min. Samples were mixed and dried in a Speedvac before being reconstituted in 0.1% TFA in ddH_2O.

High pH reverse fractionation

Sample complexity was reduced and excess TMT label was removed using the Pierce™ High pH Reversed-Phase Peptide Fractionation Kit (Thermo Fisher) according to the manufacturer's protocol. For elution of different fractions, the concentration of ACN was increase from 0% to 80% while the concentration of Triethylamine was kept constant at 0.1%. Samples were dried at 30 °C for 4 h.

Cell synchronisation to study USP54 abundance changes

U2OS cells were seeded in 10 cm dishes and incubated until 80% confluency was reached before initiating synchronisation. Cells to be harvested in G1, S and G2 phase were arrested in the respective cell cycle stage via a double thymidine block with 2 mM thymidine. To this end, thymidine was added to cell culture medium and incubated for 16 h before this first thymidine block was released for 8 h by replacing the medium. Then, the second block was initiated with another 16 h incubation step. Cells were released again into fresh medium and collected for lysis in urea lysis buffer after the indicated release times. For the collection of cells in mitosis, cells were treated with 2 mM thymidine for 24 h followed by a release from thymidine into fresh medium containing 100 ng/ml nocodazole for 18 h. Mitotic cells were collected by pipetting the mitotic cells from the dish after agitation ("mitotic shake-off"). Cells were pelleted by centrifugation at 200*g* for 5 min before resuspended in pre-warmed fresh medium to release from nocodazole. The cells were pelleted and washed twice in fresh medium before they were resuspended in Dulbecco's Modified Eagle Medium (DMEM) containing 25 mM HEPES (pH 7.2). Samples were either lysed immediately or incubated for specified time points in a water bath at 37°C before being lysed on ice using urea lysis.

Cell synchronisation to study M phase progression in U2OS cells

$9x10^4$ U2OS cells were seeded on coverslips pre-treated with poly-D-lysine in a 6-well dish in order to reach a confluency of approximately 30-40%. 24 h after seeding, thymidine was added to a final concentration of 2 mM. After 18 h, cells were released from the thymidine block by washing three times with warm PBS and culture medium was added. Directly after, the

knockdown was initiated by adding siRNA with lipofectamine. Six hours after the release, RO-3306 was added at a final concentration of 9 µM. 18 h after the addition of RO-3306, the first timepoint was collected. For other timepoints, cells were washed in warm PBS thrice before the addition of culture medium for the indicated time spans.

Stable integration of DNA in U2OS Flp-In T-REx cells

U2OS Flp-In T-REx (Thermo) cells were seeded in a T25 flask at $7x10^5$ cells to yield ~30% confluency after 24 h. After 24 h, cells were transfected with 2.9 µg pOG44 and 0.1 µg pcDNA5 using Lipofectamine 3K. 24 h after transfection, medium was replaced with fresh medium. On the next day, cells were split to T25 flasks and 3 h after splitting 200 µg/ml hygromycin B solution and 5 µg/ml blasticidin was added. Cells were grown under selection pressure for two weeks with 10% tetracycline-free FBS supplemented with 200 µg/ml hygromycin B solution and 5 µg/ml blasticidin before transferring them to T75 flasks. For generation of single-cell clones from the stable cells, cells were trypsinated and adjusted to a concentration of 5 cells/ml before transferring 100 µl per well to a 96-well plate. The plate was left in the incubator for 7 days and wells identified where one clone gave rise to a colony. Cells in these wells were trypsinated, transferred to a bigger vessel and analysed. For analysis, cells were either treated with doxycycline (0.5 µg/ml) or with control for 48 h and protein levels were compared via Western Blot.

7 References

Ahn, S., Choi, J., & Jeong, S.-H. (2023). The First Korean Adult Case of Progressive Familial Intrahepatic Cholestasis Type 7 with Novel USP53 Splicing Variants by Next Generation Sequencing. *Yonsei Medical Journal*, *64*(12), 745–749. https://doi.org/10.3349/ymj.2023.0161

Akimov, V., Barrio-Hernandez, I., Hansen, S. V. F., Hallenborg, P., Pedersen, A.-K., Bekker-Jensen, D. B., Puglia, M., Christensen, S. D. K., Vanselow, J. T., Nielsen, M. M., Kratchmarova, I., Kelstrup, C. D., Olsen, J. V., & Blagoev, B. (2018). UbiSite approach for comprehensive mapping of lysine and N-terminal ubiquitination sites. *Nature Structural & Molecular Biology*, *25*(7), 631–640. https://doi.org/10.1038/s41594-018-0084-y

Akimov, V., Henningsen, J., Hallenborg, P., Rigbolt, K. T. G., Jensen, S. S., Nielsen, M. M., Kratchmarova, I., & Blagoev, B. (2014). StUbEx: Stable Tagged Ubiquitin Exchange System for the Global Investigation of Cellular Ubiquitination. *Journal of Proteome Research*, *13*(9), 4192–4204. https://doi.org/10.1021/pr500549h

Akimov, V., Olsen, L. C. B., Hansen, S. V. F., Barrio-Hernandez, I., Puglia, M., Jensen, S. S., Solov'yov, I. A., Kratchmarova, I., & Blagoev, B. (2018). StUbEx PLUS—A Modified Stable Tagged Ubiquitin Exchange System for Peptide Level Purification and In-Depth Mapping of Ubiquitination Sites. *Journal of Proteome Research*, *17*(1), 296–304. https://doi.org/10.1021/acs.jproteome.7b00566

Alam, S., Lal, B. B., Ravindranath, A., Bavdekar, A., Dheivamani, N., Snehavardhan, P., Shah, A., Tripathi, P. R., Nagral, A., Srikanth, K. P., Shah, I., Ramakrishna, S. H., Suchismita, A., Waikar, Y., Shah, V., Nalwalla, Z., Kumar, K., Maria, A., Sibal, A., Sivaramakrishnan, M., Wadhwa, N., Ashritha, A., Sood, V., Khanna, R.s (2024). Natural course and outcomes of children with ubiquitin-specific protease 53 (USP53)-related genetic chronic cholestasis. *Journal of Pediatric Gastroenterology and Nutrition*, *79*(6), 1199–1208. https://doi.org/10.1002/jpn3.12392

Alhebbi, H., Peer-Zada, A. A., Al-Hussaini, A. A., Algubaisi, S., Albassami, A., AlMasri, N., Alrusayni, Y., Alruzug, I. M., Alharby, E., Samman, M. A., Ayoub, S. Z., Maddirevula, S., Peake, R. W. A., Alkuraya, F. S., Wali, S., & Almontashiri, N. A. M. (2020). New paradigms of USP53 disease: Normal GGT cholestasis, BRIC, cholangiopathy, and responsiveness to rifampicin. *Journal of Human Genetics*. https://doi.org/10.1038/s10038-020-0811-1

Alhebbi, H., Peer-Zada, A. A., Al-Hussaini, A. A., Algubaisi, S., Albassami, A., AlMasri, N., Alrusayni, Y., Alruzug, I. M., Alharby, E., Samman, M. A., Ayoub, S. Z., Maddirevula, S., Peake, R. W. A., Alkuraya, F. S., Wali, S., & Almontashiri, N. A. M. (2021). New paradigms of USP53 disease: Normal GGT cholestasis, BRIC, cholangiopathy, and responsiveness to rifampicin. *Journal of Human Genetics*, *66*(2), Article 2. https://doi.org/10.1038/s10038-020-0811-1

Altun, M., Kramer, H. B., Willems, L. I., McDermott, J. L., Leach, C. A., Goldenberg, S. J., Kumar, K. G. S., Konietzny, R., Fischer, R., Kogan, E., Mackeen, M. M., McGouran, J., Khoronenkova, S. V., Parsons, J. L., Dianov, G. L., Nicholson, B., & Kessler, B. M. (2011). Activity-Based Chemical Proteomics Accelerates Inhibitor Development for Deubiquitylating Enzymes. *Chemistry & Biology*, *18*(11), 1401–1412. https://doi.org/10.1016/j.chembiol.2011.08.018

Ananda Kesavan, T. M., Sreejith Kumar, K. C., & Thampi, G. P. (2022). A rare case of prolonged jaundice due to USP53 gene mutation. *Pediatric Companion*, *1*(1), 24. https://doi.org/10.4103/pedc.pedc_8_22

Anderson, J. M., Glade, J. L., Stevenson, B. R., Boyer, J. L., & Mooseker, M. S. (1989). Hepatic immunohistochemical localization of the tight junction protein ZO-1 in rat models of cholestasis. *The American Journal of Pathology*, *134*(5), 1055–1062.

Asimaki, E., Petriukov, K., Renz, C., Meister, C., & Ulrich, H. D. (2022). Fast friends – Ubiquitin-like modifiers as engineered fusion partners. *Seminars in Cell & Developmental Biology*, *132*, 132–145. https://doi.org/10.1016/j.semcdb.2021.11.013

Ateş, B. B., Ceylan, A. C., Hızal, G., Duran, F., Doğan, H. T., & Hızlı, Ş. (2023). A novel homozygous mutation in the USP53 gene as the cause of benign recurrent intrahepatic cholestasis in children: A case report. *The Turkish Journal of Pediatrics*, *65*(6), 1012–1017. https://doi.org/10.24953/turkjped.2023.367

Baek, D., Park, K. H., Lee, K.-M., Jung, S., Joung, S., Kim, J., & Lee, J. W. (2021). Ubiquitin-specific protease 53 promotes osteogenic differentiation of human bone marrow-derived mesenchymal stem cells. *Cell Death & Disease*, *12*(3), 238. https://doi.org/10.1038/s41419-021-03517-x

Berman, H. M., Westbrook, J., Feng, Z., Gilliland, G., Bhat, T. N., Weissig, H., Shindyalov, I. N., & Bourne, P. E. (2000). The Protein Data Bank. *Nucleic Acids Research*, *28*(1), 235–242. https://doi.org/10.1093/nar/28.1.235

Bertsoulaki, E., Glover, H. L., Gomes-Neto, J. I., Pizer, B., Maiato, H., Urbé, S., & Clague, M. J. (2022). *The deubiquitylase USP31 controls the Chromosomal Passenger Complex and spindle dynamics* (p. 2022.08.17.504168). bioRxiv. https://doi.org/10.1101/2022.08.17.504168

Biggs, P. J., Wooster, R., Ford, D., Chapman, P., Mangion, J., Quirk, Y., Easton, D. F., Burn, J., & Stratton, M. R. (1995). Familial cylindromatosis (turban tumour syndrome) gene localised to chromosome 16q12–q13: Evidence for its role as a tumour suppressor gene. *Nature Genetics*, *11*(4), 441–443. https://doi.org/10.1038/ng1295-441

Bingol, B., Tea, J. S., Phu, L., Reichelt, M., Bakalarski, C. E., Song, Q., Foreman, O., Kirkpatrick, D. S., & Sheng, M. (2014). The mitochondrial deubiquitinase USP30 opposes parkin-mediated mitophagy. *Nature*, *510*(7505), 370–375. https://doi.org/10.1038/nature13418

Bridges, D., & Moorhead, G. B. G. (2005). 14-3-3 Proteins: A Number of Functions for a Numbered Protein. *Science's STKE*, *2005*(296), re10–re10. https://doi.org/10.1126/stke.2962005re10

Buzuk, L., & Hellerschmied, D. (2023). Ubiquitin-mediated degradation at the Golgi apparatus. *Frontiers in Molecular Biosciences*, *10*. https://doi.org/10.3389/fmolb.2023.1197921

Cao, L., Liu, X., Zheng, B., Xing, C., & Liu, J. (2022). Role of K63-linked ubiquitination in cancer. *Cell Death Discovery*, *8*(1), 1–13. https://doi.org/10.1038/s41420-022-01204-0

Chen, L., Zhang, L., He, H., Shao, F., Yu, Z., Gao, Y., & He, J. (2024). Ubiquitin-specific protease 54 regulates GLUT1-mediated aerobic glycolysis to inhibit lung adenocarcinoma progression by modifying p53 degradation. *Oncogene*, *43*(26), 2025–2037. https://doi.org/10.1038/s41388-024-03047-8

Chernorudskiy, A. L., & Gainullin, M. R. (2013). Ubiquitin System: Direct Effects Join the Signaling. *Science Signaling*, *6*(280), pe22–pe22. https://doi.org/10.1126/scisignal.2004251

Cho, Y., Haraguchi, D., Shigetomi, K., Matsuzawa, K., Uchida, S., & Ikenouchi, J. (2022). Tricellulin secures the epithelial barrier at tricellular junctions by interacting with actomyosin. *Journal of Cell Biology*, *221*(4), e202009037. https://doi.org/10.1083/jcb.202009037

Christianson, J. C., & Ye, Y. (2014). Cleaning up in the endoplasmic reticulum: Ubiquitin in charge. *Nature Structural & Molecular Biology*, *21*(4), 325–335. https://doi.org/10.1038/nsmb.2793

Clague, M. J., Coulson, J. M., & Urbé, S. (2012). Cellular functions of the DUBs. *Journal of Cell Science*, *125*(2), 277. https://doi.org/10.1242/jcs.090985

Clague, M. J., Heride, C., & Urbé, S. (2015). The demographics of the ubiquitin system. *Trends in Cell Biology*, *25*(7), 417–426. https://doi.org/10.1016/j.tcb.2015.03.002

Clague, M. J., Urbe, S., & Komander, D. (2019). Breaking the chains: Deubiquitylating enzyme specificity begets function. *Nat Rev Mol Cell Biol*, *20*(6), 338–352. https://doi.org/10.1038/s41580-019-0099-1

Clague, M. J., Urbé, S., & Komander, D. (2019). Breaking the chains: Deubiquitylating enzyme specificity begets function. *Nature Reviews Molecular Cell Biology*, *20*(6), Article 6. https://doi.org/10.1038/s41580-019-0099-1

Crowe, S. O., Rana, A. S. J. B., Deol, K. K., Ge, Y., & Strieter, E. R. (2017). Ubiquitin Chain Enrichment Middle-Down Mass Spectrometry Enables Characterization of Branched Ubiquitin Chains in Cellulo. *Analytical Chemistry*, *89*(8), 4428–4434. https://doi.org/10.1021/acs.analchem.6b03675

Cuff, J. A., & Barton, G. J. (2000). Application of multiple sequence alignment profiles to improve protein secondary structure prediction. *Proteins: Structure, Function, and Bioinformatics*, *40*(3), 502–511. https://doi.org/10.1002/1097-0134(20000815)40:3<502::AID-PROT170>3.0.CO;2-Q

Cummins, P. M. (2012). Occludin: One Protein, Many Forms. *Molecular and Cellular Biology*, *32*(2), 242–250. https://doi.org/10.1128/MCB.06029-11

Damgaard, R. B., Nachbur, U., Yabal, M., Wong, W. W.-L., Fiil, B. K., Kastirr, M., Rieser, E., Rickard, J. A., Bankovacki, A., Peschel, C., Ruland, J., Bekker-Jensen, S., Mailand, N., Kaufmann, T., Strasser, A., Walczak, H., Silke, J., Jost, P. J., & Gyrd-Hansen, M. (2012). The Ubiquitin Ligase XIAP Recruits LUBAC for NOD2 Signaling in Inflammation and Innate Immunity. *Molecular Cell*, *46*(6), 746–758. https://doi.org/10.1016/j.molcel.2012.04.014

Danielsen, J. M. R., Sylvestersen, K. B., Bekker-Jensen, S., Szklarczyk, D., Poulsen, J. W., Horn, H., Jensen, L. J., Mailand, N., & Nielsen, M. L. (2011). Mass Spectrometric Analysis of Lysine Ubiquitylation Reveals Promiscuity at Site Level *. *Molecular & Cellular Proteomics*, *10*(3). https://doi.org/10.1074/mcp.M110.003590

Dantas, T. J. (2020). Centrosomes and cilia: Always at the center of the action. *Communications Biology*, *3*(1), 1–3. https://doi.org/10.1038/s42003-020-01519-7

Darling, S., Fielding, A. B., Sabat-Pośpiech, D., Prior, I. A., & Coulson, J. M. (2017). Regulation of the cell cycle and centrosome biology by deubiquitylases. *Biochemical Society Transactions*, *45*(5), 1125–1136. https://doi.org/10.1042/BST20170087

Denis, N. J., Vasilescu, J., Lambert, J.-P., Smith, J. C., & Figeys, D. (2007). Tryptic digestion of ubiquitin standards reveals an improved strategy for identifying ubiquitinated proteins by mass spectrometry. *PROTEOMICS*, *7*(6), 868–874. https://doi.org/10.1002/pmic.200600410

Ding, J., Chi, H., Qiu, Y.-L., Wang, R.-X., Yang, J., She, H.-Y., Zhang, J., Ling, V., Xing, Q.-H., & Wang, J.-S. (2025). Loss of hepatocyte Usp53 protects mice from a form of

xenobiotic-induced liver injury. *Biochimica et Biophysica Acta (BBA) - Molecular Basis of Disease*, *1871*(3), 167624. https://doi.org/10.1016/j.bbadis.2024.167624

Dolfe, L., Tambaro, S., Tigro, H., Del Campo, M., Hoozemans, J. J. M., Wiehager, B., Graff, C., Winblad, B., Ankarcrona, M., Kaldmäe, M., Teunissen, C. E., Rönnbäck, A., Johansson, J., & Presto, J. (2018). The Bri2 and Bri3 BRICHOS Domains Interact Differently with Aβ 42 and Alzheimer Amyloid Plaques. *Journal of Alzheimer's Disease Reports*, *2*(1), 27–39. https://doi.org/10.3233/ADR-170051

Dósa, A., & Csizmadia, T. (2022). The role of K63-linked polyubiquitin in several types of autophagy. *Biologia Futura*, *73*(2), 137–148. https://doi.org/10.1007/s42977-022-00117-4

Drozdetskiy, A., Cole, C., Procter, J., & Barton, G. J. (2015). JPred4: A protein secondary structure prediction server. *Nucleic Acids Research*, *43*(W1), W389–W394. https://doi.org/10.1093/nar/gkv332

Elia, A. E. H., Boardman, A. P., Wang, D. C., Huttlin, E. L., Everley, R. A., Dephoure, N., Zhou, C., Koren, I., Gygi, S. P., & Elledge, S. J. (2015). Quantitative Proteomic Atlas of Ubiquitination and Acetylation in the DNA Damage Response. *Molecular Cell*, *59*(5), 867–881. https://doi.org/10.1016/j.molcel.2015.05.006

Emmerich, C. H., Bakshi, S., Kelsall, I. R., Ortiz-Guerrero, J., Shpiro, N., & Cohen, P. (2016). Lys63/Met1-hybrid ubiquitin chains are commonly formed during the activation of innate immune signalling. *Biochemical and Biophysical Research Communications*, *474*(3), 452–461. https://doi.org/10.1016/j.bbrc.2016.04.141

Erpapazoglou, Z., Walker, O., & Haguenauer-Tsapis, R. (2014). Versatile Roles of K63-Linked Ubiquitin Chains in Trafficking. *Cells*, *3*(4), 1027–1088. https://doi.org/10.3390/cells3041027

Fairhead, M., & Howarth, M. (2015). Site-Specific Biotinylation of Purified Proteins Using BirA. In A. Gautier & M. J. Hinner (Eds.), *Site-Specific Protein Labeling: Methods and Protocols* (pp. 171–184). Springer. https://doi.org/10.1007/978-1-4939-2272-7_12

Fang, T.-S. Z., Sun, Y., Pearce, A. C., Eleuteri, S., Kemp, M., Luckhurst, C. A., Williams, R., Mills, R., Almond, S., Burzynski, L., Márkus, N. M., Lelliott, C. J., Karp, N. A., Adams, D. J., Jackson, S. P., Zhao, J.-F., Ganley, I. G., Thompson, P. W., Balmus, G., & Simon, D. K. (2023). Knockout or inhibition of USP30 protects dopaminergic neurons in a Parkinson's disease mouse model. *Nature Communications*, *14*(1), 7295. https://doi.org/10.1038/s41467-023-42876-1

Fassl, A., Geng, Y., & Sicinski, P. (2022). CDK4 and CDK6 kinases: From basic science to cancer therapy. *Science*, *375*(6577), eabc1495. https://doi.org/10.1126/science.abc1495

Firat-Karalar, E. N., Rauniyar, N., Yates, J. R., & Stearns, T. (2014). Proximity Interactions among Centrosome Components Identify Regulators of Centriole Duplication. *Current Biology*, *24*(6), 664–670. https://doi.org/10.1016/j.cub.2014.01.067

Foot, N., Henshall, T., & Kumar, S. (2017). Ubiquitination and the Regulation of Membrane Proteins. *Physiological Reviews*, *97*(1), 253–281. https://doi.org/10.1152/physrev.00012.2016

Fraile, J. M., Campos-Iglesias, D., Rodriguez, F., Espanol, Y., & Freije, J. M. (2016). The deubiquitinase USP54 is overexpressed in colorectal cancer stem cells and promotes intestinal tumorigenesis. *Oncotarget*, *7*(46), 74427–74434. https://doi.org/10.18632/oncotarget.12769

Fulzele, A., & Bennett, E. J. (2018). Ubiquitin diGLY Proteomics as an Approach to Identify and Quantify the Ubiquitin-Modified Proteome. *Methods in Molecular Biology (Clifton, N.J.)*, *1844*, 363–384. https://doi.org/10.1007/978-1-4939-8706-1_23

Gardino, A. K., & Yaffe, M. B. (2011). 14-3-3 proteins as signaling integration points for cell cycle control and apoptosis. *Seminars in Cell & Developmental Biology*, *22*(7), 688–695. https://doi.org/10.1016/j.semcdb.2011.09.008

Gersch, M., Gladkova, C., Schubert, A. F., Michel, M. A., Maslen, S., & Komander, D. (2017). Mechanism and regulation of the Lys6-selective deubiquitinase USP30. *Nature Structural & Molecular Biology*, *24*(11), 920–930. https://doi.org/10.1038/nsmb.3475

Gezdirici, A., Kalaycik Şengül, Ö., Doğan, M., Özgüven, B. Y., & Akbulut, E. (2023). Biallelic Novel USP53 Splicing Variant Disrupting the Gene Function that Causes Cholestasis Phenotype and Review of the Literature. *Molecular Syndromology*, *13*(6), 471–484. https://doi.org/10.1159/000523937

Goedhart, J., & Luijsterburg, M. S. (2020). VolcaNoseR is a web app for creating, exploring, labeling and sharing volcano plots. *Scientific Reports*, *10*(1), 20560. https://doi.org/10.1038/s41598-020-76603-3

Gomez-Ferreria, M. A., Bashkurov, M., Mullin, M., Gingras, A.-C., & Pelletier, L. (2012). CEP192 interacts physically and functionally with the K63-deubiquitinase CYLD to promote mitotic spindle assembly. *Cell Cycle*, *11*(19), 3555–3558. https://doi.org/10.4161/cc.21574

Grantham, J. (2020). The Molecular Chaperone CCT/TRiC: An Essential Component of Proteostasis and a Potential Modulator of Protein Aggregation. *Frontiers in Genetics*, *11*. https://doi.org/10.3389/fgene.2020.00172

Gui, D., Dong, Z., Peng, W., Jiang, W., Huang, G., Liu, G., Ye, Z., Wang, Y., Xu, Z., Fu, J., Luo, S., & Zhao, Y. (2021). Ubiquitin-specific peptidase 53 inhibits the occurrence and development of clear cell renal cell carcinoma through NF-κB pathway inactivation. *Cancer Medicine*, *10*(11), 3674–3688. https://doi.org/10.1002/cam4.3911

Gupta, G. D., Coyaud, É., Gonçalves, J., Mojarad, B. A., Liu, Y., Wu, Q., Gheiratmand, L., Comartin, D., Tkach, J. M., Cheung, S. W. T., Bashkurov, M., Hasegan, M., Knight, J. D., Lin, Z.-Y., Schueler, M., Hildebrandt, F., Moffat, J., Gingras, A.-C., Raught, B., & Pelletier, L. (2015). A Dynamic Protein Interaction Landscape of the Human Centrosome-Cilium Interface. *Cell*, *163*(6), 1484–1499. https://doi.org/10.1016/j.cell.2015.10.065

Gwon, Y., Maxwell, B. A., Kolaitis, R.-M., Zhang, P., Kim, H. J., & Taylor, J. P. (2021). Ubiquitination of G3BP1 mediates stress granule disassembly in a context-specific manner. *Science*, *372*(6549), eabf6548. https://doi.org/10.1126/science.abf6548

Haahr, P., Borgermann, N., Guo, X., Typas, D., Achuthankutty, D., Hoffmann, S., Shearer, R., Sixma, T. K., & Mailand, N. (2018). ZUFSP Deubiquitylates K63-Linked Polyubiquitin Chains to Promote Genome Stability. *Molecular Cell*, *70*(1), 165-174.e6. PubMed. https://doi.org/10.1016/j.molcel.2018.02.024

Haglund, K., Sigismund, S., Polo, S., Szymkiewicz, I., Di Fiore, P. P., & Dikic, I. (2003). Multiple monoubiquitination of RTKs is sufficient for their endocytosis and degradation. *Nature Cell Biology*, *5*(5), Article 5. https://doi.org/10.1038/ncb983

Hansen, F. M., Tanzer, M. C., Brüning, F., Bludau, I., Stafford, C., Schulman, B. A., Robles, M. S., Karayel, O., & Mann, M. (2021). Data-independent acquisition method for ubiquitinome analysis reveals regulation of circadian biology. *Nature Communications*, *12*(1), 254. https://doi.org/10.1038/s41467-020-20509-1

Hariri, H., Addison, W. N., & St-Arnaud, R. (2021). Ubiquitin specific peptidase Usp53 regulates osteoblast versus adipocyte lineage commitment. *Scientific Reports*, *11*(1), 8418. https://doi.org/10.1038/s41598-021-87608-x

Harrigan, J. A., Jacq, X., Martin, N. M., & Jackson, S. P. (2018). Deubiquitylating enzymes and drug discovery: Emerging opportunities. *Nature Reviews Drug Discovery*, *17*(1), 57–78. https://doi.org/10.1038/nrd.2017.152

Henning, N. J., Boike, L., Spradlin, J. N., Ward, C. C., Liu, G., Zhang, E., Belcher, B. P., Brittain, S. M., Hesse, M. J., Dovala, D., McGregor, L. M., Valdez Misiolek, R., Plasschaert, L. W., Rowlands, D. J., Wang, F., Frank, A. O., Fuller, D., Estes, A. R., Randal, K. L., … Nomura, D. K. (2022). Deubiquitinase-targeting chimeras for targeted protein stabilization. *Nature Chemical Biology*, *18*(4), 412–421. https://doi.org/10.1038/s41589-022-00971-2

Hershko, A., Ciechanover, A., & Rose, I. A. (1979). Resolution of the ATP-dependent proteolytic system from reticulocytes: A component that interacts with ATP. *Proceedings of the National Academy of Sciences*, *76*(7), 3107–3110. https://doi.org/10.1073/pnas.76.7.3107

Hjerpe, R., Aillet, F., Lopitz-Otsoa, F., Lang, V., England, P., & Rodriguez, M. S. (2009). Efficient protection and isolation of ubiquitylated proteins using tandem ubiquitin-binding entities. *EMBO Reports*, *10*(11), 1250–1258. https://doi.org/10.1038/embor.2009.192

Holleman, J., & Marchese, A. (2014). The ubiquitin ligase deltex-3l regulates endosomal sorting of the G protein–coupled receptor CXCR4. *Molecular Biology of the Cell*, *25*(12), 1892–1904. https://doi.org/10.1091/mbc.e13-10-0612

Hospenthal, M. K., Mevissen, T. E. T., & Komander, D. (2015). Deubiquitinase–based analysis of ubiquitin chain architecture using Ubiquitin Chain Restriction (UbiCRest). *Nature Protocols*, *10*(2), 349–361. https://doi.org/10.1038/nprot.2015.018

Hrdinka, M., Fiil, B. K., Zucca, M., Leske, D., Bagola, K., Yabal, M., Elliott, P. R., Damgaard, R. B., Komander, D., Jost, P. J., & Gyrd-Hansen, M. (2016). CYLD Limits Lys63- and Met1-Linked Ubiquitin at Receptor Complexes to Regulate Innate Immune Signaling. *Cell Reports*, *14*(12), 2846–2858. https://doi.org/10.1016/j.celrep.2016.02.062

Huang, F., Zeng, X., Kim, W., Balasubramani, M., Fortian, A., Gygi, S. P., Yates, N. A., & Sorkin, A. (2013). Lysine 63-linked polyubiquitination is required for EGF receptor degradation. *Proceedings of the National Academy of Sciences*, *110*(39), 15722–15727. https://doi.org/10.1073/pnas.1308014110

Huang, S., Liu, L., Mei, H.-F., Zhang, Q.-W., Zhang, X., Xu, X.-T., Wang, X.-Z., Huang, X., Wang, T., Jiang, Z.-Z., Zhang, L.-Y., & Sun, L.-X. (2021). Altered integrity of hepatocyte tight junctions in rats with triptolide-induced cholestasis. *Chinese Journal of Natural Medicines*, *19*(3), 188–194. https://doi.org/10.1016/S1875-5364(21)60020-1

Hunt, T., Nasmyth, K., & Novák, B. (2011). The cell cycle. *Philosophical Transactions of the Royal Society B: Biological Sciences*, *366*(1584), 3494–3497. https://doi.org/10.1098/rstb.2011.0274

Ikeda, F. (2020). Mitophagy is induced by short ubiquitin chains on mitochondria. *Journal of Cell Biology*, *219*(9), e202008031. https://doi.org/10.1083/jcb.202008031

Ikenouchi, J., Furuse, M., Furuse, K., Sasaki, H., Tsukita, S., & Tsukita, S. (2005). Tricellulin constitutes a novel barrier at tricellular contacts of epithelial cells. *Journal of Cell Biology*, *171*(6), 939–945. https://doi.org/10.1083/jcb.200510043

Isakson, P., Lystad, A. H., Breen, K., Koster, G., Stenmark, H., & Simonsen, A. (2013). TRAF6 mediates ubiquitination of KIF23/MKLP1 and is required for midbody ring degradation

by selective autophagy. *Autophagy*, *9*(12), 1955–1964. https://doi.org/10.4161/auto.26085

Iwaya, N., Kuwahara, Y., Fujiwara, Y., Goda, N., Tenno, T., Akiyama, K., Mase, S., Tochio, H., Ikegami, T., Shirakawa, M., & Hiroaki, H. (2010). A Common Substrate Recognition Mode Conserved between Katanin p60 and VPS4 Governs Microtubule Severing and Membrane Skeleton Reorganization. *Journal of Biological Chemistry*, *285*(22), 16822–16829. https://doi.org/10.1074/jbc.M110.108365

Jackson, S. P., & Durocher, D. (2013). Regulation of DNA Damage Responses by Ubiquitin and SUMO. *Molecular Cell*, *49*(5), 795–807. https://doi.org/10.1016/j.molcel.2013.01.017

Jennek, S., Mittag, S., Reiche, J., Westphal, J. K., Seelk, S., Dörfel, M. J., Pfirrmann, T., Friedrich, K., Schütz, A., Heinemann, U., & Huber, O. (2017). Tricellulin is a target of the ubiquitin ligase Itch. *Annals of the New York Academy of Sciences*, *1397*(1), 157–168. https://doi.org/10.1111/nyas.13349

Jin, J., Xie, X., Xiao, Y., Hu, H., Zou, Q., Cheng, X., & Sun, S.-C. (2016). Epigenetic regulation of the expression of Il12 and Il23 and autoimmune inflammation by the deubiquitinase Trabid. *Nature Immunology*, *17*(3), 259–268. https://doi.org/10.1038/ni.3347

Jolly, L. A., Kumar, R., Penzes, P., Piper, M., & Gecz, J. (2022). The DUB Club: Deubiquitinating Enzymes and Neurodevelopmental Disorders. *Biological Psychiatry*, *92*(8), 614–625. https://doi.org/10.1016/j.biopsych.2022.03.022

Jonsson, E., Htet, Z. M., Bard, J. A. M., Dong, K. C., & Martin, A. (2022). Ubiquitin modulates 26S proteasome conformational dynamics and promotes substrate degradation. *Science Advances*, *8*(51), eadd9520. https://doi.org/10.1126/sciadv.add9520

Jumper, J., Evans, R., Pritzel, A., Green, T., Figurnov, M., Ronneberger, O., Tunyasuvunakool, K., Bates, R., Žídek, A., Potapenko, A., Bridgland, A., Meyer, C., Kohl, S. A. A., Ballard, A. J., Cowie, A., Romera-Paredes, B., Nikolov, S., Jain, R., Adler, J., … Hassabis, D. (2021). Highly accurate protein structure prediction with AlphaFold. *Nature*, *596*(7873), 583–589. https://doi.org/10.1038/s41586-021-03819-2

Kaiser, S. E., Riley, B. E., Shaler, T. A., Trevino, R. S., Becker, C. H., Schulman, H., & Kopito, R. R. (2011). Protein standard absolute quantification (PSAQ) method for the measurement of cellular ubiquitin pools. *Nature Methods*, *8*(8), 691–696. https://doi.org/10.1038/nmeth.1649

Kamitani, T., Sakaguchi, H., Tamura, A., Miyashita, T., Yamazaki, Y., Tokumasu, R., Inamoto, R., Matsubara, A., Mori, N., Hisa, Y., & Tsukita, S. (2015). Deletion of Tricellulin Causes Progressive Hearing Loss Associated with Degeneration of Cochlear Hair Cells. *Scientific Reports*, *5*(1), 18402. https://doi.org/10.1038/srep18402

Kamran, T. E., Faisal, S., Khalid, R., Haider, Z., Inam, R., Siddiqui, Y., Iqbal, M., & Khan, S. A. (2024). A novel case report of benign recurrent intrahepatic cholestasis-associated USP53 genetic mutation in a Pakistani girl. *SAGE Open Medical Case Reports*, *12*, 2050313X241266813. https://doi.org/10.1177/2050313X241266813

Kanwal, A., Sheikh, S. A., Aslam, F., Yaseen, S., Beetham, Z., Pankratz, N., Clabots, C. R., Naz, S., & Pardo, J. V. (2023). Genome Sequencing of Consanguineous Family Implicates Ubiquitin-Specific Protease 53 (USP53) Variant in Psychosis/Schizophrenia: Wild-Type Expression in Murine Hippocampal CA 1–3 and Granular Dentate with AMPA Synapse Interactions. *Genes*, *14*(10), Article 10. https://doi.org/10.3390/genes14101921

Kasahara, K., Aoki, H., Kiyono, T., Wang, S., Kagiwada, H., Yuge, M., Tanaka, T., Nishimura, Y., Mizoguchi, A., Goshima, N., & Inagaki, M. (2018). EGF receptor kinase suppresses

ciliogenesis through activation of USP8 deubiquitinase. *Nature Communications*, *9*(1), 758. https://doi.org/10.1038/s41467-018-03117-y

Kawaguchi, T., Sakisaka, S., Sata, M., Mori, M., & Tanikawa, K. (1999). Different lobular distributions of altered hepatocyte tight junctions in rat models of intrahepatic and extrahepatic cholestasis. *Hepatology (Baltimore, Md.)*, *29*(1), 205–216. https://doi.org/10.1002/hep.510290115

Kazi, N. H., Klink, N., Gallant, K., Kipka, G.-M., & Gersch, M. (2024). *Chimeric deubiquitinase engineering reveals structural basis for specific inhibition of USP30 and a framework for DUB ligandability* (p. 2024.09.22.613429). bioRxiv. https://doi.org/10.1101/2024.09.22.613429

Kazlauskaite, A., Kondapalli, C., Gourlay, R., Campbell, D. G., Ritorto, M. S., Hofmann, K., Alessi, D. R., Knebel, A., Trost, M., & Muqit, M. M. K. (2014). Parkin is activated by PINK1-dependent phosphorylation of ubiquitin at Ser65. *Biochemical Journal*, *460*(1), 127–141. https://doi.org/10.1042/BJ20140334

Kazmierczak, M., Harris, S. L., Kazmierczak, P., Shah, P., Starovoytov, V., Ohlemiller, K. K., & Schwander, M. (2015a). Progressive Hearing Loss in Mice Carrying a Mutation in Usp53. *Journal of Neuroscience*, *35*(47), 15582–15598. https://doi.org/10.1523/JNEUROSCI.1965-15.2015

Kazmierczak, M., Harris, S. L., Kazmierczak, P., Shah, P., Starovoytov, V., Ohlemiller, K. K., & Schwander, M. (2015b). Progressive Hearing Loss in Mice Carrying a Mutation in Usp53. *J Neurosci*, *35*(47), 15582–15598. https://doi.org/10.1523/JNEUROSCI.1965-15.2015

Kim, D. I., Jensen, S. C., Noble, K. A., KC, B., Roux, K. H., Motamedchaboki, K., & Roux, K. J. (2016). An improved smaller biotin ligase for BioID proximity labeling. *Molecular Biology of the Cell*, *27*(8), 1188–1196. https://doi.org/10.1091/mbc.E15-12-0844

Kim, D. I., KC, B., Zhu, W., Motamedchaboki, K., Doye, V., & Roux, K. J. (2014). Probing nuclear pore complex architecture with proximity-dependent biotinylation. *Proceedings of the National Academy of Sciences*, *111*(24), E2453–E2461. https://doi.org/10.1073/pnas.1406459111

Kim, H., Chen, J., & Yu, X. (2007). Ubiquitin-Binding Protein RAP80 Mediates BRCA1-Dependent DNA Damage Response. *Science*, *316*(5828), 1202–1205. https://doi.org/10.1126/science.1139621

Kim, W., Bennett, E. J., Huttlin, E. L., Guo, A., Li, J., Possemato, A., Sowa, M. E., Rad, R., Rush, J., Comb, M. J., Harper, J. W., & Gygi, S. P. (2011). Systematic and Quantitative Assessment of the Ubiquitin-Modified Proteome. *Molecular Cell*, *44*(2), 325–340. https://doi.org/10.1016/j.molcel.2011.08.025

Kirkpatrick, D. S., Weldon, S. F., Tsaprailis, G., Liebler, D. C., & Gandolfi, A. J. (2005). Proteomic identification of ubiquitinated proteins from human cells expressing His-tagged ubiquitin. *PROTEOMICS*, *5*(8), 2104–2111. https://doi.org/10.1002/pmic.200401089

Kitano, T., Kitajiri, S., Nishio, S., & Usami, S. (2019). Detailed Clinical Features of Deafness Caused by a Claudin-14 Variant. *International Journal of Molecular Sciences*, *20*(18), 4579. https://doi.org/10.3390/ijms20184579

Kliza, K., & Husnjak, K. (2020). Resolving the Complexity of Ubiquitin Networks. *Frontiers in Molecular Biosciences*, *7*. https://doi.org/10.3389/fmolb.2020.00021

Kobayashi, T., & Dynlacht, B. D. (2011). Regulating the transition from centriole to basal body. *Journal of Cell Biology*, *193*(3), 435–444. https://doi.org/10.1083/jcb.201101005

Kolberg, L., Raudvere, U., Kuzmin, I., Adler, P., Vilo, J., & Peterson, H. (2023). g:Profiler—Interoperable web service for functional enrichment analysis and gene identifier mapping (2023 update). *Nucleic Acids Research*, *51*(W1), W207–W212. https://doi.org/10.1093/nar/gkad347

Komander, D., Clague, M. J., & Urbe, S. (2009). Breaking the chains: Structure and function of the deubiquitinases. *Nat Rev Mol Cell Biol*, *10*(8), 550–563. https://doi.org/10.1038/nrm2731

Komander, D., & Rape, M. (2012). The Ubiquitin Code. *Annual Review of Biochemistry*, *81*(1), 203–229. https://doi.org/10.1146/annurev-biochem-060310-170328

Kulathu, Y., Akutsu, M., Bremm, A., Hofmann, K., & Komander, D. (2009). Two-sided ubiquitin binding explains specificity of the TAB2 NZF domain. *Nature Structural & Molecular Biology*, *16*(12), 1328–1330. https://doi.org/10.1038/nsmb.1731

Kuriyama, R., Gustus, C., Terada, Y., Uetake, Y., & Matuliene, J. (2002). CHO1, a mammalian kinesin-like protein, interacts with F-actin and is involved in the terminal phase of cytokinesis. *Journal of Cell Biology*, *156*(5), 783–790. https://doi.org/10.1083/jcb.200109090

Lafont, E., Kantari-Mimoun, C., Draber, P., De Miguel, D., Hartwig, T., Reichert, M., Kupka, S., Shimizu, Y., Taraborrelli, L., Spit, M., Sprick, M. R., & Walczak, H. (2017). The linear ubiquitin chain assembly complex regulates TRAIL-induced gene activation and cell death. *The EMBO Journal*, *36*(9), 1147–1166. https://doi.org/10.15252/embj.201695699

Lange, S. M., McFarland, M. R., Lamoliatte, F., Carroll, T., Krshnan, L., Pérez-Ràfols, A., Kwasna, D., Shen, L., Wallace, I., Cole, I., Armstrong, L. A., Knebel, A., Johnson, C., De Cesare, V., & Kulathu, Y. (2024). VCP/p97-associated proteins are binders and debranching enzymes of K48–K63-branched ubiquitin chains. *Nature Structural & Molecular Biology*, *31*(12), 1872–1887. https://doi.org/10.1038/s41594-024-01354-y

Le Mercier, P., Bolleman, J., de Castro, E., Gasteiger, E., Bansal, P., Auchincloss, A. H., Boutet, E., Breuza, L., Casals-Casas, C., Estreicher, A., Feuermann, M., Lieberherr, D., Rivoire, C., Pedruzzi, I., Redaschi, N., & Bridge, A. (2022). SwissBioPics—An interactive library of cell images for the visualization of subcellular location data. *Database*, *2022*, baac026. https://doi.org/10.1093/database/baac026

Lee, B.-H., Lu, Y., Prado, M. A., Shi, Y., Tian, G., Sun, S., Elsasser, S., Gygi, S. P., King, R. W., & Finley, D. (2016). USP14 deubiquitinates proteasome-bound substrates that are ubiquitinated at multiple sites. *Nature*, *532*(7599), 398–401. https://doi.org/10.1038/nature17433

Lee, K. B., & Sharp, P. A. (2004). Transcription-Dependent Polyubiquitination of RNA Polymerase II Requires Lysine 63 of Ubiquitin. *Biochemistry*, *43*(48), 15223–15229. https://doi.org/10.1021/bi048719x

Lee, M. J., Lee, B.-H., Hanna, J., King, R. W., & Finley, D. (2011). Trimming of Ubiquitin Chains by Proteasome-associated Deubiquitinating Enzymes*. *Molecular & Cellular Proteomics*, *10*(5), R110.003871. https://doi.org/10.1074/mcp.R110.003871

Li, C. Z., Ogawa, H., Ng, S. S., Chen, X., Kishimoto, E., Sakabe, K., Fukami, A., Hu, Y.-C., Mayhew, C. N., Hellmann, J., Miethke, A., Tasnova, N. L., Blackford, S. J. I., Tang, Z. M., Syanda, A. M., Ma, L., Xiao, F., Sambrotta, M., Tavabie, O., … Asai, A. (2022). Human iPSC-derived hepatocyte system models cholestasis with tight junction protein 2 deficiency. *JHEP Reports*, *4*(4), 100446. https://doi.org/10.1016/j.jhepr.2022.100446

Li, M., Chen, D., Shiloh, A., Luo, J., Nikolaev, A. Y., Qin, J., & Gu, W. (2002). Deubiquitination of p53 by HAUSP is an important pathway for p53 stabilization. *Nature*, *416*(6881), 648–653. https://doi.org/10.1038/nature737

Ligasová, A., Frydrych, I., & Koberna, K. (2023). Basic Methods of Cell Cycle Analysis. *International Journal of Molecular Sciences*, *24*(4), Article 4. https://doi.org/10.3390/ijms24043674

Lim, K.-L., & Lim, G. G. Y. (2011). K63-linked ubiquitination and neurodegeneration. *Neurobiology of Disease*, *43*(1), 9–16. https://doi.org/10.1016/j.nbd.2010.08.001

Liu, B., Jiang, S., Li, M., Xiong, X., Zhu, M., Li, D., Zhao, L., Qian, L., Zhai, L., Li, J., Lu, H., Sun, S., Lin, J., Lu, Y., Li, X., & Tan, M. (2018). Proteome-wide analysis of USP14 substrates revealed its role in hepatosteatosis via stabilization of FASN. *Nature Communications*, *9*(1), 4770. https://doi.org/10.1038/s41467-018-07185-y

Liu, P., Chen, Z., Guo, Y., He, Q., & Pan, C. (2025). Recent advances in small molecule inhibitors of deubiquitinating enzymes. *European Journal of Medicinal Chemistry*, *287*, 117324. https://doi.org/10.1016/j.ejmech.2025.117324

Liu, X., Zheng, T., Zhang, Y., Zhao, Y., Liu, F., Dai, S., Zhang, M., Zhang, W., Zhang, C., Zhang, M., & Li, X. (2024). Endothelial Dickkopf-1 Promotes Smooth Muscle Cell-derived Foam Cell Formation via USP53-mediated Deubiquitination of SR-A During Atherosclerosis. *International Journal of Biological Sciences*, *20*(8), 2943–2964. https://doi.org/10.7150/ijbs.91957

López-Mosqueda, J., & Dikic, I. (2014). Deciphering Functions of Branched Ubiquitin Chains. *Cell*, *157*(4), 767–769. https://doi.org/10.1016/j.cell.2014.04.026

Lopitz-Otsoa, F., Rodriguez-Suarez, E., Aillet, F., Casado-Vela, J., Lang, V., Matthiesen, R., Elortza, F., & Rodriguez, M. S. (2012). Integrative analysis of the ubiquitin proteome isolated using Tandem Ubiquitin Binding Entities (TUBEs). *Journal of Proteomics*, *75*(10), 2998–3014. https://doi.org/10.1016/j.jprot.2011.12.001

Luczak, M. W., & Zhitkovich, A. (2018). Monoubiquitinated γ-H2AX: Abundant product and specific biomarker for non-apoptotic DNA double-strand breaks. *Toxicology and Applied Pharmacology*, *355*, 238–246. https://doi.org/10.1016/j.taap.2018.07.007

Maddirevula, S., Alhebbi, H., Alqahtani, A., Algoufi, T., Alsaif, H. S., Ibrahim, N., Abdulwahab, F., Barr, M., Alzaidan, H., Almehaideb, A., AlSasi, O., Alhashem, A., Hussaini, H. A., Wali, S., & Alkuraya, F. S. (2019). Identification of novel loci for pediatric cholestatic liver disease defined by KIF12, PPM1F, USP53, LSR, and WDR83OS pathogenic variants. *Genet Med*, *21*(5), 1164–1172. https://doi.org/10.1038/s41436-018-0288-x

Madeira, F., Tinti, M., Murugesan, G., Berrett, E., Stafford, M., Toth, R., Cole, C., MacKintosh, C., & Barton, G. J. (2015). 14-3-3-Pred: Improved methods to predict 14-3-3-binding phosphopeptides. *Bioinformatics*, *31*(14), 2276–2283. https://doi.org/10.1093/bioinformatics/btv133

Mangalath, C. H. (2023). A Case of Progressive Familial Intrahepatic Cholestasis 7 associated with USP53 Gene Mutation. *Journal of Clinical and Experimental Hepatology*, *13*, S157–S158. https://doi.org/10.1016/j.jceh.2023.07.140

Marmor, M. D., & Yarden, Y. (2004). Role of protein ubiquitylation in regulating endocytosis of receptor tyrosine kinases. *Oncogene*, *23*(11), 2057–2070. https://doi.org/10.1038/sj.onc.1207390

Mašindová, I., Šoltýsová, A., Varga, L., Mátyás, P., Ficek, A., Hučková, M., Sůrová, M., Šafka-Brožková, D., Anwar, S., Bene, J., Straka, S., Janicsek, I., Ahmed, Z. M., Seeman, P., Melegh, B., Profant, M., Klimeš, I., Riazuddin, S., Kádasi, Ľ., & Gašperíková, D. (2015). MARVELD2 (DFNB49) Mutations in the Hearing Impaired Central European Roma

Population—Prevalence, Clinical Impact and the Common Origin. *PLOS ONE*, *10*(4), e0124232. https://doi.org/10.1371/journal.pone.0124232

Massoumi, R., Chmielarska, K., Hennecke, K., Pfeifer, A., & Fässler, R. (2006). Cyld Inhibits Tumor Cell Proliferation by Blocking Bcl-3-Dependent NF-κB Signaling. *Cell*, *125*(4), 665–677. https://doi.org/10.1016/j.cell.2006.03.041

Matsuda, N. (2016). Phospho-ubiquitin: Upending the PINK–Parkin–ubiquitin cascade. *The Journal of Biochemistry*, *159*(4), 379–385. https://doi.org/10.1093/jb/mvv125

Matsumoto, M. L., Dong, K. C., Yu, C., Phu, L., Gao, X., Hannoush, R. N., Hymowitz, S. G., Kirkpatrick, D. S., Dixit, V. M., & Kelley, R. F. (2012). Engineering and Structural Characterization of a Linear Polyubiquitin-Specific Antibody. *Journal of Molecular Biology*, *418*(3), 134–144. https://doi.org/10.1016/j.jmb.2011.12.053

Matsumoto, M. L., Wickliffe, K. E., Dong, K. C., Yu, C., Bosanac, I., Bustos, D., Phu, L., Kirkpatrick, D. S., Hymowitz, S. G., Rape, M., Kelley, R. F., & Dixit, V. M. (2010). K11-Linked Polyubiquitination in Cell Cycle Control Revealed by a K11 Linkage-Specific Antibody. *Molecular Cell*, *39*(3), 477–484. https://doi.org/10.1016/j.molcel.2010.07.001

Mattern, M. R., Wu, J., & Nicholson, B. (2012). Ubiquitin-based anticancer therapy: Carpet bombing with proteasome inhibitors vs surgical strikes with E1, E2, E3, or DUB inhibitors. *Biochimica et Biophysica Acta (BBA) - Molecular Cell Research*, *1823*(11), 2014–2021. https://doi.org/10.1016/j.bbamcr.2012.05.005

Maxwell, B. A., Gwon, Y., Mishra, A., Peng, J., Nakamura, H., Zhang, K., Kim, H. J., & Taylor, J. P. (2021). Ubiquitination is essential for recovery of cellular activities after heat shock. *Science*, *372*(6549), eabc3593. https://doi.org/10.1126/science.abc3593

Meng, X., Chen, H., Tan, Z., Yan, W., Liu, Y., Lv, J., & Han, M. (2024). USP53 Affects the Proliferation and Apoptosis of Breast Cancer Cells by Regulating the Ubiquitination Level of ZMYND11. *Biological Procedures Online*, *26*(1), 24. https://doi.org/10.1186/s12575-024-00251-4

Metz, J., & Bressler, D. (1979). Reformation of gap and tight junctions in regenerating liver after cholestasis. *Cell and Tissue Research*, *199*(2), 257–270. https://doi.org/10.1007/BF00236137

Mevissen, T. E. T., Hospenthal, M. K., Geurink, P. P., Elliott, P. R., Akutsu, M., Arnaudo, N., Ekkebus, R., Kulathu, Y., Wauer, T., El Oualid, F., Freund, S. M. V., Ovaa, H., & Komander, D. (2013). OTU Deubiquitinases Reveal Mechanisms of Linkage Specificity and Enable Ubiquitin Chain Restriction Analysis. *Cell*, *154*(1), 169–184. https://doi.org/10.1016/j.cell.2013.05.046

Mevissen, T. E. T., & Komander, D. (2017). Mechanisms of Deubiquitinase Specificity and Regulation. *Annu Rev Biochem*, *86*, 159–192. https://doi.org/10.1146/annurev-biochem-061516-044916

Meyer, H.-J., & Rape, M. (2014). Enhanced Protein Degradation by Branched Ubiquitin Chains. *Cell*, *157*(4), 910–921. https://doi.org/10.1016/j.cell.2014.03.037

Michel, M. A., Elliott, P. R., Swatek, K. N., Simicek, M., Pruneda, J. N., Wagstaff, J. L., Freund, S. M. V., & Komander, D. (2015). Assembly and Specific Recognition of K29- and K33-Linked Polyubiquitin. *Molecular Cell*, *58*(1), 95–109. https://doi.org/10.1016/j.molcel.2015.01.042

Michel, M. A., Swatek, K. N., Hospenthal, M. K., & Komander, D. (2017). Ubiquitin Linkage-Specific Affimers Reveal Insights into K6-Linked Ubiquitin Signaling. *Molecular Cell*, *68*(1), 233-246.e5. https://doi.org/10.1016/j.molcel.2017.08.020

Müller, L., Gutschner, T., & Hatzfeld, M. (2023). Going only half the way: Cell cycle exit after the G1 restriction point. *Signal Transduction and Targeted Therapy*, *8*(1), 1–2. https://doi.org/10.1038/s41392-023-01692-1

Nakano, Y., Kim, S. H., Kim, H.-M., Sanneman, J. D., Zhang, Y., Smith, R. J. H., Marcus, D. C., Wangemann, P., Nessler, R. A., & Bánfi, B. (2009). A Claudin-9–Based Ion Permeability Barrier Is Essential for Hearing. *PLOS Genetics*, *5*(8), e1000610. https://doi.org/10.1371/journal.pgen.1000610

Narendra, D. P., Jin, S. M., Tanaka, A., Suen, D.-F., Gautier, C. A., Shen, J., Cookson, M. R., & Youle, R. J. (2010). PINK1 Is Selectively Stabilized on Impaired Mitochondria to Activate Parkin. *PLOS Biology*, *8*(1), e1000298. https://doi.org/10.1371/journal.pbio.1000298

Nayak, G., Lee, S. I., Yousaf, R., Edelmann, S. E., Trincot, C., Itallie, C. M. V., Sinha, G. P., Rafeeq, M., Jones, S. M., Belyantseva, I. A., Anderson, J. M., Forge, A., Frolenkov, G. I., & Riazuddin, S. (2013). Tricellulin deficiency affects tight junction architecture and cochlear hair cells. *The Journal of Clinical Investigation*, *123*(9), 4036–4049. https://doi.org/10.1172/JCI69031

Nayak, G., Varga, L., Trincot, C., Shahzad, M., Friedman, P. L., Klimes, I., Greinwald, J. H., Riazuddin, S. A., Masindova, I., Profant, M., Khan, S. N., Friedman, T. B., Ahmed, Z. M., Gasperikova, D., Riazuddin, S., & Riazuddin, S. (2015). Molecular genetics of MARVELD2 and clinical phenotype in Pakistani and Slovak families segregating DFNB49 hearing loss. *Human Genetics*, *134*(4), 423–437. https://doi.org/10.1007/s00439-015-1532-y

Newton, K., Matsumoto, M. L., Ferrando, R. E., Wickliffe, K. E., Rape, M., Kelley, R. F., & Dixit, V. M. (2012). Using Linkage-Specific Monoclonal Antibodies to Analyze Cellular Ubiquitylation. In R. J. Dohmen & M. Scheffner (Eds.), *Ubiquitin Family Modifiers and the Proteasome: Reviews and Protocols* (pp. 185–196). Humana Press. https://doi.org/10.1007/978-1-61779-474-2_13

Ohtake, F., Saeki, Y., Ishido, S., Kanno, J., & Tanaka, K. (2016). The K48-K63 Branched Ubiquitin Chain Regulates NF-κB Signaling. *Molecular Cell*, *64*(2), 251–266. https://doi.org/10.1016/j.molcel.2016.09.014

Ordureau, A., Heo, J.-M., Duda, D. M., Paulo, J. A., Olszewski, J. L., Yanishevski, D., Rinehart, J., Schulman, B. A., & Harper, J. W. (2015). Defining roles of PARKIN and ubiquitin phosphorylation by PINK1 in mitochondrial quality control using a ubiquitin replacement strategy. *Proceedings of the National Academy of Sciences*, *112*(21), 6637–6642. https://doi.org/10.1073/pnas.1506593112

Ordureau, A., Paulo, J. A., Zhang, J., An, H., Swatek, K. N., Cannon, J. R., Wan, Q., Komander, D., & Harper, J. W. (2020). Global Landscape and Dynamics of Parkin and USP30-Dependent Ubiquitylomes in iNeurons during Mitophagic Signaling. *Molecular Cell*, *77*(5), 1124-1142.e10. https://doi.org/10.1016/j.molcel.2019.11.013

Panda, S., & Gekara, N. O. (2018). The deubiquitinase MYSM1 dampens NOD2-mediated inflammation and tissue damage by inactivating the RIP2 complex. *Nature Communications*, *9*(1), 4654. https://doi.org/10.1038/s41467-018-07016-0

Pardo, J. V., Pardo, J. V., Sheikh, S. A., Aslam, F., Yasin, S., Kanwal, A., & Naz, S. (2021). *A USP53 p.Cys228Arg variant is associated with autosomal recessive psychosis*. https://doi.org/10.22541/au.162670946.66965381/v1

Pareja, F., Ferraro, D. A., Rubin, C., Cohen-Dvashi, H., Zhang, F., Aulmann, S., Ben-Chetrit, N., Pines, G., Navon, R., Crosetto, N., Köstler, W., Carvalho, S., Lavi, S., Schmitt, F., Dikic, I., Yakhini, Z., Sinn, P., Mills, G. B., & Yarden, Y. (2012). Deubiquitination of

EGFR by Cezanne-1 contributes to cancer progression. *Oncogene*, *31*(43), 4599–4608. https://doi.org/10.1038/onc.2011.587

Pédelacq, J.-D., Cabantous, S., Tran, T., Terwilliger, T. C., & Waldo, G. S. (2006). Engineering and characterization of a superfolder green fluorescent protein. *Nature Biotechnology*, *24*(1), 79–88. https://doi.org/10.1038/nbt1172

Peng, H., Yang, F., Hu, Q., Sun, J., Peng, C., Zhao, Y., & Huang, C. (2020). The ubiquitin-specific protease USP8 directly deubiquitinates SQSTM1/p62 to suppress its autophagic activity. *Autophagy*, *16*(4), 698–708. https://doi.org/10.1080/15548627.2019.1635381

Peng, J., Schwartz, D., Elias, J. E., Thoreen, C. C., Cheng, D., Marsischky, G., Roelofs, J., Finley, D., & Gygi, S. P. (2003). A proteomics approach to understanding protein ubiquitination. *Nature Biotechnology*, *21*(8), 921–926. https://doi.org/10.1038/nbt849

Peng, Y., Liu, Y., Gao, Y., Yuan, B., Qi, X., Fu, Y., Zhu, Q., Cao, T., Zhang, S., Yin, L., & Li, X. (2019). USP7 is a novel Deubiquitinase sustaining PLK1 protein stability and regulating chromosome alignment in mitosis. *Journal of Experimental & Clinical Cancer Research*, *38*(1), 468. https://doi.org/10.1186/s13046-019-1457-8

Pickrell, A. M., & Youle, R. J. (2015). The Roles of PINK1, Parkin, and Mitochondrial Fidelity in Parkinson's Disease. *Neuron*, *85*(2), 257–273. https://doi.org/10.1016/j.neuron.2014.12.007

Porta, G., Rigo, P. S. M., Porta, A., Pugliese, R. P. S., Danesi, V. L. B., Oliveira, E., Borges, C. C. V., Ribeiro, C., & Miura, I. K. (2021). Progressive Familial Intrahepatic Cholestasis Associated With USP53 Gene Mutation in a Brazilian Child. *Journal of Pediatric Gastroenterology and Nutrition*, *72*(5), 674–676. https://doi.org/10.1097/MPG.0000000000003110

Prus, G., Satpathy, S., Weinert, B. T., Narita, T., & Choudhary, C. (2024a). Global, site-resolved analysis of ubiquitylation occupancy and turnover rate reveals systems properties. *Cell*, *187*(11), 2875-2892.e21. https://doi.org/10.1016/j.cell.2024.03.024

Putt, K. K., Pei, R., White, H. M., & Bolling, B. W. (2017). Yogurt inhibits intestinal barrier dysfunction in Caco-2 cells by increasing tight junctions. *Food & Function*, *8*(1), 406–414. https://doi.org/10.1039/C6FO01592A

Qu, X., Liu, H., Song, X., Sun, N., Zhong, H., Qiu, X., Yang, X., & Jiang, B. (2021). Effective degradation of EGFRL858R+T790M mutant proteins by CRBN-based PROTACs through both proteosome and autophagy/lysosome degradation systems. *European Journal of Medicinal Chemistry*, *218*, 113328. https://doi.org/10.1016/j.ejmech.2021.113328

Quesada, V., Díaz-Perales, A., Gutiérrez-Fernández, A., Garabaya, C., Cal, S., & López-Otín, C. (2004). Cloning and enzymatic analysis of 22 novel human ubiquitin-specific proteases. *Biochemical and Biophysical Research Communications*, *314*(1), 54–62. https://doi.org/10.1016/j.bbrc.2003.12.050

Ramazi, S., & Zahiri, J. (2021). Post-translational modifications in proteins: Resources, tools and prediction methods. *Database*, *2021*, baab012. https://doi.org/10.1093/database/baab012

Ramirez, J., Prieto, G., Olazabal-Herrero, A., Borràs, E., Fernandez-Vigo, E., Alduntzin, U., Osinalde, N., Beaskoetxea, J., Lectez, B., Aloria, K., Rodriguez, J. A., Paradela, A., Sabidó, E., Muñoz, J., Corrales, F., Arizmendi, J. M., & Mayor, U. (2021). A Proteomic Approach for Systematic Mapping of Substrates of Human Deubiquitinating Enzymes. *International Journal of Molecular Sciences*, *22*(9), Article 9. https://doi.org/10.3390/ijms22094851

Reiche, J., & Huber, O. (2020). Post-translational modifications of tight junction transmembrane proteins and their direct effect on barrier function. *Biochimica et Biophysica Acta (BBA) - Biomembranes*, *1862*(9), 183330. https://doi.org/10.1016/j.bbamem.2020.183330

Renart, J., Reiser, J., & Stark, G. R. (1979). Transfer of proteins from gels to diazobenzyloxymethyl-paper and detection with antisera: A method for studying antibody specificity and antigen structure. *Proceedings of the National Academy of Sciences*, *76*(7), 3116–3120. https://doi.org/10.1073/pnas.76.7.3116

Renz, C., Asimaki, E., Meister, C., Albanèse, V., Petriukov, K., Krapoth, N. C., Wegmann, S., Wollscheid, H.-P., Wong, R. P., Fulzele, A., Chen, J.-X., Léon, S., & Ulrich, H. D. (2024). Ubiquiton—An inducible, linkage-specific polyubiquitylation tool. *Molecular Cell*, *84*(2), 386-400.e11. https://doi.org/10.1016/j.molcel.2023.11.016

Reyes-Alvarez, E., Walker, T. J., & Mulligan, L. M. (2022). Evaluating Cell Membrane Localization and Intracellular Transport of Proteins by Biotinylation. In S. L. Christian (Ed.), *Cancer Cell Biology: Methods and Protocols* (pp. 197–209). Springer US. https://doi.org/10.1007/978-1-0716-2376-3_15

Rhind, N., & Russell, P. (2012). Signaling Pathways that Regulate Cell Division. *Cold Spring Harbor Perspectives in Biology*, *4*(10), a005942. https://doi.org/10.1101/cshperspect.a005942

Riazuddin, S., Ahmed, Z. M., Fanning, A. S., Lagziel, A., Kitajiri, S., Ramzan, K., Khan, S. N., Chattaraj, P., Friedman, P. L., Anderson, J. M., Belyantseva, I. A., Forge, A., Riazuddin, S., & Friedman, T. B. (2006). Tricellulin Is a Tight-Junction Protein Necessary for Hearing. *The American Journal of Human Genetics*, *79*(6), 1040–1051. https://doi.org/10.1086/510022

Rigden, D. J., Liu, H., Hayes, S. D., Urbé, S., & Clague, M. J. (2009). Ab initio protein modelling reveals novel human MIT domains. *FEBS Letters*, *583*(5), 872–878. https://doi.org/10.1016/j.febslet.2009.02.012

Roux, K. J., Kim, D. I., & Burke, B. (2013). BioID: A Screen for Protein-Protein Interactions. *Current Protocols in Protein Science*, *74*(1), 19.23.1-19.23.14. https://doi.org/10.1002/0471140864.ps1923s74

Rusilowicz-Jones, E. V., Barone, F. G., Lopes, F. M., Stephen, E., Mortiboys, H., Urbé, S., & Clague, M. J. (2022). Benchmarking a highly selective USP30 inhibitor for enhancement of mitophagy and pexophagy. *Life Science Alliance*, *5*(2). https://doi.org/10.26508/lsa.202101287

Rusilowicz-Jones, E. V., Jardine, J., Kallinos, A., Pinto-Fernandez, A., Guenther, F., Giurrandino, M., Barone, F. G., McCarron, K., Burke, C. J., Murad, A., Martinez, A., Marcassa, E., Gersch, M., Buckmelter, A. J., Kayser-Bricker, K. J., Lamoliatte, F., Gajbhiye, A., Davis, S., Scott, H. C., … Clague, M. J. (2020). USP30 sets a trigger threshold for PINK1–PARKIN amplification of mitochondrial ubiquitylation. *Life Science Alliance*, *3*(8), e202000768. https://doi.org/10.26508/lsa.202000768

Samak, G., Gangwar, R., Meena, A. S., Rao, R. G., Shukla, P. K., Manda, B., Narayanan, D., Jaggar, J. H., & Rao, R. (2016). Calcium Channels and Oxidative Stress Mediate a Synergistic Disruption of Tight Junctions by Ethanol and Acetaldehyde in Caco-2 Cell Monolayers. *Scientific Reports*, *6*(1), 38899. https://doi.org/10.1038/srep38899

Samanta, A., Parveen, N., Sen Sarma, M., Poddar, U., & Srivastava, A. (2024). Cholestatic Liver Disease due to Novel *USP53* Mutations: A Case Series of Three Indian Children. *Journal of Clinical and Experimental Hepatology*, *14*(2), 101290. https://doi.org/10.1016/j.jceh.2023.10.001

Sambrotta, M., Strautnieks, S., Papouli, E., Rushton, P., Clark, B. E., Parry, D. A., Logan, C. V., Newbury, L. J., Kamath, B. M., Ling, S., Grammatikopoulos, T., Wagner, B. E., Magee, J. C., Sokol, R. J., Mieli-Vergani, G., Smith, J. D., Johnson, C. A., McClean, P., Simpson, M. A., … Thompson, R. J. (2014). Mutations in TJP2 cause progressive cholestatic liver disease. *Nature Genetics*, *46*(4), 326–328. https://doi.org/10.1038/ng.2918

Sanchez, A. D., & Feldman, J. L. (2017). Microtubule-organizing centers: From the centrosome to non-centrosomal sites. *Current Opinion in Cell Biology*, *44*, 93–101. https://doi.org/10.1016/j.ceb.2016.09.003

Sapmaz, A., Berlin, I., Bos, E., Wijdeven, R. H., Janssen, H., Konietzny, R., Akkermans, J. J., Erson-Bensan, A. E., Koning, R. I., Kessler, B. M., Neefjes, J., & Ovaa, H. (2019). USP32 regulates late endosomal transport and recycling through deubiquitylation of Rab7. *Nature Communications*, *10*(1), 1454. https://doi.org/10.1038/s41467-019-09437-x

Sato, Y., Yoshikawa, A., Mimura, H., Yamashita, M., Yamagata, A., & Fukai, S. (2009). Structural basis for specific recognition of Lys 63-linked polyubiquitin chains by tandem UIMs of RAP80. *The EMBO Journal*, *28*(16), 2461–2468. https://doi.org/10.1038/emboj.2009.160

Satpathy, S., Wagner, S. A., Beli, P., Gupta, R., Kristiansen, T. A., Malinova, D., Francavilla, C., Tolar, P., Bishop, G. A., Hostager, B. S., & Choudhary, C. (2015). Systems-wide analysis of BCR signalosomes and downstream phosphorylation and ubiquitylation. *Molecular Systems Biology*, *11*(6), 810. https://doi.org/10.15252/msb.20145880

Savio, M. G., Wollscheid, N., Cavallaro, E., Algisi, V., Di Fiore, P. P., Sigismund, S., Maspero, E., & Polo, S. (2016). USP9X Controls EGFR Fate by Deubiquitinating the Endocytic Adaptor Eps15. *Current Biology*, *26*(2), 173–183. https://doi.org/10.1016/j.cub.2015.11.050

Schindelin, J., Arganda-Carreras, I., Frise, E., Kaynig, V., Longair, M., Pietzsch, T., Preibisch, S., Rueden, C., Saalfeld, S., Schmid, B., Tinevez, J.-Y., White, D. J., Hartenstein, V., Eliceiri, K., Tomancak, P., & Cardona, A. (2012). Fiji: An open-source platform for biological-image analysis. *Nature Methods*, *9*(7), 676–682. https://doi.org/10.1038/nmeth.2019

Schwertman, P., Lagarou, A., Dekkers, D. H. W., Raams, A., van der Hoek, A. C., Laffeber, C., Hoeijmakers, J. H. J., Demmers, J. A. A., Fousteri, M., Vermeulen, W., & Marteijn, J. A. (2012). UV-sensitive syndrome protein UVSSA recruits USP7 to regulate transcription-coupled repair. *Nature Genetics*, *44*(5), 598–602. https://doi.org/10.1038/ng.2230

Seguin, L., Liot, C., Mzali, R., Harada, R., Siret, A., Nepveu, A., & Bertoglio, J. (2009). CUX1 and E2F1 Regulate Coordinated Expression of the Mitotic Complex Genes Ect2, MgcRacGAP, and MKLP1 in S Phase. *Molecular and Cellular Biology*, *29*(2), 570–581. https://doi.org/10.1128/MCB.01275-08

Shannon, P., Markiel, A., Ozier, O., Baliga, N. S., Wang, J. T., Ramage, D., Amin, N., Schwikowski, B., & Ideker, T. (2003). Cytoscape: A software environment for integrated models of biomolecular interaction networks. *Genome Research*, *13*(11), 2498–2504. https://doi.org/10.1101/gr.1239303

Shatokhina, O., Semenova, N., Demina, N., Dadali, E., Polyakov, A., & Ryzhkova, O. (2021). A Two-Year Clinical Description of a Patient with a Rare Type of Low-GGT Cholestasis Caused by a Novel Variant of USP53. *Genes*, *12*(10), Article 10. https://doi.org/10.3390/genes12101618

Shi, X., Liu, X., Zong, Y., Zhao, Z., & Sun, Y. (2024). Novel compound heterozygous variants in causing autosomal recessive hearing loss in two Chinese families. *Molecular Genetics & Genomic Medicine*, *12*(8), e2502. https://doi.org/10.1002/mgg3.2502

Shi, Y., Chan, D. W., Jung, S. Y., Malovannaya, A., Wang, Y., & Qin, J. (2011). A Data Set of Human Endogenous Protein Ubiquitination Sites*. *Molecular & Cellular Proteomics*, *10*(5), M110.002089. https://doi.org/10.1074/mcp.M110.002089

Shiba-Fukushima, K., Arano, T., Matsumoto, G., Inoshita, T., Yoshida, S., Ishihama, Y., Ryu, K.-Y., Nukina, N., Hattori, N., & Imai, Y. (2014). Phosphorylation of Mitochondrial Polyubiquitin by PINK1 Promotes Parkin Mitochondrial Tethering. *PLOS Genetics*, *10*(12), e1004861. https://doi.org/10.1371/journal.pgen.1004861

Shrestha, R. K., Ronau, J. A., Davies, C. W., Guenette, R. G., Strieter, E. R., Paul, L. N., & Das, C. (2014). Insights into the Mechanism of Deubiquitination by JAMM Deubiquitinases from Cocrystal Structures of the Enzyme with the Substrate and Product. *Biochemistry*, *53*(19), 3199–3217. https://doi.org/10.1021/bi5003162

Sims, J. J., Scavone, F., Cooper, E. M., Kane, L. A., Youle, R. J., Boeke, J. D., & Cohen, R. E. (2012). Polyubiquitin-sensor proteins reveal localization and linkage-type dependence of cellular ubiquitin signaling. *Nature Methods*, *9*(3), 303–309. https://doi.org/10.1038/nmeth.1888

Snyder, N. A., & Silva, G. M. (2021). Deubiquitinating enzymes (DUBs): Regulation, homeostasis, and oxidative stress response. *The Journal of Biological Chemistry*, *297*(3), 101077. https://doi.org/10.1016/j.jbc.2021.101077

Sobol, A., Askonas, C., Alani, S., Weber, M. J., Ananthanarayanan, V., Osipo, C., & Bocchetta, M. (2017). Deubiquitinase OTUD6B Isoforms Are Important Regulators of Growth and Proliferation. *Molecular Cancer Research*, *15*(2), 117–127. https://doi.org/10.1158/1541-7786.MCR-16-0281-T

Sonoi, R., & Hagihara, Y. (2021). Tight junction stabilization prevents HepaRG cell death in drug-induced intrahepatic cholestasis. *Biology Open*, *10*(6), bio058606. https://doi.org/10.1242/bio.058606

Srinivas Sankaranarayanan, M. V. (2021). *Biallelic Mutations in Ubiquitin-Specific Peptidase 53 (USP53) Causing Progressive Intrahepatic Cholestasis. Report of a Case With Review of Literature*. https://journals.sagepub.com/doi/full/10.1177/10935266211051175

Steger, M., Demichev, V., Backman, M., Ohmayer, U., Ihmor, P., Müller, S., Ralser, M., & Daub, H. (2021). Time-resolved in vivo ubiquitinome profiling by DIA-MS reveals USP7 targets on a proteome-wide scale. *Nature Communications*, *12*(1), 5399. https://doi.org/10.1038/s41467-021-25454-1

Stes, E., Laga, M., Walton, A., Samyn, N., Timmerman, E., De Smet, I., Goormachtig, S., & Gevaert, K. (2014). A COFRADIC Protocol To Study Protein Ubiquitination. *Journal of Proteome Research*, *13*(6), 3107–3113. https://doi.org/10.1021/pr4012443

Stringer, D. K., & Piper, R. C. (2011). Terminating protein ubiquitination. *Cell Cycle*, *10*(18), 3067–3071. https://doi.org/10.4161/cc.10.18.17191

Sun, M., Zhang, Q., Zhao, B., Huang, Q., Wu, W., Fan, P., Zhang, L., & Zhang, X. (2023). Antibody-free approach for ubiquitination profiling by selectively clicking the ubiquitination sites. *Analytica Chimica Acta*, *1246*, 340877. https://doi.org/10.1016/j.aca.2023.340877

Sun, M., & Zhang, X. (2022). Current methodologies in protein ubiquitination characterization: From ubiquitinated protein to ubiquitin chain architecture. *Cell & Bioscience*, *12*(1), 126. https://doi.org/10.1186/s13578-022-00870-y

Sun, X.-X., Li, Y., Sears, R. C., & Dai, M.-S. (2021). Targeting the MYC Ubiquitination-Proteasome Degradation Pathway for Cancer Therapy. *Frontiers in Oncology*, *11*. https://doi.org/10.3389/fonc.2021.679445

Sun, Y., Zhao, X., Ding, N., Gao, H., Wu, Y., Yang, Y., Zhao, M., Hwang, J., Song, Y., Liu, W., & Rao, Y. (2018). PROTAC-induced BTK degradation as a novel therapy for mutated BTK C481S induced ibrutinib-resistant B-cell malignancies. *Cell Research*, *28*(7), 779–781. https://doi.org/10.1038/s41422-018-0055-1

Swatek, K. N., & Komander, D. (2016). Ubiquitin modifications. *Cell Research*, *26*(4), 399–422. https://doi.org/10.1038/cr.2016.39

Swatek, K. N., Usher, J. L., Kueck, A. F., Gladkova, C., Mevissen, T. E. T., Pruneda, J. N., Skern, T., & Komander, D. (2019). Insights into ubiquitin chain architecture using Ub-clipping. *Nature*, *572*(7770), 533–537. https://doi.org/10.1038/s41586-019-1482-y

Szklarczyk, D., Kirsch, R., Koutrouli, M., Nastou, K., Mehryary, F., Hachilif, R., Gable, A. L., Fang, T., Doncheva, N. T., Pyysalo, S., Bork, P., Jensen, L. J., & von Mering, C. (2023). The STRING database in 2023: Protein-protein association networks and functional enrichment analyses for any sequenced genome of interest. *Nucleic Acids Research*, *51*(D1), D638–D646. https://doi.org/10.1093/nar/gkac1000

Taghipour-Sheshdeh, A., Nemati-Zargaran, F., Zarepour, N., Tahmasebi, P., Saki, N., Tabatabaiefar, M. A., Mohammadi-Asl, J., & Hashemzadeh-Chaleshtori, M. (2019). A novel pathogenic variant in the *MARVELD2* gene causes autosomal recessive non-syndromic hearing loss in an Iranian family. *Genomics*, *111*(4), 840–848. https://doi.org/10.1016/j.ygeno.2018.05.008

Takagi, M., Yamauchi, M., Takada, K., & Ohkawa, K. (2002). Serum Ubiquitin-Protein Conjugates in Normal Subjects and Patients With Alcoholic Liver Diseases: Immunoaffinity Isolation and Electrophoretic Mobility. *Alcoholism: Clinical and Experimental Research*, *26*(11), 1692–1696. https://doi.org/10.1111/j.1530-0277.2002.tb02472.x

Tan, F., Lu, L., Cai, Y., Wang, J., Xie, Y., Wang, L., Gong, Y., Xu, B., Wu, J., Luo, Y., Qiang, B., Yuan, J., Sun, X., & Peng, X. (2008). Proteomic analysis of ubiquitinated proteins in normal hepatocyte cell line Chang liver cells. *PROTEOMICS*, *8*(14), 2885–2896. https://doi.org/10.1002/pmic.200700887

Tan, S., Tan, H. T., & Chung, M. C. M. (2008). Membrane proteins and membrane proteomics. *PROTEOMICS*, *8*(19), 3924–3932. https://doi.org/10.1002/pmic.200800597

Tang, Y., Tu, H., Zhang, J., Zhao, X., Wang, Y., Qin, J., & Lin, X. (2019). K63-linked ubiquitination regulates RIPK1 kinase activity to prevent cell death during embryogenesis and inflammation. *Nature Communications*, *10*(1), 4157. https://doi.org/10.1038/s41467-019-12033-8

Terawaki, S., Vasilev, F., Moriwaki, T., & Otomo, T. (2023). HOPS, CORVET and newly-identified Hybrid tethering complexes contribute differentially towards multiple modes of endocytosis. *Scientific Reports*, *13*(1), 18734. https://doi.org/10.1038/s41598-023-45418-3

The UniProt Consortium. (2025). UniProt: The Universal Protein Knowledgebase in 2025. *Nucleic Acids Research*, *53*(D1), D609–D617. https://doi.org/10.1093/nar/gkae1010

Thorslund, T., Ripplinger, A., Hoffmann, S., Wild, T., Uckelmann, M., Villumsen, B., Narita, T., Sixma, T. K., Choudhary, C., Bekker-Jensen, S., & Mailand, N. (2015). Histone H1 couples initiation and amplification of ubiquitin signalling after DNA damage. *Nature*, *527*(7578), 389–393. https://doi.org/10.1038/nature15401

Tomaiuolo, F. (2016). *Functional characterization of Myl6B: A protein required for spindle and midbody orientation in HeLa cell*. https://doi.org/10.58015/tomaiuolo-francesco_phd2016

Tomas, A., Futter, C. E., & Eden, E. R. (2014). EGF receptor trafficking: Consequences for signaling and cancer. *Trends in Cell Biology*, *24*(1), 26–34. https://doi.org/10.1016/j.tcb.2013.11.002

Trulsson, F., Akimov, V., Robu, M., van Overbeek, N., Berrocal, D. A. P., Shah, R. G., Cox, J., Shah, G. M., Blagoev, B., & Vertegaal, A. C. O. (2022). Deubiquitinating enzymes and the proteasome regulate preferential sets of ubiquitin substrates. *Nature Communications*, *13*(1), 2736. https://doi.org/10.1038/s41467-022-30376-7

Tsuchiya, H., Burana, D., Ohtake, F., Arai, N., Kaiho, A., Komada, M., Tanaka, K., & Saeki, Y. (2018). Ub-ProT reveals global length and composition of protein ubiquitylation in cells. *Nature Communications*, *9*(1), 524. https://doi.org/10.1038/s41467-018-02869-x

Tyanova, S., Temu, T., Sinitcyn, P., Carlson, A., Hein, M. Y., Geiger, T., Mann, M., & Cox, J. (2016). The Perseus computational platform for comprehensive analysis of (prote)omics data. *Nature Methods*, *13*(9), 731–740. https://doi.org/10.1038/nmeth.3901

Uehara, T., Yamada, M., Umetsu, S., Nittono, H., Suzuki, H., Fujisawa, T., Takenouchi, T., Inui, A., & Kosaki, K. (2020). Biallelic Mutations in the *LSR* Gene Cause a Novel Type of Infantile Intrahepatic Cholestasis. *The Journal of Pediatrics*, *221*, 251–254. https://doi.org/10.1016/j.jpeds.2020.01.064

Valenzano, M. C., DiGuilio, K., Mercado, J., Teter, M., To, J., Ferraro, B., Mixson, B., Manley, I., Baker, V., Moore, B. A., Wertheimer, J., & Mullin, J. M. (2015). Remodeling of Tight Junctions and Enhancement of Barrier Integrity of the CACO-2 Intestinal Epithelial Cell Layer by Micronutrients. *PLoS ONE*, *10*(7), e0133926. https://doi.org/10.1371/journal.pone.0133926

Valkevich, E. M., Sanchez, N. A., Ge, Y., & Strieter, E. R. (2014). Middle-Down Mass Spectrometry Enables Characterization of Branched Ubiquitin Chains. *Biochemistry*, *53*(30), 4979–4989. https://doi.org/10.1021/bi5006305

Vassilev, L. T. (2006). Cell Cycle Synchronization at the G2/M Phase Border by Reversible Inhibition of CDK1. *Cell Cycle*, *5*(22), 2555–2556. https://doi.org/10.4161/cc.5.22.3463

Vermeulen, K., Van Bockstaele, D. R., & Berneman, Z. N. (2003). The cell cycle: A review of regulation, deregulation and therapeutic targets in cancer. *Cell Proliferation*, *36*(3), 131–149. https://doi.org/10.1046/j.1365-2184.2003.00266.x

Wagner, S. A., Beli, P., Weinert, B. T., Nielsen, M. L., Cox, J., Mann, M., & Choudhary, C. (2011). A Proteome-wide, Quantitative Survey of In Vivo Ubiquitylation Sites Reveals Widespread Regulatory Roles. *Molecular & Cellular Proteomics*, *10*(10). https://doi.org/10.1074/mcp.M111.013284

Waltho, A., Popp, O., Lenz, C., Pluska, L., Lambert, M., Dötsch, V., Mertins, P., & Sommer, T. (2024). K48- and K63-linked ubiquitin chain interactome reveals branch- and length-specific ubiquitin interactors. *Life Science Alliance*, *7*(8). https://doi.org/10.26508/lsa.202402740

Wang, B., Hu, B., & Yang, S. (2015). Cell junction proteins within the cochlea: A review of recent research. *Journal of Otology*, *10*(4), 131–135. https://doi.org/10.1016/j.joto.2016.01.003

Wendrich, K., Gallant, K., Recknagel, S., Petroulia, S., Kazi, N. H., Hane, J. A., Führer, S., Bezstarosti, K., O'Dea, R., Demmers, J., & Gersch, M. (2024). Discovery and

mechanism of K63-linkage-directed deubiquitinase activity in USP53. *Nature Chemical Biology*, 1–12. https://doi.org/10.1038/s41589-024-01777-0

Wickström, S. A., Masoumi, K. C., Khochbin, S., Fässler, R., & Massoumi, R. (2010). CYLD negatively regulates cell-cycle progression by inactivating HDAC6 and increasing the levels of acetylated tubulin. *The EMBO Journal*, *29*(1), 131–144. https://doi.org/10.1038/emboj.2009.317

Wijdeven, R. H., Berlin, I., Jansen, G., Janssen, H., van Veelen, P., & Neefjes, J. (2017). USP54 is a novel regulator of cytoskeletal dynamics. Part of *Dissertation*.

Wu, X., & Karin, M. (2015). Emerging roles of Lys63-linked polyubiquitylation in immune responses. *Immunological Reviews*, *266*(1), 161–174. https://doi.org/10.1111/imr.12310

Xolalpa, W., Mata-Cantero, L., Aillet, F., & Rodriguez, M. S. (2016). Isolation of the Ubiquitin-Proteome from Tumor Cell Lines and Primary Cells Using TUBEs. In R. Matthiesen (Ed.), *Proteostasis: Methods and Protocols* (pp. 161–175). Springer. https://doi.org/10.1007/978-1-4939-3756-1_8

Xu, G., & Jaffrey, S. R. (2013). Proteomic identification of protein ubiquitination events. *Biotechnology and Genetic Engineering Reviews*, *29*(1), 73–109. https://doi.org/10.1080/02648725.2013.801232

Xu, G., Paige, J. S., & Jaffrey, S. R. (2010). Global analysis of lysine ubiquitination by ubiquitin remnant immunoaffinity profiling. *Nature Biotechnology*, *28*(8), Article 8. https://doi.org/10.1038/nbt.1654

Xue, Y., Ouyang, K., Huang, J., Zhou, Y., Ouyang, H., Li, H., Wang, G., Wu, Q., Wei, C., Bi, Y., Jiang, L., Cai, Z., Sun, H., Zhang, K., Zhang, Y., Chen, J., & Fu, X.-D. (2013). Direct Conversion of Fibroblasts to Neurons by Reprogramming PTB-Regulated MicroRNA Circuits. *Cell*, *152*(1), 82–96. https://doi.org/10.1016/j.cell.2012.11.045

Yan, K., Ponnusamy, M., Xin, Y., Wang, Q., Li, P., & Wang, K. (2018). The role of K63-linked polyubiquitination in cardiac hypertrophy. *Journal of Cellular and Molecular Medicine*, *22*(10), 4558–4567. https://doi.org/10.1111/jcmm.13669

Yan, Q., Dutt, S., Xu, R., Graves, K., Juszczynski, P., Manis, J. P., & Shipp, M. A. (2009). BBAP Monoubiquitylates Histone H4 at Lysine 91 and Selectively Modulates the DNA Damage Response. *Molecular Cell*, *36*(1), 110–120. https://doi.org/10.1016/j.molcel.2009.08.019

Yang, Q., Zhao, J., Chen, D., & Wang, Y. (2021). E3 ubiquitin ligases: Styles, structures and functions. *Molecular Biomedicine*, *2*, 23. https://doi.org/10.1186/s43556-021-00043-2

Yang, Y., Liu, M., Li, D., Ran, J., Gao, J., Suo, S., Sun, S.-C., & Zhou, J. (2014). CYLD regulates spindle orientation by stabilizing astral microtubules and promoting dishevelled-NuMA-dynein/dynactin complex formation. *Proceedings of the National Academy of Sciences*, *111*(6), 2158–2163. https://doi.org/10.1073/pnas.1319341111

Yang, Y., Ran, J., Liu, M., Li, D., Li, Y., Shi, X., Meng, D., Pan, J., Ou, G., Aneja, R., Sun, S.-C., & Zhou, J. (2014). CYLD mediates ciliogenesis in multiple organs by deubiquitinating Cep70 and inactivating HDAC6. *Cell Research*, *24*(11), 1342–1353. https://doi.org/10.1038/cr.2014.136

Yao, Y., Ma, W., Guo, Y., Liu, Y., Xia, P., Wu, X., Chen, Y., Wang, K., Mei, C., Wang, G., Li, X., Zhang, Z., Chen, X., & Yuan, Y. (2022). USP53 plays an antitumor role in hepatocellular carcinoma through deubiquitination of cytochrome c. *Oncogenesis*, *11*(1), Article 1. https://doi.org/10.1038/s41389-022-00404-8

Yasukawa, T., Tsutsui, A., Tomomori-Sato, C., Sato, S., Saraf, A., Washburn, M. P., Florens, L., Terada, T., Shimizu, K., Conaway, R. C., Conaway, J. W., & Aso, T. (2020). NRBP1-

Containing CRL2/CRL4A Regulates Amyloid β Production by Targeting BRI2 and BRI3 for Degradation. *Cell Reports*, *30*(10), 3478-3491.e6. https://doi.org/10.1016/j.celrep.2020.02.059

Yau, R. G., Doerner, K., Castellanos, E. R., Haakonsen, D. L., Werner, A., Wang, N., Yang, X. W., Martinez-Martin, N., Matsumoto, M. L., Dixit, V. M., & Rape, M. (2017). Assembly and Function of Heterotypic Ubiquitin Chains in Cell-Cycle and Protein Quality Control. *Cell*, *171*(4), 918-933.e20. https://doi.org/10.1016/j.cell.2017.09.040

Ye, Y., Scheel, H., Hofmann, K., & Komander, D. (2009). Dissection of USP catalytic domains reveals five common insertion points. *Molecular BioSystems*, *5*(12), 1797–1808. https://doi.org/10.1039/B907669G

Yi Liu, Wei Tang, & Feng Yao. (2023). USP53 Exerts Tumor-Promoting Effects in Triple-Negative Breast Cancer by Deubiquitinating CRKL. *Cancers*. https://www.mdpi.com/2072-6694/15/20/5033

Yuan, W.-C., Lee, Y.-R., Lin, S.-Y., Chang, L.-Y., Tan, Y. P., Hung, C.-C., Kuo, J.-C., Liu, C.-H., Lin, M.-Y., Xu, M., Chen, Z. J., & Chen, R.-H. (2014). K33-Linked Polyubiquitination of Coronin 7 by Cul3-KLHL20 Ubiquitin E3 Ligase Regulates Protein Trafficking. *Molecular Cell*, *54*(4), 586–600. https://doi.org/10.1016/j.molcel.2014.03.035

Yue, W., Chen, Z., Liu, H., Yan, C., Chen, M., Feng, D., Yan, C., Wu, H., Du, L., Wang, Y., Liu, J., Huang, X., Xia, L., Liu, L., Wang, X., Jin, H., Wang, J., Song, Z., Hao, X., & Chen, Q. (2014). A small natural molecule promotes mitochondrial fusion through inhibition of the deubiquitinase USP30. *Cell Research*, *24*(4), 482–496. https://doi.org/10.1038/cr.2014.20

Zacharias, D. A., Violin, J. D., Newton, A. C., & Tsien, R. Y. (2002). Partitioning of Lipid-Modified Monomeric GFPs into Membrane Microdomains of Live Cells. *Science*, *296*(5569), 913–916. https://doi.org/10.1126/science.1068539

Zhang, C., Ma, X., Wei, G., Zhu, X., Hu, P., Chen, X., Wang, D., Li, Y., Ruan, T., Zhang, W., Tao, K., & Wu, C. (2023). Centrosomal protein 120 promotes centrosome amplification and gastric cancer progression via USP54-mediated deubiquitination of PLK4. *IScience*, *26*(1), 105745. https://doi.org/10.1016/j.isci.2022.105745

Zhang, D., Raasi, S., & Fushman, D. (2008). Affinity Makes the Difference: Nonselective Interaction of the UBA Domain of Ubiquilin-1 with Monomeric Ubiquitin and Polyubiquitin Chains. *Journal of Molecular Biology*, *377*(1), 162–180. https://doi.org/10.1016/j.jmb.2007.12.029

Zhang, J., Yang, Y., Gong, J. Y., Li, L. T., Li, J. Q., Zhang, M. H., Lu, Y., Xie, X. B., Hong, Y. R., Yu, Z., Knisely, A. S., & Wang, J. S. (2020). Low-GGT intrahepatic cholestasis associated with biallelic USP53 variants: Clinical, histological and ultrastructural characterization. *Liver Int*, *40*(5), 1142–1150. https://doi.org/10.1111/liv.14422

Zhang, M., Berk, J. M., Mehrtash, A. B., Kanyo, J., & Hochstrasser, M. (2022). A versatile new tool derived from a bacterial deubiquitylase to detect and purify ubiquitylated substrates and their interacting proteins. *PLOS Biology*, *20*(6), e3001501. https://doi.org/10.1371/journal.pbio.3001501

Zhang, Y., Mao, D., Roswit, W. T., Jin, X., Patel, A. C., Patel, D. A., Agapov, E., Wang, Z., Tidwell, R. M., Atkinson, J. J., Huang, G., McCarthy, R., Yu, J., Yun, N. E., Paessler, S., Lawson, T. G., Omattage, N. S., Brett, T. J., & Holtzman, M. J. (2015). PARP9-DTX3L ubiquitin ligase targets host histone H2BJ and viral 3C protease to enhance interferon signaling and control viral infection. *Nature Immunology*, *16*(12), 1215–1227. https://doi.org/10.1038/ni.3279

Zhang, Y., Yan, M., Yu, Y., Wang, J., Jiao, Y., Zheng, M., & Zhang, S. (2024). 14–3-3ε: A protein with complex physiology function but promising therapeutic potential in cancer. *Cell Communication and Signaling*, *22*(1), 72. https://doi.org/10.1186/s12964-023-01420-w

Zhao, J., Molitor, T. P., Langston, J. W., & Nichols, R. J. (2015). LRRK2 dephosphorylation increases its ubiquitination. *Biochemical Journal*, *469*(1), 107–120. https://doi.org/10.1042/BJ20141305

Zhao, X., Wu, X., Wang, H., Yu, H., & Wang, J. (2020). USP53 promotes apoptosis and inhibits glycolysis in lung adenocarcinoma through FKBP51-AKT1 signaling. *Molecular Carcinogenesis*, *59*(8), 1000–1011. https://doi.org/10.1002/mc.23230

Zheng, Y., Guo, H., Chen, L., Cheng, W., Yan, K., Zhang, Z., Li, M., Jin, Y., Hu, G., Wang, C., Zhou, C., Zhou, W., Jia, Z., Zheng, B., & Liu, Z. (2024). Diagnostic yield and novel candidate genes by next generation sequencing in 166 children with intrahepatic cholestasis. *Hepatology International*, *18*(2), 661–672. https://doi.org/10.1007/s12072-023-10553-6

Zhou, C., Zhang, X., Ma, H., Zhou, Y., Meng, Y., Chen, C., Shi, G., Yu, W., & Zhang, J. (2024). USP54 is a potential therapeutic target in castration-resistant prostate cancer. *BMC Urology*, *24*(1), 32. https://doi.org/10.1186/s12894-024-01418-7

Zihni, C., Mills, C., Matter, K., & Balda, M. S. (2016). Tight junctions: From simple barriers to multifunctional molecular gates. *Nature Reviews Molecular Cell Biology*, *17*(9), 564–580. https://doi.org/10.1038/nrm.2016.80

8 Abbreviations

ABP: Activity-based probe

ACN: Acetonitrile

AP-MS: Affinity purification-mass spectrometry

B: Blot

CAA: Chloroacetamide

CCCP: Carbonyl cyanide *m*-chlorophenyl hydrazine

CD: Catalytic domain

CHMP: Charged multivesicular body protein

Cmpd: Compound

Ct: Threshold cycle

DAPI: 4′,6-diamidino-2-phenylindole

DDA: Data-dependent acquisition

DDR: DNA-Damage response

DIA: Data-independent acquisition

DMEM: Dulbecco's Modified Eagle Medium

DMSO: Dimethyl sulfoxide

DNA: Desoxyribunucleic acid

Dox: Doxycycline

DSB: DNA double-strand breaks

DTT: Dithiothreitol

DUB: Deubiquitinase

EDTA: Ethylenediaminetetraacetic acid

EGF: Epidermal growth factor

EGFR: EGF receptor

emGFP: Enhanced monomeric GFP

ER: Endoplasmic reticulum

ERAD: ER-associated degradation

ESCRT: Endosomal sorting complexes required for transport

Eto: Etoposide

FA: Formic acid

FBS: Fetal bovine serum

FL: Full-length

GFP: Green fluorescent protein

HA: Hemagglutinin

HEK: Human embryonic kidney cells

HeLa: Henrietta Lacks cells

HF: High fidelity

HOPS: Homotypic fusion and vacuole protein sorting

IB: Immunoblot

IF: Immunofluorescence

IP: Immunoprecipitation

IPTG: Isopropyl-1-thio-β-D-galactopyranoside

JAMM: Zn-dependent JAB1/MPN/MOV34 metalloprotease family

kDa: Kilo Dalton

LDS: Lithium dodecyl sulfate

MES: 2-(N-morpholino) ethanesulfonic acid

MESNA: Sodium 2-mercaptoetanesulfonate

MINDY: Motif interacting with ubiquitin-containing novel DUB family

MIT: Microtubule interacting and transport

MonoUb: Monoubiquitin

MS: Mass spectrometry

MT: Mutant

MVB: Multivesicular body

MW: Molecular weight

NEM: N-Ehtylmaleimide

NZF: Npl4 zinc finger

OCEL: occluding/ELL domain

OE: (Ectopic) overexpression

OMM: Outer mitochondrial membrane

OtUBD: *Orientia tsutsugamushi* ubiquitin-binding domain

OTU: Ovarian tumour protease

PA: Propargylamide gel electrophoresis

PAGE: Polyacrylamide

PBS: Phosphate-buffered saline

PCR: Polymerase chain reaction

PD: Parkinson's disease

PD: Pulldown

PEI: Polyethyleneimine

PMSF: Phenylmethylsulfonyl fluoride

PolyUb: Polyubiquitin

PPM: Parts per million

PQC: Protein quality control

PTM: Post-translational modification

qPCR: Quantitative PCR

SDS: Sodium dodecyl sulfate

SH3: Src homology 3

shRNA: Small hairpin RNA

siRNA: Small interfering RNA

siR: siRNA-resistant

SN: Supernatant

SOE: Splicing-by-overlap extension

TAMP: Tight-junction-associated MARVEL proteins

TCEP: Tris-(2-carboxyethyl)-phosphine

TFA: Trifluoracetic acid

TJ: Tight junction

TJP: Tight junction proteins

TMT: Tandem mass tag

tTJ: Tricellular tight junction

TUBE: Tandem-repeated ubiquitin-binding entities

UBD: Ubiquitin-binding domain

UCH: Ubiquitin C-terminal hydrolase

UIM: Ubiquitin-interacting motif

UPS: Ubiquitin-mediated protein degradation system

USP: Ubiquitin-specific protease

VS: Vinyl methyl sulfone

WB: Western Blot

WT: Wild-type

YFP: Yellow fluorescent protein

ZO: Zonula occludens

ZUP: Zinc finger containing ubiquitin peptidase